HOKKAIDO UNIVERSITY

Title	Study on Adsorption Heat Pump Using Composite Natural Mesoporous Material as Low-Carbon Air Conditioning
Author(s)	,
Citation	. ( ) 14242
Issue Date	2020-09-25
DOI	10.14943/doctoral.k14242
Doc URL	http://hdl.handle.net/2115/79440
Type	theses (doctoral)
File Information	Sung-Hoon_Seol.pdf

Instructions for use

STUDY ON ADSORPTION HEAT PUMP USING COMPOSITE NATURAL MESOPOROUS MATERIAL AS LOW-CARBON AIR CONDITIONING

Presented by: Sung-Hoon Seol

Supervisor: Prof. Katsunori Nagano

北海道大学

2020

Division of Human Environmental Systems

Graduate School of Engineering

Hokkaido University

CONTENTS OF THE THESIS

I

4. **Modeling of AHP System Based on Experimental Estimation of Heat and Mass Transfer Coefficients**

5. **Simulation on Annual Performance of Solar AHP Using WSS Composite for Low-carbon Air Conditioning**

学 位 論 文 内 容 の 要 旨
DISSERTATION ABSTRACT

空間性能システム専攻　　　博士（工学）　　　氏名　SEOL Sung-Hoon

学 位 論 文 題 名
Title of dissertation submitted for the degree

Study on Adsorption Heat Pump Using Composite Natural Mesoporous Material as Low-Carbon Air Conditioning

（天然メソポーラス材料を用いた吸着式ヒートポンプによる低炭素空調）

The energy demand on heating, cooling and domestic hot water supply, which account for around half of the energy in the residential sector, are primary factor increasing the energy consumption in the sector throughout the world. Also the cases require cooling or refrigeration all day are frequently found in commercial facilities and office buildings in urban area. Meanwhile, the massive amount of low-level waste heat around 80 ℃ is discharged from co-generation systems and industries to the environment. In order to supply cooling energy, refrigeration systems are needed. They are categorized into the vapor compression and thermally-driven systems. In terms of the thermally-driven systems, absorption chillers employing sorbents such as lithium bromide and adsorption chillers applying adsorbents such as a silica gel are the most representative. Among them, the system that can utilize the low-level thermal energy more efficiently is known to be the adsorption cooling system, and it is commonly named adsorption heat pump (AHP). The concept of technology of the adsorption has been existed from the past. However, low effective thermal conductivity due to the porosity of the adsorbent leads limitation of enhancement of heat and mass transfer rate have resulted in the huge system volume of AHP systems. Additionally, high-performance synthesis is too expensive, and the AHP system itself could not obtain economic competitiveness yet. For these reasons, there are only several commercial AHP units throughout the world yet, and the chance to utilize an AHP system properly at energetic and economic aspects is highly limited. Based on these background, this research deals with a low cost and high-performance AHP system applying the natural mesoporous material named Wakkanai Siliceous Shale (WSS) and its application. WSS is obtained from the north part of Hokkaido and mainly consists of silicon dioxide (SiO_2).

In Chapter 1, researches and developments of AHP are reviewed including the general background and cost of commercialized units. Upon them, this chapter describes the motivation and target of this study.

In Chapter 2, the natural mesoporous material based composite adsorbent impregnated with lithium chloride (LiCl) is introduced. Equilibrium adsorption characteristics, so called, isotherms of the adsorbents are experimentally measured under the operating pressure and temperature of AHP. At the same time, it is confirmed that LiCl concentration preventing carryover is 20 wt.%

for the case of WSS.

In Chapter 3, the measurement of mass transfer of water vapor on the coated composite adsorbent is provided. The composite material is prepared by mixing the submicron-scale WSS particles, LiCl solution and acrylic binder which does not disturb water vapor adsorption severely. The particles of adsorbent is able to be sprayed on the metal surface of the sample plate owing to its fine particle size. Samples which are coated by the adsorbent layer with the different thickness are used to separate interfacial mass transfer at the surface and internal mass transfer inside of the layer. The interfacial mass transfer characteristics are successfully yielded by the novel experimental method making the coated adsorbent layer as thin as possible and the Linear Driving Force (LDF) model.

In Chapter 4, heat and mass transfer coefficients of the WSS composite filled between the fins of the corrugated-type heat exchanger are measured. For the comparison, the same experiments applying the A-type silica gel are also conducted. The zero-dimensional simulation model based on these experimental estimation of coefficients calculates the cooling performance of AHP. As a result, the adsorber applying the WSS composite presents 6-17 % higher COP compared to the A-type silica gel, proving the competitiveness of the WSS composite.

In Chapter 5, the performance of a solar AHP applying a WSS composite is estimated, together with analysis on reduction of CO_2 emission and economic advantages according to local electricity cost of various major regions. Four regions having distinct climate conditions are selected as targets in this chapter, namely, Hawaii, Dubai, Florida and Tokyo. As a result, Hawaii presents the shortest payback period of 6.6 years owing to the expansive electricity cost in it. Although CO_2 reduction in Dubai is the highest, the payback period in Dubai is 15.6 years due to the low local electricity cost.

In Chapter 6, energy and exergy analysis through the experimental data using 1 kW-scale AHP unit are conducted. The cooling capacity with the regeneration temperature of 70 ℃ is about 36 % reduced than that of the case with the regeneration water of 80 ℃, meanwhile the exergy efficiency is approximately 20 % increased by lowering the chilled water temperature as 10 ℃.

In Chapter 7, the hybrid system combining CO_2 compression and AHP systems are introduced as a future research, and the general conclusions of the research are provided.

It is valuable in this study that the heat and mass transfer coefficients of the composite natural adsorbent are estimated by the novel experimental methodology. These characteristics are essential information in designing the AHP system. Also the actual cooling performance of the AHP system which can produce cooling energy by using the low-level heat source below 80 ℃ is proved. Furthermore, application effect of the solar AHP system in four major regions are studied based on its annual performance, economic and environmental analysis. It is believed that these research works above contribute to the low-carbon society.

NOMENCLATURE

Abbreviations

AHP	Adsorption heat pump
COP	Coefficient of performance
EHP	Electric heat pump
LDF	Linear driving force
SCP	Specific cooling power
WSS	Wakkanai siliceous shale

Symbols

A	Area [m^2], Constant of isotherm equation [-]
A_0	Constant of Eq. (4-3), (4-4)
B_0	Constant of Eq. (4-3), (4-4)
C	Constant of isotherm equation [-], Heat capacity [J/K]
c	Gas phase water vapor concentration [g$_{vapor}$/m$^3_{gas}$]
C_p	Specific heat of water [J/gK]
D_e	Effective diffusivity [m^2/s]
D_p	Pore diameter [nm]
D_h	Hydraulic diameter [m]
d	Coated thickness [m]
$F_R\tau\alpha$	Intercept efficiency of solar collector [-]
$F_R U_L$	First-order coefficient of collector efficiency [W/m^{2}K]
E_a	Activation energy [J/g]
E_c	Characteristic energy [J/g]
F_H	Fin height [m]
F_p	Fin pitch [m]
F_{th}	Fin thickness [m]
h	Enthalpy [J/g] or convective heat transfer coefficient [W/m^{2}K]
I	Solar radiation [W/m^2]
$\dot{I}$	Irreversibility [kW]
K	Slope of sorption isotherm [m$^3_{vapor}$/g$_{solid}$]

K_m	Overall mass transfer coefficient [s^{-1}]
k	Thermal conductivity [W/mK]
k_f	Interfacial mass transfer coefficient [s^{-1}]
k_s	Internal mass transfer coefficient [s^{-1}]
M	Mass [g]
$\dot{m}$	Cooling water flow rate [g/s]
Nu	Nusselt number [-]
N_M	Isotherm constant of Eq. (2-23) [-]
n	Surface heterogeneity [-]
P	Pressure [kPa]
Q	Heat capacity [W]
q	Average water vapor sorption amount [g_{vapor}/g_{solid}]
q^*	Equilibrium water vapor sorption amount [g_{vapor}/g_{solid}]
R	Mass transfer resistance [s], gas constant [J/gK]
S	Surface area [m^2/g]
T	Temperature [°C]
TCR	Thermal contact resistance [K/Wm^2]
t	Time [s]
UA	Overall Heat transfer coefficient [W/K]
V	Volume [m^3]
W_P	Pump power [kW]

Greek letters

α	Temperature ratio [-]
β	Constant of isotherm equation [-]
τ	Characteristic time [-]
$\triangle H$	Heat of adsorption [J/g]
ε	Heat transfer effectiveness [-]
$\emptyset$	Constant of isotherm equation [-]
ρ	Density [g/m^3]
φ	Exergy [J/g]

η	Efficiency [-]

Subscripts

a	Adsorbent
ad	Adsorption
amb	Ambient
b	Adsorption bed
c	Cooling
cal	Calculated
cf	Cross area of fin
cond	Condenser
cycle	Cycle
des	Desorption
e	Evaporation
exp	Experiment
evap	Evaporator
f	Interfacial
fin	Fin
HEX	Heat exchanger
i	Inlet
L	Loss
load	Cooling load
r	Refrigerant
SC	Solar collector
s	Internal
sat	Saturation
tw	Tube wall, tank wall
unfin	Unfinned
v	Vapor
w	Water
metal	Metal
m	Maximum

LIST OF FIGURES

CHAPTER 3

CHAPTER 7

LIST OF TABLES

CHAPTER 6

CHAPTER 1. INTRODUCTION

1.1 ENERGY CONSUMPTION AND ENVIRONMENTAL ISSUES

Advancement of industry and improved standard of living have tended to be coupled with increase of energy consumption. It eventually has been bringing out issues such as depletion of reserves, various environmental problems and economic matters regarding fuel price. Indeed, the world ultimate oil reserve is assumed to be about 2000 billion barrel, and the world daily oil consumption amount is estimated to be around 71.7 million barrels [1]. Also World Energy Annual Report has provided world historical and projected oil production in which the production amount decreases as from 2010 (Fig. 1. 1) [2]. Coal and natural gas, which are the other energy sources used for thermal power generation, also reported to have significantly reduced production by 2050 (Fig. 1. 2, Fig. 1. 3) [3].
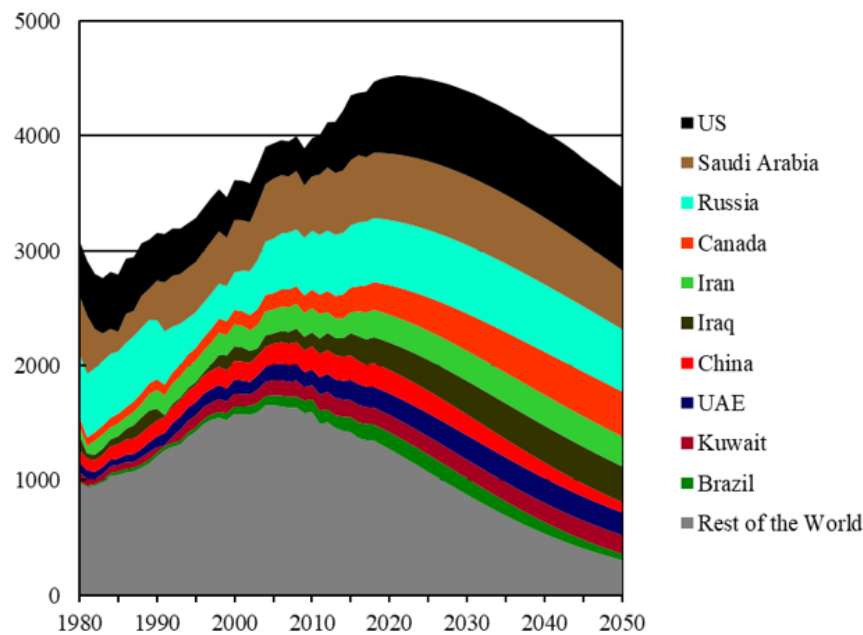
Fig. 1. 1 Extraction of reserved oil from 1980 to 2050 [2]

The U.S. Energy Information Administration (EIA) estimates that the energy consumed for air-conditioning will increase the most drastically among other uses in the building sector by 2050 (Fig. 1. 4) [4]. The entire delivered energy consumption amount in the building sectors is expected to increase by 7% because of increased demand for energy use. Furthermore, International Institute of Refrigeration (IIR) defined that the refrigeration and air-conditioning sector consume approximately 17% of the overall electricity use of the worldwide [5].
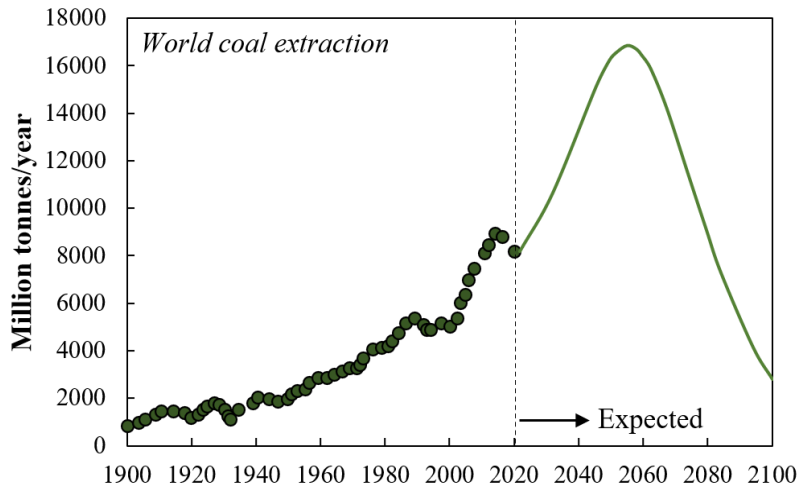
Fig. 1. 2 Extraction of reserved coal from 1900 to 2100 [3]
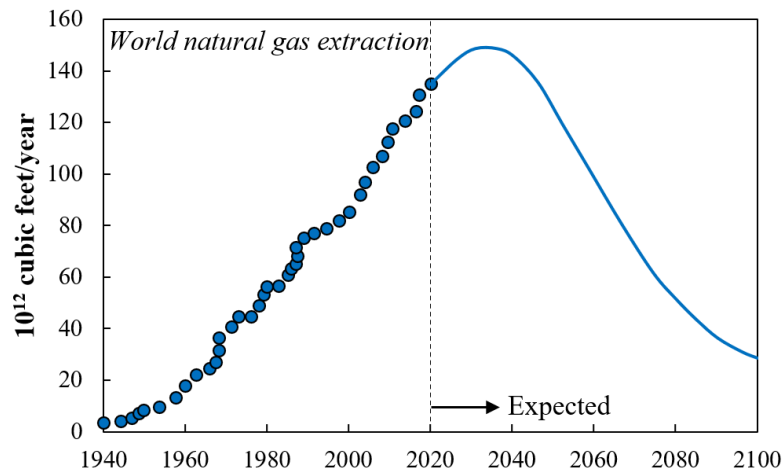
Fig. 1. 3 Extraction of reserved natural gas from 1940 to 2100 [3]

Vapor compressions system which is the most commonly used in air-conditioning and refrigeration systems are driven by the electric energy of the compressor. Assuming that the energy efficiency for electrical generation ranges between 40~50 %, it can be noticed that the large amount energy loss occurs to the environment with the temperature between 70 ~200 ℃ [6]. Furthermore, the by-products of generation process such as carbon dioxide, sulfur and nitrogen oxide greatly contribute to global warming. Aside from the generation process, most of vapor compression systems themselves include environmental pollutants refrigerant. CFC (Chlorofluorocarbon) and HCFC (Hydrochlorofluorocarbon) are already under regulation by the Montreal protocol because of its contribution to depletion of ozone layers. Furthermore, their substation

2

substances called HFC (Hydrofluorocarbon) are also designated as one of global warming pollutant by Kyoto protocol, and their usages are supposed to be reduced and regulated [7].
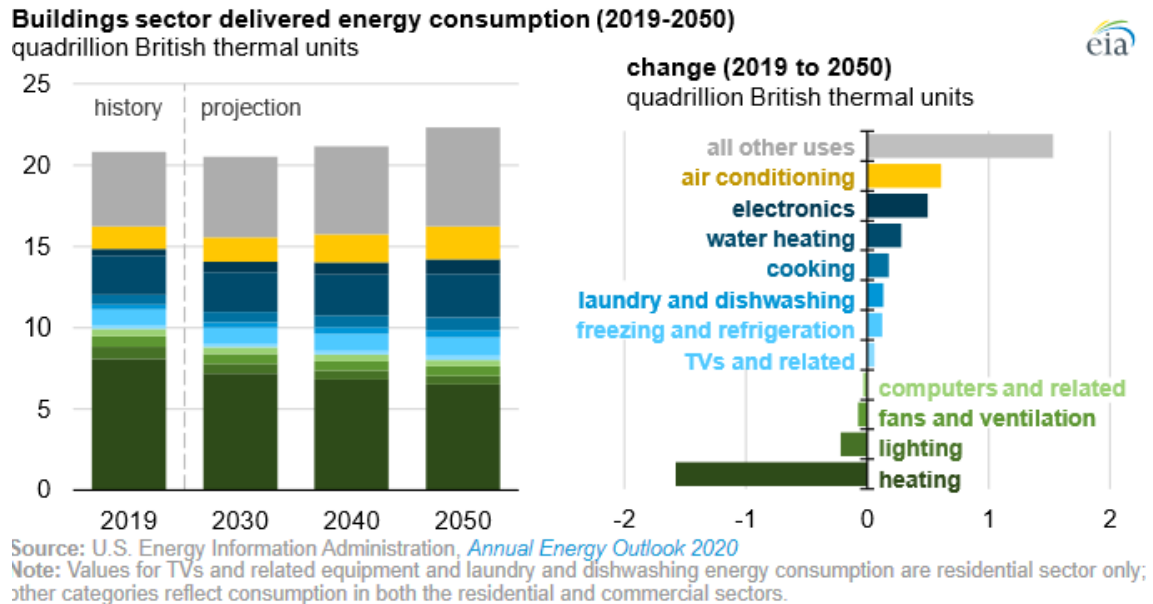
Fig. 1. 4 Building sector delivered energy consumption (2019-2050) [4]

In contrast, adsorption heat pump (AHP) systems normally apply nature refrigerants such as water and ammonia whose Ozone Depletion Potential (ODP) and Global Warming Potential (GDP) are zero. Furthermore, the AHP systems consume much less electric energy compared to the vapor compression systems since they are thermally driven system rather than being driven electrically. More details about refrigerants of AHP systems so called working pairs will be provided in the latter part of this chapter, and more explanation about the system will be given in the following sections of this chapter.

1.2 WORLD CO₂ EMISSION AND REDUCTION TARGET

In 2018, International Panel on Climate Change (IPCC) reported that unprecedented changes in all aspects of society are required to limit global warming to 1.5 °C. It was suggested that the human-caused emissions of carbon dioxide (CO_2) needs to be reduced by approximately 45 % compared to 2010 level by 2030. Fig. 1.5 describes total global annual emissions of fossil CO_2 by sectors. The greenhouse gas emissions have been increased steadily since the early 21 century. Developed countries announced their plan for reducing CO_2 emissions to mitigate rising global temperature and greenhouse gas emissions, as shown in Fig. 1. 6.
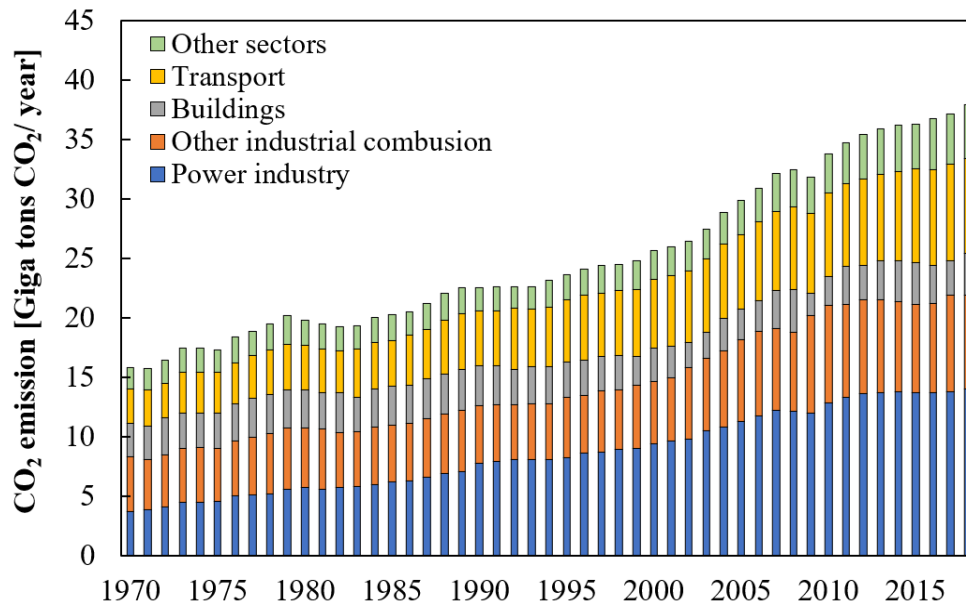
Fig. 1. 5 Total global annual emissions of fossil CO_2 in $GTCO_2$/year by sector [8]

Although U.S. decided to be withdrawn from the Paris Agreement in 2019, a lot of countries target to reduce the emissions of CO_2 in all possible aspects. In terms of power industry, which takes the largest portion, the amount of the CO_2 emission per kWh is dependent on the energy source of the generation: 1.00kgCO₂/kWh for coal, 0.417 kgCO₂/kWh for natural gas, 0.957 kgCO₂/kWh. The generation by using renewable energy source shows far more attractive values in the CO_2 emissions. The lowest was 10gCO₂/kWh for hydropower, followed by 34gCO₂/kWh for wind power, solar PV 50gCO₂/kWh. Though it is quite controversial, nuclear power generation is also known

as relatively low-carbon generation. Since the emission factor tends to decrease as the portion of renewable energy and nuclear power increase throughout the world [9–11], the entire emission amount is expected to decrease in accordance with the trend. Also, the emission from the transport section also expected to decrease as electric and hydrogen vehicles are commercialized.

Post 2020 National CO_2 Emission Reduction Targets
from United Nations Framework Convention on Climate Change

Country	Reduction target
U.S.A	**By 2025** reduce 26 ~ 28 % compared to 2005
China	**By 2030** *carbon intensity of its GDP* reduce 60 ~ 65 % compared to 2005
EU	**By 2030** reduce 40 % compared to 2005
Japan	**By 2030** reduce 26 % compared to 2013
Russia	**By 2030** reduce 70 ~ 75% compared to 1990
Korea	**By 2030** reduce 37 % compared to BAU
India	**By 2030** *carbon intensity of its GDP* reduce 33 ~ 35% compared to 2005

Fig. 1. 6 CO_2 emission reduction targets of several countries after 2020 [12]

In terms of the building air-conditioning section, application of thermally-driven heat pumps have attracted interest. Furthermore, use of the low-level waste heat source from industries have been one of the key word for energy saving, in recent decades. Thermal-driven cooling systems give significant energy saving compared to traditional vapor compression systems and have low GWP and ODP [13]. As a part of the heat-driven systems, adsorption heat pump (AHP) has attracted huge interest due to its eco-friendly operation and applicability of low-level heat sources less than 100 ℃. In addition, utilization of solar energy makes the AHP far more attractive because it significantly decreases fossil energy input for the operation the system. AHP systems have an

advantage compared to absorption cycles that the heat source with the lower temperature can be used [14,15].

Fig. 1.7 represents a schematic diagram of the combined cooling system with EHP and AHP. As the thermally driven AHP supports the EHP to provide cooling energy to the target building, the entire electric energy consumption significantly decreases. This finally not only results in reduction of CO_2 emission but also brings out economic benefit. The detailed analysis on the application effect of the AHP system will be introduced in Chapter 5 of this thesis.
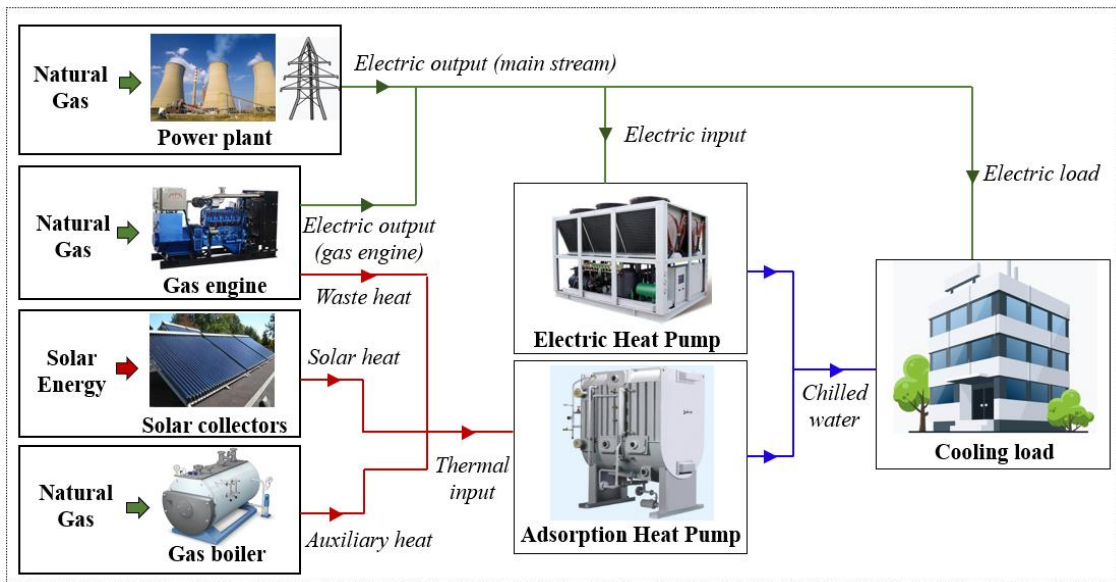
Fig. 1. 7 Schematic diagram of the combined cooling system with EHP and AHP
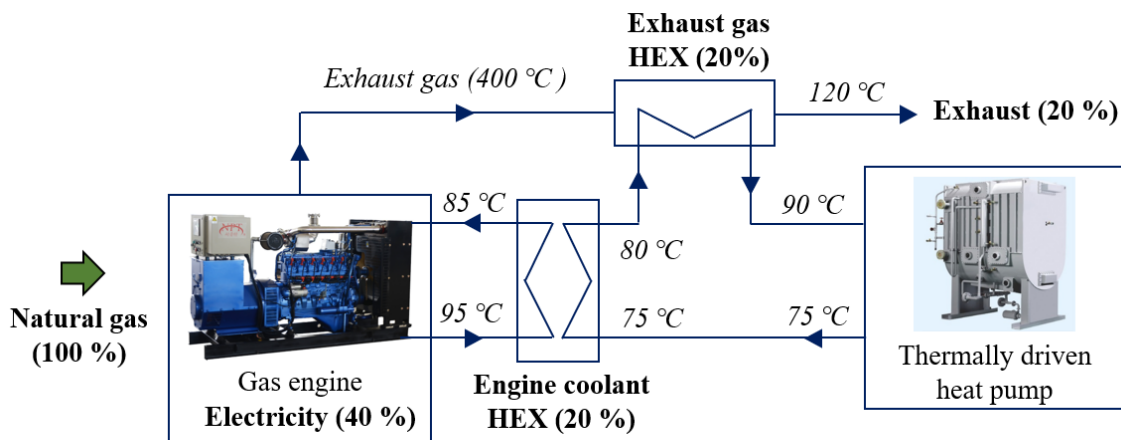
Fig. 1. 8 Example of heat recovery from gas engine [16]

1.3 ADSORPTION HEAT PUMP (AHP) SYSTEM

When it comes to the history of adsorption, the earliest the adsorption phenomena was found by Faraday in 1840 that cooling effect can be occurred when ammonia is adsorbed by AgCl. After that, an application of adsorption cooling effects was proposed by Hulse [6]. The system targeted for food storage in trains and applied silica gel-SO_2 working pair. The combustion of propane was used as a heat source for the desorption and the adsorber was cooled by air. The lowest refrigeration temperature was known to reach 12 °C [17]. For adsorption technologies, the energy crisis occurred in 1970s was a good chance owing to the advantage that it consumes less electric energy and can be operated by using solar and waste heat energy [18]. The other chance was in 1990s in which the environmental issues resulted from using CFCs started to rear up.

An AHP system can be divided into two categories with a thermodynamic point of view: heat engine and heat pump. As presented in Fig. 1. 9, an AHP system has two heat sources with different temperature levels and two heat sinks. That is, the system works within three different temperature levels; desorption occurs at the high temperature level (T_H), adsorption and condensation happen at the intermediate level (T_{amb}) and evaporation takes place at the low temperature level (T_L).

The AHP system consist of adsorbers, an evaporator and a condenser. The naming of the system differ according to the number of adsorber (i.e., single-bed in case the number of adsorber is one, two-bed for two adsorbers). The adsorber normally comprises a heat exchanger in which a porous media are packed (filled) between its fins or coated on the surface its fins. Heat transfer fluid circulates the heat exchanger to deliver or extract heat from the adsorbent during the adsorption/desorption process. Since it takes similar roles with a compressor of a vapor compression system, it is sometimes called thermally driven compressor [19].

Fig. 1. 10 describes a Clapeyron diagram of ideal AHP system which shows four thermodynamic processes of AHP.
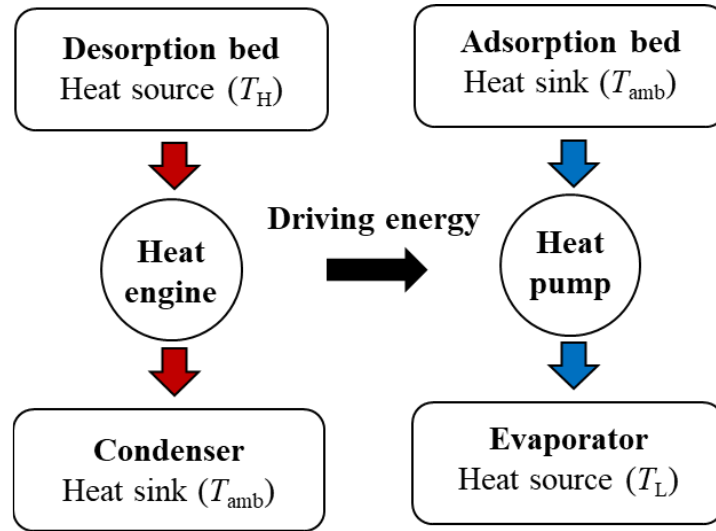
Fig. 1. 9 Schematic diagram of ideal thermodynamic adsorption heat pump [19]
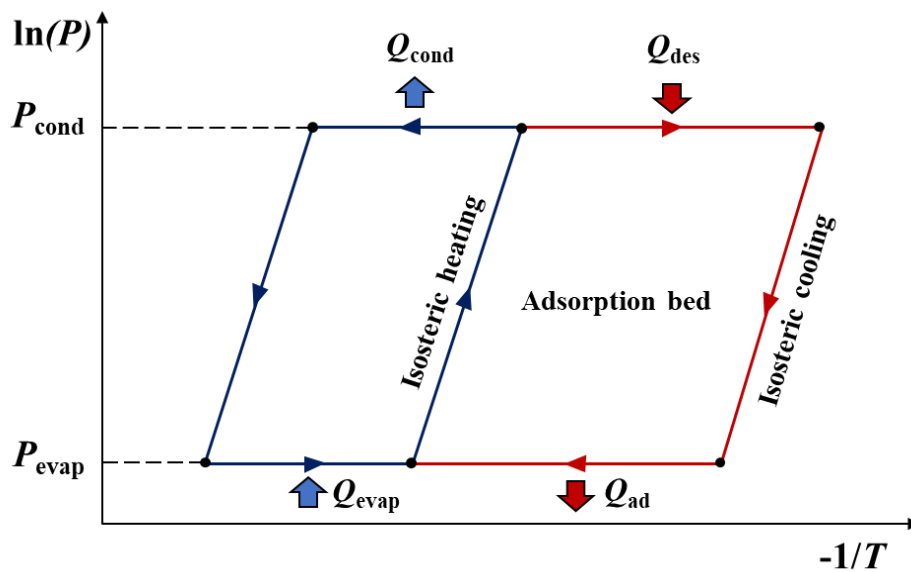
Fig. 1. 10 Clapeyron diagram of ideal adsorption heat pump [19]

In general, operation of an AHP system comprises four steps: Pre-heating, desorption, Pre-cooling and adsorption processes. Fig. 1. 11 depicts operation pattern of typical two-bed AHP system, and followings describes the four steps of the operation.

Firstly, the heat source with high temperature around 80 ℃ flows into the adsorber during the pre-heating process to heat the adsorbent up. In this period, the mass transfer

channel (valve 3) installed between the adsorber and the condenser is closed. Of course the valve 4 which is installed between the adsorber and the evaporator is kept closed. That is, the heat transfer is conducted to increase the bed temperature sensibly in the closed system, thereby increase of vapor pressure in the chamber is induced.

After then, during the desorption process, the heating by the heat transfer fluid having high temperature level lasts. In this period, in contrast, the valve 3 installed between the adsorber and the condenser is kept opened. The transfer of vapor through the mass transfer channel occurs. Thus the temperature of adsorbent keeps increasing and the vapor pressure in the adsorber start to decrease as the water vapor moves to the condenser to be condensed until its vapor pressure becomes the same as the condensation pressure.

Meanwhile, the other adsorption bed undergoes pre-cooling and adsorption process. The adsorber which finished the desorption process having the highest temperature and the pressure level around the condensation pressure starts to be cooled by the cooling fluid. In the same way, the mass transfer channel (valve 2) installed between the adsorber and the condenser and the valve 1 installed between the adsorber and the evaporator are closed in this period. Therefore, both temperature of the adsorbent and the vapor pressure in the adsorber fall down up to the cooling temperature and the equilibrium pressure at this temperature.

The practical cooling capacity in generated during the adsorption process by opening the valve installed between the adsorber and the evaporator. The adsorbent keeps adsorbed water vapor evaporated from the evaporator, and the adsorbed water vapor exists in the adsorbent after being converted to the other phase namely the adsorbed phase. These continuous mass transfer enables the liquid state refrigerant to evaporate continuously. During this process, cooling water with the intermediate temperature level flow the adsorber to remove the heat generated by the adsorption.

(a) Pre-heating process
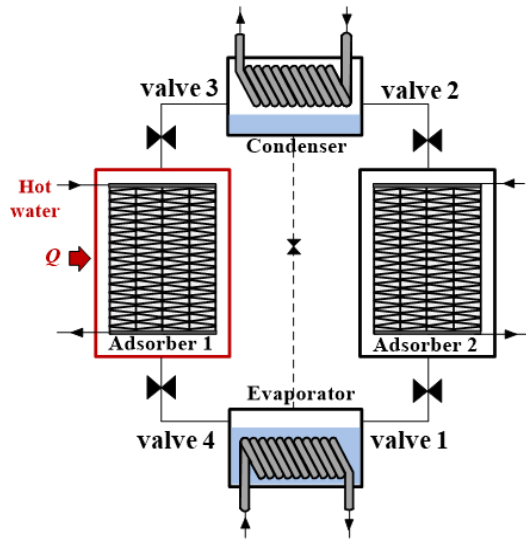
(b) Desorption process
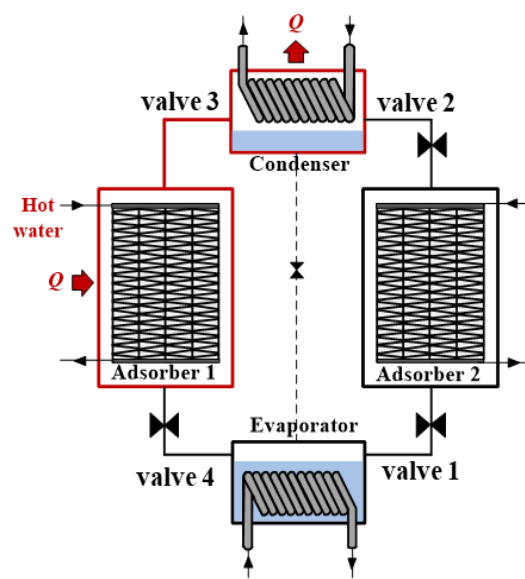
(c) Pre-cooling process
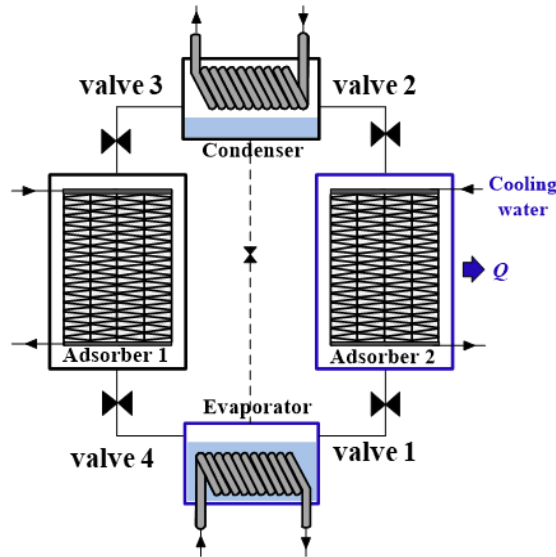
(d) Adsorption process
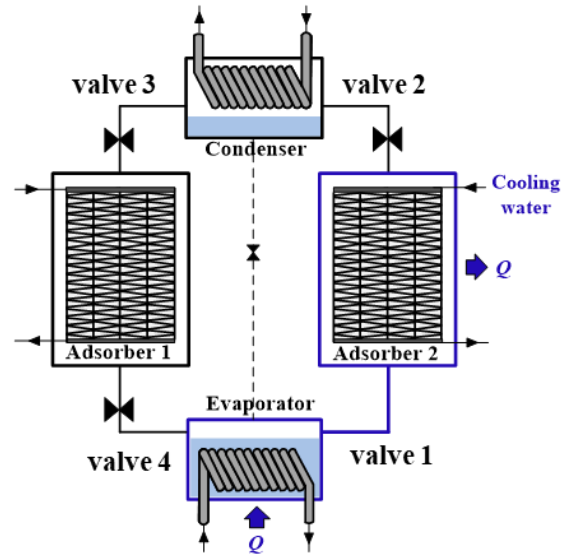
Fig. 1. 11 Operation processes of typical AHP systems

1.4 ADVANTAGES AND LIMITATIONS OF AHP

As mentioned earlier, there are two main factors making AHP more attractive compared to the traditional vapor compression systems. The first one is advantages with energy saving aspect and the other one is benefit with environmental aspect. Although researches and investments did not focus on AHP systems due to less competitiveness in the past, the circumstances have been changed a lot during recent decades. Experience of two times of energy crisis, continuous worries on environmental issues and interest on utilization of waste heat and solar energy are all positive factors making the worth of AHP enhanced.

The major advantages of AHP are listed as followings.

Advantages [20]

- Consumes less electrical power since it is mainly driven by thermal energy.
- Becomes much more attractive if the low-level waste heat can be obtainable.
- Operates with relatively less noise and vibration due to absence of a compressor.
- Normally uses eco-friendly working fluids having zero ODP and GWP.
- Longer lifetime compared to vapor compression and absorption heat pump [21].
- Suitable in conditions with serious vibration such as fishing boat compared to absorption heat pump [22].

Although AHP following disadvantages need to be improved to overcome the limitation of the application and foster commercialization of AHP [23] .

Disadvantage

- Inferior COP to that of vapor compression systems.
- Large system volume and expensive initial cost.
- Intermittently operating cooling.

To sum up, having those advantages have been proved competitiveness of AHP in various applications, at the same time, having those limitations means the further researches and developments are required for AHP to widespread.

1.5 RESEARCHES ON VARIOUS AHP CYCLES

There have been various tries to improve AHP system performance by adjusting components of the system (e.g., two-stage and multi-bed AHP [24–29]), or by using waste heat source (e.g., solar assisted AHP [30–34] and AHP for automobiles). Several representative researches on AHP system development are as shown followings.

1.5.1 Multi-bed Adsorption Cycle

Fig. 1. 12 present schematic diagram of 3-bed AHP system. The main advantage of this cycle is to reduce temperature fluctuation in the evaporator and condenser. Therefore, more continuous chilled water temperature can be achievable. The 3-bed AHP system consists of an evaporator, a condenser and three adsorption beds. The system operates with four modes of pre-cooling, adsorption, pre-heating and desorption, just same as 2-bed systems. The difference is that the 3-bed systems contains 12 steps [25,26]. Owing to this subdivided step, for example, the temperature of the adsorber supposed to start adsorption mode is already pre-cooled. The mass recovery can be additionally applied for the further performance enhancement [28].
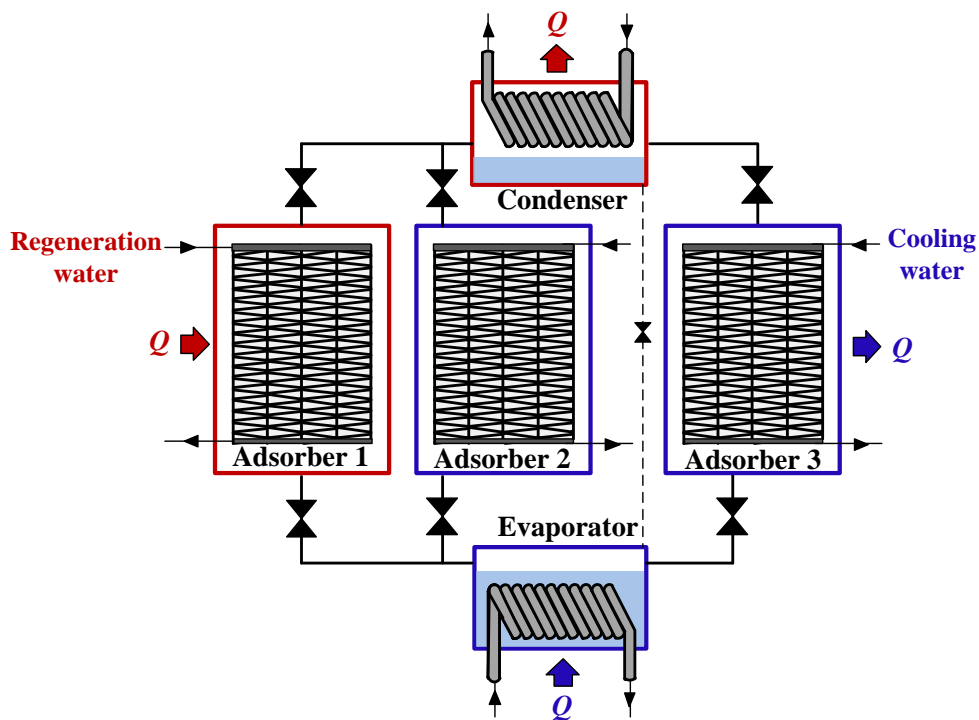
Fig. 1. 12 Schematic diagram of 3-bed AHP system [26]

The 3-bed with dual evaporators also can be found in literatures [27]. In this configuration, evaporators are divided into the low-pressure evaporator and high-pressure evaporator, respectively. Thus, the operation modes are more subdivided into five process: Pre-cooling, high-pressure adsorption, low-pressure adsorption, pre-heating and desorption. Miyazaki et al. has addressed that the dual step evaporation enables the water flowing the evaporator to have the larger temperature difference [27].

Aside from increasing the number of adsorbers with a single stage, several researches on making the arrangement of adsorbers into multi-stage can be found in literatures [29]. Fig. 1. 13 and Fig. 1. 14 show schematic diagram and the Duhring diagram of two-stage AHP system. For the case of silica gel, it is hard to expect proper cooling performance with a cooling water temperature around 30 ℃ if the regeneration temperature falls below 60 ℃ [34]. These multi-stage (2-stages or 3-stages) cycles enables the AHP system to produce cooling capacity even when the regeneration temperature is achievable only between 45 ℃ to 60 ℃ [31]. To explain, the water vapor desorbed in the low-stage adsorber by the heat source around 50 ℃ moves to the high-stage adsorber, the instead toward the condenser for the case of the single-stage cycles. Here, the reason made the low-stage be able to desorb water vapor with 50 ℃ was the lower desorption pressure than the condensation pressure. In the perspective of the high-stage adsorber, the equilibrium adsorption amount at the cooling temperature increases because the adsorption pressure increased. It eventually enables the high-stage adsorber to desorb water vapor even with heat source around 50 ℃ at the typical condensation pressure.
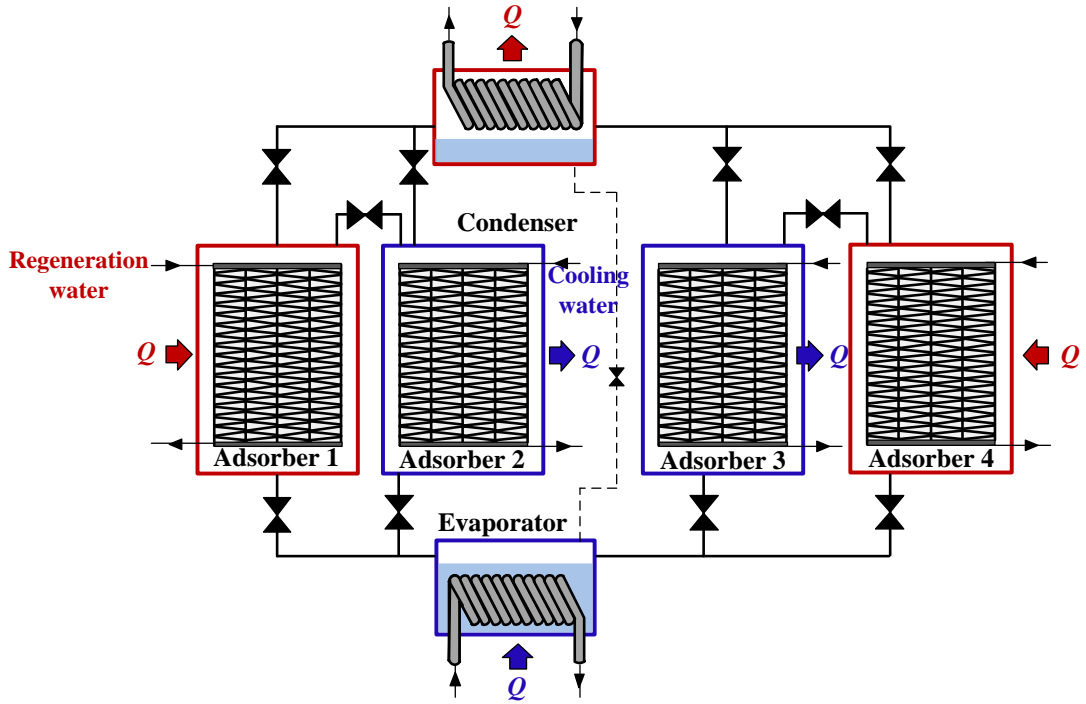
Fig. 1. 13 Schematic diagram of two-stage AHP system [29]
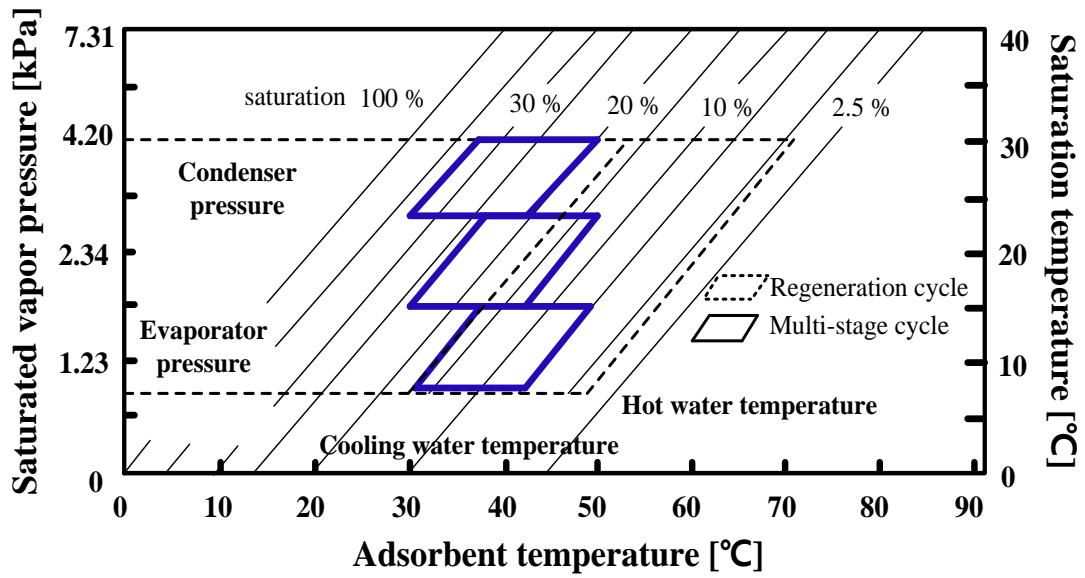
Fig. 1. 14 Duhring diagram of the multi-stage AHP system [29]

1.5.2 Solar Assisted AHP Systems

Utilization of solar energy makes the AHP far more attractive because it significantly decreases fossil energy input for the operation the system. Furthermore, the coincidence of the peak cooling load with the amount of available solar energy is also positive factor in terms of application of the AHP [35]. Followings introduces previous studies related to the solar adsorption heat pump systems.

Zhai et al. [30] installed a solar AHP system at the Shanghai Research Institute of Building Science. They could obtain average cooling power of 15.3kW using AHP, referring solar fraction of 0.71. Habib et al. [31] applied experimentally obtained heat source temperature data from 22 units of solar collectors into a mathematical model of an AHP. They introduced a two-stage and four beds cooling system which enables effective operation when the heat source temperature is below 60 °C. Koronaki et al. [32] examined the application of an AHP under climatic conditions of eastern Mediterranean area based on a mathematical modeling. They also provided overall energy and exergy efficiencies of the cooling system using hybrid photovoltaic-thermal (PV/T) collector. El-Sharkawy et al. [33] compared performances of the AHP in two cases which are with and without the hot water buffer storage by using a mathematical modeling. They addressed that the time which shows the maximum cooling capacity is revealed different for these two cases with and without the hot water tank.
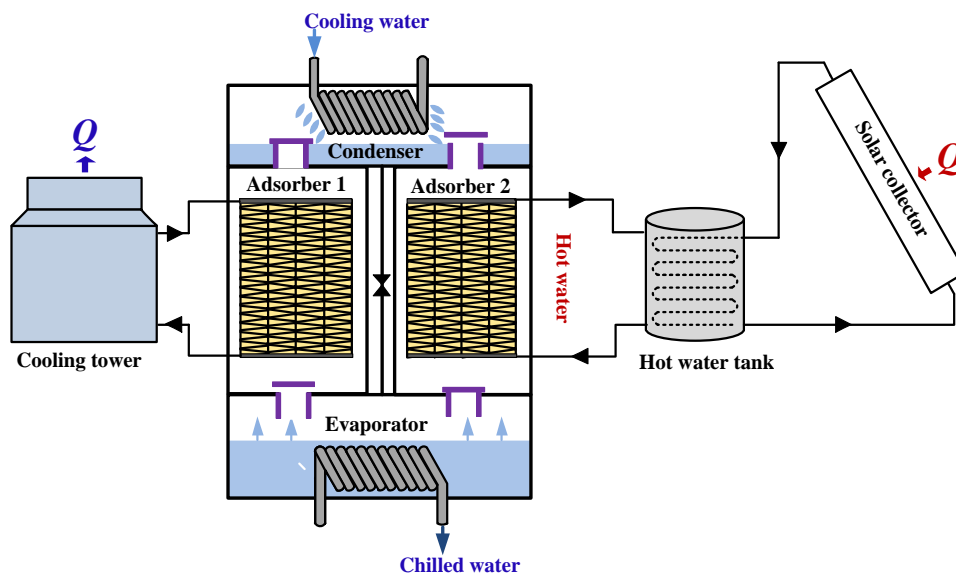
Fig. 1. 15 Schematic diagram of solar assisted AHP system [32]

1.5.3 Utilization of Automobile Engine Waste Heat

Fig. 1. 16 shows schematic diagram of AHP utilizing engine waste heat of a truck. The engine of automobiles exhausts substantial amount of thermal energy. According to Zhang [36], about 35 % of the input energy is wasted in the coolant of water-cooled engine. On the other hand, certain extra load is imposed to the engine by operating an air-conditioning system of the vehicles, which result in more fuel consumption and emission heat [37]. Thus, the overall fuel energy can be utilized more effectively by the waste heat recovery. The waste heat can immediately be utilized to control the cabin climate [38].

Generally, the temperature of the engine coolant lies between 80 °C and 95 °C [39].

The regeneration water from the engine flows toward adsorber to let the adsorbent desorb water vapor. In case of the adsorption loop, on the other hand, the circulating cooling water releases heat of adsorption to the ambient.
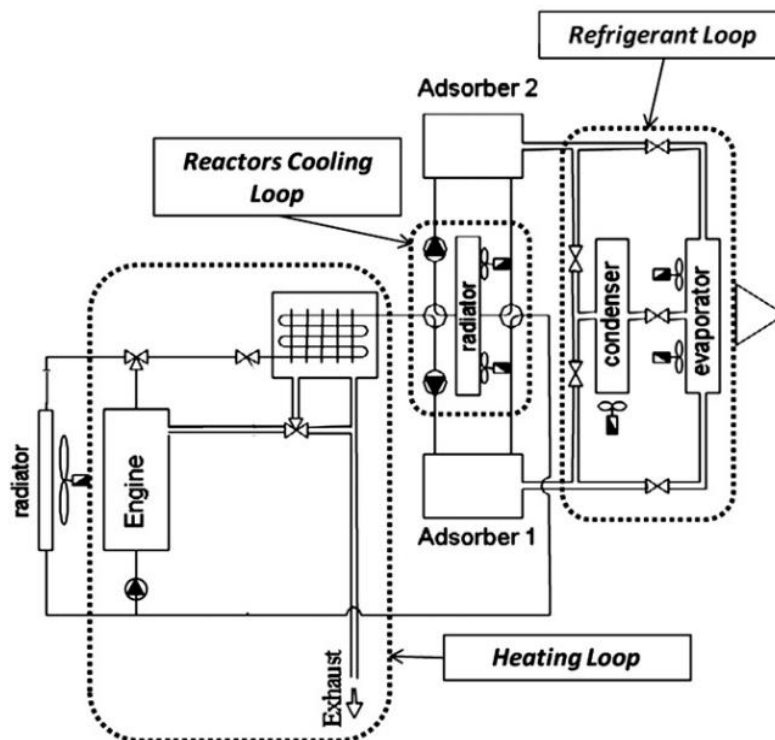
Fig. 1. 16 Schematic diagram of AHP utilizing engine waste heat of trucks [39]

1.5.4 Combined AHP System with ORC

Fig. 1. 17 shows schematic diagram of multi-bed AHP for cooling and electricity generation. There has been many researches which integrate the cooling system (e.g., adsorption, absorption chiller) and power generation cycle (e.g., ORC) [40,41]. An ORC system has the advantage that it utilizes low-grade heat source to generate electricity. However, its low efficiency compared to other utilization methods such as thermally driven cooling systems. Therefore, Al-Mousawi et al insisted that the overall efficiency may be enhanced by converting low-grade heat to the cooling and electricity simultaneously [40].

Jiang et al. [41] applied the R245fa and $CaCl_2$/$BaCl_2$-ammonia working pair to ORC and AHP system, respectively. They could achieve the electricity generation and cooling capacity of 300~560 W and 2.17~ 2.97 kW, respectively with the heat source between 78 to 98 °C. Here, the total energy and exergy efficiency ranged from 0.10~ 0.13 and 0.18~0.20, respectively.
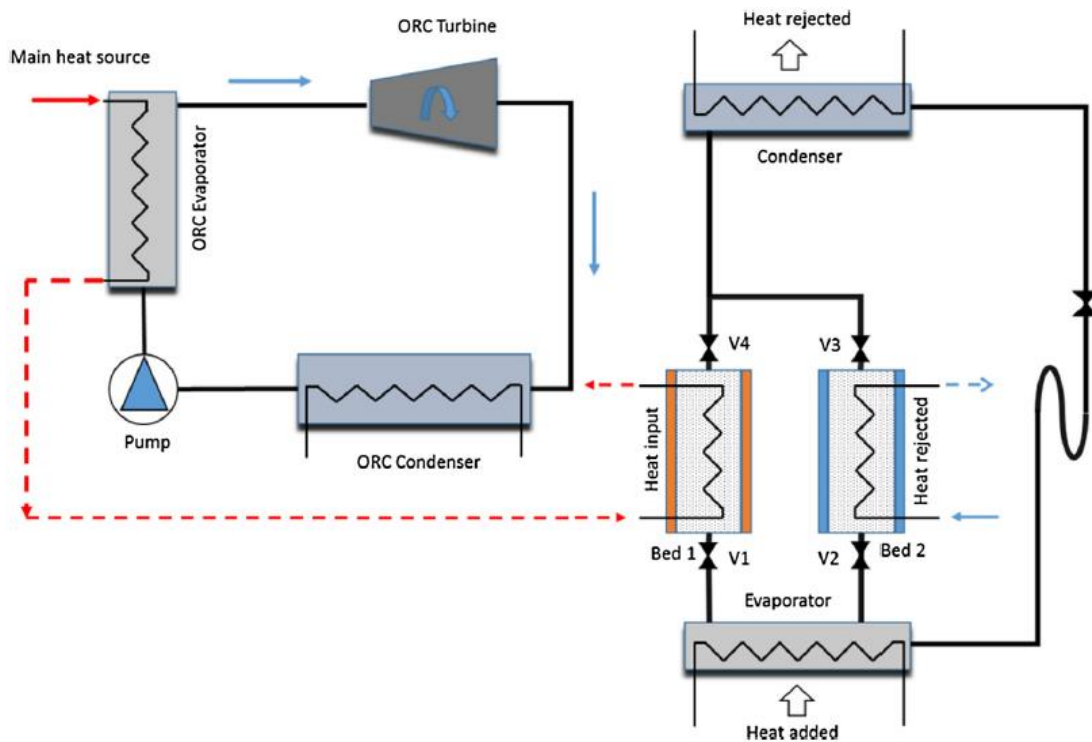
Fig. 1. 17 Schematic diagram of multi-bed AHP for cooling and electricity generation [40]

1.6 WORKING PAIRS OF AHP

The working pairs of AHP can be classified into physical and chemical working pairs. The former one occurs by the van der Waals force between adsorbate molecules of adsorbents and adsorbates. On the other hand, the latter one can be defined as a reaction between adsorbate and the surface molecules of the adsorbent [6]. Followings briefly introduces several typical working pairs.

1.6.1 Silica Gel-water Pair

Silica gel is made synthetized silicon dioxide having porous structure. The high density silica gels which are commonly used in AHP systems are Fuji Davison types 'A' and 'RD' silica gel having D_p around 2.0-3.5 nm, V_p around 0.3-0.4 cm^3/g, S_{BET} around 400-700 m^2/g [19]. The other types of silica gel having higher pore diameter can be used for making composite material. The minimum-required regeneration temperature of silica gels is about 50 °C, and the heat of adsorption is about 2500 kJ/kg [22].

1.6.2 Zeolite-water Pair

Zeolite-water working pair has advantages of a wide regeneration range (70-250 °C). It has advantages that the high temperature heat source (e.g., exhaust gases from engine) can directly be used. 4A, 5A, 10X and 13X zeolite molecular sieves are most frequently used materials in AHP systems. Meanwhile, the zeolite-water working pair has higher heat of adsorption (3300-4200 kJ/kg) compared to that of silica gel-water pair, which results in low COP [19]. Researches on developing a zeolite applicable at low temperature and having relatively lower heat of adsorption have been conducted. Novel synthetic functionalized material called 'AQSOA' which belongs to the class SAPO zeolites has been commercialized by Mitubishi Plastic Incorporation [42]. Since AQSOAs present outstanding regeneration at low temperature (< 80 °C) and they show S-shape curves, it is expected that these materials foster the AHPs to widespread more if the issues on high capital cost is relieved.

1.6.3 Activated Carbon-ammonia/methanol Pair

The raw material becomes activated carbon after undergoing certain treatment at 700-800 °C [19]. Activated carbon has advantages of large surface area between 800 and 1500 m^2/g. Also, its heat of adsorption is relatively lower (1800-2000 kJ/kg) than that of silica gel-water and zeolite-water working pairs. However, thermal conductivity of activated carbon is known to be low. The measured thermal conductivity of the activated carbon fiber was approximately 0.089 W/mK [43]. The 'MAXSORB III' recently invented by Kansai Coke and Chemicals in Japan has been attracting lot of attention from the field. This is a form of high surface area activated carbon presenting much higher uptake compared to traditional activate carbons [44–46]. Besides, MAXSORB III/ ethanol working pair presents outstanding uptake and specific cooling energy [47].

1.6.4 Composite Adsorbents-water Pair

The composite materials are usually combination of porous material and chemical adsorbent. Metal chlorides, such as $CaCl_2$, $BaCl_2$ and $LiCl$, are representative chemical adsorbents. Even though the advantage having large sorption uptake of chemical adsorbents, low stability resulted from swelling and agglomeration phenomena are considered as a factor limiting application of the chemical adsorbent in AHP purposes [48,49]. Thus the synthetized composite adsorbents enhance adsorption capacity of physical porous media, at the same time, improve shortcomings of chemical adsorbent such as swelling, agglomeration and low thermal conductivity [6,19,22,50]. The silica gel and chlorides, suggested by Aristov et al. [51–54], are the most representative composite adsorbents for AHP applications.

Following Table 1.1 summarizes the studies using composite working pairs in the field of AHPs.

Table 1. 1 Summary of studies using composite working pairs [55]

Authors	Working pairs	Heat source	Contents
Aristov et al. [51–53]	SWS-1L/ SWS-1S -water	120-150 ℃	Equilibrium adsorption characteristics of SWS-1L/SWS-1S and water vapor were studied. The effects of grain size on the dynamic characteristics at various temperature (33-69 ℃) were provided.
Aristov et al. [54]	SWS-9L -water	70-90 ℃	Effects of ad/desorption time composition at certain fixed total cycle time were studied. The total cycle time was varied 385~600 second, and precooling and preheating time were fixed.
Freni et al. [56,57]	SWS-1L/ SWS-2L -water	95-130 ℃	The effects of thermal conductivity on the cooling performance were given, which emphasizes enhancement of heat transfer of the adsorption bed. The experiment on the coated adsorbent presented much higher specific cooling power than that of the pallet types.
Freni et al. [58]	SWS-8L -water	75-90 ℃	The new composite of silica gel modified by calcium nitrate ($Ca(NO_3)_2$) was tested in the relatively low regeneration temperature. The isoteric diagram is calculated from experimentally obtained equilibrium adsorption data.
Sapienza et al. [59]	SWS-9V -water	68 ℃, 90 ℃	Adsorption equilibrium of the new composite using natural rock vermiculite was demonstrated. Search on the ratio between adsorption and desorption time was conducted, and the result presented increased cooling performance by adjusting the time ratio.
Saha et al. [60]	SWS-1L -water	60-90 ℃	The application effect of SWS-1L was compared to the traditional silica gel by using a lumped mathematical model. The result showed relatively increased cooling capacity at the high regeneration temperature.
Gordeeva et al. [61]	Mesoporous silica gel (KSK)+LiCl-methanol	70-90 ℃	Lithium chloride is confined in silica gel to adsorb methanol vapor at the saturation pressure around approx. 7 ℃. The effects of salt contents, number of layers and grain size were studied, and dynamic characteristics were fitted by exponential curve.

Table 1.1 Continued

Authors	Working pairs	Heat source	Contents
Lu et al. [62]	Mesoporous silica gel+LiCl-methanol	85 ℃	LiCl/silica gel- methanol working pair is test under the conditions for air-conditionings and cold storages. The system could produce chilled water around 7 ℃, and system performance could be enhanced by applying mass recovery process for 230 seconds.
Chen et al. [63]	Attapulgite +LiCl-water	170 ℃	Composite materials using attapulgite and LiCl (30%) were prepared by the mixing method. The higher adsorption equilibrium than traditional adsorbents was confirmed by TG/DTA analysis. The sorption heat of the composite material was intermediate level between zeolite 13X and silica gel.
Wang et al. [64]	Expanded graphite +$CaCl_2$-Ammonia	150 ℃	Adsorption and thermal performance of three types of materials ($CaCl_2$ powder, simple composite, consolidated composite adsorbent) were compared. The consolidated material presented 3200% higher thermal conductivity than $CaCl_2$ powder. Furthermore, its high volumetric cooling capacity and the better anti-sway performance made it promising to be applied in ice makers on fishing boats.
Tokarev et al. [65]	MCM-41 +$CaCl_2$-water	90 ℃ <	37.7 wt.% of $CaCl_2$ is confined in the granules of MCM-41 (S_{BET}= 1050 m^2/g, D_p=3.8 nm, V_p=1.1 cm^3/g). Equilibrium sorption amount of 0.75g/g and most of adsorbed water could be desorbed at the temperature between 70 ℃ and 120 ℃.

1.7 COMMERCIALIZED AHP UNITS

Bry-Air company specializes dehumidifiers, dryers, both small scale and large scale adsorption chillers having cooling capacity between 11 to 35 kW, and 35 to 1180 kW. With the optimal conditions, the chilled water of 7 ℃ can be obtained from 12 ℃ water with COP around 0.55.

The German company GBU produces an adsorption chiller called NAK, COP of 0.6 is obtainable at hot water temperature of 90 ℃, cooling water temperature of 30 ℃. The cooling capacity is between 50 to 430 kW.

MYCOM [66] NOA uses zeolite (AQSOA)-water working pair and presents chilling capacity from 50 to 430 kW. The applicable range of the regeneration water temperature ranges from 60 to90 ℃. The cooling performance using zeolite (AQSOA) shows almost constant performance above the heat source temperature of 70 ℃, otherwise that of silica gel tends to be proportional to the temperature.

The German company InvenSor [67] developed the adsorption chiller with directly coated zeolite (AQSOA)-water. Units having cooling capacity of 10 kW is available in the market.

According to the literature, the capital costs of the units having cooling capacities of 10, 20, 50, and 100 kW could be 10,000, 15,000, 30,000, and 50,000 US dollars, respectively [68].

Fig. 1. 18 Commercialized AHP system (left: MYCOM [66], right: InvenSor [67])

1.8 OBJECTIVE AND SCOPE OF THE THESIS

The main objective of this research is to develop an adsorption heat pump (AHP) system using composite natural mesoporous material, called Wakkanai Siliceous Shale (WSS). Furthermore, this research aims to estimate applicability of the developed AHP system with energetic and economic perspectives.

As mentioned earlier, AHP systems have various advantages in environmental and energetic view. However, they still need improvement in terms of cooling performance, cost and system volume. Therefore, this work focuses on characteristics of AHP, such as heat and mass transfer, for the better design and performance prediction.

Followings summarize objectives and scopes of this thesis:

1) The first objective is to provide comparison of adsorption characteristics of Wakkanai Siliceous Shale (WSS) as a host matrix of the composite adsorbent with traditional adsorbents, including silica gel-based composite adsorbents.

2) The second object is to estimate heat and mass transfer characteristics experimentally to predict dynamic performance of AHP.

3) The third object is to conduct performance analysis of annual operation of the solar assisted AHP in various climate conditions. This performance prediction will include simple economic analysis to verify competitiveness of AHP.

4) The fourth object is to provide energy and exergy analysis based on 1 kW-scale unit applying WSS composite to show actual cooling performance of AHP.

1.9 OUTLINE OF THE THESIS

This thesis consists of seven chapters, and followings are brief description on each chapter.

Chapter 1 presents general introduction about AHP systems. To provide general background concerning AHP systems following contents are introduced: working principles, advantages and disadvantages, various AHP systems, types of working pairs and commercialized AHP units.

In **Chapter 2**, theories regarding physical and equilibrium properties of adsorbents are provided. Also, application of WSS as a host matrix of composite material with lithium chloride is investigated. Lastly, effects of impregnation of lithium chloride on the physical and equilibrium adsorption characteristics of the porous media are studied to emphasize advantage of WSS as a host matrix.

In **Chapter 3**, the novel methodology to separate the effects of the interfacial and internal mass transfers of water vapor at a coated adsorbent will be given, based on both experimental methods and the LDF model. For the adsorbent, the composite WSS is used to enhance the adsorption performance. The mass transfer performance of a composite WSS is also compared with that of A-type silica gel to prove its competitiveness.

Chapter 4 focuses on experimentally estimated heat and mass transfer characteristics. The overall mass transfer coefficients were measured at various adsorbent temperatures in the range of 30–60 °C. Additionally, the overall heat transfer coefficients of the adsorbers were experimentally estimated when the inlet water temperature was changed from 80 to 30 °C to analyze the actual working conditions of AHP systems. The estimated coefficients were utilized for numerical modeling to analyze the AHP performance characteristics.

Chapter 5 provides analysis of annual cooling performance of AHP based on the mathematical model under the different weather conditions. Four metropolises having distinct climatic characteristics are selected: Tokyo (35 $^{\circ}$ N, 139 $^{\circ}$ E), Florida (28 $^{\circ}$ N, 81

$^{\mathrm{o}}$ W), Hawaii (19 $^{\mathrm{o}}$ N, 155 $^{\mathrm{o}}$ W), Dubai (25 $^{\mathrm{o}}$ N, 55 $^{\mathrm{o}}$ E). Lastly, the economic analysis of solar AHP system is provided to show economic competitiveness of the system.

In **Chapter 6**, experimental investigation on energy and exergy of AHP systems using 1kW-scale experimental system applying WSS impregnated with 20 wt.% of LiCl was provided. The heat exchangers filled with the WSS composite are kept in the transparent acrylic chamber of the AHP system to observe the operation status. Based on the experimental data, thermodynamic characteristics regarding energy and exergy are analyzed.

Finally, **Chapter 7** summarizes general conclusions of this thesis and suggest future research topics.

1.10 REFERENCE

[1]   M. ASIF, T. MUNEER, Energy supply, its demand and security issues for developed and emerging economies, Renew. Sustain. Energy Rev. 11 (2007) 1388–1413.

[2]   M. Li, World Oil 2018-2050: World Energy Annual Report, 2018.

[3]   L.D. Roper, Fossil-Fuels Depletion, 2019.

[4]   Annual Energy Outlook 2020, 2020.

[5]   UNEP, Refrigeration, Air Conditioning and Heat Pumps, 2018 Assessment Report, 2018.

[6]   R. Wang, L. Wang, J. Wu, Adsorption Refrigeration Technology, Wiley, 2014.

[7]   Y. Heredia-Aricapa, J.M. Belman-Flores, A. Mota-Babiloni, J. Serrano-Arellano, J.J. García-Pabón, Overview of low GWP mixtures for the replacement of HFC refrigerants: R134a, R404A and R410A, Int. J. Refrig. 111 (2020) 113–123.

[8]   Global Warming Policy Forum, Greta Eff. Glob. CO2 Emiss. Increased By 1.9% 2018. (2019).

[9]   J. Liu, Q. Yang, Y. Zhang, W. Sun, Y. Xu, Analysis of CO2 Emissions in China's Manufacturing Industry Based on Extended Logarithmic Mean Division Index Decomposition, Sustainability. 11 (2019) 226.

[10]   E.& I.S. Department for Business, 2019 Government Greenhouse Gas Conversion Factors For Company Reporting, 2019.

[11]   K. Treyer, C. Bauer, The environmental footprint of UAE's electricity sector: Combining life cycle assessment and scenario modeling, Renew. Sustain. Energy Rev. 55 (2016) 1234–1247.

[12]   気候変動枠組条約第 21 回締約国会議, Japan Center for Climate Change Actions, (2015). https://www.jccca.org/trend_world/conference_report/cop21/.

[13]   R. Narayanan, Heat-driven cooling technologies, 2017.

[14]   S. Akhtar, T.S. Khan, S. Ilyas, M.S. Alshehhi, Feasibility and Basic Design of Solar Integrated Absorption Refrigeration for an Industry, Energy Procedia. 75 (2015) 508–513.

[15]   J. Cerezo Román, R. Javier Romero Domínguez, A. Rodríguez Martínez, P. Soto Parra, Thermal Analysis of an Absorption and Adsorption Cooling Chillers Using a Modulating Tempering Valve, in: Zero Net Zero Energy, IntechOpen, 2019: p. 13.

[16]   CIBSE Journal, High-Efficiency Waste Heat-Powered Lithium Bromide Absorpt. Chill. (2016).

[17]   G.. Hulse, Freight car refrigeration by an adsorption system employing silica gel, Refrig. Eng. 17 (1929) 41–54.

[18] H. Tyagi, P.R. Chakraborty, S. Powar, A.K. Agarwal, Introduction to Solar Energy: Systems, Challenges, and Opportunities, in: 2020: pp. 3–12.

[19] M.B. Elsheniti, O.A. Elsamni, R.K. Al-dadah, S. Mahmoud, E. Elsayed, K. Saleh, Adsorption Refrigeration Technologies, in: Sustain. Air Cond. Syst., InTech, 2018.

[20] F. Meunier, Adsorptive cooling: A clean technology, Clean Prod. Process. 3 (2001) 8–20.

[21] A. Li, Experimental and Theoretical Studies on the Heat Transfer Enhancement of Adsorbent Coated Heat Exchangers, National University of Singapore, 2014.

[22] T. Oh, Silica gel / Water Based Adsorption Cooling System Employing Compact Fin-Tube Heat Exchanger, Kyushu University, 2013.

[23] H. Demir, M. Mobedi, S. Ülkü, A review on adsorption heat pump: Problems and solutions, Renew. Sustain. Energy Rev. 12 (2008) 2381–2403.

[24] M. Chorowski, P. Pyrka, Z. Rogala, P. Czupryński, Experimental Study of Performance Improvement of 3-Bed and 2-Evaporator Adsorption Chiller by Control Optimization, Energies. 12 (2019) 3943.

[25] G. Gullì, A. Sapienza, A. Caprì, F. Costa, D. La Rosa, V. Palomba, A. Freni, Innovative Adsorption Chiller for Marine Applications: Design and Building, Energy Procedia. 82 (2015) 432–438.

[26] B.B. Saha, S. Koyama, J.B. Lee, K. Kuwahara, K.C.A. Alam, Y. Hamamoto, A. Akisawa, T. Kashiwagi, Performance evaluation of a low-temperature waste heat driven multi-bed adsorption chiller, Int. J. Multiph. Flow. 29 (2003) 1249–1263.

[27] T. Miyazaki, A. Akisawa, B.B. Saha, The performance analysis of a novel dual evaporator type three-bed adsorption chiller, Int. J. Refrig. 33 (2010) 276–285.

[28] M.Z.I. Khan, B.B. Saha, K.C.A. Alam, A. Akisawa, T. Kashiwagi, Study on solar/waste heat driven multi-bed adsorption chiller with mass recovery, Renew. Energy. 32 (2007) 365–381.

[29] B.B. Saha, S. Koyama, T. Kashiwagi, A. Akisawa, K.C. Ng, H.T. Chua, Waste heat driven dual-mode, multi-stage, multi-bed regenerative adsorption system, Int. J. Refrig. 26 (2003) 749–757.

[30] X.Q. Zhai, R.Z. Wang, J.Y. Wu, Y.J. Dai, Q. Ma, Design and performance of a solar-powered air-conditioning system in a green building, Appl. Energy. 85 (2008) 297–311.

[31] K. Habib, B. Choudhury, P.K. Chatterjee, B.B. Saha, Study on a solar heat driven dual-mode adsorption chiller, Energy. 63 (2013) 133–141.

[32] I.P. Koronaki, E.G. Papoutsis, V.D. Papaefthimiou, Thermodynamic modeling and exergy analysis of a solar adsorption cooling system with cooling tower in Mediterranean conditions, Appl. Therm. Eng. 99 (2016) 1027–1038.

[33] I.I. El-Sharkawy, H. AbdelMeguid, B.B. Saha, Potential application of solar powered adsorption cooling systems in the Middle East, Appl. Energy. 126 (2014) 235–245.

[34] B.B. Saha, S. Koyama, K. Choon Ng, Y. Hamamoto, A. Akisawa, T. Kashiwagi, Study on a dual-mode, multi-stage, multi-bed regenerative adsorption chiller, Renew. Energy. 31 (2006) 2076–2090.

[35] A. Alahmer, X. Wang, R. Al-Rbaihat, K.C. Amanul Alam, B.B. Saha, Performance evaluation of a solar adsorption chiller under different climatic conditions, Appl. Energy. 175 (2016) 293–304.

[36] L.Z. Zhang, Design and testing of an automobile waste heat adsorption cooling system, Appl. Therm. Eng. 20 (2000) 103–114.

[37] M. Hamdy, A. Askalany, K. Harbi, N. Koura, An overview on adsorption cooling systems powered by waste heat from internal combustion engine, Renew. Sustain. Energy Rev. 51 (2016) 1223–1234.

[38] S. Maeda, K. Thu, T. Maruyama, T. Miyazaki, Critical Review on the Developments and Future Aspects of Adsorption Heat Pumps for Automobile Air Conditioning, Appl. Sci. 8 (2018) 2061.

[39] M. Verde, L. Cortés, J.M. Corberán, A. Sapienza, S. Vasta, G. Restuccia, Modelling of an adsorption system driven by engine waste heat for truck cabin A/C. Performance estimation for a standard driving cycle, Appl. Therm. Eng. 30 (2010) 1511–1522.

[40] F.N. Al-Mousawi, R. Al-Dadah, S. Mahmoud, Integrated adsorption-ORC system: Comparative study of four scenarios to generate cooling and power simultaneously, Appl. Therm. Eng. 114 (2017) 1038–1052.

[41] L. Jiang, L. Wang, R. Wang, P. Gao, F. Song, Investigation on cascading cogeneration system of ORC (Organic Rankine Cycle) and CaCl2/BaCl2 two-stage adsorption freezer, Energy. 71 (2014) 377–387.

[42] A. Freni, B. Dawoud, L. Bonaccorsi, S. Chmielewski, A. Frazzica, L. Calabrese, G. Restuccia, Characterization of Zeolite-Based Coatings for Adsorption Heat Pumps, 2015.

[43] Y. Hamamoto, K.C.A. Alam, B.B. Saha, S. Koyama, A. Akisawa, T. Kashiwagi, Study on adsorption refrigeration cycle utilizing activated carbon fibers. Part 1. Adsorption characteristics, Int. J. Refrig. 29 (2006) 305–314.

[44] M.M. Younes, I.I. El-Sharkawy, A.E. Kabeel, B.B. Saha, A review on adsorbent-adsorbate pairs for cooling applications, Appl. Therm. Eng. 114 (2017) 394–414.

[45] J.Y. San, W.M. Lin, Comparison among three adsorption pairs for using as the working substances in a multi-bed adsorption heat pump, Appl. Therm. Eng. 28 (2008) 988–997.

[46] I.I. El-Sharkawy, M. Hassan, B.B. Saha, S. Koyama, M.M. Nasr, Study on adsorption of methanol onto carbon based adsorbents, Int. J. Refrig. 32 (2009)

1579–1586.

[47]   I.I. El-Sharkawy, B.B. Saha, S. Koyama, J. He, K.C. Ng, C. Yap, Experimental investigation on activated carbon-ethanol pair for solar powered adsorption cooling applications, Int. J. Refrig. 31 (2008) 1407–1413.

[48]   L.W. Wang, R.Z. Wang, J.Y. Wu, K. Wang, Compound adsorbent for adsorption ice maker on fishing boats, Int. J. Refrig. 27 (2004) 401–408.

[49]   X.B. Bu, Z.N. Lu, L.B. Wang, Preparation of composite adsorbent with high performance of heat and mass transfer, Chinese Sci. Bull. 58 (2013) 3709–3714.

[50]   S.M.N. Mehr, Development of Adsorber Beds for Air Conditioning in Vehicle Applications, Simon Fraser University, 2016.

[51]   Y.I. Aristov, M.M. Tokarev, G. Cacciola, G. Restuccia, Selective water sorbents for multiple applications, 1. CaCl2 confined in mesopores of silica gel: Sorption properties, React. Kinet. Catal. Lett. 59 (1996) 325–333.

[52]   Y.I. Aristov, M.M. Tokarev, G. Restuccia, G. Cacciola, Selective water sorbents for multiple applications, 2. CaCl2 confined in micropores of silica gel: Sorption properties, React. Kinet. Catal. Lett. 59 (1996) 335–342.

[53]   Y.I. Aristov, I.S. Glaznev, A. Freni, G. Restuccia, Kinetics of water sorption on SWS-1L (calcium chloride confined to mesoporous silica gel): Influence of grain size and temperature, Chem. Eng. Sci. 61 (2006) 1453–1458.

[54]   Y.I. Aristov, A. Sapienza, D.S. Ovoshchnikov, A. Freni, G. Restuccia, Reallocation of adsorption and desorption times for optimisation of cooling cycles, Int. J. Refrig. 35 (2012) 525–531.

[55]   H. Liu, Study on Open and Closed Chemical Thermal Energy Storage Technology with Low-regeneration Temperature, Hokkaido University, n.d.

[56]   A. Freni, M.M. Tokarev, G. Restuccia, A.G. Okunev, Y.. Aristov, Thermal conductivity of selective water sorbents under the working conditions of a sorption chiller, Appl. Therm. Eng. 22 (2002) 1631–1642.

[57]   A. Freni, F. Russo, S. Vasta, M. Tokarev, Y.I. Aristov, G. Restuccia, An advanced solid sorption chiller using SWS-1L, Appl. Therm. Eng. 27 (2007) 2200–2204.

[58]   A. Freni, A. Sapienza, I.S. Glaznev, Y.I. Aristov, G. Restuccia, Experimental testing of a lab-scale adsorption chiller using a novel selective water sorbent "silica modified by calcium nitrate," Int. J. Refrig. 35 (2012) 518–524.

[59]   A. Sapienza, I.S. Glaznev, S. Santamaria, A. Freni, Y.I. Aristov, Adsorption chilling driven by low temperature heat: New adsorbent and cycle optimization, Appl. Therm. Eng. 32 (2012) 141–146.

[60]   B.B. Saha, A. Chakraborty, S. Koyama, Y.I. Aristov, A new generation cooling device employing CaCl2-in-silica gel-water system, Int. J. Heat Mass Transf. 52 (2009) 516–524.

[61] L.G. Gordeeva, Y.I. Aristov, Composite sorbent of methanol " LiCl in mesoporous silica gel" for adsorption cooling: Dynamic optimization, Energy. 36 (2011) 1273–1279.

[62] Z.S. Lu, R.Z. Wang, Study of the new composite adsorbent of salt LiCl/silica gel-methanol used in an innovative adsorption cooling machine driven by low temperature heat source, Renew. Energy. 63 (2014) 445–451.

[63] H. Chen, Q. Cui, Y. Tang, X. Chen, H. Yao, Attapulgite based LiCl composite adsorbents for cooling and air conditioning applications, Appl. Therm. Eng. 28 (2008) 2187–2193.

[64] K. Wang, J.Y. Wu, R.Z. Wang, L.W. Wang, Composite adsorbent of $CaCl_2$ and expanded graphite for adsorption ice maker on fishing boats, Int. J. Refrig. 29 (2006) 199–210.

[65] M. Tokarev, L. Gordeeva, V. Romannikov, I. Glaznev, Y. Aristov, New composite sorbent $CaCl_2$ in mesopores for sorption cooling/heating, Int. J. Therm. Sci. 41 (2002) 470–474.

[66] MYCOM, (n.d.). www.mayekawa.com/.

[67] INVENSOR, INVENSOR, (n.d.). www.invensor.com/.

[68] M. Ebrahimi, A. Keshavarz, 2 - CCHP Technology, in: M. Ebrahimi, A.B.T.-C.C. Keshavarz   Heating and Power (Eds.), Elsevier, Boston, 2015: pp. 35–91.

CHAPTER 2. PHYSICAL AND EQUILIBRIUM CHARACTERISTICS OF WAKKANAI SILICEOUS SHALE

2.1 INTRODUCTION

Since adsorbents induces circulation of working fluids in the AHP system, same as a compressor of a vapor compression system [1], comprehensive understanding about the adsorbent is required. Porous media which have highly porous structure and large surface area are used as adsorbents of AHP systems. According to International Union of Pure and Applied Chemistry (IUPAC), the pore are classified into three categories according to the pore diameter (D_p): micro-pores ($D_p < 2$nm), meso-pores (2nm $< D_p < 50$nm), macro-pores ($D_p > 50$ nm). The physical characteristics of adsorbents such as pore size distributions, pore volume and surface area are normally investigated from the N_2 gas adsorption isotherm at -196 ℃ [2]. Firstly, the surface area is estimated based on the multimolecular adsorption theory suggested by Brunauer, Emmett and Teller (1938) [3]. The theory extended the monolayer adsorption theory suggested by Langmuir (1916). The pore distribution and the pore volume are normally determined based on the capillary evaporation which occurs as decreasing pressure from the unity [4].

The adsorbents can be classified into physical and chemical working pairs. The former one occurs by the van der Waals force between adsorbate molecules of adsorbents and adsorbates. On the other hand, the latter one can be defined as a reaction between adsorbate and the surface molecules of the adsorbent [5]. Meanwhile, it is well known that a good adsorbent should have large adsorption capacity and strong affinity with adsorbate [6]. In recent decades, researches on 'Composites Salt in Porous Matrix (CSPMS)', which enhance equilibrium adsorption amount compared to the traditional working pair, were conducted actively throughout the world [7–10].

This chapter includes following topics. 1) theories regarding physical properties such as B.E.T and B.J.H theories are briefly introduced. 2) Several representative isotherm equations describing equilibrium adsorption characteristics are provided. 3) Experimentally measured physical and equilibrium adsorption characteristics of WSS will be given, together with those of silica gels for comparison. 4) Application of WSS as a host matrix of composite material with lithium chloride is investigated. 5) Lastly, effects of impregnation of lithium chloride on the physical and equilibrium adsorption characteristics of the porous media are studied to emphasize advantage of WSS as a host matrix.

2.2 THEORIES ON PHYSICAL PROPERTIES OF ADSORBENTS

2.2.1 B.E.T Surface Area [3]

The BET theory provides isotherm for multimolecular layers by simplifying several assumptions, which is similar to monolayer Langmuir theory. First, S_0, S_1, S_2, …, S_i present the surface area covered by only 0, 1, 2, …, i layers of adsorbate molecules. It is assumed that the adsorption rate of i layer is proportional to pressure (P) and surface area (S) covered by *i-1* layers. On the other hand, the desorption rate is proportional to surface area covered by i layer. Thus it can be expressed as following Eq. (2-1).

$$a_1 P S_0 = b_1 S_1 e^{-E_1/RT} \tag{2-1}$$

By extending the Eq. (2-1) to consecutive layers, Eq. (2-2) is derived.

$$a_2 P S_1 = b_2 S_2 e^{-E_2/RT} \tag{2-2a}$$

$$a_3 P S_2 = b_3 S_3 e^{-E_3/RT} \tag{2-2b}$$

$$a_i P S_{i-1} = b_i S_i e^{-E_i/RT} \tag{2-2c}$$

Here, several the Eq. (2-2) can be simplified by applying several assumptions as followings: $E_2 = E_3 = \dots E_i = E_L$ and $(b_2/a_2) = (b_3/a_3) = \dots (b_i/a_i) = g$. Thus the equations above can be simplified as followings Eq. (2-3).

$$S_1 = yS_0, \text{ where } y = \left(\frac{a_1}{b_1}\right) P e^{-E_L/RT} \tag{2-3a}$$

$$S_2 = xS_1, \text{ where } x = \left(\frac{P}{g}\right) P e^{-E_L/RT} \tag{2-3b}$$

$$S_3 = xS_2 = x^2 S_1 = x^2 yS_0 \tag{2-3c}$$

$$S_i = x^{i-1} yS_0 = cx^i S_0, \text{ Where } c = (y/x) \tag{2-3d}$$

The total surface area can be calculated by the summation of surface area covered by each number of layer as shown in Eq. (2-4).

$$A = \sum_{i=0}^{\infty} S_i \tag{2-4}$$

The total volume (V) adsorbed is obtained by Eq. (2-5).

$$V = V_0 \sum_{i=0}^{\infty} iS_i \tag{2-5}$$

Here, V_0 refers to the volume of adsorbed gas per one square centimeter in which the surface of the adsorbent is completely covered by monolayer molecules. By arranging Eq. (2-1) ~ (2-5), then following Eq. (2-6) is obtained.

$$\frac{V}{AV_0} = \frac{V}{V_m} = \frac{\sum_{i=0}^{\infty} iS_i}{\sum_{i=0}^{\infty} S_i} = \frac{cS_0 \sum_{i=1}^{\infty} ix^i}{S_0\{1 + c \sum_{i=1}^{\infty} x^i\}} = \frac{cx}{(1-x)(1-x+cx)} \tag{2-6}$$

Finally, the isotherm equation based on B.E.T theory can be represented with Eq. (2-7).

$$V = \frac{V_m c \left(\frac{P}{P_0}\right)}{\left(1 - \frac{P}{P_0}\right)\left(1 + (c-1)\frac{P}{P_0}\right)} \tag{2-7}$$

The Eq. (2-7) can be again simplified into the convenient form by converting it to the linear straight line, as shown in Eq. (2-8).

$$\frac{P}{V(P_0 - P)} = \frac{1}{V_m c} + \frac{c-1}{V_m c} \frac{P}{P_0} \tag{2-8}$$

In the Eq. (2-8), the two constants of V_m and c can be evaluated based on the intercept ($1/V_m c$) and the slope ((c-1)/ $V_m c$) of the equation.

2.2.2 B.J.H Pore Distribution and Volume [4]

B.J.H methods requires an assumption that all pores are filled with liquid adsorbate at the initial relative pressure (P/P_o) around 0.95. At this state, the largest pores having radius of r_{p1} contains the physically adsorbed nitrogen layer with thickness of t_1. The evaporation occurs at inner capillary (r) of the pore as the pressure decreases. The relationship between the pore volume V_{p1} and the inner capillary V_{K1} is given by Eq. (2-9)

$$V_{p1} = \frac{V_{K1} r_{p1}{}^2}{r_{K1}{}^2} \qquad (2\text{-}9)$$

In the Eq. (2-9), V_1 means the desorbed volume of nitrogen from the pore as the relative pressure is reduced from $(P/P_0)_1$ to $(P/P_0)_2$. This volume of V_1 include two factors: the volume for emptying the condensate in the largest pores and the portion resulted from reduction of the layer which is physically adsorbed (Δt_1). The volume of the largest pore is described as following Eq. (2-10).

$$V_{p1} = V_1 \left(\frac{r_{p1}}{r_{K1} + \Delta t_1} \right)^2 \qquad (2\text{-}10)$$

As the relative pressure decreases to $(P/P_0)_3$, the additional factor to consider occurs. That is, the volume of desorption contains not only the condensate from the second largest pore but also the desorption amount from the second thinning portion of physically adsorbed layer in the largest pore. The volume V_{p2} desorbed from pores of the second largest pore is shown as Eq. (2-11).

$$V_{p2} = \left(\frac{r_{p2}}{r_{K2} + \Delta t_2} \right)^2 \left(V_2 - V_{\Delta t_2} \right) \qquad (2\text{-}11)$$

Assuming that $V_{\Delta t2}$ is $V_{\Delta t_2} = \Delta t_2 A_{c1}$, where A_{c1} is the average area of physically adsorbed gas is desorbed at previous status, Eq. (2-12) can be generalized to represent any step of a stepwise desorption.

$$V_{\Delta t_n} = \Delta t_n \sum_{j=1}^{n-1} A_{cj} \tag{2-12}$$

By combining Eq. (2-11) and (2-12), the expression for calculating pore volumes at various relative pressures becomes as following Eq. (2-13).

$$V_{pn} = \left(\frac{r_{pn}}{r_{Kn} + \Delta t_n}\right)^2 \left(\Delta V_n - \Delta t_n \sum_{j=1}^{n-1} A_{cj}\right) \tag{2-13}$$

Since the quantity of Ac tends to change according to (P/P_o), the area of each pore which is a constant and can be obtained from the pore volume will be used instead. By putting that $A_p = 2V_p/r_p$, the pore areas can be cumulatively summed so that for any step in the desorption process is known. The average capillary radius is expressed as $\bar{r}_c = \bar{r}_p - \bar{t}_r$, where $\bar{t}_r$ is the thickness of the adsorbed layer at the average radius in the interval in the current pressure decrement. The term c is known as $c = \bar{r}_c/\bar{r}_p = (\bar{r}_p - \bar{t}_r)/\bar{r}_p$.

Eq. (2-14) now can be used as the final generalized B.J.H method form as shown following.

$$V_{pn} = \left(\frac{r_{pn}}{r_{Kn} + \Delta t_n}\right)^2 \left(\Delta V_n - \Delta t_n \sum_{j=1}^{n-1} A_{pj}c_j\right) \tag{2-14}$$
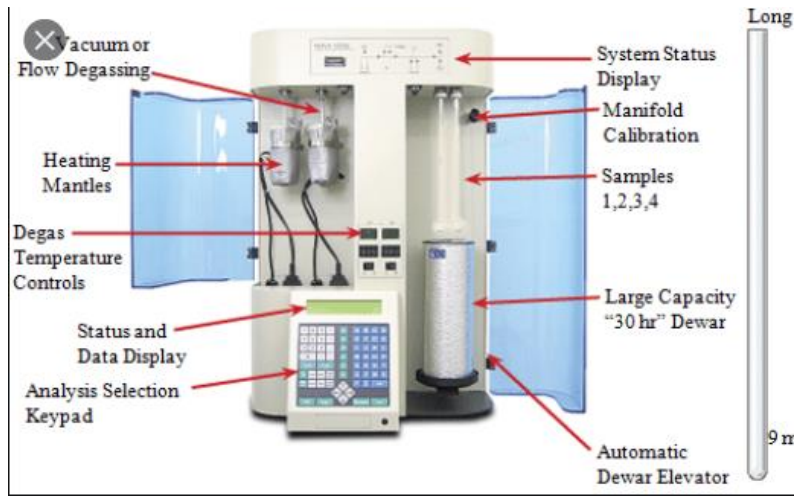
Fig. 2. 1 Experimental device for measuring adsorbent properties

2.2.3 Estimation of Physical Properties of WSS and Silica Gels

A natural mesoporous hard mudstone called the WSS mined from the northern part of Hokkaido in Japan [11–18]. It is naturally derived from diatoms and planktonic organisms composed primarily of SiO_2 and changes into siliceous shale with a crystalline structure at high temperatures and pressures. Fig. 2.2 shows mining places and a raw material of WSS. It exists as belt-shaped foothills with its height of 50 meters across about 30 km in the direction of North-South. Also, its underground distribution exists more than 1 km in the depth under the surface layer [17]. Fig. 2.3 presents measured data by the experimental data of Quantachrome NOVA 1000, as the form of Eq. (2-8). As explained in the previous chapter, the specific surface area estimated by the B.E.T method is about 150 m^2/g. Fig. 2.3 also provides B.E.T straight lines of an A-type and a B-type silica gels for the comparison. The specific surface area of an A-type and a B-type silica gels estimated by the B.E.T method are about 712.4 m^2/g and 513.6 m^2/g, respectively.
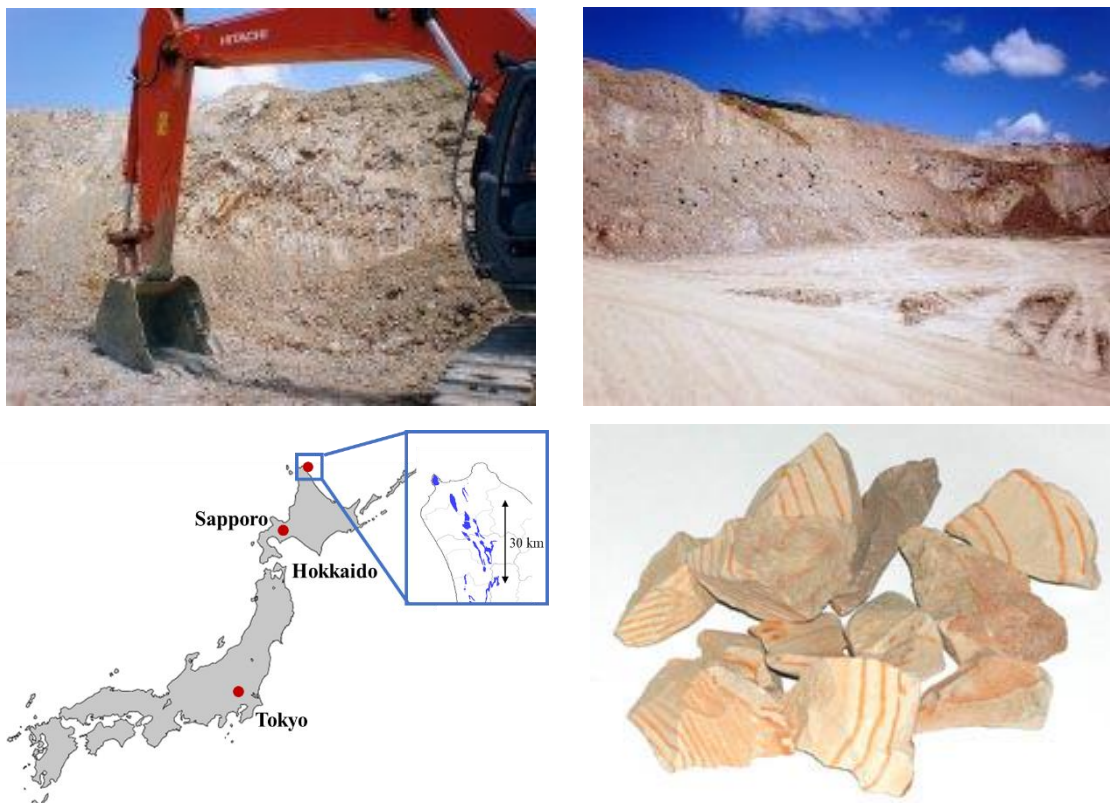
Fig. 2. 2 Mining place and raw material of Wakkanai Siliceous Shale (WSS)

Similarly, Fig. 2.4 depicts the typical straight form of B.E.T plot to compare surface area according to the impregnation amount of LiCl. The surface area of pores tend to be reduced because certain part of the pores of the host matrix WSS are filled with LiCl particles, and the reduction amount increases as impregnating the more amount of LiCl. The detailed physical characteristics of the composite materials are listed in Table 2. 1.
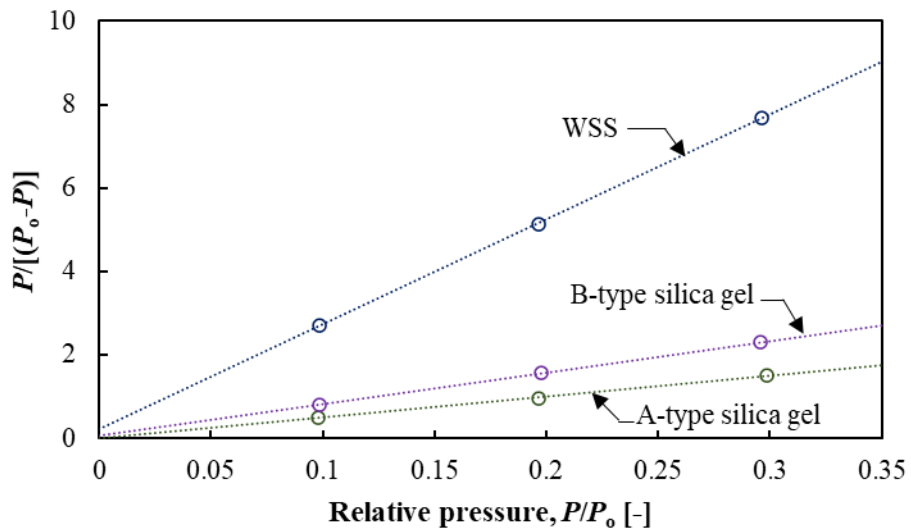
Fig. 2. 3 Typical B.E.T plot presenting straight line (WSS, A and B-type silica gels)
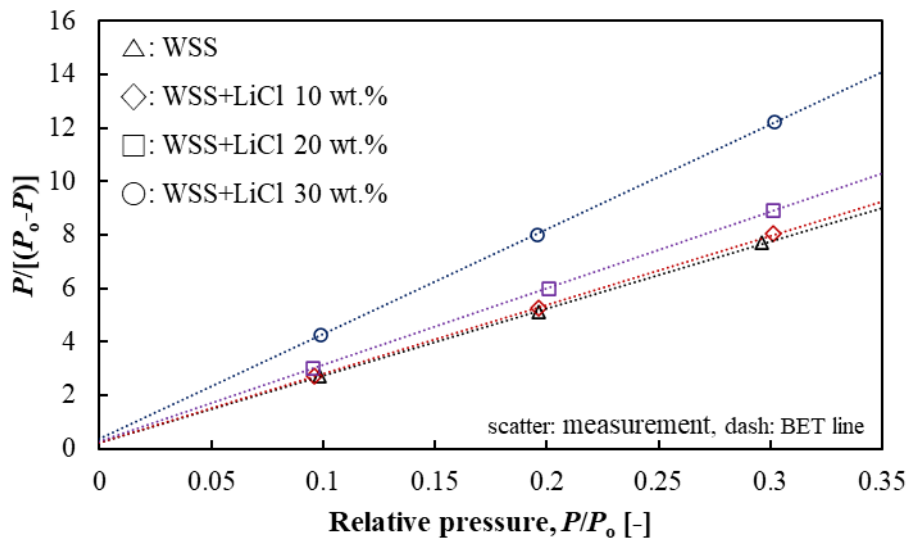
Fig. 2. 4 Typical B.E.T plot presenting straight line (Pure WSS and composites)

As presented in Fig. 2.5, the WSS mainly consists of meso-pores whose size normally ranges from 4 to 20 nm. The estimated pore volume based on the B.J.H method is about 0.36 cm3/g. On the other hand, the micro-pores are observed in the A-type silica gel. Its average pore size and average volume are estimated to be about 2.5 nm and 0.454 cm3/g, respectively (Fig. 2.6). The B-type silica gel has similar pore distribution showing the peak value of log differential pore volume around 7 nm and average pore diameter with WSS (Fig. 2.7). The mesoporous silica gel is often used as a porous matrix of many composite materials such as SWS-1L and SWS-2L [7–10].

Fig. 2.8 shows pore distributions of WSS composites according to the LiCl amounts. The volume of pores tend to be reduced because certain part of the pores of the host matrix WSS are filled with LiCl particles, and the reduction amount increases as impregnating the more amount of LiCl. The detailed physical characteristics of the composite materials are listed in Table 2. 1.
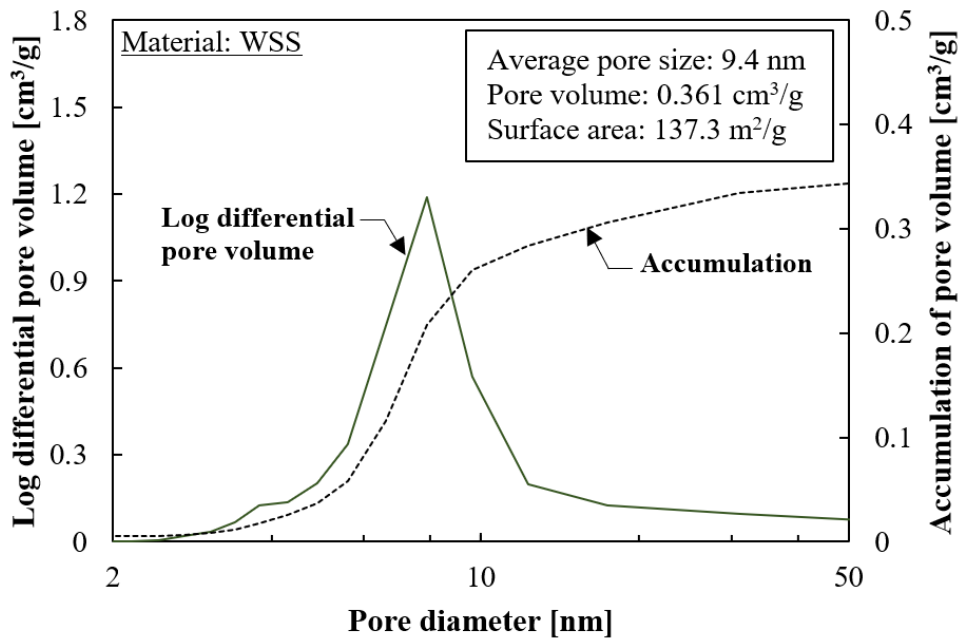
Fig. 2. 5 Log differential pore volume of WSS
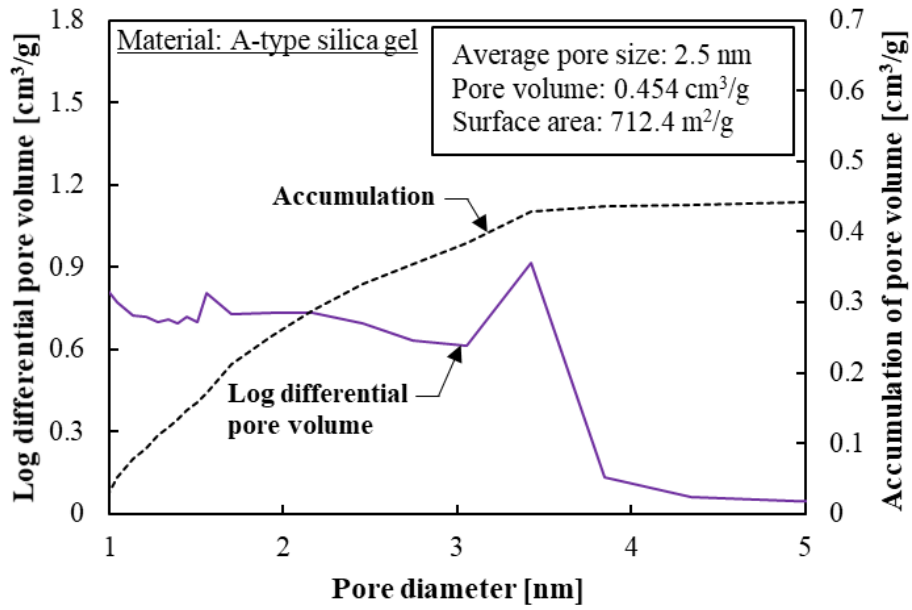
Fig. 2. 6 Log differential pore volume of A-type silica gel
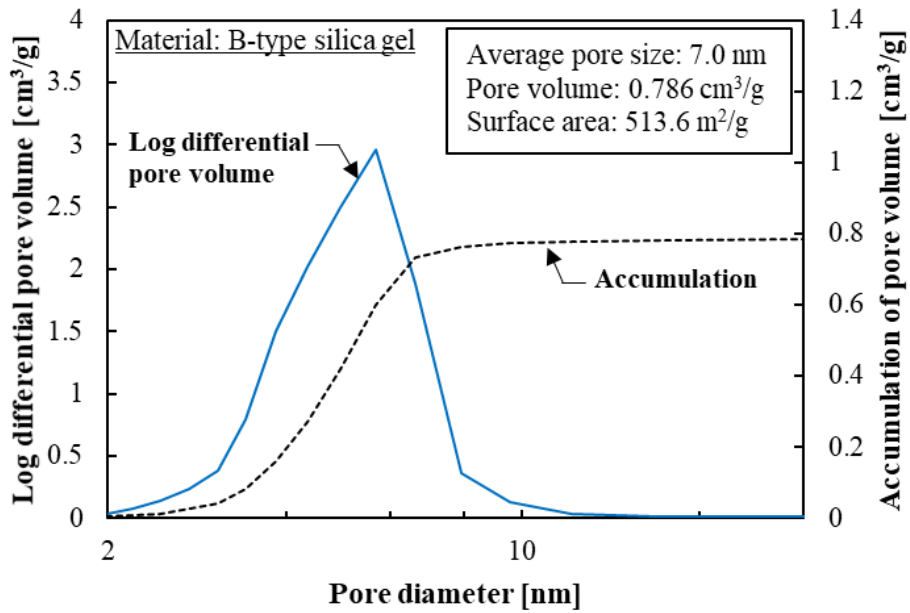
Fig. 2. 7 Log differential pore volume of B-type silica gel
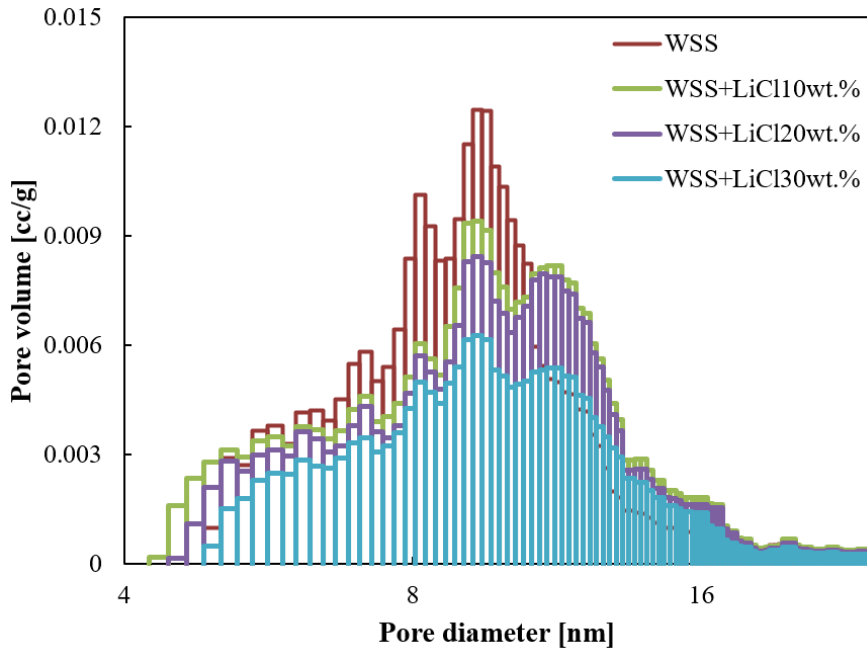
Fig. 2. 8 Pore volume distribution according to pore diameter of various composite

Table 2. 1 Physical characteristics of WSS-based composite materials

Sample No.	1	2	3	4
LiCl content [wt. %]	0	10	20	30
Surface area [m^2/g]	137.28	133.79	120.35	87.88
Pore volume [cm^3/g]	0.361	0.354	0.320	0.244
Average pore size [nm]	9.4	9.4	9.4	9.4

2.3 EQUILIBRIUM ADSORTPION PROPERTIES

2.3.1 Measurement of Equilibrium Adsorption Amount [19]

The adsorption equilibrium amount of the adsorbents was measured by using experimental device, named 'Quantachrome HYDROSORB 1000'. The device measures amount of water vapor dosed to the sample cell from the manifold. The process supplying water vapor to the sample cell is called 'dose action', and this actions are repeated until the sample reaches to certain target pressure. That is, if the sample fails to reach to the equilibrium at certain pressure, the amount supplied during the dose action is recorded and proceed to the next dose action. The water vapor amount transferred from the manifold to the sample cell at the dose action i (m_i) can be expressed as following Eq. (2-15). As shown in Fig. 2.10, the two different temperature levels exist in HYDROSORB; the cold zone in which the sample cell is partially immersed with certain constant temperature, and the hot zone heated by the electric heater to supply water vapor. The temperatures of cold and hot zone are represented as T_H and T_c, respectively. V_H and V_c refer to volume of each zone, and V_A indicates volume of the solid sample in the cell. ΔP_i is the pressure difference between start and end of the particular dose action, and P_i is the end pressure of the particular dose action. The α means non-ideality correction factor, and the value of 3 x 10^{-5} torr^{-1} are according to the user manual.

$$m_i = \sum_{i=1}^{n-1} \frac{\Delta P_i}{R} \left[\frac{V_H}{T_H} + \frac{(V_c - V_A)(1 + \alpha P_i)}{T_c} \right] \qquad (2\text{-}15)$$

If the sample succeed to achieve the equilibrium, then the summation of the mass of water vapor adsorbed by the sample during the dose actions is regarded as equilibrium adsorption amount at the set pressure (m_e) as shown in Eq. (2-16). Here, ΔP_e and P_e are Pressure difference between start and end of dose being equilibrium and final equilibrium pressure, respectively.

$$m_e = \frac{\Delta P_e}{R} \left[\frac{V_H}{T_H} + \frac{(V_c - V_A)(1 + \alpha P_e)}{T_c} \right] \qquad (2\text{-}16)$$

One more parameter that needs to be considered is the amount of water vapor required to achieve the set pressure without adsorption. The amount (m_B) needs to be ready before the measurement by conducting sample cell calibration at the corresponding cell temperature. Finally, the measured adsorption equilibrium at certain target pressure is obtained as Eq. (2-17).

$$m = \sum_{i=1}^{n-1} m_i + m_e - m_B \qquad (2\text{-}17)$$
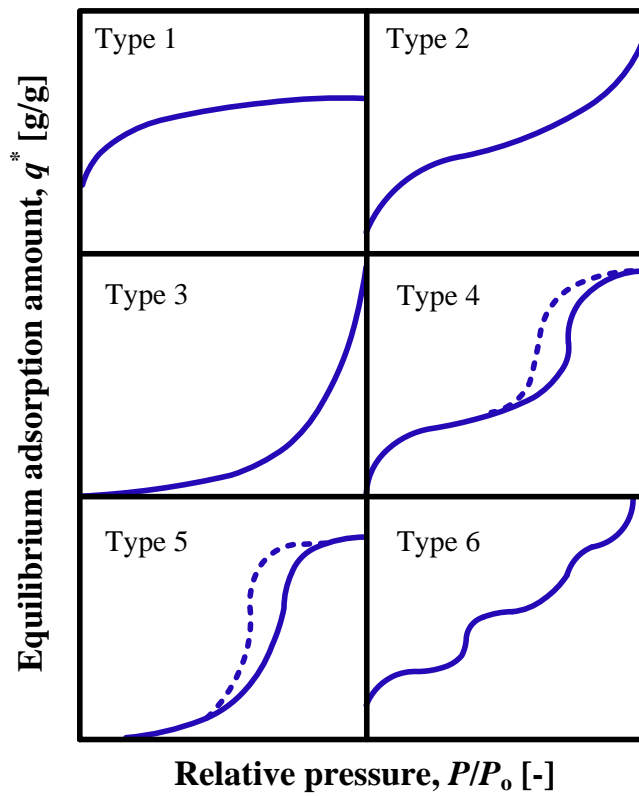
Fig. 2. 9 Classification of the isotherm types according to IUPAC
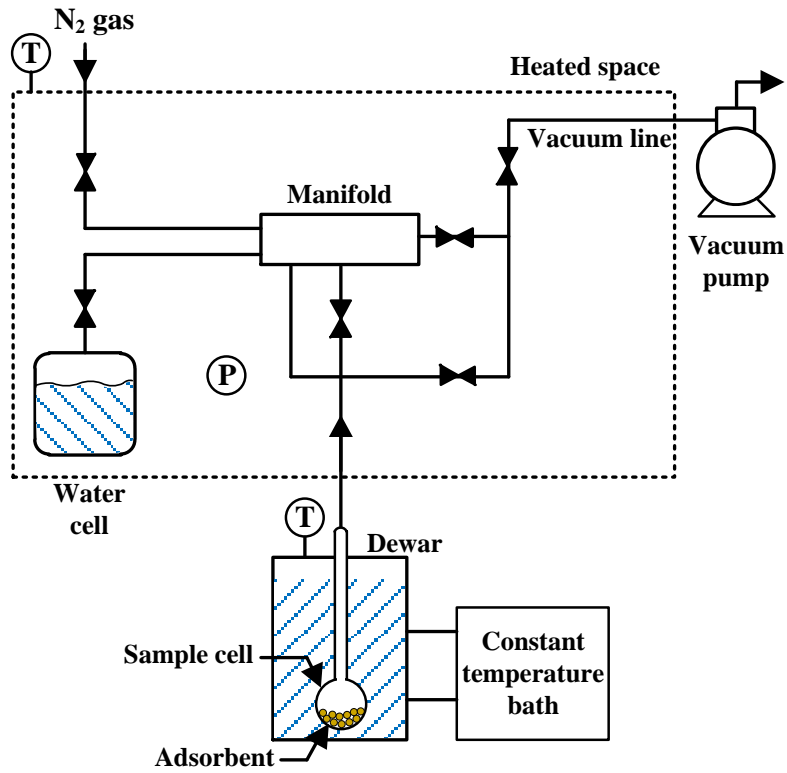
Fig. 2. 10 Schematic diagram of Quantachrome HYDROSORB 1000 [19]

Fig. 2. 11 Actual feature of Quantachrome HYDROSORB 1000

2.3.2 Adsorption Isotherm Equations

Adsorption isotherm equations describe equilibrium adsorption characteristics of certain working pairs mathematically. Theses equations correlate adsorption amount with adsorbent temperature and adsorbate pressure, such as *q= f(P,T)* [6]. There are numerous isotherm equation models suggested to describe various types of isotherms.

The some of the most representative and frequently used isotherm equations are as introduced as followings.

1) Langmuir isotherm

This equation bases on the monomolecular film adsorption theory. That is, the adsorption sites uniformly exist on the surface of adsorbent to provide place for the adsorbate molecules to be adsorbed. The theory implies that there will not be more adsorption phenomena once the sites are occupied. The traditional form of the Langmuir isotherm is as shown in Eq. (2-18) [20]. Modified form of the Langmuir equations suggested by several researchers can easily found in the literatures [21–23].

$$\frac{q^*}{q_{\mathrm{m}}} = \frac{K_L P}{1 + K_L P} \qquad (2\text{-}18)$$

Here, K_L named Langmuir equilibrium constant refers to the ratio between adsorption desorption rate.

2) Freundlich isotherm

This model is well known as the most primitive equation depicting the adsorption mechanism. The modified form of this model is widely used to describe adsorption equilibrium of various types of working pairs [24–26].

$$q^* = A(T_a) \left[\frac{P}{P_{\mathrm{sat}}(T_a)}\right]^{B(T_a)} \qquad (2\text{-}19\text{a})$$

$$A(T_a) = A_0 + A_1 T_a + A_2 T_a{}^2 + A_3 T_{\mathrm{a}}{}^3 \qquad (2\text{-}19\text{b})$$

$$B(T_a) = B_0 + B_1 T_a + B_2 T_a{}^2 + B_3 T_{\mathrm{a}}{}^3 \qquad (2\text{-}19\text{c})$$

3) Tòth isotherm

Freundlich equation tends to be improper at low and high relative pressure. Tòth equation presented in Eq. (2-20) [27,28], which is based on the multi-layer adsorption, can satisfy the monolayer coverage and the multi-layer adsorption.

$$\frac{q^*}{q_{\mathrm{m}}} = \frac{\beta P}{[1 + (\beta P)^t]^{\frac{1}{t}}}$$

(2-20)

The parameter β depends on temperature and can be expressed as $\beta = \beta_o exp(Q/(RT))$, where Q represents heat of adsorption. It can be noticed that the form of Tòth equation becomes Langmuir model if *t*=1, describing monolayer adsorption phenomenon [29].

4) D-A isotherm

The D-A equation is known to describe adsorption phenomenon on the microporous adsorbents such as activated carbons, which characteristically have high heterogeneous pores. The equilibrium adsorption amount is expressed as Eq. (2-21) [30,31].

$$\frac{q^*}{q_{\mathrm{m}}} = \exp\left\{-\left(\frac{RT_{\mathrm{a}}}{E_{\mathrm{c}}}\ln\frac{P_{\mathrm{sat}}}{P}\right)^{\gamma}\right\}$$

(2-21)

Here, E_{c} and *n* are the characteristic energy and the heterogeneity constant, respectively.

5) Li and Ng model

Various studies to simulate adsorption type 5 isotherms have been reported [21,32]. The newly proposed mathematical equation which describes S-shape isotherms can be found in researches of Li [33,34] and Ng [35]. They proved that the proposed isotherm successfully depict various types of adsorption working pairs (e.g., silica gel and FAM-Z01). The isotherm model is explained as following Eq. (2-22). They also emphasized that the model requires only four parameters to be estimated for the description of various working pairs, and the error of numerical fitting is obviously lower than traditional

models [34].

$$\frac{q^*}{q_{\mathrm{m}}} = \frac{A\emptyset\, exp\left(\beta\, \frac{P}{P_{\mathrm{sat}}}\right)\frac{P}{P_{\mathrm{sat}}} + C\, \frac{P}{P_{\mathrm{sat}}}}{\left\{1 + \emptyset\, exp\left(\beta\, \frac{P}{P_{\mathrm{sat}}}\right)\frac{P}{P_{\mathrm{sat}}}\right\}^n} \tag{2-22a}$$

$$\beta = \exp\left(\frac{E_{\mathrm{c}}}{RT_{\mathrm{a}}}\right) \tag{2-22b}$$

$$A = \frac{\{1 + \emptyset\exp(\beta)\}^n - C}{\emptyset\exp(\beta)} \tag{2-22c}$$

5) Yahia model

The isotherm equation which suitable for describing type 6 isotherms is suggested by Yahia et al. [36]. They assumed that the four levels of adsorption energy exist in each adsorption site. According to the authors, $P_{\mathrm{i}} = 1, 2, 3, 4$ represents the pressure at each adsorption site, n_{i} is the number of molecules per site, N_{mi} is the density of receptor sites, and E_{ai} refers to the molar adsorption energy of gases at site i. The mathematical equation of the model is as shown in Eq. (2-23).

$$q^* = \frac{n_1 N_{\mathrm{M1}}\left(\frac{P}{P_1}\right)^{n_1}}{1 + \left(\frac{P}{P_1}\right)^{n_1}} + \frac{n_2 N_{\mathrm{M2}}\left(\frac{P}{P_2}\right)^{n_2}}{1 + \left(\frac{P}{P_2}\right)^{n_2}} + \frac{n_3 N_{\mathrm{M3}}\left(\frac{P}{P_3}\right)^{n_3}}{1 + \left(\frac{P}{P_3}\right)^{n_3}} + \frac{n_4 N_{\mathrm{M4}}\left(\frac{P}{P_4}\right)^{n_4}}{1 + \left(\frac{P}{P_4}\right)^{n_4}} \tag{2-23a}$$

$$P_{\mathrm{i}} = P_{\mathrm{sat}}\exp\left(\frac{\Delta E_{\mathrm{a,i}}}{RT_{\mathrm{a}}}\right) \tag{2-23b}$$

2.3.3 Equilibrium Adsorption Properties of WSS and Silica Gels

'Composites Salt in Porous Matrix (CSPMS)' enhance equilibrium adsorption amount compared to the traditional working pair. WSS could be used as a sort of the porous matrix owing to its mesoporous structure. The thing that should be dealt with carefully in using the composite materials is to avoid carryover of deliquescing solution. That is, the host matrix no longer contains the deliquescing chloride solution as its volume exceeds the maximum pore capacity of the host matrix. This phenomenon eventually results in a severe decrease in the adsorption capacity and the problems regarding corrosions. The previous member of our research team Nakabayshi et al. [17] investigated the proper impregnation amount of lithium chlorides to prevent carryover problem, based on the pore volume.

Fig. 2.12 shows adsorption isotherms of WSS composite with LiCl at various amount. The obvious enhancement of the equilibrium adsorption amount was obtained by impregnating LiCl into the pure WSS. With the consideration that the adsorption pressure of AHP system ranges from 1.0 kPa (T_{sat}: 7 °C) to 1.7 kPa (T_{sat}: 15 °C), it was observed that the equilibrium adsorption amount at the relative pressure 0.53, which equals to 1.7 kPa, could almost reach the WSS pore volume. Therefore, the maximum applicable amount of the lithium chloride for preventing carryover was determined to be 20 wt.%.
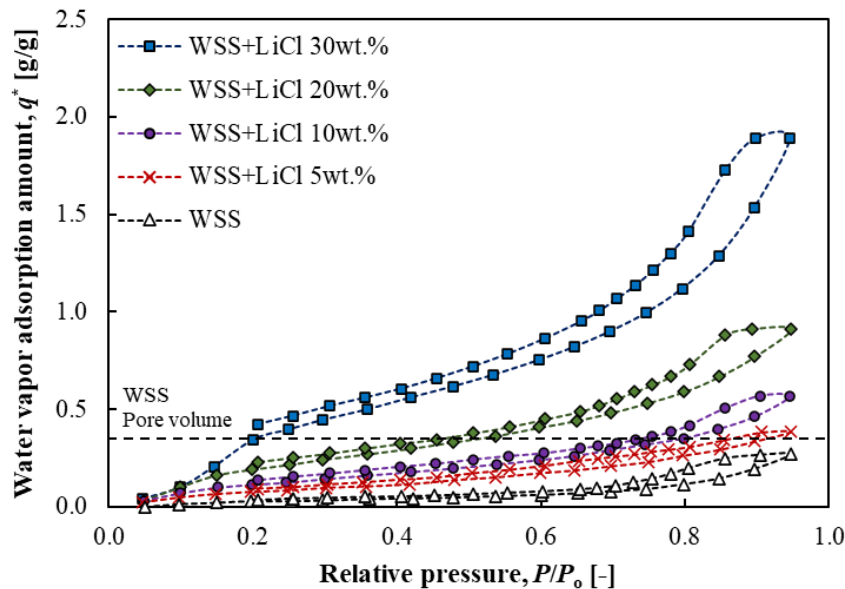
Fig. 2. 12 Adsorption isotherms of WSS composite with LiCl at various amount

As presented in Fig. 2.13, the isotherm of WSS composite tends to show two-steps at 0.1 kPa and 0.5 kPa, which is similar shape with type 6 isotherm equations. Therefore, the isotherm of WSS + LiCl 20 wt.% has been expressed using the equation proposed by Yahia et al. [36] shown in Eq. (2-23).

On the other hand, the isotherm of the A-type silica gel was fitted numerically using the equation proposed by Li et al. [33], as expressed in Eq. (2-22) because of its high accuracy.

Table 2. 2 summarizes the value of numerically fitted constants. The equilibrium adsorption amount of the A-type silica gel and WSS + LiCl 20 wt.% were measured in four temperature levels between 30 and 50 °C, as shown in Fig. 2.13 and Fig. 2.14. The pressure range of the measurement was the relative pressure of 0 to 0.6. In the case of WSS + LiCl 20 wt.%, the average number of measuring points was 22, and the points were placed more densely at the zone exhibiting stepwise adsorption characteristics. The average and maximum deviations between the measured and calculated equilibrium loading of WSS + LiCl 20 wt.% were 0.0081 and 0.06 g/g, respectively ($R^2 = 99.24$).

Regarding the A-type silica gel, the average number of measuring points was 12. The average and maximum deviations between the measured and calculated equilibrium loading of the A-type silica gel were 0.0048 and 0.0164 g/g, respectively ($R^2 = 99.58$).

The accuracies of the pressure transducer, PT-100 temperature sensor in the dewar, and electric balance measuring the sample weight were ±0.5 % that of the reading, ±0.25 °C, and ±0.1 mg, respectively. The estimated mean value of uncertainty of the measurement based on the user manual and that of Li et al. [19] was ±2.98 × 10^{-3} g/g (±1.09%).
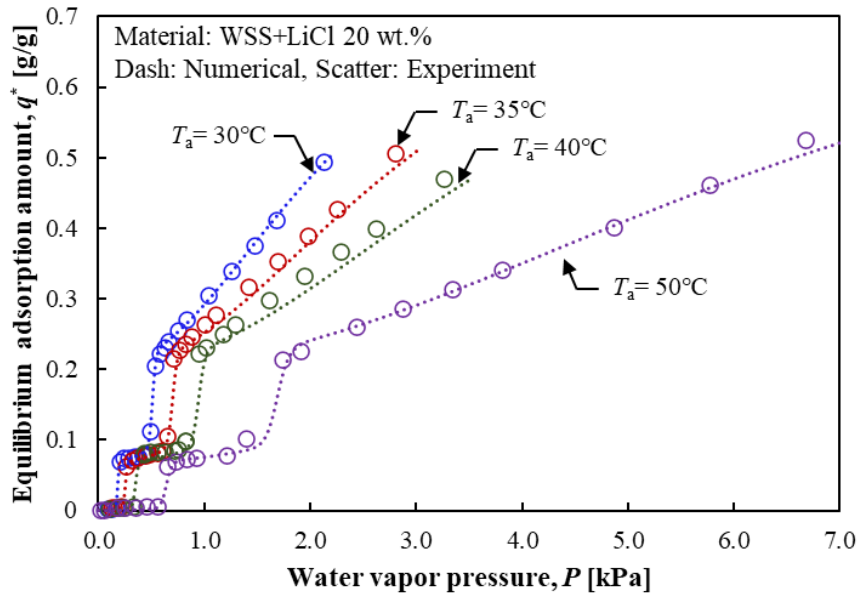
Fig. 2. 13 Isotherm equation of WSS+LiCl 20wt .% at various temperature
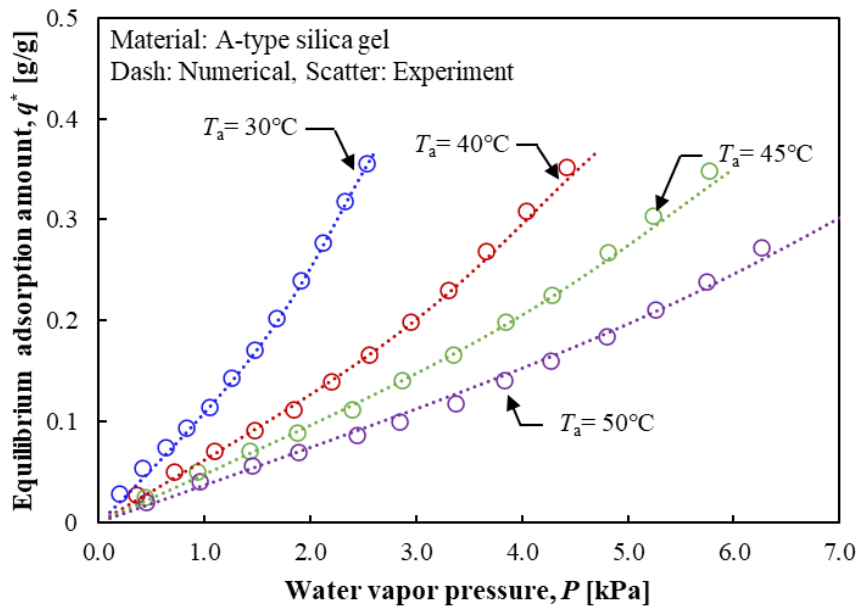
Fig. 2. 14 Isotherm equation of A-type silica gel at various temperature

Table 2. 2 Constants for isotherms for WSS+LiCl 20wt.% and A-type silica gel

Constant	WSS+ LiCl 20 wt.%	Constant	A-type silica gel
n_1	2.211	q_m	0.464
n_2	31.564	E_c	323.015
n_3	25.044	$\emptyset$	3.89×10^{-3}
n_4	3.738	C	0.9753
N_{m1}	0.271	n	0.9878
N_{m2}	4.3×10^{-3}	-	-
N_{m3}	2.7×10^{-3}	-	-
N_{m4}	1.22	-	-
E_{a1}	-1.67×10^3	-	-
E_{a2}	-5.34×10^3	-	-
E_{a3}	-7.94×10^3	-	-
E_{a4}	5.40×10^3	-	-

2.4 EFFECT OF IMPREGNATION ON ADSORPTION PROPERTIES

The combination of porous materials and chemical adsorbents enlarges adsorption capacity of the porous matrix, at the same time enhances physical stability and thermal conductivity of chemical adsorbent. The chemical adsorbents tend to swell and agglomerate in the adsorption process [5]. Our research member Kurokawa et al. pointed out that the impregnation of chloride may affect physical property of the host matrix [12]. Zhao et al. also presented the results that particles of the zeolite dissolved as putting the material into the $CaCl_2$ solution at its concentration above 20 wt.% [37], which shows physical change in the porous matrix resulting from the impregnation.

Therefore, the porous matrixes are washed once after being impregnated with lithium chloride of 20 wt.% to investigate physical changes in the porous structure. As presented in Fig. 2.15~ Fig. 2.18, pore distribution of the washed A-type and B-type silica gels after impregnation is greatly changed. That is, the washed porous media showed obviously decreased portion of small pores compared to the original state. It implies the physical

characteristics or properties of the porous media has been changed. The comparison of the equilibrium adsorption amount between the 'original' state and the 'washed after impregnation' in Fig. 2.15~ Fig. 2.18 prove the changes in porous structures by impregnating lithium chloride into the porous matrix. For the case of the A-type silica gel, much obvious degradation in the equilibrium adsorption amount was observed because most of micro-pores and small pores (< 4 nm) are broken. The surface area of the original state A-type silica gel is about 712.4 m^2/g, meanwhile that of the washed A-type silica gel after impregnation with LiCl is 412.9 m^2/g, approximately 42% reduced value. The B-type silica gel also presented degradation in the equilibrium adsorption amount, especially at relative pressure above 0.6. The surface area of the B-type silica gel is decreased from 531.61 m^2/g to 379.62 m^2/g by impregnating LiCl. On the other hand, WSS hardly shows change in physical properties after impregnation and the equilibrium adsorption amount also did not changed. The detailed physical characteristics of the composite materials are listed in Table 2. 3.

From these results, the strong pore structure of WSS has been verified compared to physically weak pores of silica gels. Having constant physical pore structures after impregnation can be connected to the issue regarding stability and long-term usage of the composite adsorbent. Therefore, WSS is expected to be utilized as a host matrix of composite adsorbent in terms of both enhanced equilibrium adsorption amount and physically stable pore structures.

Table 2. 3 Physical characteristics of host matrix before and after impregnation

Sample No.	Surface area [m^2/g]	Pore volume [cm^3/g]	Average pore size [nm]
A-type silica gel: Original	712.44	0.454	2.58
A-type silica gel: Washed	412.92	0.441	5.08
B-type silica gel: Original	531.61	0.786	7.03
B-type silica gel: Washed	379.62	0.752	7.03
WSS: Original	137.28	0.361	9.41
WSS: Washed	138.59	0.372	9.41
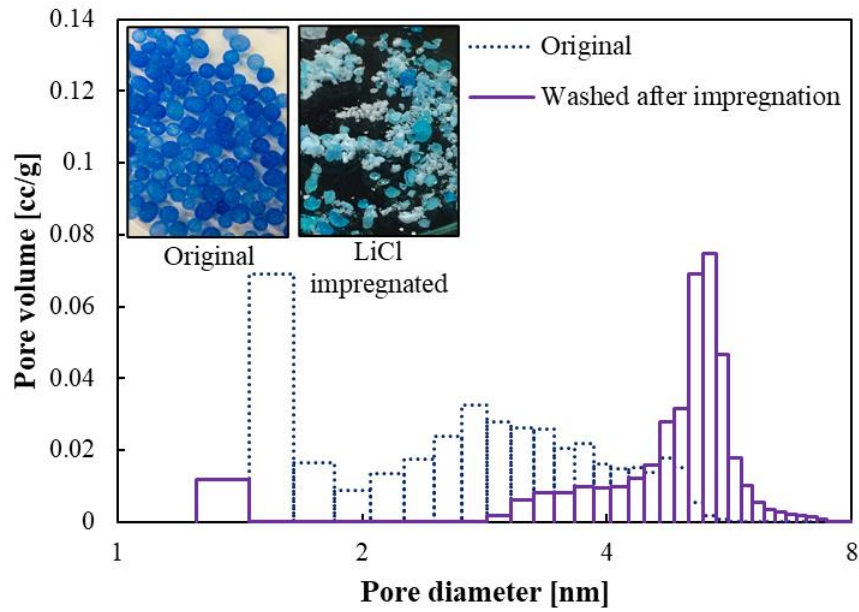
Fig. 2. 15 Comparison of pore volume and diameter:
Before and after washing impregnated LiCl in A-type silica gel
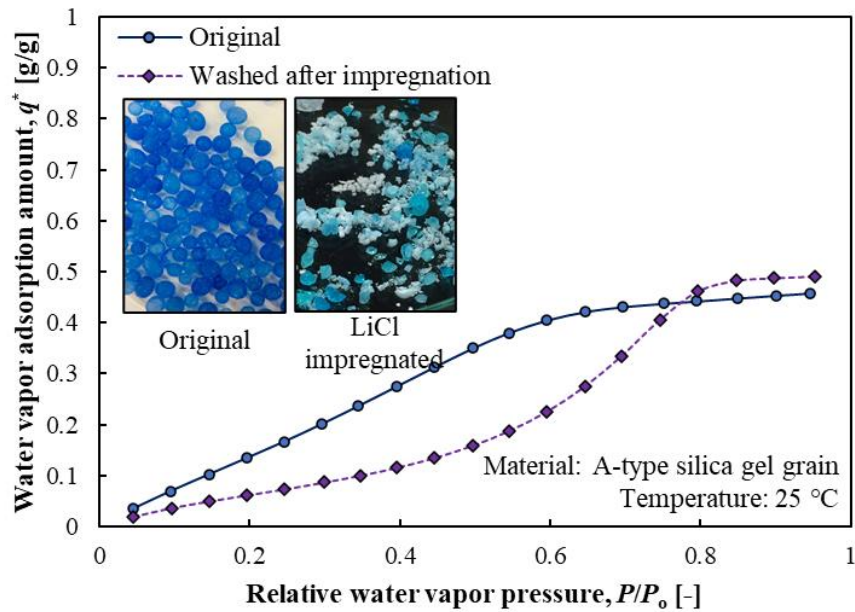
Fig. 2. 16 Comparison of equilibrium adsorption amount:
Before and after washing impregnated LiCl in A-type silica gel
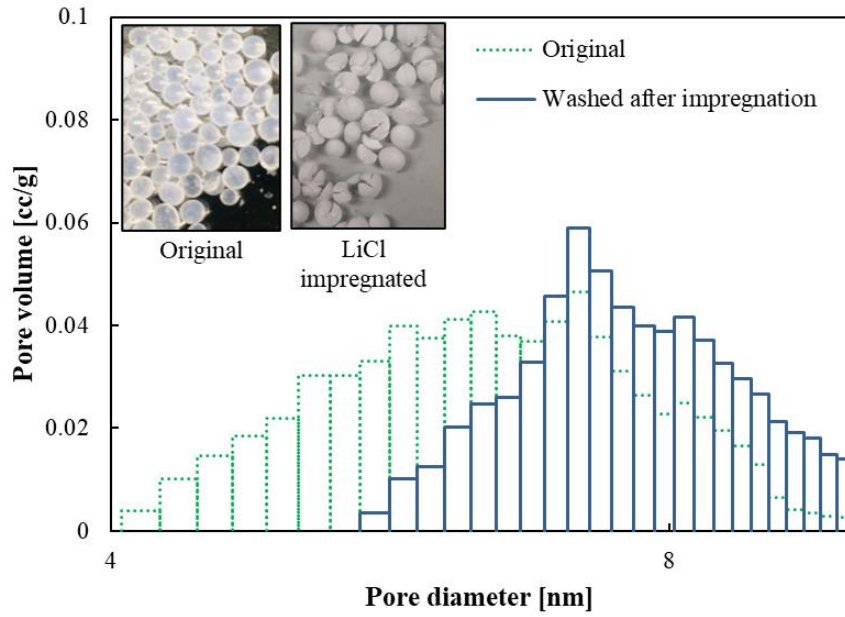
Fig. 2. 17 Comparison of pore volume and diameter:
Before and after washing impregnated LiCl in B-type silica gel
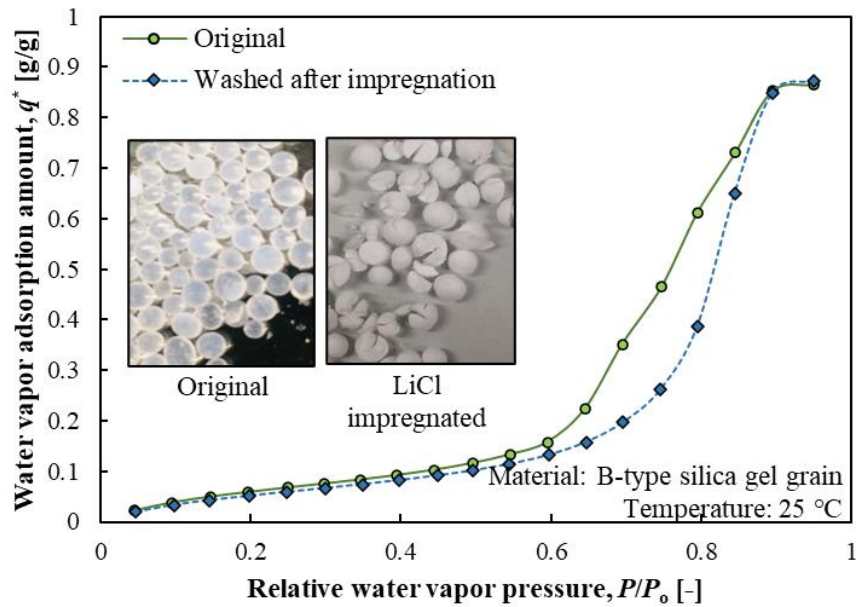
Fig. 2. 18 Comparison of equilibrium adsorption amount:
Before and after washing impregnated LiCl in B-type silica gel
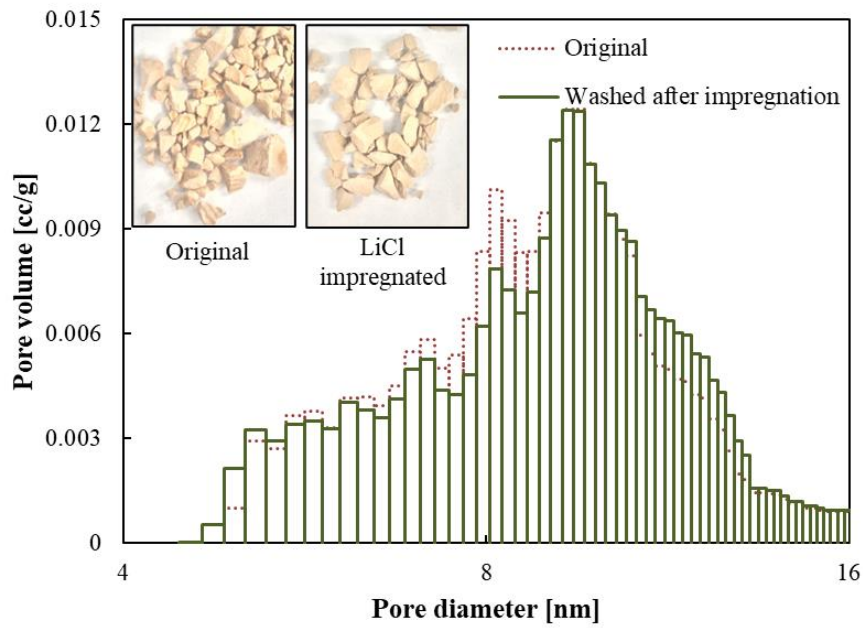
Fig. 2. 19 Comparison of pore volume and diameter:
Before and after washing impregnated LiCl in WSS
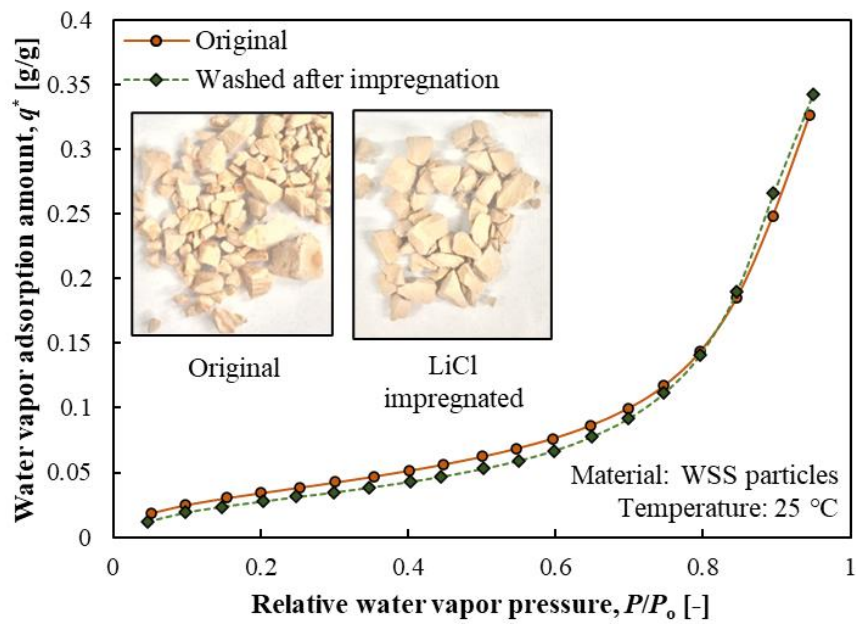
Fig. 2. 20 Comparison of equilibrium adsorption amount:
Before and after washing impregnated LiCl in WSS

2.5 SUMMARY

In this chapter, experimental investigation of physical and equilibrium characteristics of WSS and its composite with lithium chloride are provided. Furthermore, those characteristics of silica gels (A-type and B-type) are given for the comparison. Lastly, effects of impregnation of lithium chloride on the physical and equilibrium adsorption characteristics of the porous media are studied to emphasize advantage of WSS as a host matrix. Followings summarize the contents of this chapter.

1) The specific surface area estimated by the B.E.T method is about 150 m^2/g. WSS mainly consists of meso-pores whose size normally ranges from 4 to 20 nm. The estimated pore volume based on the B.J.H method is about 0.36 cm^3/g. The surface area of pores tend to be reduced because certain part of the pores of the host matrix WSS are filled with LiCl particles.

2) The B-type silica gel has similar pore distribution showing the peak value of log differential pore volume around 7 nm and average pore diameter with WSS. Meanwhile, the micro-pores are observed in the A-type silica gel. Its average pore size and average volume are estimated to be about 2.5 nm and 0.454 cm^3/g, respectively.

3) The obvious enhancement of the equilibrium adsorption amount was obtained by impregnating LiCl into the pure WSS. The maximum applicable amount of the lithium chloride for preventing carryover was determined to be 20 wt.%, based on its pore volume.

4) The isotherms of WSS+LiCl 20 wt.% is numerically fitted to the model suggested by Yahia et al. The model successfully described two-stepwise isotherm, and the average and maximum deviations between the measured and calculated equilibrium loading of WSS + LiCl 20 wt.% were 0.0081 and 0.06 g/g, respectively ($R^2 = 99.24$). The isotherms of A-type silica gel, which will be used in further chapters for the comparison, are fitted to the model suggested by Li et al. The average and maximum deviations between the measured and calculated equilibrium loading of the A-type silica gel were 0.0048 and 0.0164 g/g, respectively ($R^2 = 99.58$).

5) The surface areas of both A-type and B-type silica gels are decreased by impregnating LiCl. Also their equilibrium adsorption amount tended to be decreased due to the destroyed or changed pore structure. On the other hand, WSS hardly shows change in physical properties after impregnation and the equilibrium adsorption amount also did not changed.

Therefore, WSS is expected to be utilized as a host matrix of composite adsorbent in terms of both enhanced equilibrium adsorption amount and physically stable pore structures.

2.6 REFERENCE

[1]   M.B. Elsheniti, O.A. Elsamni, R.K. Al-dadah, S. Mahmoud, E. Elsayed, K. Saleh, Adsorption Refrigeration Technologies, in: Sustain. Air Cond. Syst., InTech, 2018.

[2]   R.S. Mikhail, S. Brunauer, Surface area measurements by nitrogen and argon adsorption, J. Colloid Interface Sci. 52 (1975) 572–577.

[3]   S. Brunauer, P.H. Emmett, E. Teller, Adsorption of Gases in Multimolecular Layers, J. Am. Chem. Soc. 60 (1938) 309–319.

[4]   E.P. Barrett, L.G. Joyner, P.P. Halenda, The Determination of Pore Volume and Area Distributions in Porous Substances. I. Computations from Nitrogen Isotherms, J. Am. Chem. Soc. 73 (1951) 373–380.

[5]   R. Wang, L. Wang, J. Wu, Adsorption Refrigeration Technology, Wiley, 2014.

[6]   H.Z. Hassan, A.A. Mohamad, Y. Alyousef, H.A. Al-Ansary, A review on the equations of state for the working pairs used in adsorption cooling systems, Renew. Sustain. Energy Rev. 45 (2015) 600–609.

[7]   Y.I. Aristov, M.M. Tokarev, G. Cacciola, G. Restuccia, Selective water sorbents for multiple applications, 1. CaCl2 confined in mesopores of silica gel: Sorption properties, React. Kinet. Catal. Lett. 59 (1996) 325–333.

[8]   Y.I. Aristov, I.S. Glaznev, A. Freni, G. Restuccia, Kinetics of water sorption on SWS-1L (calcium chloride confined to mesoporous silica gel): Influence of grain size and temperature, Chem. Eng. Sci. 61 (2006) 1453–1458.

[9]   A. Freni, M.M. Tokarev, G. Restuccia, A.G. Okunev, Y.. Aristov, Thermal conductivity of selective water sorbents under the working conditions of a sorption chiller, Appl. Therm. Eng. 22 (2002) 1631–1642.

[10]   A. Freni, F. Russo, S. Vasta, M. Tokarev, Y.I. Aristov, G. Restuccia, An advanced solid sorption chiller using SWS-1L, Appl. Therm. Eng. 27 (2007) 2200–2204.

[11]   H. Liu, K. Nagano, J. Togawa, A composite material made of mesoporous siliceous shale impregnated with lithium chloride for an open sorption thermal energy storage system, Sol. Energy. 111 (2015) 186–200.

[12]   A. Kurokawa, J. Togawa, Y. Nabeshima, K. Nagano, The Evaluation of the Moisture Sorption Mechanism of Chloride-Impregnated Wakkanai Siliceous Shale, KAGAKU KOGAKU RONBUNSHU. 37 (2011) 394–399.

[13]   J. Togawa, A. Kurokawa, K. Nagano, Water sorption property and cooling performance using natural mesoporous siliceous shale impregnated with LiCl for adsorption heat pump, Appl. Therm. Eng. 173 (2020) 115241.

[14]   S.H. Seol, K. Nagano, J. Togawa, Modeling of adsorption heat pump system based on experimental estimation of heat and mass transfer coefficients, Appl. Therm. Eng. 171 (2020) 115089.

[15]   H. Liu, K. Nagano, J. Togawa, H. Liu, K. Nagano, J. Togawa, Performance of LiCl

Impregnated Mesoporous Material Coating over Corrugated Heat Exchangers in a Solid Sorption Chiller, Energies. 11 (2018) 1565.

[16]   S.H. Seol, K. Nagano, J. Togawa, A new experimental method to separate interfacial and internal mass transfer on coated adsorbent, Appl. Therm. Eng. 159 (2019) 113869.

[17]   S. Nakabayashi, K. Nagano, M. Nakamura, J. Togawa, A. Kurokawa, Improvement of water vapor adsorption ability of natural mesoporous material by impregnating with chloride salts for development of a new desiccant filter, Adsorption. 17 (2011) 675–686.

[18]   A. Kurokawa, J. Togawa, Y. Nabeshima, K. Nagano, The Evaluation of the Moisture Sorption Mechanism of Chloride-Impregnated Wakkanai Siliceous Shale, KAGAKU KOGAKU RONBUNSHU. 37 (2011) 394–399.

[19]   A. Li, A. Bin Ismail, K. Thu, M.W. Shahzad, K.C. Ng, B.B. Saha, Formulation of Water Equilibrium Uptakes on Silica Gel and Ferroaluminophosphate Zeolite for Adsorption Cooling and Desalination Applications, Evergreen. 1 (2014) 37–45.

[20]   B. Sun, A. Chakraborty, Thermodynamic frameworks of adsorption kinetics modeling: Dynamic water uptakes on silica gel for adsorption cooling applications, Energy. 84 (2015) 296–302.

[21]   B. Sun, A. Chakraborty, Thermodynamic formalism of water uptakes on solid porous adsorbents for adsorption cooling applications, Appl. Phys. Lett. 104 (2014) 201901.

[22]   S. Azizian, S. Eris, L.D. Wilson, Re-evaluation of the century-old Langmuir isotherm for modeling adsorption phenomena in solution, Chem. Phys. 513 (2018) 99–104.

[23]   S. Sohn, D. Kim, Modification of Langmuir isotherm in solution systems - Definition and utilization of concentration dependent factor, Chemosphere. 58 (2005) 115–123.

[24]   Z.Z. Xia, C.J. Chen, J.K. Kiplagat, R.Z. Wang, J.Q. Hu, Adsorption equilibrium of water on silica gel, J. Chem. Eng. Data. 53 (2008) 2462–2465.

[25]   P.G. Youssef, R.K. Al-Dadah, S.M. Mahmoud, H.J. Dakkama, A. Elsayed, Effect of Evaporator and Condenser Temperatures on the Performance of Adsorption Desalination Cooling Cycle, Energy Procedia. 75 (2015) 1464–1469.

[26]   L.X. Gong, R.Z. Wang, Z.Z. Xia, C.J. Chen, Adsorption Equilibrium of Water on a Composite Adsorbent Employing Lithium Chloride in Silica Gel, J. Chem. Eng. Data. 55 (2010) 2920–2923.

[27]   M.M. Younes, I.I. El-sharkawy, A.E. Kabeel, K. Uddin, A. Pal, S. Mitra, K. Thu, B.B. Saha, Synthesis and characterization of silica gel composite with polymer binders for adsorption cooling applications, Int. J. Refrig. 98 (2019) 161–170.

[28]   M.M. Rahman, A. Pal, K. Uddin, K. Thu, B.B. Saha, Statistical Analysis of Optimized Isotherm Model for Maxsorb III/Ethanol and Silica Gel/Water Pairs,

Evergreen. 5 (2018) 1–12.

[29] M.M. Rahman, M. Muttakin, A. Pal, A.Z. Shafiullah, B.B. Saha, A statistical approach to determine optimal models for IUPAC-classified adsorption isotherms, Energies. 12 (2019).

[30] L.X. Gong, R.Z. Wang, Z.Z. Xia, C.J. Chen, Design and performance prediction of a new generation adsorption chiller using composite adsorbent, Energy Convers. Manag. 52 (2011) 2345–2350.

[31] I.I. El-Sharkawy, B.B. Saha, S. Koyama, K. Srinivasan, Isosteric heats of adsorption extracted from experiments of ethanol and HFC 134a on carbon based adsorbents, Int. J. Heat Mass Transf. 50 (2007) 902–907.

[32] M. Hefti, L. Joss, Z. Bjelobrk, M. Mazzotti, On the potential of phase-change adsorbents for CO 2 capture by temperature swing adsorption, Faraday Discuss. 192 (2016) 153–179.

[33] A. Li, K. Thu, A. Bin Ismail, M.W. Shahzad, K.C. Ng, Performance of adsorbent-embedded heat exchangers using binder-coating method, Int. J. Heat Mass Transf. 92 (2016) 149–157.

[34] A. Li, Experimental and Theoretical Studies on the Heat Transfer Enhancement of Adsorbent Coated Heat Exchangers, National University of Singapore, 2014.

[35] K.C. Ng, K. Thu, S.J. Oh, L. Ang, M.W. Shahzad, A. Bin Ismail, Recent developments in thermally-driven seawater desalination: Energy efficiency improvement by hybridization of the MED and AD cycles, Desalination. 356 (2015) 255–270.

[36] M. Ben Yahia, Y. Ben Torkia, S. Knani, M.A. Hachicha, M. Khalfaoui, A. Ben Lamine, Models for type VI adsorption isotherms from a statistical mechanical formulation, Adsorpt. Sci. Technol. 31 (2013) 341–357.

[37] H. Zhao, S. Jia, J. Cheng, X. Tang, M. Zhang, H. Yan, W. Ai, Experimental investigations of composite adsorbent 13X/CaCl2 on an adsorption cooling system, Appl. Sci. 7 (2017).

CHAPTER 3. EXPERIMENTAL SEPARATION OF INTERFACIAL AND INTERNAL MASS TRANSFER ON COATED ADSORBENT

3.1 INTRODUCTION

In recent decades, adsorption heat pumps (AHP) have attracted significant interest worldwide because they can utilize low-level heat sources less than 100 °C. Especially, it is possible for AHP to utilize the heat source characterized by the lower temperature as compared to absorption chillers [1]. However, the relatively huge system volume, low COP results from the low adsorption performance and high initial cost remain crucial disadvantages. Since it is a natural adsorbent, Wakkanai Siliceous Shale (WSS) is less costly than other newly developed adsorbents. Furthermore, its adsorption performance can be markedly improved by impregnating salts such as lithium chloride [2]. Sharkawy et al. compared the water vapor adsorption on an RD silica gel and a $CaCl_2$ confined to KSK silica gel to prove the improved adsorption amount by impregnating chloride into the classical material [3]. Aristov et al. found that the chlorides of $CaCl_2$ and LiBr impregnated in micro and mesoporous silica gels could adsorb a significantly higher amount of water vapor compared with pure silica gels [4]. Many studies have proven that the adsorption capacity of a silica gel can also be improved by impregnating salts. However, according to Kurokawa et al. [5], the pores of silica gel expand because of impregnated chlorides when the synthesized amount exceeds 5 wt.%. The expansion results in the matrix dissolution and unsustainable pore structures. Meanwhile, WSS showed advantages of a strong pore structure, which maintains a stable pore size after the chloride impregnation due to the presence of crystalized silica [2]. Future studies on the durability and mechanical strength of a porous matrix impregnated with salts should be conducted for more details. Aside from silica gels, Lass-Seyoum et al. reported a substantial adsorption capacity of water vapor on hydrophobic substrates such as an attapulgite and an activated carbon by impregnating $CaCl_2$, $MgCl_2$ and $MgSO_4$ [6]. Chan et al. presented the effects of calcium ion exchange on the adsorption properties of zeolite 13X impregnated with $CaCl_2$. Enlarged total pore volume due to the ion exchange facilitated impregnation of $CaCl_2$. As a result, the difference in equilibrium uptake amount between 25 °C and 75 °C of the zeolite 13X with 40 wt.% of $CaCl_2$ was 419% higher than that of the pure zeolite 13X [7]. Mccague et al. [8] and Zheng et al. [9] studied the effects of the pore size of substrates (6~15 nm and 2~10 nm, respectively), which revealed the lower water uptake amount per dry sorbent mass at the adsorbent with

smaller pore diameters. However, according to Glaznev et al., adsorbents with pore diameters of 8.1 nm and 11.8 nm showed almost similar isotherms for the case of the $CaCl_2$ confined SBA-15 [10].

One of the main problems of adsorption heat pump systems is the low heat transfer efficiency between an adsorbent that contacts a heat exchanger and a heat transfer fluid [11,12]. In particular, poor heat transfer of an adsorbent in granular shape results in a steep decrease in adsorption rate [13]. The heat transfer rate can be improved by forming a mono-layer pellet or increasing the area that directly contacts a heat exchanger surface [14]. Based on this principle, a coated adsorbent layer enables the material to markedly enhance the heat transfer rate, which improves the mass transfer. The heat and mass transfer characteristics strongly depend on the coated thickness. Frazzica et al. [15] conducted an experimental evaluation of the kinetic performance of the coated SAPO 34 layers with various thickness. Heyden et al. [16] used an AIPO-18 material to evaluate the adsorption kinetic characteristics with respect to the coated thickness of 0.08~0.75 mm. Dawoud [17] compared the sorption speeds obtained from coated layers with various thicknesses and loose pellets with a moderate radius. Grabowska et al. [18] provided comprehensive analysis on selection of adsorbents and granular size for the coated bed systems. They obtained the thermal conductivity of sorbents by using an experimental device, called 'LFA 457 MicroFlash' and revealed that the thermal conductivity of the coated layer is enhanced 2.6 times compared to that of the fixed layer [19]. Their numerical simulations on the temperature distribution shows that average temperature of the coated layer was 321.12 K, 17 K higher than that of the fixed layer, when the heat source temperature is 343 K [20].

In general, the adsorption kinetics based on experimental studies can evaluate the mass transfer coefficients at various conditions. The measurement methods of the adsorption dynamics are divided into a large pressure jump (LPJ) method [15,21,22] and a large temperature jump (LTJ) method [23–25]. Both methods are considered useful instruments to comparatively evaluate the adsorption performance of different sample configurations [15]. A gravimetric method that measures the adsorption dynamics is considered an improved method compared with a volumetric one due to a direct weighing of the samples [26].

The linear driving force (LDF) model is widely used to simulate the dynamic behavior

of adsorption chillers because of its simplicity. Analytical approach including an interfacial (or called external film) mass transfer for the LDF model can be found in related researches [27,28]. Their models consider both interfacial and internal mass transfer phenomena, which can be expressed by an overall term. Also, mass conservation models can reflect an interfacial mass transfer at their boundary conditions as shown by Wang et al. [29] and Medved et al. [30]. However, many of mass conservation models assume the interfacial adsorbate concentration to be equal to the bulk phase concentration [31–34]. Many of researches using the LDF model [3,35–37] also consider the internal mass transfer as the overall mass transfer and assumed a saturated concentration at the interface between two phases. This assumption may be acceptable if the mass transfer resistance at the interface is minor, or if the internal mass transfer resistance is sufficiently large to ignore the effect of the interfacial mass transfer. Otherwise, the adsorption dynamic characteristics based on the LDF approximation may yield huge errors compared with the actual experimental data.

This study separates the effects of the interfacial and internal mass transfers of water vapor at a coated adsorbent based on both experimental methods and the LDF model. In terms of the adsorbent, the chloride-impregnated composite natural rock called Wakkanai Siliceous Shale (WSS) is used to enhance the adsorption performance. The mass transfer performance of a composite WSS is also compared with that of A-type silica gel to prove its competitiveness.

3.2 EXPERIMENTAL METHODOLOGY

This study aims to estimate an interfacial mass transfer resistance using an experimental method. Fig. 3. 1 (a) summarizes the methodology to separate the interfacial and internal mass transfers, and Fig. 3. 1 (b) shows the cross-section diagram of a coated sample. First, the mass transfer in the range of thickness with negligible internal mass transfer resistance, which is called the subsurface (interfacial) zone, is experimentally observed. The experiments assume that the internal mass transfer resistance is negligible if two sufficiently thin samples present almost identical adsorption dynamic curves. On the other hand, the overall mass transfer resistance can be estimated through experiments using relatively thicker samples (d= 0.19 ~ 0.75 mm). Then, the internal mass transfer resistance

is calculated by subtracting the interfacial resistance from the overall resistance. Finally, the average effective diffusivity is calculated based on the obtained internal mass transfer resistance using the LDF model.

   The large pressure jump (LPJ) method was used to determine the adsorption dynamic characteristics. The adsorption process is triggered by a sudden and large pressure difference between the initially vacuumed chamber and the supplied vapor. Fig. 3. 2 introduces the experimental system to measure the adsorption dynamics. The system can be divided into two sections according to the purpose of the experiments: to analyze the interfacial mass transfer and overall mass transfer. Chamber 1 and Chamber 2 were used for each purpose, and both chambers included an electric balance to gravimetrically measure the adsorption dynamics. Since the samples used in the experiments of the interfacial mass transfer were too thin and light, even a small measuring error from the use of a cooling plate would greatly affect the results. Thus, Chamber 1 used indirect cooling through a rolled-type copper heat exchanger surrounding the sample to remove the adsorption heat. In terms of experiments for the overall mass transfer using Chamber 2, a cooling plate in direct contact with the sample was used to remove the relatively higher adsorption heat, which is proportional to the water vapor sorption amount. During the experiments, the pressure in the chambers could reach the target pressure within 5 seconds because of use of the large size pipe with its diameter of 75 mm, which connects the chamber and the evaporator. Cooling water of 30 °C from a constant temperature bath circulated both cooling devices. The other temperature bath supplied a heat source of 20 °C to an evaporator to generate water vapor, and the entire system was placed into a constant temperature room with an identical temperature level.
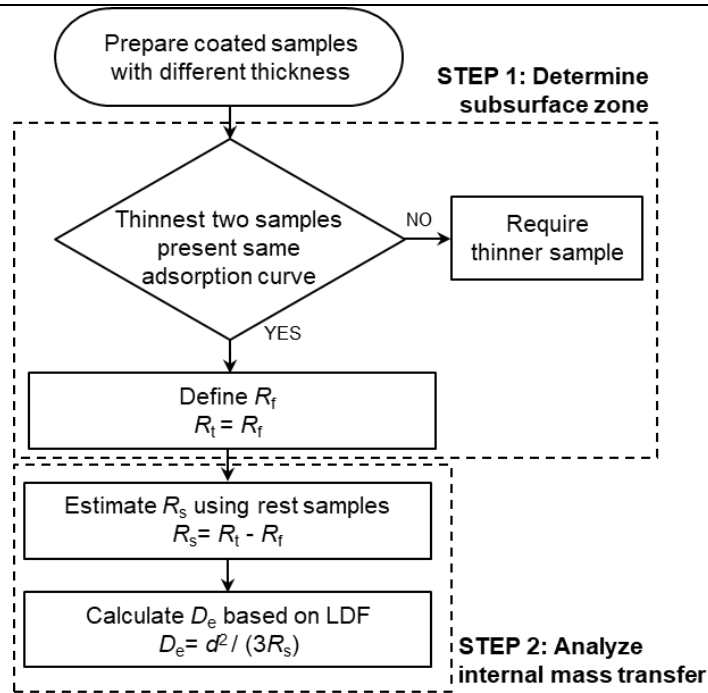
Fig. 3. 1 (a) Methodology for separating interfacial and internal mass transfer resistance
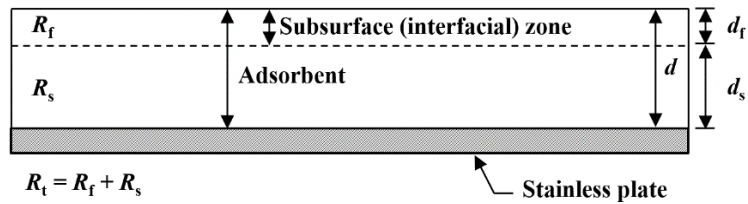
Fig. 3. 1 (b) Cross-section diagram of coated adsorbent on plate

- Chamber 1: Φ 450 mm x 150 mm (Tube: Φ 75 mm)
- Chamber 2: Φ 450 mm x 150 mm (Tube: Φ 75 mm)
- Evaporator: Φ 300 mm x 180 mm

- Accuracy resolution:
  - Electric balance 1: 0.001 g (Max. 310 g)
  - Electric balance 2: 0.01g (Max. 3100 g)
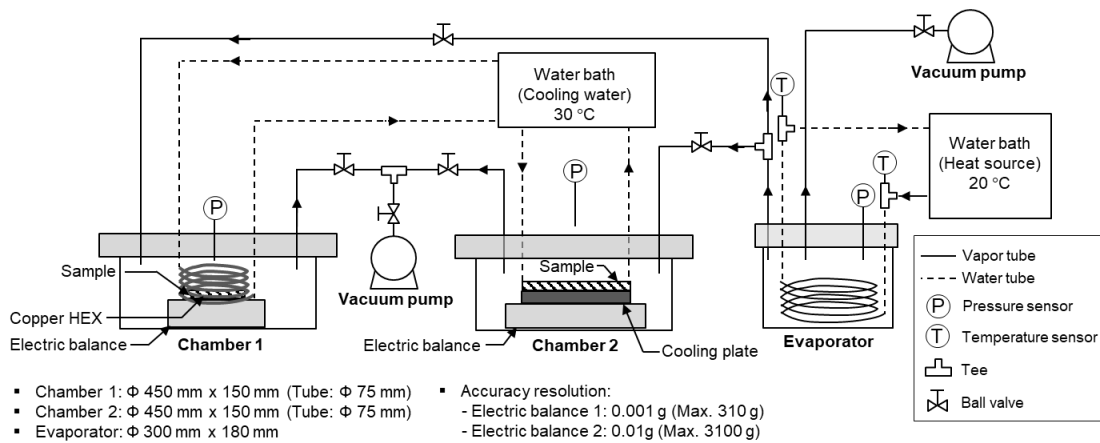
Fig. 3. 2 Schematic diagram of experimental system for measuring sorption dynamic

3.3 ANALYSIS METHODOLOGY

3.3.1 Linear Driving Force (LDF) Model

In general, adsorption dynamic characteristics are obtained through experimental methods and analyzed using various models. The linear driving force (LDF) model, which is one of the most frequently used models, assumes that the mass transfer rate between the adsorbent and the surrounding fluid is proportional to the difference between the concentration at the solid-fluid interface and the average concentration in the adsorbent [38]. In other words, both mass transfer at an interface and an internal side of the adsorbent affect the entire mass transfer. The following equations explain how the mass transfer phenomena are divided into interfacial and internal mass transfers. First of all, mass flux of water vapor from the bulk phase to the interface of the coated layer can be expressed as Eq. (3-1).

$$\frac{\partial q}{\partial t} = k_\mathrm{f} K (c - c_\mathrm{f}) \qquad (3\text{-}1)$$

An instantaneous partial adsorption equilibrium condition is assumed to calculate slope K of the adsorption isotherm. From the simple case having a linear equilibrium adsorption isotherm, it can be written that $q^*=Kc$ and $q_\mathrm{f}=Kc_\mathrm{f}$ [28]. Thus, Eq. (3-1) can be written as Eq. (3-2).

$$\frac{\partial q}{\partial t} = k_\mathrm{f}(q^* - q_\mathrm{f}) \qquad (3\text{-}2)$$

Mass flux of water vapor from the interface to the internal part of the coated layer can be described as Eq. (3-3).

$$\frac{\partial q}{\partial t} = k_\mathrm{s}(q_\mathrm{f} - q) \qquad (3\text{-}3)$$

The overall term of the mass transfer from the bulk phase to the internal part of the coated layer becomes Eq. (3-4).

$$\frac{\partial q}{\partial t} = K_{\mathrm{m}}(q^* - q) \tag{3-4}$$

Considering $q^* - q = (q^* - q_{\mathrm{f}}) + (q_{\mathrm{f}} - q)$ and Eq. (3-2) ~ (3-4), Eq. (3-5) is yielded.

$$\frac{1}{K_{\mathrm{m}}} = \frac{1}{k_{\mathrm{f}}} + \frac{1}{k_{\mathrm{s}}} = R_{\mathrm{f}} + R_{\mathrm{s}} = R_{\mathrm{f}} + \frac{d^2}{3D_{\mathrm{e}}} \tag{3-5}$$

The internal mass transfer resistance (R_{s}) was calculated as $d^2/3D_{\mathrm{e}}$ based on Patton et al. [39] that provided LDF approximations for various geometries of adsorbents.

3.3.2 Assumptions Regarding Non-isothermal Mass Transfer

Some assumptions were required to simplify the experiment and analysis. It is difficult to maintain a constant adsorbent temperature, meaning that the process becomes non-isothermal adsorption. Increase of the adsorbent temperature affects both equilibrium adsorption amount (q^*) and the effective diffusivity (D_{e}) in many cases using the LDF model. Dependence of the equilibrium adsorption amount on the adsorbent temperature can be easily measured by experimental methods and be expressed through the isotherm equation simply. On the other hand, the analysis of the non-isothermal intraparticle diffusion is particularly onerous in case of temperature effects, since the heat and mass balances are strongly coupled [40]. In most of researches on the numerical modeling of AHP systems, the adsorption rate is assumed to be controlled by the surface diffusion [41] expressed as the function of the adsorbent temperature [36]. Even this approach requires a pre-exponential diffusion constant that is normally taken from previous researches and is mostly applicable for the adsorbents frequently used such as a silica gel and a zeolite [42–44]. In contrast, it seems limited to apply this approach in cases of the composite adsorbents since the values are dependent on the kind of the impregnated material and its amount. Sharkawy [3] has applied the same pre-exponential value of the RD silica gel to the $CaCl_2$ confined KSK silica gel, and researches which have used constant the diffusion coefficient value independent on the temperature can be found [15,35,45,46].

This study also allowed the temperature rise and ignored the effect of the adsorbent temperature on the intraparticle diffusion. That is, the most representative effective diffusivity (D_e) which fits the adsorption dynamic curve the most was estimated through each sample. Meanwhile, the effect of temperature rise was considered in calculating the equilibrium adsorption amount (q^*) [35,47]. Following Eq. (3-6) presents heat balance in the coated adsorbent to fit the experimentally obtained temperature rise [36,48,49].

$$\left(C_a + C_{\text{plate}} + M_{\text{ad}} q c_{\text{p,v}}\right) \frac{dT_a}{dt}$$

$$= M_a \Delta H \frac{dq}{dt} - M_a \frac{dT_a}{dt} c_{\text{p,v}} (T_a - T_v) - \varepsilon \dot{m}_w c_p (T_{\text{w,i}} - T_a) \tag{3-6}$$

3.3.3 Importance of Reflecting Interfacial Mass Transfer

The mass flux from the vapor bulk to the interface should be identical to that from the interface to the internal part of the adsorbent. Many studies using the LDF model assume a saturated concentration at an interface between the vapor and the porous material, which may yield huge errors compared with actual data. Fig. 3. 3 contains three adsorption dynamic curves of WSS impregnated with 20 wt.% of lithium chloride to present possible error resulted from assuming the saturated condition at the interface: LDF based on experimentally estimated K_m marked with 'LDF_based on K_m', calculated data based on the LDF model including interfacial mass transfer resistance marked with 'LDF_with R_f', calculated data based on the LDF model assuming the saturated concentration at the interface and ignoring interfacial mass transfer resistance marked with 'LDF_without R_f'. The calculation of 'LDF_with R_f' was based on Eq. (3-3). Here, q_f was calculated by Eq. (3-2). Regarding 'LDF_without R_f', q_f of the Eq. (3-3) is assumed to be q^*, and k_s is considered as K_m according to the assumption. The mass transfer coefficients were calculated following the methodology presented in Fig. 3. 1 (a), and the detailed process will be discussed in the chapter 4. As shown in Fig. 3. 3, ignoring the interfacial mass transfer resistance (R_f) results in an evident error compared with the actual adsorption data; in particular, the thinner coated layer presented a substantial deviation. That is because the internal mass transfer resistance (R_s) becomes larger when the coated thickness (d) gets thicker, diminishing influence of the interfacial mass transfer resistance

(R_f).

Therefore, the effect of the interfacial mass transfer on the total mass transfer should be more carefully considered for coated adsorption beds, since a coated adsorbent layer is usually thinner than the diameter of an adsorbent grain. This study used an experimental method to define the interfacial mass transfer characteristics, i.e., the mass transfer of sufficiently thin-coated samples ($d=$ 27~79 μm) to ignore the internal mass transfer resistance was considered the interfacial mass transfer.

Finally, an effective diffusivity (D_e) is estimated based on the methodology presented in Fig. 3. 1 (a) to calculate the overall mass transfer coefficient (K_m) according to various thicknesses based on Eq. (3-5).
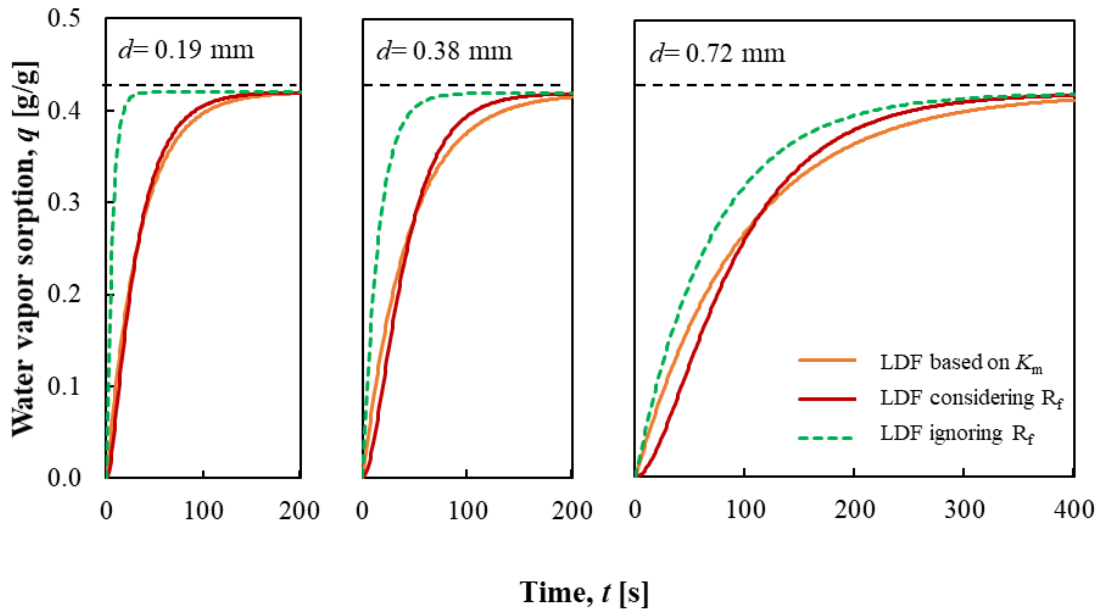
Fig. 3. 3 Comparison of sorption dynamic data according to calculation method

3.4 MATERIALS AND SAMPLES

3.4.1 Adsorbent

Recently, invented adsorbents with high adsorption performance have contributed to the commercialization of AHP. However, the high initial cost occupied by the adsorbents is considered one of the biggest hindrances for the widespread application of AHP. Composites Salt in Porous Matrix (CSPMS), particularly natural rock-based materials, have the advantages of cheap price and high adsorption performance enhancement [50–52]. Among them, Wakkanai Siliceous Shale (WSS) is a natural mesoporous hard mudstone mined from the northern part of Hokkaido, Japan. It is naturally derived from diatoms and planktonic organisms, mostly composed of silicon dioxide (SiO_2) and changed into siliceous shale with a crystal structure as a result of the increased temperature and pressure [53]. In this study, the mass transfer performance of a composite WSS is compared with that of A-type silica gel to prove its competitiveness. The adsorption equilibrium equations of the WSS composite [54] and the A-type silica gel [55] are described in Chapter 2 of this equation.

3.4.2 Samples

In this study, the adsorption dynamics were measured using stainless plates coated by WSS+LiCl 20 wt.% and A-type silica gel. A composite material of WSS was synthesized as follows. Micro powder of WSS was dried at 120 °C overnight and mixed into the prepared LiCl solution at room temperature. Then, the mixture was placed in a vacuum chamber for 30 minutes to promote the synthetization of lithium chloride into the matrix. The liquid state organic concrete additive (LDM6680, Celvolit) of 10 wt.% was added to the mixture to adhere adsorbent particles onto the sample plate properly. Finally, the composite material was dried in an oven after it is sprayed onto the stainless plates. Fig. 3. 4 shows the slurry state of composite WSS impregnated by lithium chloride and the stainless plate before and after they have been coated. The A-type silica gel was prepared and coated onto the plates using the same methods but without the impregnation of lithium chloride. In the coating process, the plate was placed onto a hot plate, through which hot water of 90 °C circulated to immediately dry the material as soon as it was sprayed. The coated thickness was measured at nine different spots of the sample using

an automatic thickness-measuring device (MJ-TG77, SATO Tech) three times. In this study, two separated experiments based on a gravimetric LPJ method were conducted. The first experiment was to analyze the mass transfer that occurred at the interface of the adsorbent. The coating thickness of the samples for this experiment was minimized to ignore the effect of internal diffusion and is, presenting the values between 27 and 79 μm. The other experiment was to measure the overall mass transfer from water vapor to the coated sample. Samples for this experiment were prepared considering possible coating thickness in actual use of adsorption heat pumps. Detailed specifications of the coated samples are shown in Table 3. 1.

(a) WSS+LiCl slurry

(b) Empty plate
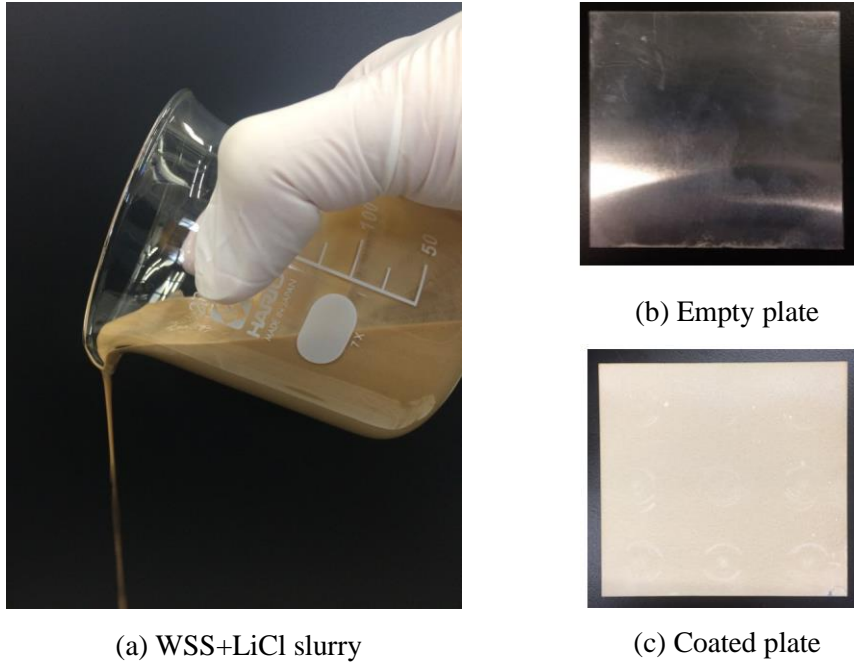
(c) Coated plate

Fig. 3. 4 (a) Slurry state WSS+LiCl 20 wt.%, (b) empty plate and (c) coated sample

Table 3. 1 Specifications of coated samples by WSS+LiCl 20wt.% and A-type silica gel

Material	Thickness [mm]	Coated amount [g/cm^2]
A-type silica gel	0.05	2.11 x 10^{-3}
	0.08	4.55 x 10^{-3}
	0.19	8.10 x 10^{-3}
	0.37	1.61 x 10^{-2}
	0.75	3.66 x 10^{-2}
WSS+LiCl 20 wt.%	0.03	2.28 x 10^{-3}
	0.07	4.64 x 10^{-3}
	0.19	9.10 x 10^{-3}
	0.38	1.71 x 10^{-2}
	0.71	3.86 x 10^{-2}

3.5 RESULTS AND DISCUSSIONS

3.5.1 Interfacial Mass Transfer

As mentioned, the point of this study is to separate the effects of interfacial and internal mass transfers from the overall mass transfer using an experimental method. Sufficiently thin samples to ignore the effects of the internal mass transfer resistance were prepared and tested (d= 27~79 µm). Fig. 3. 5 (a) and (b) show the measured water vapor sorption amount of samples coated by A-type silica gel and WSS+LiCl 20wt.%, respectively. The samples with different thicknesses presented almost identical calculated overall mass transfer coefficients, which implies that the obtained mass transfer characteristics may be considered interfacial mass transfer characteristics. During the experiments, the generated heat of adsorption was indirectly removed through a rolled-type copper heat exchanger. Fig. 3. 6 (a) and (b) represent the change of the adsorbent temperature and water vapor pressure according to time: (a) A-type silica gel, (b) WSS+LiCl 20 wt.%. The pressure inside of the chamber was kept around 1.7 kPa corresponding to the saturation temperature of 15℃. The calculated values of the samples with each thickness were almost related. Those values are almost identical, which supports that the internal mass transfer resistance can be ignored in this case as initially intended. For all cases, the LDF model presents acceptable consistency with experimental data. Based on the experiment, the estimated interfacial mass transfer coefficients are 0.026 s^{-1} and 0.035 s^{-1} for A-type silica gel and WSS+LiCl 20wt.%, respectively.
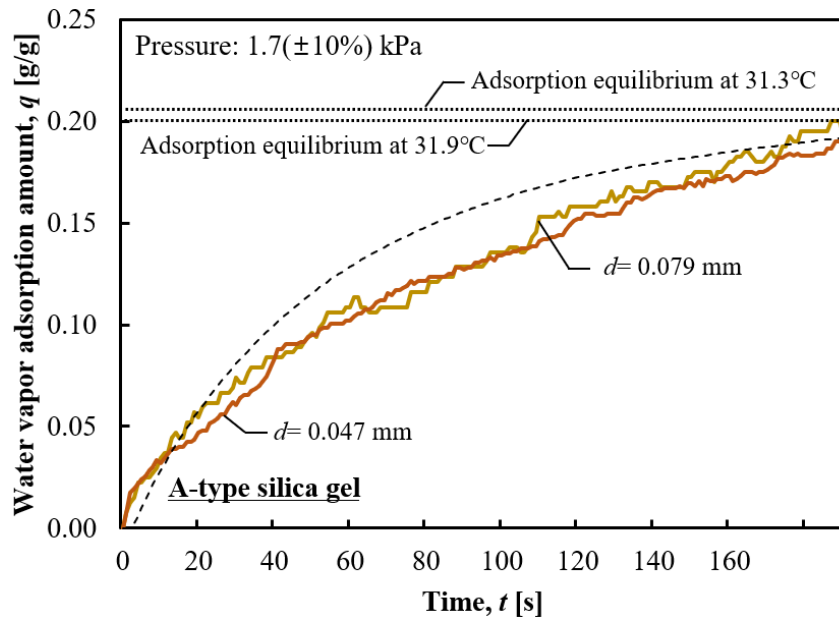
(a) A-type silica gel
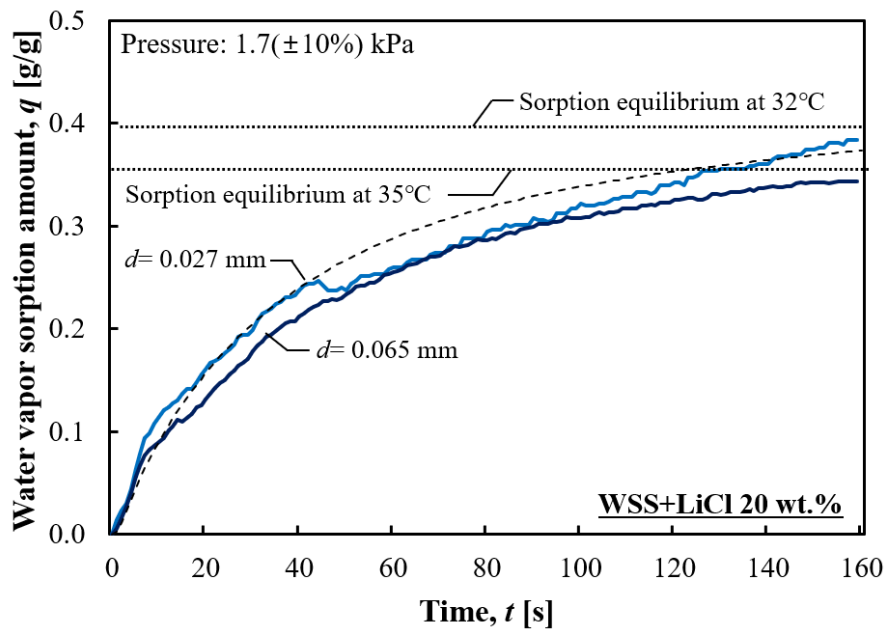
(b) WSS+LiCl 20 wt.%

Fig. 3. 5 Estimation of interfacial mass transfer coefficient (line: experiment, dash: LDF)
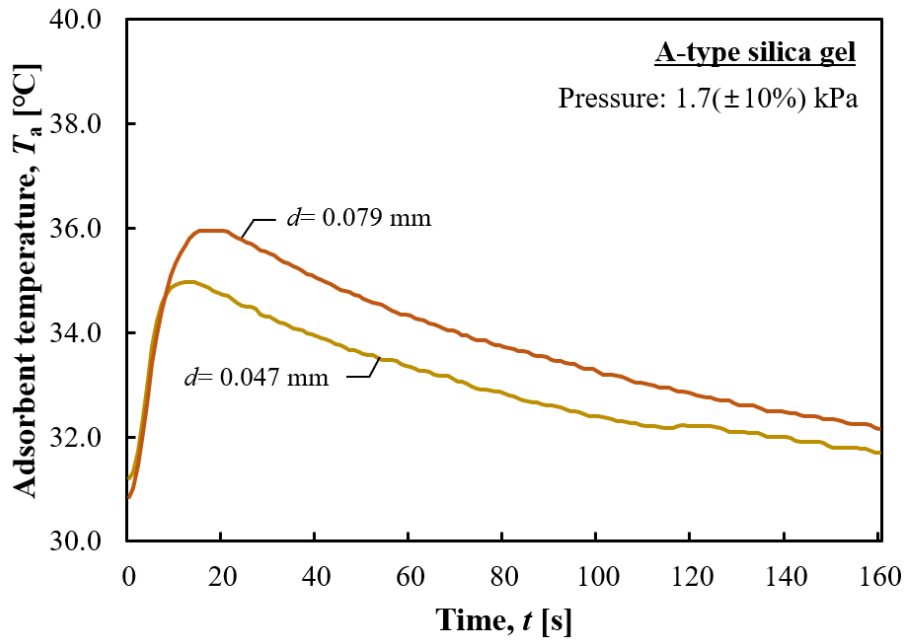
(a) A-type silica gel
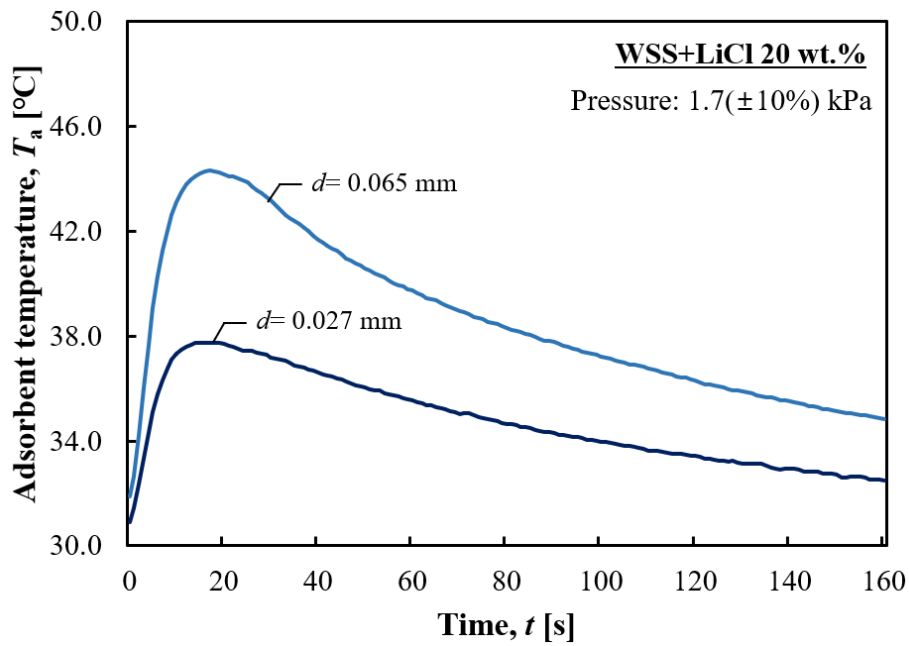
(b) WSS+LiCl 20 wt.%

Fig. 3. 6 Adsorbent temperature and pressure change (line: temperature, dash: pressure)

74

3.5.2 Overall Mass Transfer

The overall mass transfer characteristic of the samples with thickness of 0.19~0.75 mm was gravimetrically measured to calculate each overall mass transfer coefficient. The generated heat of adsorption was removed through the cooling plate that directly contacted the samples. Fig. 3. 7 (a) and (b) show the water vapor adsorption amount of coated A-type silica gel and WSS+LiCl 20 wt.% with different thicknesses, respectively. The adsorption dynamics of the samples were obviously revealed differently according to their thickness. In general, the calculated data using the LDF model tended to underestimate adsorption rate at the beginning of the adsorption process. The reason for this is because this research did not consider effect of the temperature change on the diffusivity. That is, the fitted adsorption dynamic curve was calculated based on the constant and representative effective diffusivity. According to Wang et al. [29] and Rezk et al. [56], the diffusivity depends on the surface temperature; a higher diffusivity value is obtainable when the surface temperature is higher. Fig. 3. 8 (a) and (b) represent the change of the adsorbent temperature and water vapor pressure according to time; the plane line refers to the experimentally obtained data, and the dash is the fitted one using the heat balance model of Eq. (3-6). As revealed in the figure, the adsorbent temperature rises as the water vapor is adsorbed by the adsorbents, showing the peak temperature between 35~44 °C. Therefore, the actual effective diffusivity is expected higher than the calculated representative effective diffusivity in all cases. However, the calculated model could be matched relatively properly after the mid-latter half as the adsorbent is cooled down.

Table 3. 2 summarizes adsorption characteristic times to reach 50 %, 80 % and 90 % of the saturation obtained from experimental data. Obviously, a thicker sample required more time to become saturated. The characteristic time between τ_0 and $\tau_{0.5}$ was merely approximately 15 % of that between $\tau_{0.5}$ and $\tau_{0.9}$. The A-type silica gel presented lower overall mass transfer coefficients than WSS+LiCl 20 wt.%. The small average pore size and large surface area of A-type silica gel are possible reasons for its decrease in adsorption rate. According to Dawoud et al. [21], a microporous silica gel requires longer time to reach saturation than a mesoporous silica gel. Also, the relatively higher adsorbent temperature of WSS+LiCl 20 wt.% can be a possible reason for this as mentioned earlier.
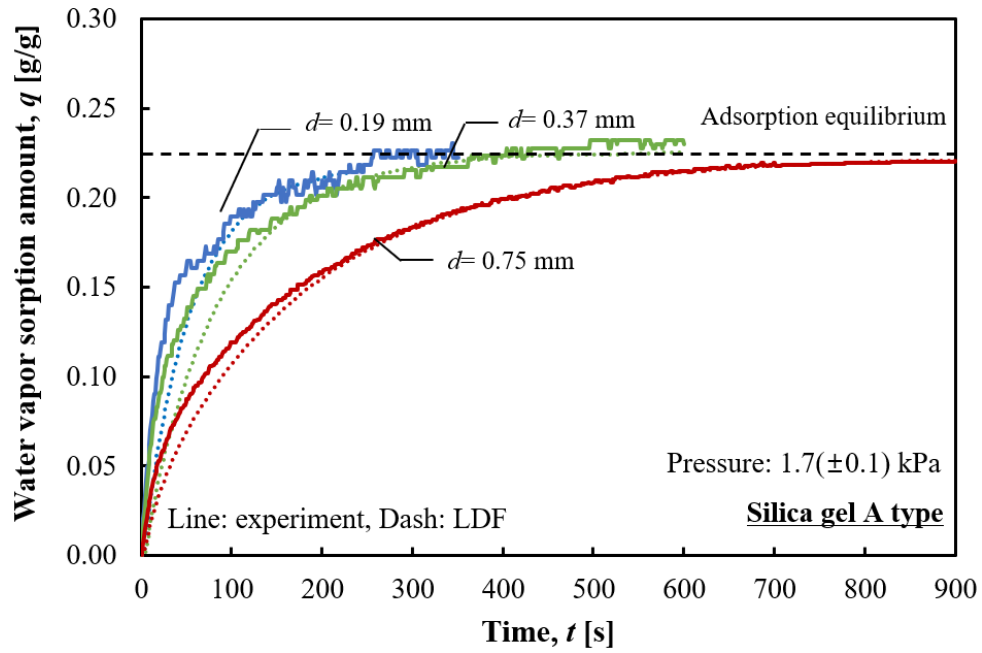
(a) A-type silica gel
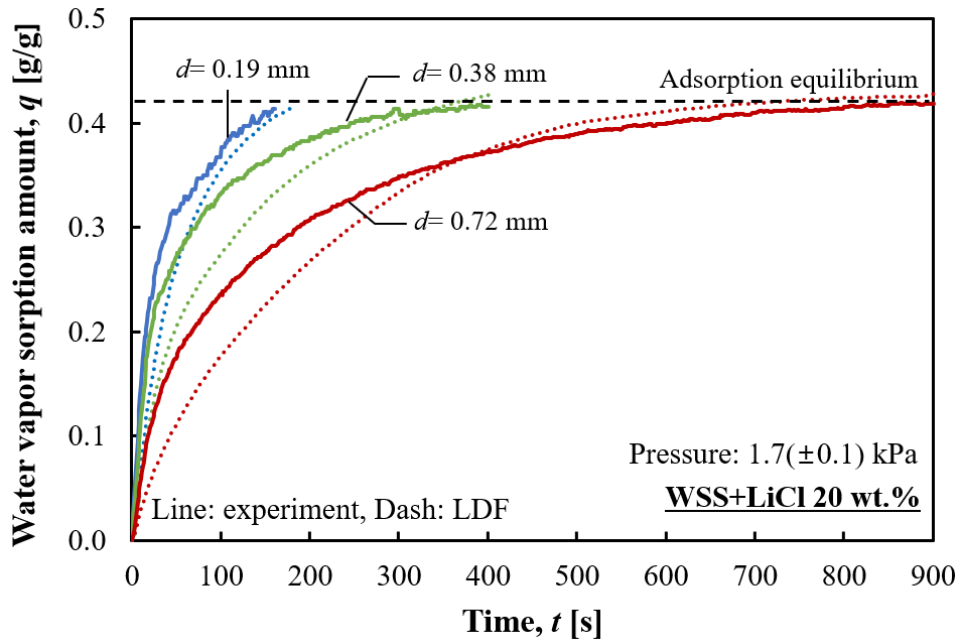
(b) WSS+LiCl 20 wt.%

Fig. 3. 7 Dynamic water vapor sorption amount of samples with different thickness

(line: experiment, dash: LDF)
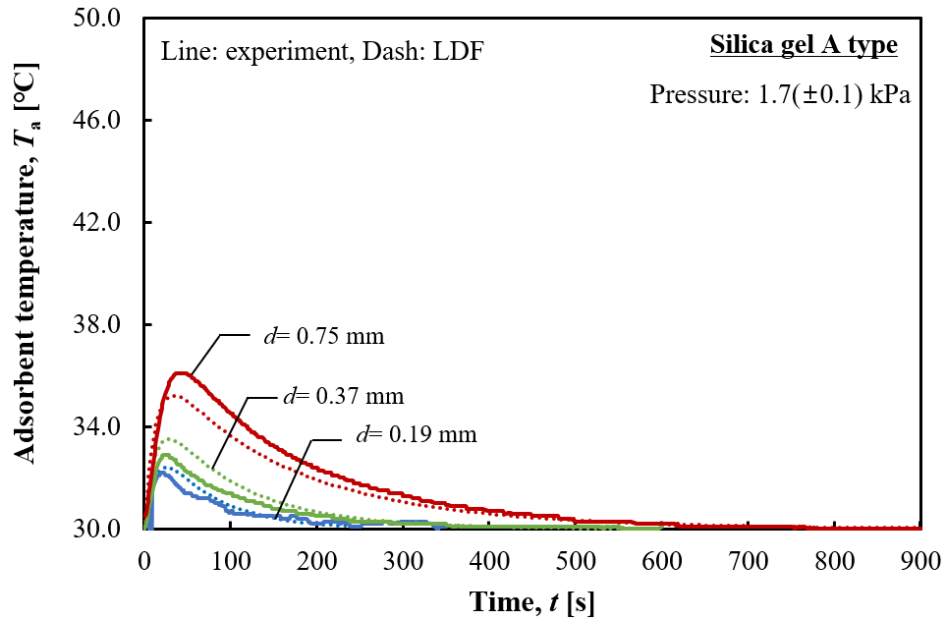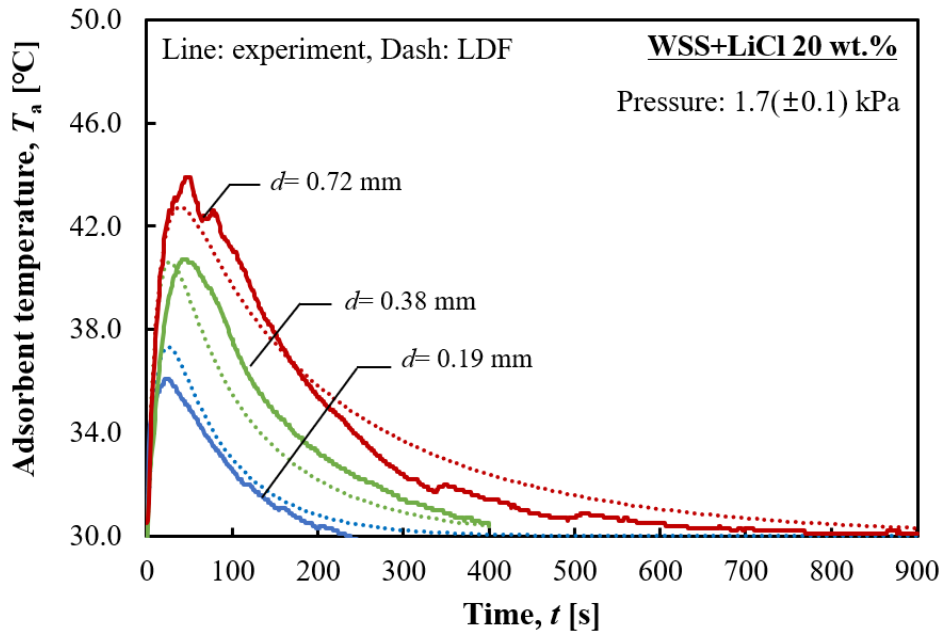
(a) A-type silica gel

(b) WSS+LiCl 20 wt.%

Fig. 3. 8 Adsorbent temperature and pressure change (line: experiment, dash: model)

Table 3. 2 Characteristic time and overall mass transfer coefficient of tested samples

	A-type silica gel			WSS+LiCl 20 wt.%		
d [mm]	0.19	0.37	0.75	0.19	0.38	0.72
$\tau_{0.5}$ [s]	21	33	97	18	24	73
$\tau_{0.8}$ [s]	92	143	314	71	103	252
$\tau_{0.9}$ [s]	150	219	522	100	176	423

3.5.3 Separation of Interfacial and Internal Mass Transfer

The effects of the interfacial and internal mass transfers were separated based on the obtained experimental data. The interfacial mass transfer characteristics were obtained from experiments using samples with thin-coated layers and assumed to be constant regardless of the coated thickness. The overall mass transfer coefficients of samples with thickness of 0.19~0.75 mm are experimentally obtained. The LDF model of Eq. (3-1)~(3-5) were applied to separate the mass transfer resistance at the interface and inner side of the material from the obtained overall mass transfer resistance. Finally, the effective diffusivity of each sample was calculated to estimate an overall mass transfer coefficient at random coated thickness. Table 3.3 summarizes the experimentally obtained, calculated mass transfer coefficients and average effective diffusivity of the samples.

Table 3. 3 Experimentally obtained, calculated mass transfer coefficients and effective diffusivities

	A-type silica gel			WSS+LiCl 20 wt.%		
d [mm]	0.19	0.37	0.75	0.19	0.38	0.72
k_f_exp [s⁻¹]	2.56×10^{-2}	2.56×10^{-2}	2.56×10^{-2}	3.55×10^{-2}	3.55×10^{-2}	3.55×10^{-2}
K_m_exp [s⁻¹]	2.35×10^{-2}	1.67×10^{-2}	1.11×10^{-3}	2.87×10^{-2}	2.26×10^{-2}	1.01×10^{-2}
K_m_cal [s⁻¹]	2.32×10^{-2}	1.86×10^{-2}	1.02×10^{-3}	3.01×10^{-2}	2.01×10^{-2}	1.02×10^{-2}
D_e [m²/s]	3.68×10^{-9}	2.25×10^{-9}	3.69×10^{-9}	1.84×10^{-9}	3.13×10^{-9}	2.42×10^{-9}
	(average: 3.21×10^{-9})			(average: 2.46×10^{-9})		

3.5.4 Optimization of Coated Thickness

The heat transfer resistance between a heat exchanger and an adsorbent can be reduced by coating the material onto the heat exchanger, which improves the heat and mass transfer rate. Furthermore, a coated adsorbent more quickly reaches the adsorption equilibrium than loose grains or granular adsorbers because of its thin-coated layer. The shortened cycle time causes the higher evaporation capacity and enhanced SCP, but frequent switches of the ad/desorption modes simultaneously result in the lower COP. The adsorption rate is strongly dependent on the coated thickness at non-isothermal conditions, and the evaporation capacity, SCP and COP are affected by the cycle time. Therefore, it is essential to analyze the adsorption dynamic characteristics at various coated thickness according to the cycle time. Both mass and heat transfer models of Eq. (3-1)~(3-5) and Eq. (3-6) were used for the optimization analysis. The experimentally obtained D_e and k_f were substituted, and the heat transfer model was utilized when calculating q^*.

Fig. 3. 9 (a), (b) represent the analysis on evaporation capacity of the samples coated by A-type silica gel and WSS+LiCl 20 wt.%, and Fig. 3. 10 (a), (b) depict the presumed SCP (specific cooling power) of the samples. The evaporation capacity was calculated by multiplying the evaporation latent heat of water at 15 °C and the water vapor sorption amount of each sample then divided by the adsorption time. In the case of A-type silica gel, the sample with coated thickness of 0.4 mm revealed obviously lower Q_e compared to others during the entire t_{ad}. Q_e of the sample with the thickness of 1.0 mm was similar or rather lower than those of the samples with d= 0.8 mm up to t_{ad} of 1.5 minutes. After that, it presented almost slightly higher Q_e than that of the sample of 0.8 mm. Thus, it is analyzed that thickness of the layer coated by A-type silica gel is not supposed to exceed 0.8 mm when considering both Q_e and SCP. In general, the samples coated with WSS+LiCl 20 wt.% showed quite similar tendency. The difference of Q_e between the sample having thickness of 0.8 and 1.0 mm was larger than that of A-type silica gel, which signifies applicability of thickness of 1.0 mm.
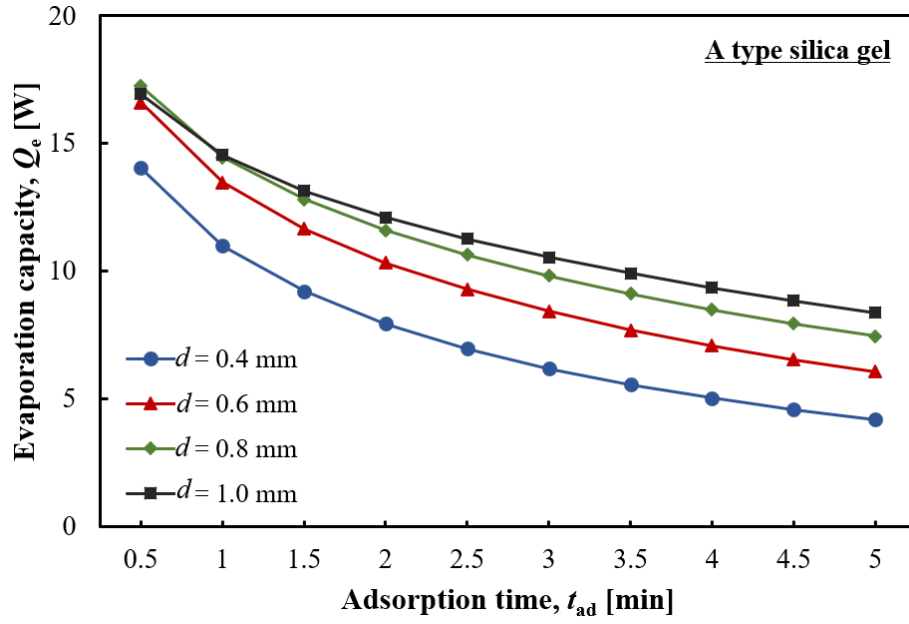
(a) A-type silica gel
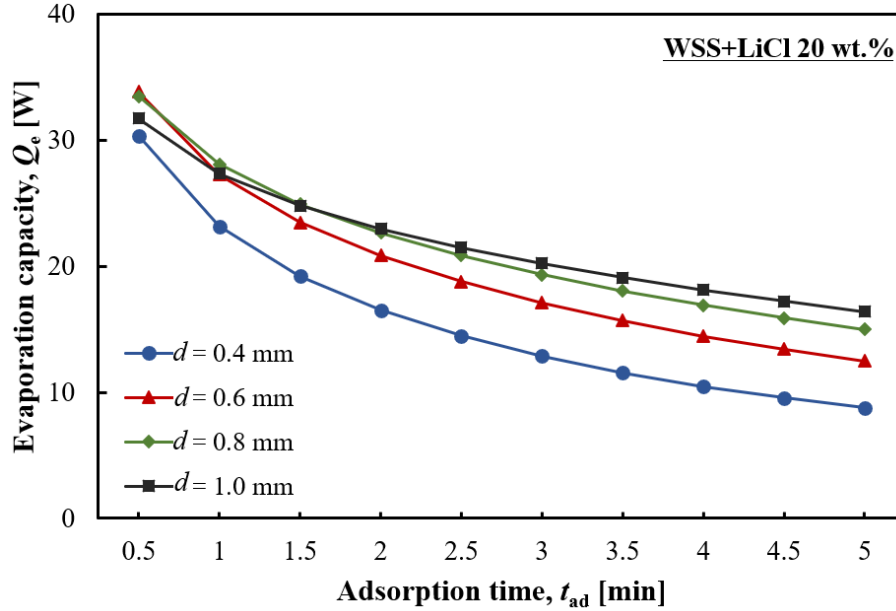
(b) WSS+LiCl 20 wt.%

Fig. 3. 9 Effect of coated thickness on evaporation capacity of samples according to sorption time
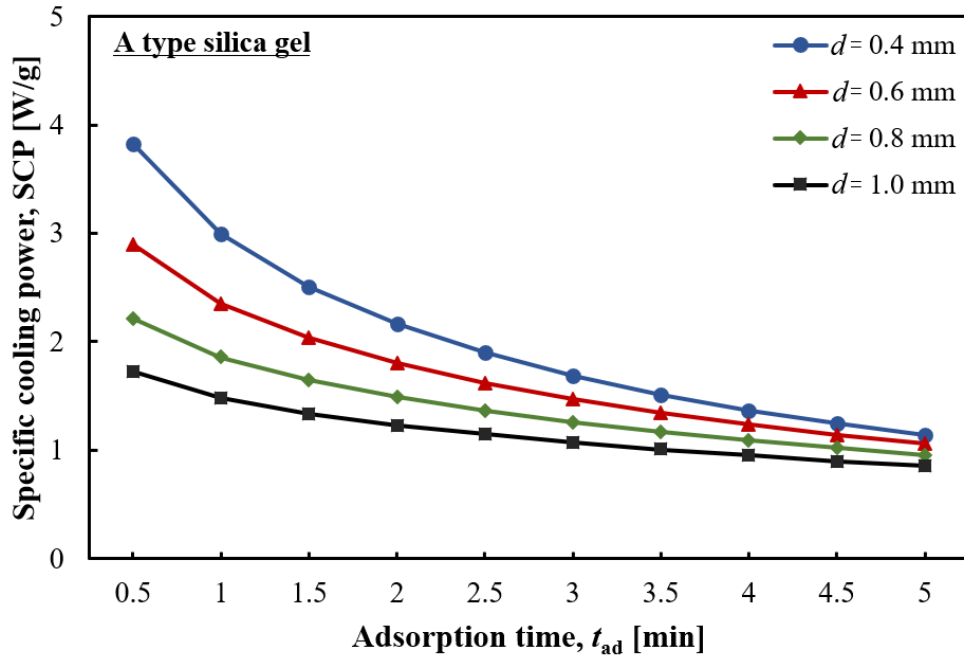
(a) A-type silica gel
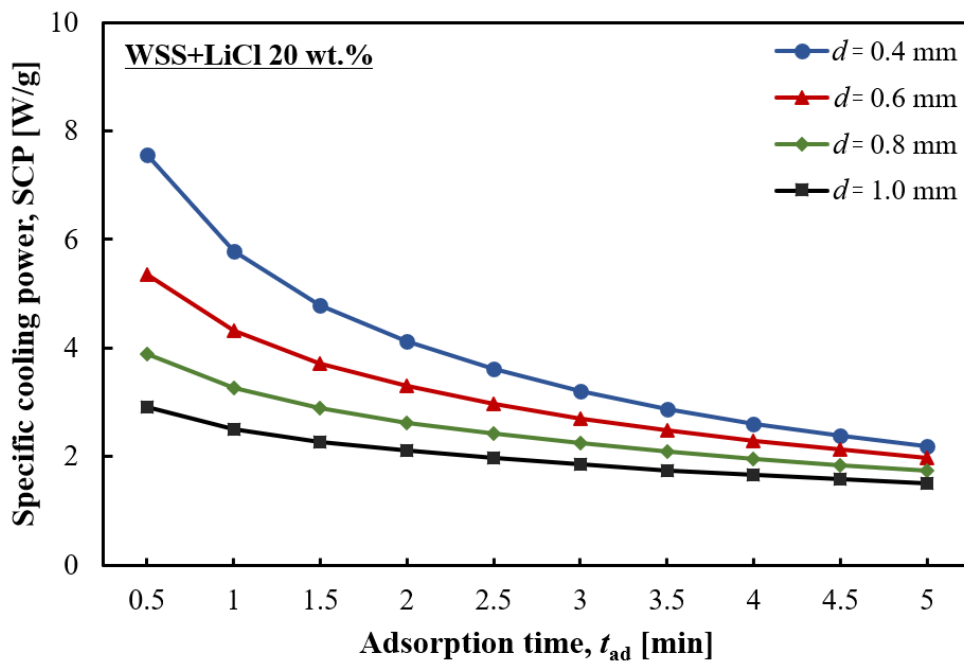
(b) WSS+LiCl 20 wt.%

Fig. 3. 10 Effect of coated thickness on SCP of samples according to sorption time

3.6 SUMMARY

In this study, the adsorption dynamic characteristics of the samples coated by two different adsorbents were experimentally studied: WSS+LiCl 20 wt.% and A-type silica gel. The experiments followed a gravimetric LPJ method, and the obtained data were analyzed using the LDF model.

This study separated the effect of interfacial and internal mass transfers using experimental methods and the LDF model. Ignoring the interfacial mass transfer resistance in the calculation of the overall mass transfer coefficient using the LDF model results in notable discrepancy with the actual data. After the interfacial mass transfer coefficient has been experimentally estimated, the interfacial and internal mass transfer resistance can be separated from the overall mass transfer resistance of the coated sample at 0.19~0.75 mm. The effective diffusivity of the coated layers can also be estimated based on the LDF model, which enables us to calculate the overall mass transfer coefficient at any random thickness of coated layers. The experimentally obtained and calculated overall mass transfer coefficients based on the LDF model were matched acceptably.

The A-type silica gel presented lower overall mass transfer coefficients than those of WSS+LiCl 20 wt.%. The small average pore size, large surface area of the A-type silica gel, effect of non-isothermal adsorption are possible reasons for this.

When considering the mechanical strength of the coated layer and the water vapor sorption amount, WSS appears to be a possible matrix of the impregnation to enhance the adsorption performance. The effects of the impregnation amount and type of salts on the adsorption dynamic should be analyzed in future studies.

3.7 REFERENCE

[1]   M. Chorowski, P. Pyrka, Modelling and experimental investigation of an adsorption chiller using low-temperature heat from cogeneration, Energy. 92 (2015) 221–229.

[2]   S. Nakabayashi, K. Nagano, M. Nakamura, J. Togawa, A. Kurokawa, Improvement of water vapor adsorption ability of natural mesoporous material by impregnating with chloride salts for development of a new desiccant filter, Adsorption. 17 (2011) 675–686.

[3]   I.I. El-Sharkawy, On the linear driving force approximation for adsorption cooling applications, Int. J. Refrig. 34 (2011) 667–673.

[4]   Y.. Aristov, G. Restuccia, G. Cacciola, V.. Parmon, A family of new working materials for solid sorption air conditioning systems, Appl. Therm. Eng. 22 (2002) 191–204.

[5]   A. Kurokawa, J. Togawa, Y. Nabeshima, K. Nagano, The Evaluation of the Moisture Sorption Mechanism of Chloride-Impregnated Wakkanai Siliceous Shale, KAGAKU KOGAKU RONBUNSHU. 37 (2011) 394–399.

[6]   A. Lass-Seyoum, D. Borozdenko, T. Friedrich, K. Schönfeld, J. Adler, S. Mack, Experimental Investigation on Adsorption and Surface Characteristics of Salt Hydrates and Hydrophobic Porous Matrix Based Composites, Mod. Environ. Sci. Eng. 3 (2017) 67–81.

[7]   H. Zhao, S. Jia, J. Cheng, X. Tang, M. Zhang, H. Yan, W. Ai, Experimental investigations of composite adsorbent 13X/CaCl2 on an adsorption cooling system, Appl. Sci. 7 (2017).

[8]   K. Fayazmanesh, C. Mccague, M. KALRA, M. Bahrami, Water adsorption of CaCl2 confined in mesoporous silica gel with various pore sizes, 2014.

[9]   X. Zheng, T.S. Ge, R.Z. Wang, Recent progress on desiccant materials for solid desiccant cooling systems, Energy. 74 (2014) 280–294.

[10]   I. Glaznev, I. Ponomarenko, S. Kirik, Y. Aristov, Composites CaCl2/SBA-15 for adsorptive transformation of low temperature heat: Pore size effect, Int. J. Refrig. 34 (2011) 1244–1250.

[11]   H. Demir, M. Mobedi, S. Ülkü, A review on adsorption heat pump: Problems and solutions, Renew. Sustain. Energy Rev. 12 (2008) 2381–2403.

[12]   A. Freni, L. Bonaccorsi, L. Calabrese, A. Caprì, A. Frazzica, A. Sapienza, SAPO-34 coated adsorbent heat exchanger for adsorption chillers, Appl. Therm. Eng. 82 (2015) 1–7.

[13]   L.Z. Zhang, L. Wang, Performance estimation of an adsorption cooling system for automobile waste heat recovery, Appl. Therm. Eng. 17 (1997) 1127–1139.

[14]   Y.I. Aristov, I.S. Glaznev, I.S. Girnik, Optimization of adsorption dynamics in adsorptive chillers: Loose grains configuration, Energy. 46 (2012) 484–492.

[15]   A. Frazzica, G. Füldner, A. Sapienza, A. Freni, L. Schnabel, Experimental and theoretical analysis of the kinetic performance of an adsorbent coating composition for use in adsorption chillers and heat pumps, Appl. Therm. Eng. 73 (2014) 1022–1031.

[16]   H. van Heyden, G. Munz, L. Schnabel, F. Schmidt, S. Mintova, T. Bein, Kinetics of water adsorption in microporous aluminophosphate layers for regenerative heat exchangers, Appl. Therm. Eng. 29 (2009) 1514–1522.

[17]   B. Dawoud, Water vapor adsorption kinetics on small and full scale zeolite coated adsorbers; A comparison, Appl. Therm. Eng. 50 (2013) 1645–1651.

[18]   K. Grabowska, J. Krzywanski, W. Nowak, M. Wesolowska, Construction of an innovative adsorbent bed configuration in the adsorption chiller - Selection criteria for effective sorbent-glue pair, Energy. 151 (2018) 317–323.

[19]   K. Grabowska, M. Sosnowski, J. Krzywanski, K. Sztekler, W. Kalawa, A. Zylka, W. Nowak, The Numerical Comparison of Heat Transfer in a Coated and Fixed Bed of an Adsorption Chiller, J. Therm. Sci. 27 (2018) 421–426.

[20]   K. Grabowska, M. Sosnowski, J. Krzywanski, K. Sztekler, W. Kalawa, A. Zylka, W. Nowak, Analysis of heat transfer in a coated bed of an adsorption chiller, MATEC Web Conf. 240 (2018) 0–3.

[21]   B. Dawoud, Y. Aristov, Experimental study on the kinetics of water vapor sorption on selective water sorbents, silica gel and alumina under typical operating conditions of sorption heat pumps, Int. J. Heat Mass Transf. 46 (2003) 273–281.

[22]   L. Schnabel, M. Tatlier, F. Schmidt, A. Erdem-Şenatalar, Adsorption kinetics of zeolite coatings directly crystallized on metal supports for heat pump applications (adsorption kinetics of zeolite coatings), Appl. Therm. Eng. 30 (2010) 1409–1416.

[23]   A. Sapienza, A. Velte, I. Girnik, A. Frazzica, G. Füldner, L. Schnabel, Y. Aristov, "Water - Silica Siogel" working pair for adsorption chillers: Adsorption equilibrium and dynamics, Renew. Energy. 110 (2017) 40–46.

[24]   S. Santamaria, A. Sapienza, A. Frazzica, A. Freni, I.S. Girnik, Y.I. Aristov, Water adsorption dynamics on representative pieces of real adsorbers for adsorptive chillers, Appl. Energy. 134 (2014) 11–19.

[25]   J. Ammann, B. Michel, P.W. Ruch, Characterization of transport limitations in SAPO-34 adsorbent coatings for adsorption heat pumps, Int. J. Heat Mass Transf. 129 (2019) 18–27.

[26]   A. Sapienza, S. Santamaria, A. Frazzica, A. Freni, Y.I. Aristov, Dynamic study of adsorbers by a new gravimetric version of the Large Temperature Jump method, Appl. Energy. 113 (2014) 1244–1251.

[27]   M.C. Annesini, L. Marrelli, V. Piemonte, L. Turchetti, Mass Transfer Coefficient, in: Artif. Organ Eng., Springer London, London, 2017: pp. 23–31.

[28]   D.O. Cooney, Determining external film mass transfer coefficients for adsorption columns, AIChE J. 37 (1991) 1270–1274.

[29] K. Wang, S. Qiao, X. Hu, Study of isosteric heat of adsorption and activation energy for surface diffusion of gases on activated carbon using equilibrium and kinetics information, Sep. Purif. Technol. 34 (2004) 165–176.

[30] I. Medveď, R. Černý, Surface diffusion in porous media: A critical review, Microporous Mesoporous Mater. 142 (2011) 405–422.

[31] W.D. Abdelmottaleb Ouederni, Estimate of Effective Diffusivity Starting from the Phenol Adsorption Profiles on an Activated Carbon in Discontinuous Suspension, J. Chem. Eng. Process Technol. 05 (2013) 2020.

[32] A. Kapoor, R.T. Yang, Contribution of concentration-dependent surface diffusion to rate of adsorption, Chem. Eng. Sci. 46 (1991) 1995–2002.

[33] A. Freni, G. Maggio, F. Cipitì, Y.I. Aristov, Simulation of water sorption dynamics in adsorption chillers: One, two and four layers of loose silica grains, Appl. Therm. Eng. 44 (2012) 69–77.

[34] Y.I. Aristov, Optimal adsorbent for adsorptive heat transformers: Dynamic considerations, Int. J. Refrig. 32 (2009) 675–686.

[35] A. Velte, G. Füldner, E. Laurenz, L. Schnabel, Advanced Measurement and Simulation Procedure for the Identification of Heat and Mass Transfer Parameters in Dynamic Adsorption Experiments, Energies. 10 (2017) 1130.

[36] A. Sakoda, M. Suzuki, Fundamental study on solar powered adsorption cooling system, J. Chem. Eng. Japan. 17 (1984) 52–57.

[37] A.M. Ribeiro, T.P. Sauer, C.A. Grande, R.F.P.M. Moreira, J.M. Loureiro, A.E. Rodrigues, Adsorption equilibrium and kinetics of water vapor on different adsorbents, Ind. Eng. Chem. Res. 47 (2008) 7019–7026.

[38] M. Gwadera, K. Kupiec, Investigation of water vapour adsorption on silica gel grains coated on a metal pipe, Adsorpt. Sci. Technol. 33 (2015) 499–511.

[39] A. Patton, B.D. Crittenden, S.P. Perera, Use of the Linear Driving Force Approximation to Guide the Design of Monolithic Adsorbents, Chem. Eng. Res. Des. 82 (2004) 999–1009.

[40] J.H. Hills, Non-isothermal adsorption in a pellet, Chem. Eng. Sci. 46 (1991) 69–74.

[41] Marlinda, A.S. Uyun, T. Miyazaki, Y. Ueda, A. Akisawa, Marlinda, A.S. Uyun, T. Miyazaki, Y. Ueda, A. Akisawa, Performance Analysis of a Double-effect Adsorption Refrigeration Cycle with a Silica Gel/Water Working Pair, Energies. 3 (2010) 1704–1720.

[42] L.X. Gong, R.Z. Wang, Z.Z. Xia, C.J. Chen, Design and performance prediction of a new generation adsorption chiller using composite adsorbent, Energy Convers. Manag. 52 (2011) 2345–2350.

[43] M. Verde, K. Harby, R. de Boer, J.M. Corberán, Performance evaluation of a waste-heat driven adsorption system for automotive air-conditioning: Part I –

Modeling and experimental validation, Energy. 116 (2016) 526–538.

[44] S. Bruckner, T. Demmer, M. Ganswind, D. Bathen, Modeling of Water Adsorption in SAPO-34-Coated Aluminum Foam, Chemie-Ingenieur-Technik. 89 (2017) 757–764.

[45] J. Xiao, L. Tong, D. Cossement, P. Bénard, R. Chahine, CFD simulation for charge–discharge cycle of cryo-adsorptive hydrogen storage on activated carbon, Int. J. Hydrogen Energy. 37 (2012) 12893–12904.

[46] S. Li, S. Deng, L. Zhao, R. Zhao, M. Lin, Y. Du, Y. Lian, Mathematical modeling and numerical investigation of carbon capture by adsorption: Literature review and case study, Appl. Energy. 221 (2018) 437–449.

[47] J. Xiao, R. Peng, D. Cossement, P. Bénard, R. Chahine, Heat and mass transfer and fluid flow in cryo-adsorptive hydrogen storage system, Int. J. Hydrogen Energy. 38 (2013) 10871–10879.

[48] M. Verde, L. Cortés, J.M. Corberán, A. Sapienza, S. Vasta, G. Restuccia, Modelling of an adsorption system driven by engine waste heat for truck cabin A/C. Performance estimation for a standard driving cycle, Appl. Therm. Eng. 30 (2010) 1511–1522.

[49] J. Xiao, R. Li, P. Bénard, R. Chahine, Heat and mass transfer model of multicomponent adsorption system for hydrogen purification, Int. J. Hydrogen Energy. 40 (2015) 4794–4803.

[50] H. Chen, Q. Cui, Y. Tang, X. Chen, H. Yao, Attapulgite based LiCl composite adsorbents for cooling and air conditioning applications, Appl. Therm. Eng. 28 (2008) 2187–2193.

[51] A. Sapienza, I.S. Glaznev, S. Santamaria, A. Freni, Y.I. Aristov, Adsorption chilling driven by low temperature heat: New adsorbent and cycle optimization, Appl. Therm. Eng. 32 (2012) 141–146.

[52] G. Bulut, M. Chimeddorj, F. Esenli, M.S. Çelik, Production of desiccants from Turkish bentonites, Appl. Clay Sci. 46 (2009) 141–147.

[53] H. Liu, K. Nagano, J. Togawa, H. Liu, K. Nagano, J. Togawa, Performance of LiCl Impregnated Mesoporous Material Coating over Corrugated Heat Exchangers in a Solid Sorption Chiller, Energies. 11 (2018) 1565.

[54] M. Ben Yahia, Y. Ben Torkia, S. Knani, M.A. Hachicha, M. Khalfaoui, A. Ben Lamine, Models for type VI adsorption isotherms from a statistical mechanical formulation, Adsorpt. Sci. Technol. 31 (2013) 341–357.

[55] A. Li, Experimental and Theoretical Studies on the Heat Transfer Enhancement of Adsorbent Coated Heat Exchangers, National University of Singapore, 2014.

[56] A. Rezk, R. Al-Dadah, S. Mahmoud, A. Elsayed, Experimental investigation of metal organic frameworks characteristics for water adsorption chillers, Proc. Inst. Mech. Eng. Part C J. Mech. Eng. Sci. 227 (2013) 992–1005.

CHAPTER 4. MODELING OF AHP SYSTEM BASED ON EXPERIMENTAL ESTIMATION OF HEAT AND MASS TRANSFER COEFFICIENTS

4.1 INTRODUCTION

Because of increasing environmental issues and sustainable energy consumption, the adsorption heat pump (AHP) has attracted considerable interest owing to its ecofriendly operation. Typically, it utilizes natural refrigerants such as water and ammonia instead of chlorofluorocarbons and hydrochlorofluorocarbons, which cause ozone depletion [1]. Additionally, the applicability of low-level heat sources (<100 °C) enables the utilization of waste heat and solar energy. However, several disadvantages, such as large system volume, discontinuous cooling effect, low coefficient of performance (COP), and high initial cost, have hindered the commercialization of AHP systems [2]. As the overall performance of AHP systems strongly relies on the heat and mass transfer characteristics of the adsorbate into the adsorbent, numerous studies have been conducted to improve adsorption behavior. According to these studies, composite adsorbents, which are porous host matrices impregnated with inorganic salts, exhibit high equilibrium adsorption capacities compared with traditional working pairs. Following studies have verified the enhanced adsorption capacity of silica gels impregnated with additional salts. Aristov et al. [3] demonstrated that KSK silica gel impregnated with 33.7 wt.% $CaCl_2$ exhibited an uptake amount that was approximately five times larger than that of pure silica gel. Sharkawy et al. [4] compared the water vapor adsorption dynamics of RD and KSK silica gel impregnated with $CaCl_2$ to verify the improved adsorption amount, using impregnation. Daou et al. [5] compared the saturation adsorption amount of composite materials that had different impregnation ratios. Zheng et al. [6] studied the effects of the pore size of silica gels, demonstrating that a smaller water uptake amount per dry sorbent mass was observed for adsorbents with smaller pore diameters. Zhang et al. reported the advantages of using $CaCl_2$ such as thermal stability, low cost, and large sorption capacity [7]. They also indicated that LiCl with crystal water produced HCL when the drying temperature was beyond 98 °C. Not only studies regarding the enhancement of adsorption capacity, but also those on the adsorption dynamic characteristics and system performance of silica gel-based composite materials have been reported. Aristov et al. [8] measured the adsorption and desorption dynamic characteristics of SWS-1L at isobaric conditions and proved the idea of compact adsorption units using SWS-1L. Furthermore, they estimated the effective diffusivity of composite materials at various working

temperatures and pressures [9]. Finally, Saha et al. [10] demonstrated improved system performance by applying SWS-1L based on a simulation model. However, Kurokawa et al. [11] reported that the pores of silica gel expanded because of impregnated chlorides when the synthesized amount exceeded 5 wt.%. The expansion resulted in matrix dissolution and unsustainable pore structures. To address the challenges of using porous media as a parent matrix for impregnating chloride, Wakkanai siliceous shale (WSS) was adopted in the current study. Detailed explanations about this natural mesoporous material will be provided in Chapter 2. Our research team has previously reported the enhanced adsorption capacity of WSS composites compared with traditional adsorbents and verified the applicability of WSS as a parent matrix of a composite adsorbent. Nakabayashi et al. [12] proposed an appropriate supporting amount of chlorides based on water sorption amount and pore volume to prevent a carryover. Liu et al. [13] presented the stability of WSS impregnated with LiCl by repeating adsorptions (0.55 g/g, 25 °C, RH 95 %) and desorption (0.1 g/g, 60 °C, RH 5 %) for 250 repetitions. Furthermore, WSS impregnated with LiCl presented a two-step-like sorption isotherm at pressures around 0.6 kPa when the adsorbent temperature was 30 °C, which was attractive for lower cooling temperatures [14]. However, studies regarding adsorption dynamics using WSS as a host matrix of chloride is insufficient. Therefore, experimental studies must be performed to estimate adsorption rates. Large temperature jump (LTJ) [15,16] and large pressure jump (LPJ) [17,18] are the most representative methods. In the LTJ method, the adsorbent temperature is adjusted at a certain pressure to promote adsorption, whereas in the LPJ method, the adsorption pressure is controlled. Experimentally obtained adsorption kinetics data have been analyzed using various dynamic models. Aristov et al. [9,19] employed a Fickian diffusion model to fit the data of spherical pellets. A model for slab-shaped particles has been used by Freni et al. [20]. A model employing the mass-conservation equation was utilized by Wang et al. [21] and Medved et al. [22]. Sun et al. developed a kinetic formulation from the rigor of the partition function of each adsorptive site and the kinetics theory of adsorbate molecules with the analogy of Langmuir kinetics [23]. The linear driving force (LDF) model is widely used to simulate the dynamic behavior of adsorption chillers owing to its simplicity [24]. This model comprises two main parameters: the mass transfer coefficient and driving force. The driving force is the difference between the equilibrium and current average adsorption amount. The mass

transfer coefficient can be obtained according to the relationship between the size of the adsorbent, its geometric shape [25], and its diffusivity. Generally, in numerical AHP models, the thermal effect on the intraparticle diffusivity is calculated using the equation proposed by Sakoda et al. [26]. This equation contains terms corresponding to the activation energy and adsorbent temperature, as well as a pre-exponential constant that varies according to the material. The lumped modeling of AHP systems, which has been proposed by numerous researchers, employs the LDF model and the equation proposed by Sakoda et al. [26]. Verde et al. [27] modeled and tested AHP systems powered by wasted engine heat. Gong et al. [28] developed a numerical model involving mass recovery between two adsorbers. Chahbani et al. [29] studied heat and mass transfer rates using a numerical model. In this model, heat transfer was analyzed from a one-dimensional viewpoint, but the lumped LDF model was used to estimate the mass transfer. Meanwhile, the actual mass transfer through porous media can be categorized into intra- and interparticle diffusion [30]. Intraparticle diffusion depends on the particle size [9,16], diffusion mechanisms such as surface diffusion [22,31], and the Knudsen diffusion [32]. Meanwhile, the viscous flow through particles, namely interparticle diffusion, depends on the porosity of the bed [33] and number of particle layers [34,35]. Furthermore, the effect of heat transfer on mass transfer must be considered because they are coupled [36]. Freni et al. [37] compared the adsorbent temperature and uptake mapping according to the grain configuration, and the results showed that the water adsorption was noticeably faster for the grain monolayer owing to the more efficient heat transfer.

As cited above, parameters pertaining to the geometric structure, such as the particle size and number of layers, affect mass transfer characteristics significantly. However, the LDF model calculates the adsorption rate according to the particle size and do not consider the effect of number of layers [24–29,38–41]. This can result in a large error in the calculated adsorption amount. Multidimensional interparticle diffusion analysis is required to assess the effect of such geometric characteristics; however, it increases the computational time and diminishes the simplicity and ability to perform quick calculations, which are the greatest advantages of zero-dimensional modeling. Similarly, the filled density of the adsorbent can impose a similar effect on the adsorption rate. For filled adsorbents, this effect can be easily analyzed by experimentally estimating the mass transfer coefficients at various filled densities.

Studies regarding the experimental estimation of a heat transfer coefficient of an adsorption heat exchanger have been performed by Li et al. [42]. Furthermore, theoretical models for calculating the overall heat transfer coefficient have been reported [43–45]. Computational fluid dynamics has been widely used for the numerical analysis of heat transfer. Grabowska et al. verified the heat transfer enhancement of a coated layer compared with a fixed layer, based on a numerical comparison using Ansys FLUENT [46]. Sosnowski et al. proposed a polyhedral meshing method for more accurate solutions achieved using a lower cell amount [47]. More recently, artificial-intelligence-based approaches have been applied in the analysis of heat transfer. Grabowska et al. proposed artificial intelligence algorithms that comprise fuzzy logic to analyze heat transfer coefficients based on a specific set of received input data [48].

This study focused on zero-dimensional AHP system simulations based on experimentally estimated heat and mass transfer characteristics for minimizing errors resulting from traditional heat and mass transfer evaluations. The direct measurement of heat and mass transfer characteristics of an entire adsorption heat exchanger is intuitive because complicated multidimensional numerical analyses are not required. Furthermore, the methodology can be considered applied engineering; hence, it can be easily applied to various types of materials. The heat and mass transfer coefficients of the adsorbers, which were filled with an A-type silica gel or WSS impregnated with 20 wt.% LiCl at different filling densities, were experimentally estimated. The overall mass transfer coefficients were measured at various adsorbent temperatures in the range of 30–60 °C. Additionally, the overall heat transfer coefficients of the adsorbers were experimentally estimated when the inlet water temperature was changed from 80 to 30 °C to analyze the actual working conditions of AHP systems. The estimated coefficients were utilized for numerical modeling to analyze the AHP performance characteristics. Finally, the performance of the system employing the WSS composite was compared with that of the system employing the A-type silica gel to validate its effectiveness.

4.2 EXPERIMENTAL ESTIMATION OF COEFFICIENT

4.2.1 Adsorbent

Composite "salt inside porous matrix" is an adsorbent that exhibits an enhanced equilibrium adsorption amount compared with that of traditional working pairs. As a type of porous matrix, a natural mesoporous hard mudstone called the WSS mined from the northern part of Hokkaido in Japan can be used [6, 7, 31, 32].

4.2.2 Experimental Methodology

Table 4. 1 summarizes the geometric specifications of the heat exchanger used in this study, and Fig. 4. 1 provides its schematics. In the adsorption heat exchanger, PT-100 sensors (HAYASHI DENKO, ±0.25 °C) measured the water inlet/outlet temperature, and thermocouples (±0.5 °C, diameter 1 mm) that were inserted between fins measured the temperature of each spot. In this study, the four temperatures measured by the inserted thermocouples were assumed as the adsorbent temperature at each spot, and finally their average value was used as the final adsorbent temperature. In this research, the instantaneous equilibrium condition between adsorbent particles and water vapor flow through the particles was assumed [51].
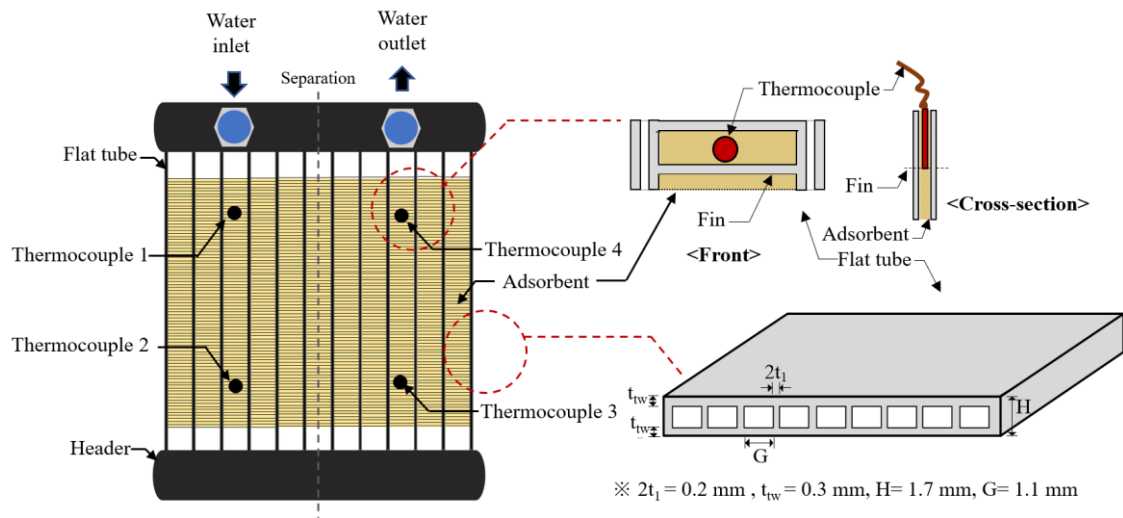
Fig. 4. 1 Schematics of sketch of adsorption heat exchanger

Table 4. 1 Geometric specifications of the adsorption heat exchanger

Parameters	Value
Blank HEX including headers (W/H/D) [mm]	140/ 110/ 12
Primary area of HEX, A_p [m^2]	0.247
Inner surface area of flat tube, A_i [m^2]	0.032
Convective heat transfer coefficient, h_i [W/m^{2}K]	3357
Thermal conductivity of metal, k_{metal} [W/mK]	160
Fin height (F_H) / Fin thickness (F_{th})/ Fin pitch (F_p) [mm]	8/ 0.11/ 1
Thickness of tube wall, d_{tw} [mm]	0.3
Number of fin pack / hydraulic passages [-]	12/ 2
Weight of heat exchanger with/ without header [g_cal]	198 / 71.9
Weight of heat transfer fluid in HEX with/ without header [g_cal]	41.5 / 12.8
Filled density [g/L] (A-type silica gel / WSS+LiCl 20 wt.%) excluding volume of headers (S1, S2/ W1, W2)	223, 305 / 233, 329

Fig. 4. 2 presents the schematics of the experimental system for measuring the adsorption dynamics. The LPJ method was used to estimate the adsorption dynamic characteristics of the adsorbers filled with the A-type silica gel and WSS composite. The system comprised a chamber for adsorption and desorption, an evaporator, two vacuum pumps, and three constant temperature baths. One water bath was used for the heat source of the evaporator, and the two remaining water baths supplied regeneration water for desorption and cooling water for eliminating the heat of adsorption. This study focused on evaluating the mass transfer characteristics of the adsorbers with respect to the adsorbent temperature. During the experiments, the adsorbent temperature was controlled by adjusting the temperature of the cooling water from 30 to 60 °C. The adsorber was placed on an electric balance in the chamber, and regeneration water was flowed through it to desorb the water vapor, under a vacuum. After entering the vacuum, the cooling water cooled the adsorbent until the adsorbent reached the target temperature.

Subsequently, adsorption was induced by opening the valve installed between the chamber and evaporator. The chambers attained the target pressure within 5 s because the pipe that connected the chamber and evaporator had a diameter of 75 mm. The heat transfer coefficients at the adsorbers were estimated while the adsorbent temperature was reduced from 80 to 30 °C at a certain water vapor pressure. These coefficients reflected the actual operating conditions of AHP systems.
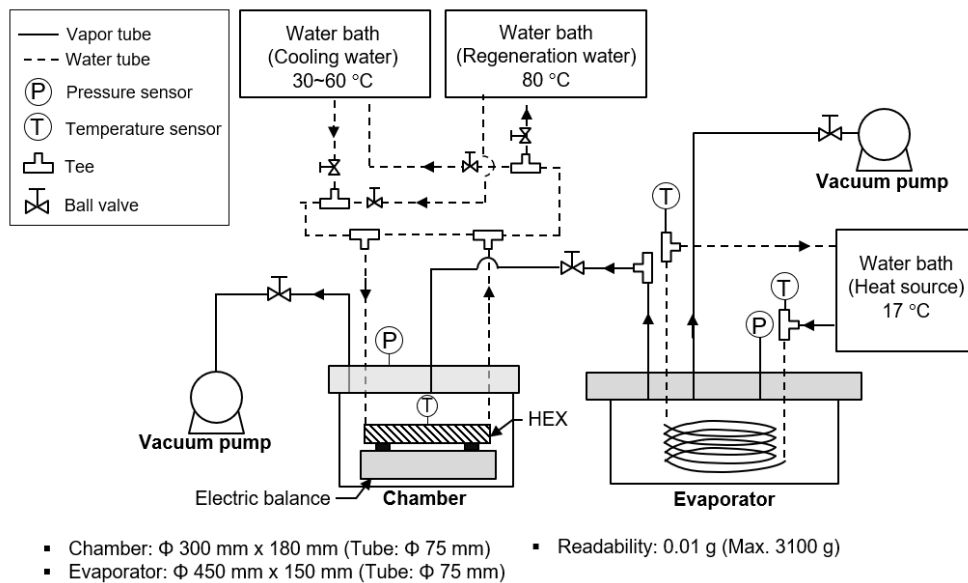
Fig. 4. 2 Schematics of experimental system for measuring adsorption dynamic

4.2.3 Estimation of Mass Transfer

Fig. 4. 3 shows the dynamic water vapor adsorption amount of each adsorber at various temperatures. As mentioned in the previous sections, the adsorption temperature was changed by controlling the temperature of the cooling water. Fig. 4. 4 shows the change in the adsorbent temperature during the adsorption process. Notably, an inevitable increase in the adsorbent temperature occurred at the beginning of the cycle, and the increase was larger at a lower adsorption temperature because of the larger instantaneous adsorption amount. However, the increase in the adsorbent temperature was less than 3–8 °C, which was considered an acceptable level to reflect the thermal effects on the mass transfer. Fig. 4. 5 shows an approach to quantify mass transfer limitation [52,53]. Unlike the typically used LDF model, which defines the driving force of mass transfer as the concentration gradient, the temperature gradient between the equilibrium temperature and the adsorbent temperature was applied to describe mass transfer performance. The advantage afforded by this method was the quantification of heat and mass transfer performance using the same unit of temperature, which enabled a direct comparison of importance between heat and mass transfer. The driving temperature of mass transfer is T_{eq}-T_{ad}, as shown in Fig. 4. 5. If the adsorbent temperature approximately reaches the equilibrium temperature, then the heat transfer must be enhanced to increase mass transfer. WSS + LiCl 20 wt.% has a relatively higher driving temperature in a wide range of uptake amount compared with the A-type silica gel. This implies that WSS + LiCl 20 wt.% exhibits a higher adsorption capability, which allows the actual cooling system using this adsorbent to be operated with a longer cycle time to reduce the heat loss that occurs when switching between adsorption and desorption modes.
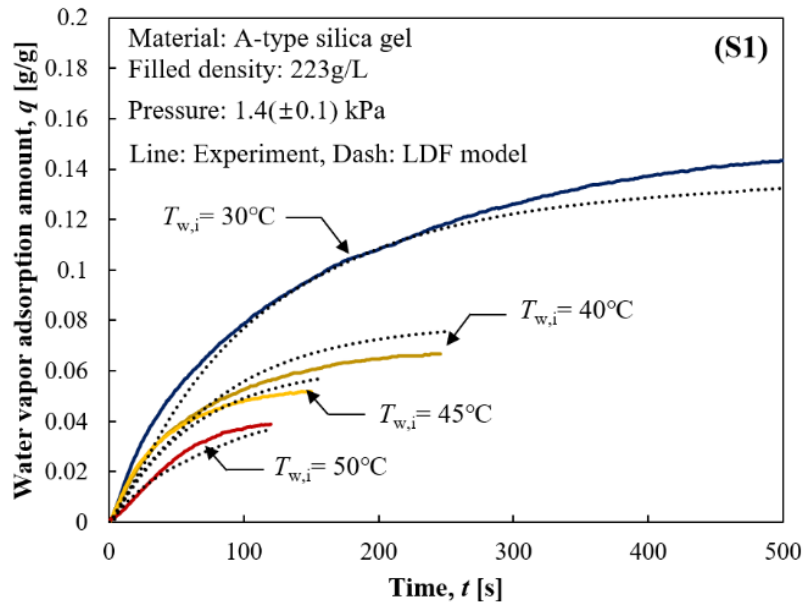
Fig. 4. 3 (a) Dynamic water vapor sorption amount at various temperature:
A-type silica gel (223g/L)
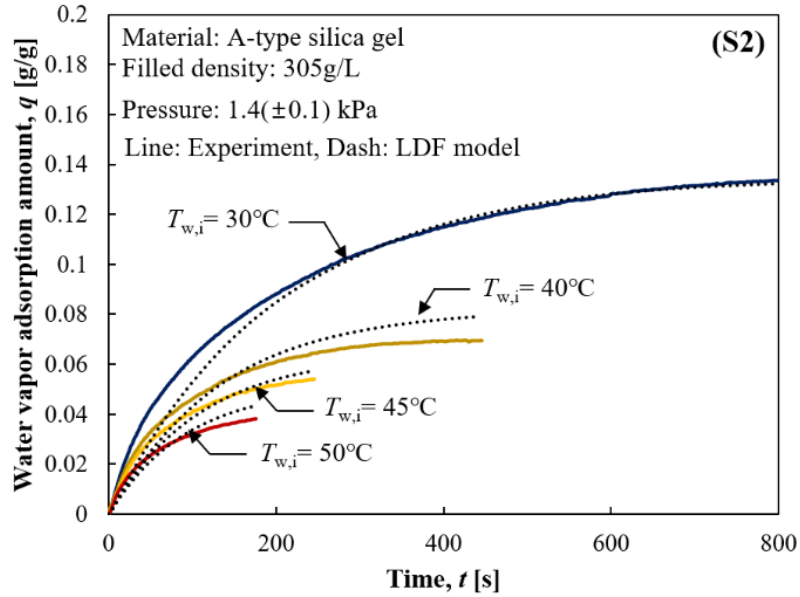
Fig. 4. 3 (b) Dynamic water vapor sorption amount at various temperature:
A-type silica gel (305g/L)
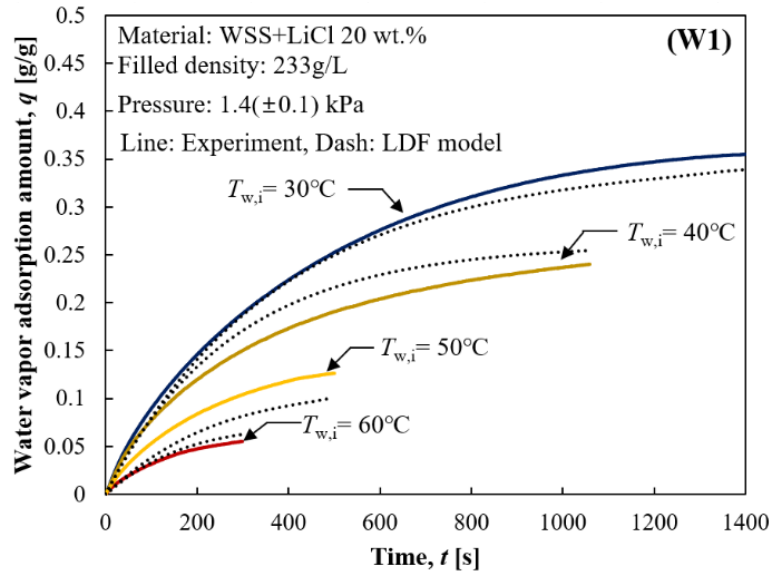
Fig. 4. 3 (c) Dynamic water vapor sorption amount at various temperature: WSS+LiCl 20 wt.% (233g/L)
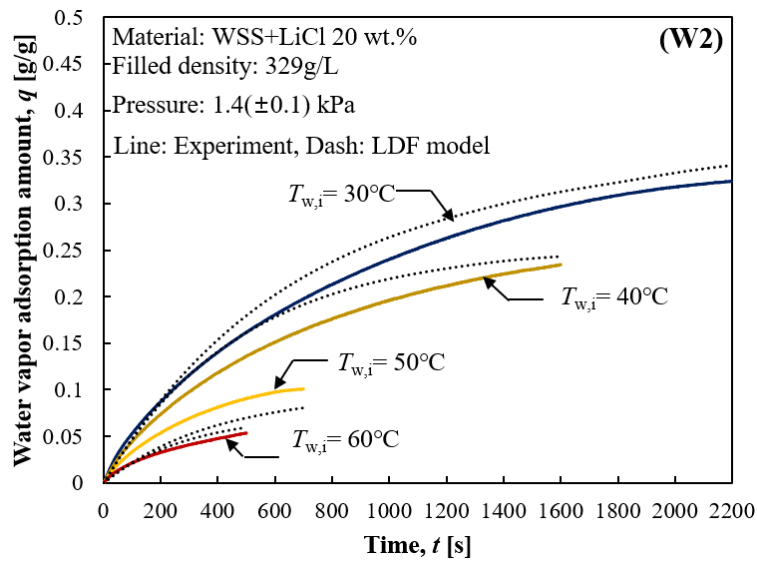
Fig. 4. 3 (d) Dynamic water vapor sorption amount at various temperature: WSS+LiCl 20 wt.% (329g/L)
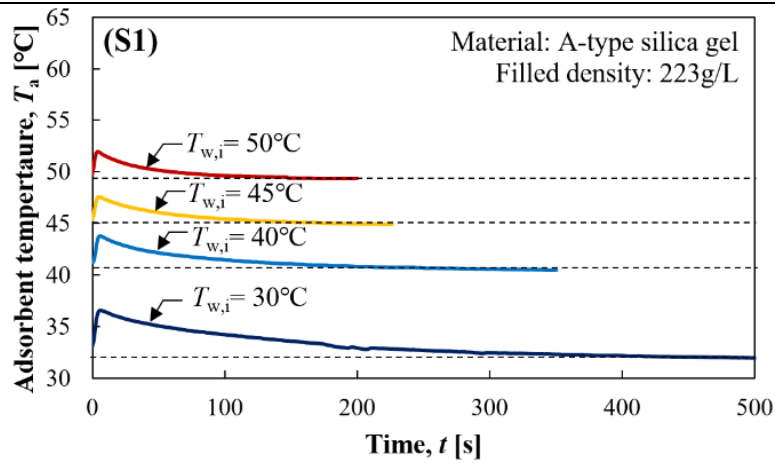
Fig. 4. 4 (a) Adsorbent temperature change during: A-type silica gel (223g/L)
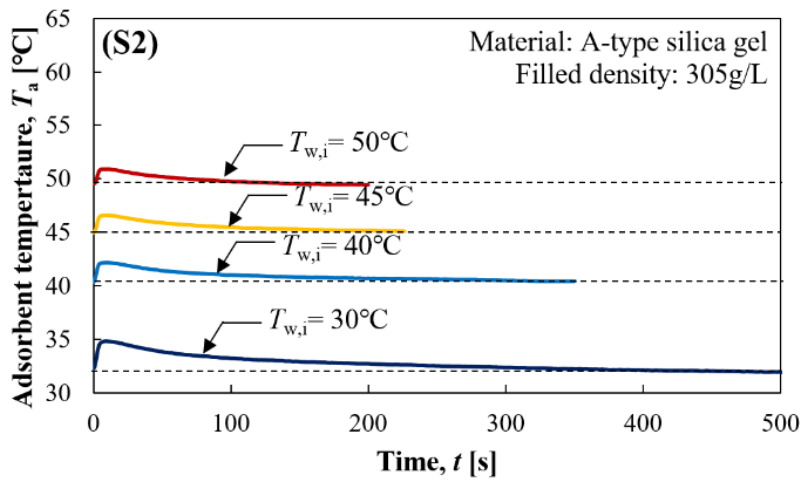
Fig. 4. 4 (b) Adsorbent temperature change during: A-type silica gel (305g/L)
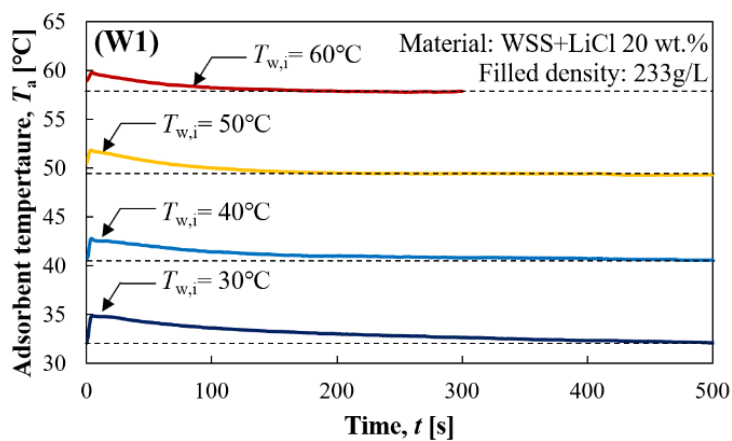
Fig. 4. 4 (c) Adsorbent temperature change during: WSS+LiCl 20wt.% (233g/L)
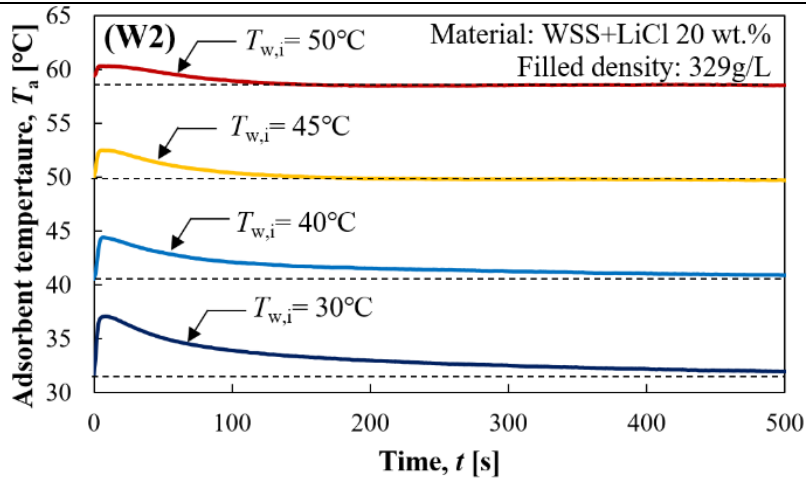
Fig. 4. 4 (d) Adsorbent temperature change during: WSS+LiCl 20wt.% (329g/L)
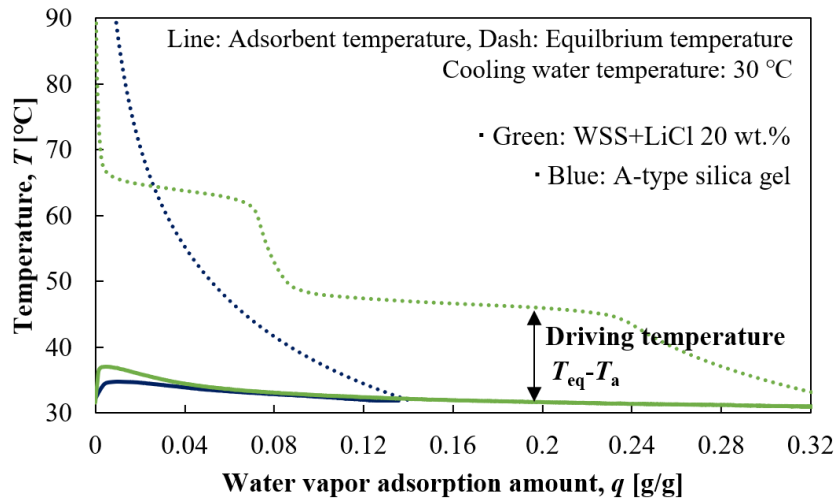
Fig. 4. 5 Equilibrium and adsorbent temperature according to water vapor adsorption amount

The experimentally obtained dynamic mass transfer data were analyzed using the LDF model, as indicated by Eq. (4-1). The overall mass transfer coefficient (K_m) was calculated using Eq. (4-2) [54].

$$\frac{dq}{dt} = K_m(q^* - q) \qquad (4\text{-}1)$$

$$K_\mathrm{m} = \frac{q(t + \Delta t) - q(t)}{(q^*(t) - q(t))\Delta t} \tag{4-2}$$

During non-isothermal adsorption, an increase in the adsorbent temperature affects the equilibrium adsorption amount (q^*) and overall mass transfer coefficient (K_m). According to the vapor pressure and adsorbent temperature, the value of q^* is expressed using the isotherm equations which were introduce in Chapter 2 (Eq. (2-22) ~ (2-23)). The thermal effects on K_m or the effective diffusivity, which is closely related to K_m, can be expressed by Eq. (4-3) and (4-4) [55,56]

$$K_\mathrm{m} = B_0 \exp\left\{-\frac{A_0 E_\mathrm{a}}{R T_a}\right\} \tag{4-3}$$

$$\ln K_\mathrm{m} = -A_0 \left(\frac{E_\mathrm{a}}{R T_\mathrm{a}}\right) + \ln B_0 \tag{4-4}$$

Eq. (4-4) represents the first-order linear function of the logarithmic K_m having a variable of $E_\mathrm{a}/RT_\mathrm{a}$ and a y-intercept of $\ln B_0$. Using the calculated K_m based on the experimentally measured instantaneous adsorption amount and the adsorption temperature and pressure, the coefficients of the function (A_0, B_0) can be fitted. Fig. 4. 6 shows the variation in the value of $\ln K_\mathrm{m}$ based on the adsorbent temperature. The numerically fitted values for each case of the adsorbers are presented in Table 4. 2.
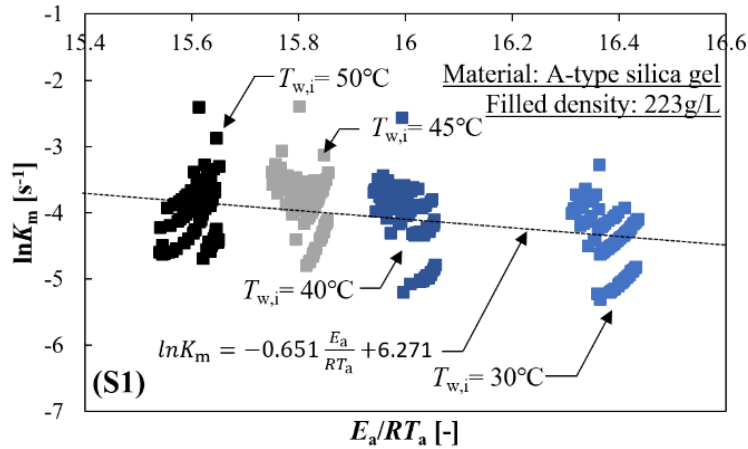
Fig. 4. 6 (a) $\ln K_\mathrm{m}$ value according to temperature: A-type silica gel (233g/L)
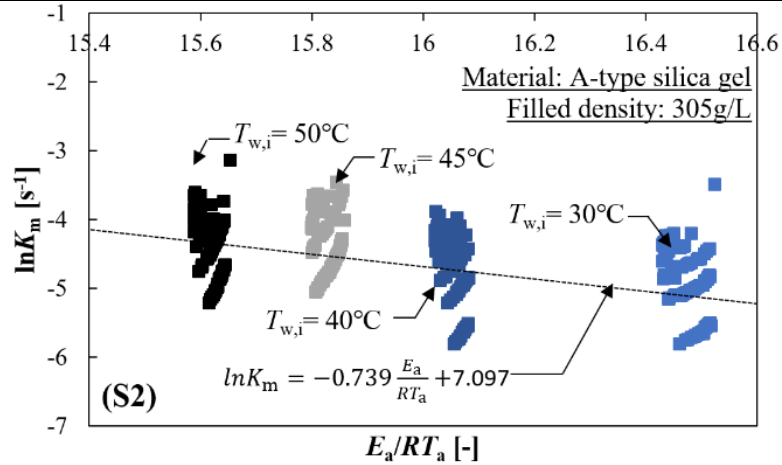
Fig. 4. 6 (b) $\ln K_m$ value according to temperature: A-type silica gel (305g/L)
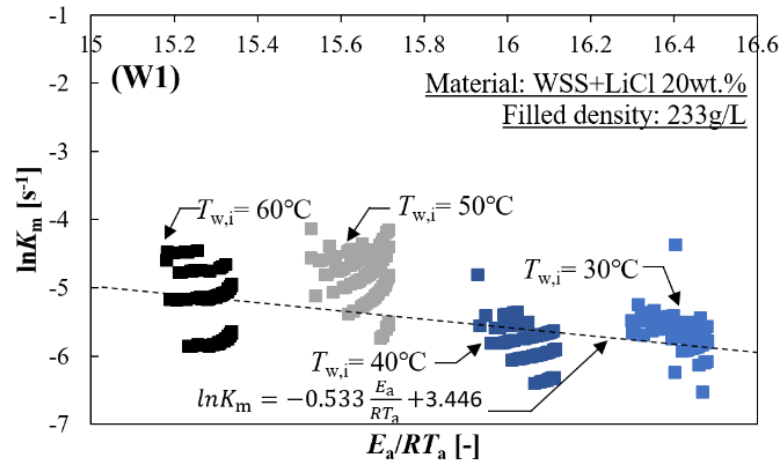
Fig. 4. 6 (c) $\ln K_m$ value according to temperature: WSS+LiCl 20 wt.% (233g/L)
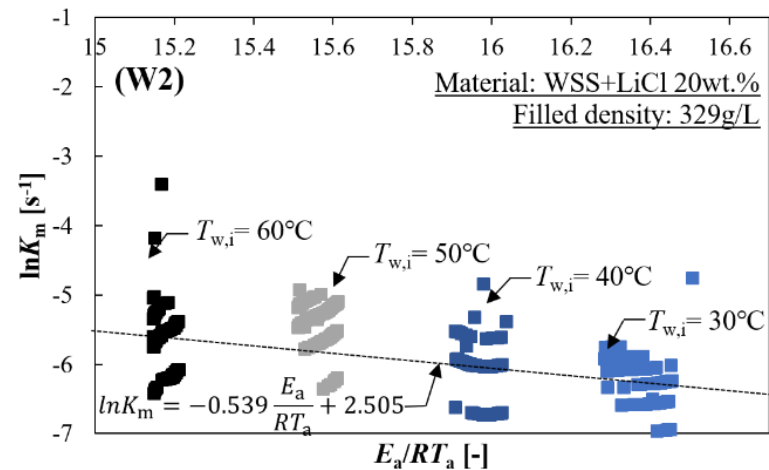
Fig. 4. 6 (d) $\ln K_m$ value according to temperature: WSS+LiCl 20 wt.% (329g/L)

Table 4. 2 Coefficients of straight fitting line in Eq. (4-4)

HEX No.	HEX	A_0	B_0
S1	A-type silica gel (223g/L)	0.651	6.271
S2	A-type silica gel (305/L)	0.739	7.097
W1	WSS+LiCl 20wt.% (233g/L)	0.533	3.446
W2	WSS+LiCl 20wt.% (329g/L)	0.539	2.505

4.2.4 Estimation of Heat Transfer

Fig. 4. 7 shows the experimentally estimated average *UA* when the adsorbent temperature was changed from 80 to 30 °C. Eq. (4-5) was used to calculate the *UA* value [42].

$$UA = \frac{\dot{m}_w C_{p,w}\left(T_{w,o} - T_{w,i}\right)}{T_a - T_{w,i}} \qquad (4\text{-}5)$$

The obtained *UA* value exhibited a similar tendency to that obtained by Li et al. [42]. In the applied simulation model, the heat transfer coefficient is required to calculate the heat exchanger efficiency (ε), as indicated by Eq. (4-6).

$$\varepsilon = 1 - \exp(-\frac{UA}{\dot{m}_w C_{p,w}}) \qquad (4\text{-}6)$$

Fig. 4. 8 depicts the schematics of heat transfer resistances for the theoretical calculation of the *UA* value [44,45]. In this study, seven types of thermal resistances were considered in the heat transfer between the heat transfer fluid to the adsorbent bed: convection thermal resistance from the heat transfer fluid to inner-side flat tube wall (R_i); conduction thermal resistance across the flat tube wall (R_{tw}) and from outer-side flat tube wall to fins (R_{fin}), including the thermal contact resistance between the fin and tube (TCR_{metal});

thermal contact resistances between the adsorbent layers and metal surface of tubes or fins (TCR_{ad}); and conduction thermal resistance from the metal surface of the fins to the adsorbent layer (R_{fin-ad}) and from the tubes to the adsorbent layers (R_{tw-ad}). Therefore, the total thermal resistance can be estimated using Eq. (4-7)–(4-10), where $h_i = Nu_D k_w / D_h$, $R_{tw} = d_t / k_{tw} A_{tw}$, $R_{fin} = 0.5 F_H / k_{fin} A_{cf}$, $R_{fin-ad} = 0.5 F_p / k_{ad} A_{fin}$, and $R_{tw-ad} = 0.5 F_H / k_{ad} A_{unfin}$. In this study, k_{ad} was considered 0.198 W/mK [44], TCR_{metal} and TCR_{ad} were assumed to be 1/15,000 and 1/300 m^2K/W, respectively [57].

$$R_{eq,1} = TCR_{fin} A_{cf} + R_{fin} + TCR_a A_{fin} + R_{fin-a} \qquad (4\text{-}7)$$

$$R_{eq,2} = TCR_a A_{unfin} + R_{tw-a} \qquad (4\text{-}8)$$

$$R_{eq,3} = \frac{R_{eq,1} \times R_{eq,2}}{R_{eq,1} + R_{eq,2}} \qquad (4\text{-}9)$$

$$UA = \left(R_i + R_{tw} + R_{eq,3}\right)^{-1} \qquad (4\text{-}10)$$

Herein, D_h refers to the hydraulic diameter of the microchannel in the flat tube, and all dimensions for Eq. (4-11) are provided in Fig. 4. 1 [58].

$$D_h = \frac{4(H - 2t_{tw}) \times (G - 2t_1)}{2(H + G - 2(t_1 + t_{tw}))} \qquad (4\text{-}11)$$

As shown in Eq. (4-12), the Nusselt number of the flow can be calculated by an empirical equation when *Re* is less than 1000 [59], where α refers to $(H\text{-}2t_{tw})/G$. This empirical equation was applied since *Re* of this paper is around 360.

$$Nu_D = 2.253 + 8.164 \left(\frac{\alpha}{\alpha + 1}\right)^{1.5} \qquad (4\text{-}12)$$
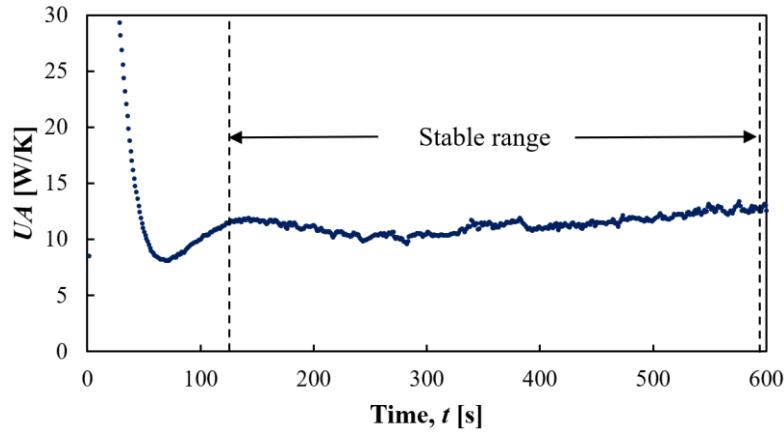
Fig. 4. 7 Estimation of *UA* values during the adsorbent temperature change from 80°C to 30°C
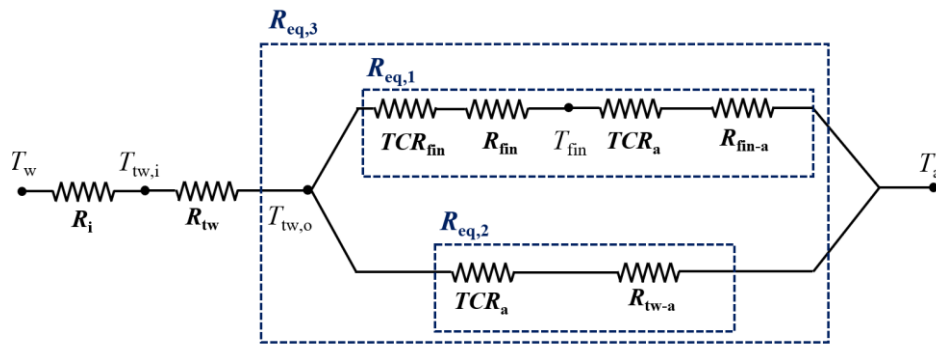
Fig. 4. 8 Schematic diagram of the adsorption heat transfer resistances

Table 4. 3 Comparison of experimentally estimated and calculated *UA* value

	UA [W/K]	*U* [W/m²K]
EXP: Fig. 4. 7	11.38	45.97
Calculated: Eq (4-10)	11.75	47.48
Reference [42]	-	Approx. 50

Table 4. 3 shows the comparison of experimentally obtained average *UA* value in the stable range shown in Fig. 4. 7, the calculated *UA* value based on Eq. (4-10), and the *UA* value that was estimated experimentally by Li et al. [42].

According to the heat-balance equation of Eq. (4-13) [38–41], the adsorbent temperatures measured experimentally and calculated by the model were compared to verify the estimated heat exchanger coefficient (ε).

$$
\left(C_{\mathrm{a}} + C_{\mathrm{HEX}} + M_{\mathrm{a}} q c_{\mathrm{p,w}}\right)\frac{dT_{\mathrm{a}}}{dt}
$$
$$
= M_{\mathrm{a}}\Delta H \frac{dq}{dt} - M_{\mathrm{a}}\frac{dT_{\mathrm{a}}}{dt} c_{\mathrm{p,v}}(T_{\mathrm{a}} - T_{\mathrm{v}}) \tag{4-13}
$$
$$
- \varepsilon \dot{m}_{\mathrm{w}} c_{\mathrm{p,w}}\left(T_{\mathrm{w,i}} - T_{\mathrm{a}}\right)
$$

Fig. 4. 9 presents the results of the comparison between the experimentally estimated and calculated adsorbent-temperature variation. These results indicate that the proposed model calculates the adsorbent temperature adequately.
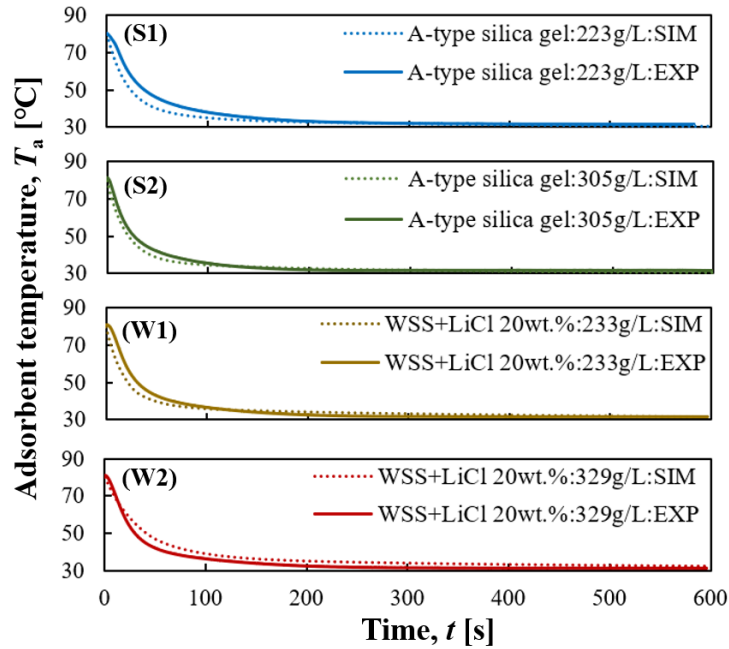
Fig. 4. 9 Comparison between experimentally measured and calculated adsorbent temperature variation

4.2.5 Uncertainty Analysis

The combined uncertainty of the evaluated parameters was determined through the propagation of individual uncertainties. The following equation for the combined uncertainties of the measured parameters $(\omega_{x_1}, \omega_{x_2} \cdots \omega_{x_n})$ was used to calculate the uncertainty of the evaluated parameters (ω_X) [60].

$$\omega_X = \sqrt{\left(\frac{\partial X}{\partial x_1}\right)^2 \omega_{x_1}{}^2 + \left(\frac{\partial X}{\partial x_2}\right)^2 \omega_{x_2}{}^2 + \cdots + \left(\frac{\partial X}{\partial x_n}\right)^2 \omega_{x_n}{}^2} \qquad (4\text{-}14)$$

Table 4. 4 presents the uncertainties of the measured and evaluated parameters in the experimental estimation of the heat and mass transfer coefficients of the adsorbent-filled heat exchangers.

Table 4. 4 Uncertainty in measured and evaluated parameters

Parameter	Uncertainty
T [℃]	$\pm$ 0.5 (Thermocouple T)
	$\pm$ 0.25 (PT-100)
P [kPa]	$\pm$ 0.05
$\dot{m}_w$ [g/s]	$\pm$ 0.083
q [g/g]	$\pm$ 2.76 x 10^{-4}
q^* [g/g]	$\pm$ 2.98 x 10^{-3}
K_m [1/s]	$\pm$ 4.51 x 10^{-4}
UA [W/K]	$\pm$ 0.322

4.3 MATHEMATICAL MODELING OF AHP SYSTEM

4.3.1 Assumptions

The following assumptions were applied in the proposed model [27].

- The temperature and pressure distributions were uniform in each component.
- The adsorption and desorption processes were considered under non-equilibrium conditions, and their rates were considered to be identical if the temperature was the same for both processes.
- The pressure of each component depended on the instantaneous mass of the water vapor.
- The vapor satisfied the ideal gas equation.
- The evaporation and condensation temperature is assumed to be saturation corresponding to the pressure.

4.3.2 Adsorption/Desorption Model

The governing equations applied to the two beds of the AHP modeling are as follows. For adsorption bed 1, which was initially in the desorption mode, the adsorbent temperature (T_a) and outlet water temperature ($T_{b,w,o}$) were calculated using Eqs. (4-15) and (4-16).

$$\left(C_{a1} + C_{HEX} + M_a q C_{p,w}\right)\frac{dT_{a1}}{dt} = M_a \frac{dq}{dt}\Delta H(T_{a1}) + \dot{Q}_1 \tag{4-15}$$

$$C_{b1,w}\frac{dT_{b1,w,o}}{dt} = \dot{m}_{b,w}C_{p,w}\left(T_{b1,w,i} - T_{b1,w,o}\right) - \dot{Q}_1 \tag{4-16}$$

$$\dot{Q}_1 = \varepsilon_{b1}\dot{m}_{b1,w}C_{p,w}\left(T_{b1,w,i} - T_{a1}\right) \tag{4-17}$$

As indicated by the left-hand side of Eq. (4-15), the thermal capacities of the adsorbent, adsorbate, and metal were considered. The first term on the right-hand side represents the heat consumed by the adsorbent to desorb water vapor. Here, the instantaneous adsorption amount was obtained using Eq. (4-1), and the heat of adsorption of 2710 J/g was applied in this research [69]. The second term of Eq. (4-15) represents the heat flux entering the

desorption bed.

In Eq. (4-16), the heat flux entering the control volume was calculated according to the difference between the water inlet and outlet temperatures. The heat flux exiting the system was calculated using the temperature difference between the regeneration water and the adsorbent. Similarly, for adsorption bed 2, the temperatures of the adsorbent and the secondary water outlet, during the adsorption mode, were obtained using Eqs. (4-18) and (4-19).

$$
\left(C_{\text{a2}} + C_{\text{HEX}} + M_a q C_{\text{p,w}}\right)\frac{dT_{\text{a2}}}{dt}
$$

$$
= M_a \frac{dq}{dt}\left\{\Delta H(T_{\text{b2}}) - C_{\text{p,v}}\left(T_{\text{a2}} - T_{\text{evap}}\right)\right\} - \dot{Q}_2 \tag{4-18}
$$

$$
C_{\text{b2,w}}\frac{dT_{\text{b2,w,o}}}{dt} = -\dot{m}_{\text{b2,w}}C_{\text{p,w}}\left(T_{\text{b2,w,o}} - T_{\text{b2,w,i}}\right) - \dot{Q}_2 \tag{4-19}
$$

$$
\dot{Q}_2 = \varepsilon_{\text{b2}}\dot{m}_{\text{b2,w}}C_{\text{p,w}}\left(T_{\text{a2}} - T_{\text{b2,w,i}}\right) \tag{4-20}
$$

In contrast to the case of the desorption mode, the first term on the right-hand side of Eq. (4-18) refers to the heat generated by adsorption. Additionally, the newly added second term represents the cooling effect that occurs when cold water vapor from the evaporator establishes contact with the relatively hot adsorbent. The outlet temperature of the cooling water was calculated using the same principle that was employed for the desorption mode, as indicated by Eq. (4-19).

The amount of residual vapor inside each bed was determined according to the following mass-balance equations (Eqs. (4-21)–(4-23)).

$$
\frac{dm_v}{dt} = -M_a \frac{dq}{dt} - \dot{m}_{v,o} + \dot{m}_{v,i} \tag{4-21}
$$

$$
\dot{m}_{v,o} = A_{\text{cond}}\sqrt{2\rho_v(P_b - P_{\text{cond}})} \tag{4-22}
$$

$$
\dot{m}_{v,i} = A_{\text{evap}}\sqrt{2\rho_v(P_{\text{evap}} - P_b)} \tag{4-23}
$$

The terms $\dot{m}_{v,o}$ and $\dot{m}_{v,i}$ represent the instantaneous flow rates leaving and entering

the adsorption bed, respectively. These values are valid only when the bed pressure is higher than the condensation pressure during the desorption cycle and lower than the evaporation pressure during the adsorption mode.

Additionally, the change in the bed pressure with respect to time was calculated using the change ratio of the residual vapor and bed temperature, as given by Eq. (4-24).

$$\frac{dP_b}{dt} = P_b \left(\frac{1}{m_v} \frac{dm_v}{dt} + \frac{1}{T_a} \frac{dT_a}{dt} \right) \tag{4-24}$$

4.3.3 Evaporation and Condenser Model

The condensation rate was calculated using the energy-conservation equation of Eq. (4-25), and the variation in the condensation pressure was expressed as a function of the residual vapor amount and condensation temperature, as indicated by Eq. (4-26). Finally, the variation in the water outlet temperature was obtained through the energy-conservation equations of Eqs. (4-27) and (4-28).

$$\dot{m}_{cond} = \frac{\dot{m}_{cond,w} C_{p,w} (T_{cond,w,o} - T_{cond,w,i})}{C_{p,v} (T_{cond,v,i} - T_{cond}) + h(P_{cond})} \tag{4-25}$$

$$\frac{dP_{cond}}{dt} = \frac{\left(\frac{P_{cond}}{m_{cond,v}} \right) \times \left(\frac{dm_v}{dt} \right)}{1 - \frac{P_{cond}}{T_{cond}} \frac{dT_{sat}}{dP}} \tag{4-26}$$

$$C_{cond,w} \frac{dT_{cond,w,o}}{dt} = \dot{m}_{cond,w} C_{p,w} (T_{cond,w,i} - T_{cond,w,o}) - \dot{Q}_{cond} \tag{4-27}$$

$$\dot{Q}_{cond} = \varepsilon_{cond} \dot{m}_{cond,w} C_{p,w} \left\{ \begin{array}{c} \left(\alpha(T_{cond,w,i} - T_{cond}) + \right. \\ \left. (1 - \alpha)(\frac{T_{cond,w,o} - T_{cond}}{1 - \varepsilon_{cond}}) \right\} \end{array} \tag{4-28}$$

The values of these parameters for the evaporator were determined using the same calculation method and Eq. (4-29)–(4-32).

$$\dot{m}_{\text{evap}} = \frac{-\dot{m}_{\text{evap,w}} C_{\text{p,w}}(T_{\text{evap,w,i}} - T_{\text{evap,w,o}})}{C_{\text{p,w}}(T_{\text{cond}} - T_{\text{evap}}) - h(P_{\text{evap}})} \tag{4-29}$$

$$\frac{dP_{\text{evap}}}{dt} = \frac{\left(\frac{P_{\text{evap}}}{m_{\text{evap,v}}}\right) \times \left(\frac{dm_{\text{v}}}{dt}\right)}{1 - \frac{P_{\text{evap}}}{T_{\text{evap}}} \frac{dT_{\text{sat}}}{dP}} \tag{4-30}$$

$$C_{\text{evap,w}} \frac{dT_{\text{evap,w,o}}}{dt} = \dot{m}_{\text{evap,w}} C_{\text{p,w}}(T_{\text{evap,w,i}} - T_{\text{evap,w,o}}) - \dot{Q}_{\text{evap}} \tag{4-31}$$

$$\dot{Q}_{\text{evap}} = \varepsilon_{\text{evap}} \dot{m}_{\text{evap,w}} C_{\text{p,w}} \left\{ \begin{array}{l} \left(\alpha(T_{\text{evap,w,i}} - T_{\text{evap}}) + \right. \\ (1 - \alpha)(\frac{T_{\text{evap,w,o}} - T_{\text{evap}}}{1 - \varepsilon_{\text{evap}}}) \end{array} \right\} \tag{4-32}$$

The values of $C_{\text{cond,w}}$ (Eq. (4-27)) and $C_{\text{evap,w}}$ (Eq. (4-32)) include the heat capacity of metal of the evaporator and condenser, as well as that of water in the heat exchanger. α describes the weighting factor of the temperature difference between the inlet and outlet water temperatures and the bed temperature. According to Verde et al. [27,61], the value of $\alpha = 0.8$ can be used in a wide range of operating conditions.

4.4 SIMULATION RESULTS AND DISCUSSIONS

4.4.1 Validation of Mathematical Model

The mathematical model, including the experimentally estimated heat and mass transfer coefficients, was validated by comparing between the calculated and experimental values. Fig. 4. 10 shows the comparison results for the adsorption process. The cooling capacities (Q_c) and chilled-water temperatures ($T_{evap,w,o}$) obtained from the experiment and simulation were compared. Generally, the simulation values closely matched the experimental values, except at the beginning of the process when the adsorbent temperature and pressure changed significantly. This marked change in the properties was attributed to the relatively large imprecision in the calculations. Notably, the values were successfully predicted after 100 s, which may be considered as short term compared with the duration of the entire process. Furthermore, the error between the average values of the cooling capacity between the experimental and simulation results was 6.4%, and its maximum value after 100 s was 12.7%. In the actual evaporation, the time for the liquid in the evaporator to evaporate and reach the lower temperature is required. Meanwhile, the model assumes that the evaporation temperature varies immediately as the pressure changes, which results in the higher cooling capacity at the beginning of the cycle. Therefore, the error at the beginning of the cycle should be reduced by reflecting the temperature change according to the pressure change, rather than assuming the saturated condition in the evaporator and condenser.

Parameters	EXP	SIM	Error
Q_{c_ave} [W]	28.55	30.37	6.4 %
T_{evap,w,o_ave} [°C]	15.84	15.59	1.6 %
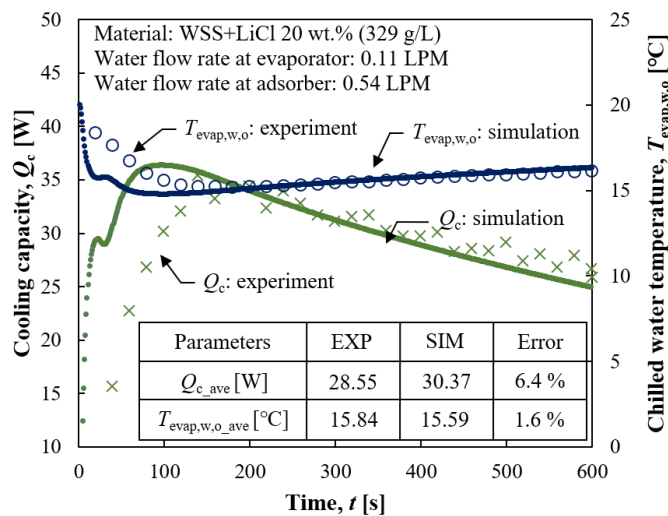
Fig. 4. 10 Comparison of values obtained from experiment and simulation

4.4.2 Simulation Results for AHP

Fig. 4. 11 and Fig. 4. 12 present the simulation results for the changes in the pressure and temperature, respectively, over time. The results for the adsorbers filled with different materials of similar densities, i.e., 305 and 329 g/L, were compared. In the case of the A-type silica gel, the desorption and condensation pressures increased rapidly because of the high mass transfer rate at high adsorbent temperatures. Furthermore, it appeared that the actual desorption had already completed in the middle of the desorption process, where the condensation and desorption pressures were almost the same. Therefore, the adsorbent temperature at the beginning of the desorption cycle increased more slowly for the A-type silica gel than for the WSS composite. Because of the difference in the mass transfer rates of the A-type silica gel and WSS composite, the temperature variation with respect to time was different. The average evaporation pressure for both cases was approximately 1.57 kPa, resulting in chilled water with a temperature of 15 °C.
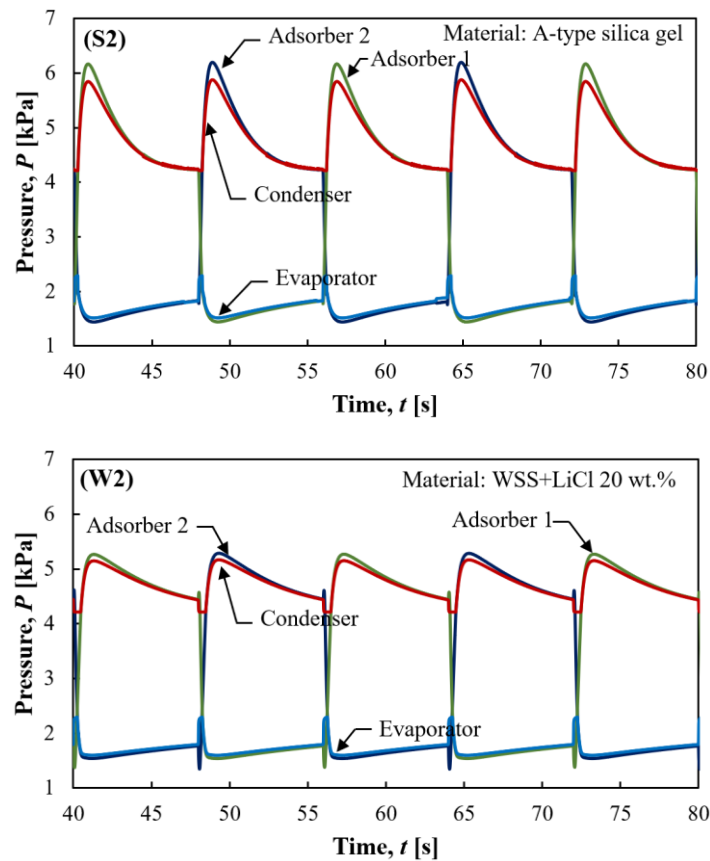
Fig. 4. 11 Simulation results of pressure change according to time: (S2) A-type silica gel: 305 g/L, (W2) WSS+LiCl 20 wt.%: 329 g/L
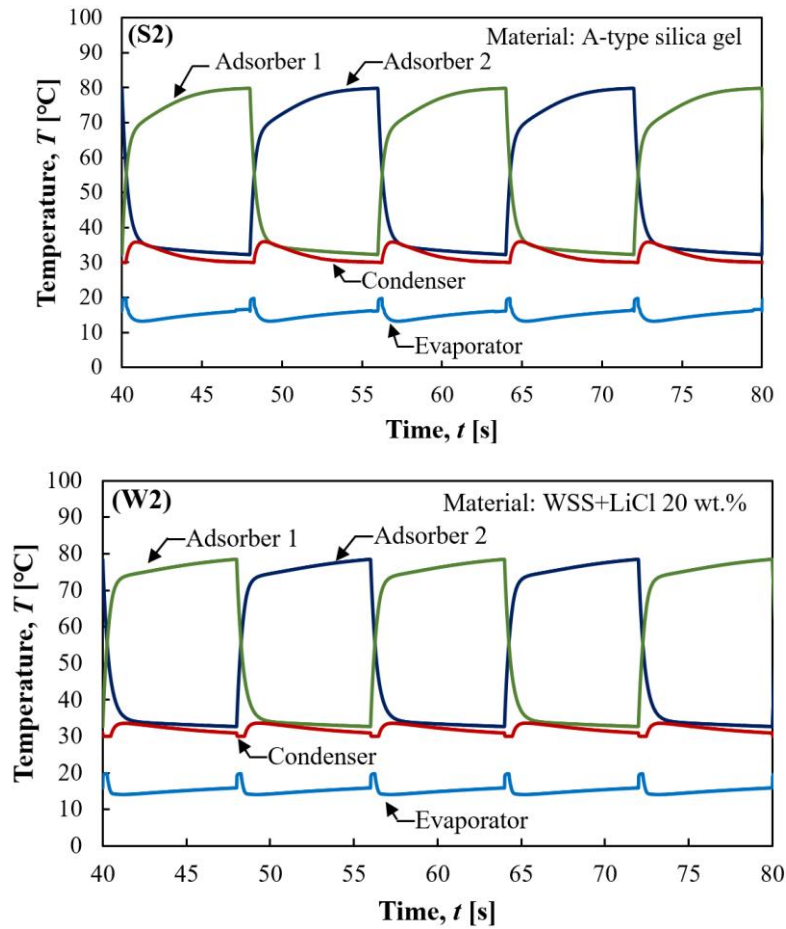
Fig. 4. 12 Simulation results of temperature change according to time:
(S2) A-type silica gel: 305 g/L, (W2) WSS+LiCl 20 wt.%: 329 g/L

Fig. 4. 13 compares the equilibrium and adsorber temperatures during one cycle of both the A-type silica gel and WSS + LiCl 20 wt.%. The temperature difference between the T_{eq} and T_{ad} of the A-type silica gel was much smaller than that of the WSS composite, meaning that the A-type silica gel reached equilibrium faster. Indeed, the calculated overall mass transfer coefficient of the A-type silica gel based on the LDF model was approximately four times higher than that of the WSS composite. Meanwhile, the WSS composite exhibited a relatively higher driving temperature in a wide range of uptake amount compared with the A-type silica gel. This implies that WSS + LiCl 20 wt.% exhibited a higher adsorption capability, which enabled the actual cooling system using this adsorbent to be operated with a longer cycle time to reduce the heat loss that occurred

when switching between adsorption and desorption modes.
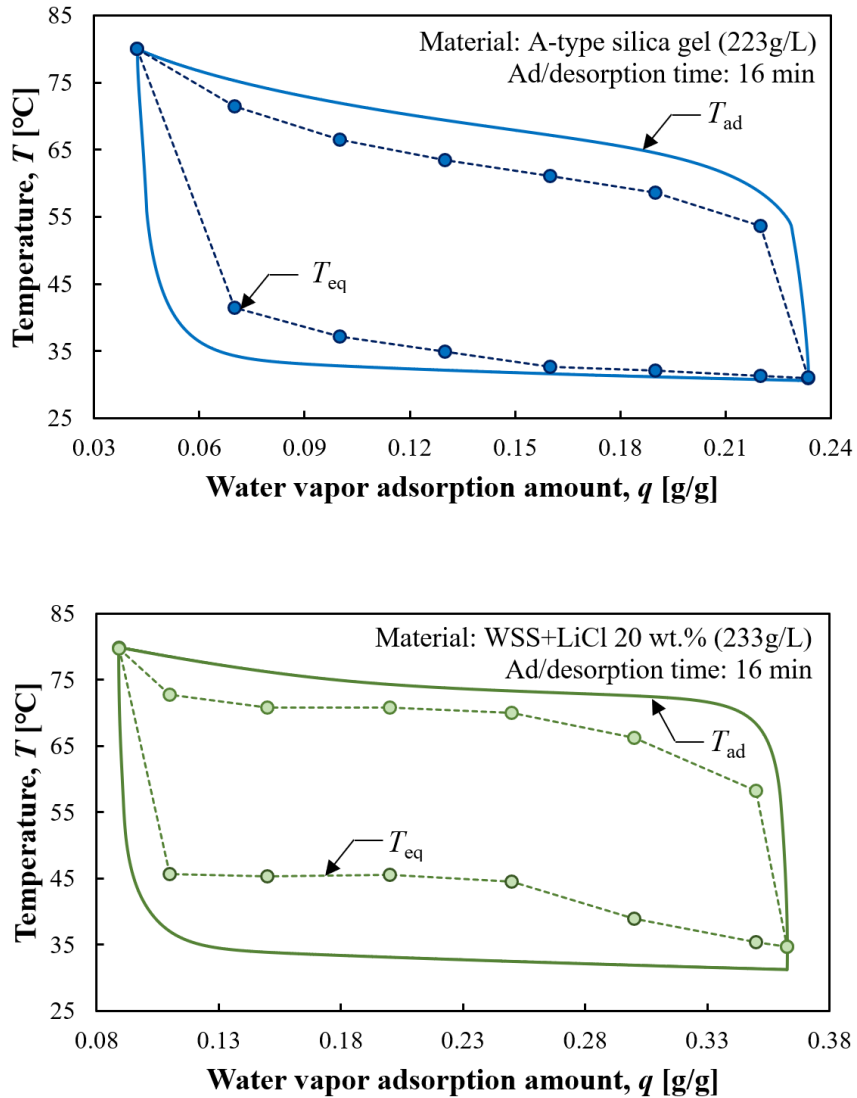
Fig. 4. 13 Equilibrium and adsorbent temperature according to water vapor adsorption amount during one cycle

Fig. 4. 14 shows the difference between saturation temperature of the adsorber and that of the evaporator or condenser. The difference between $T_{sat}(P_{ad})$ and T_{evap} or T_{cond} was significantly dependent on the size of the mass transfer path between the adsorber and evaporator or condenser. If the path was not sufficiently large, for example, the evaporated water vapor from the evaporator could not move to the adsorber optimally, thereby resulting in an increase in P_{evap} (T_{evap}) and decrease in P_b (T_b). The same principle can be applied to the condenser. In this case, the equilibrium temperature decreases owing

to the decreased adsorption pressure, which means the driving force for the mass transfer becomes limited.

Fig. 4. 15 shows a comparison of the cooling capacity based on the filled density for both adsorbents. A significant difference between the cooling-capacity distributions of the A-type silica gel and WSS composite was observed. The A-type silica gel exhibited a rapid decrease in its cooling capacity because it quickly reached the saturated state. The reduction in the cooling capacity for the WSS composite was moderate during the adsorption cycle. Additionally, the adsorber with a lower filling density exhibited a steeper decrease in the cooling capacity. Therefore, the rate of reduction of the cooling capacity was proportional to the mass transfer rate.
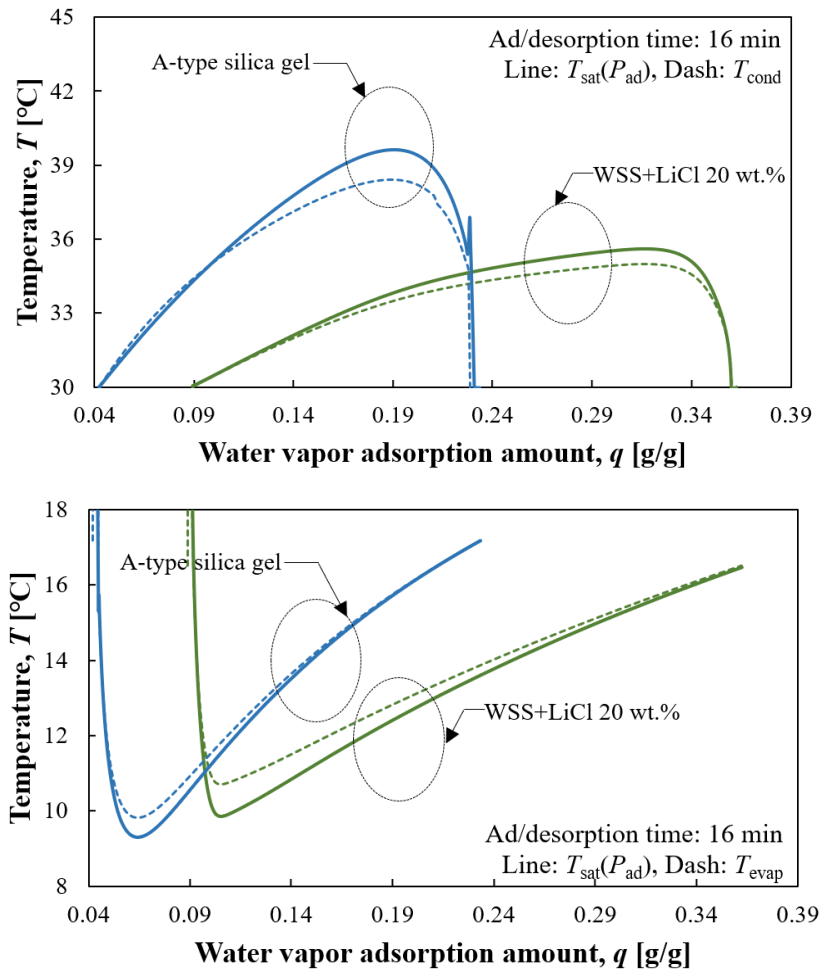
Fig. 4. 14 Saturation temperature at adsorber, condenser and evaporator (top: condenser, bottom: evaporator)
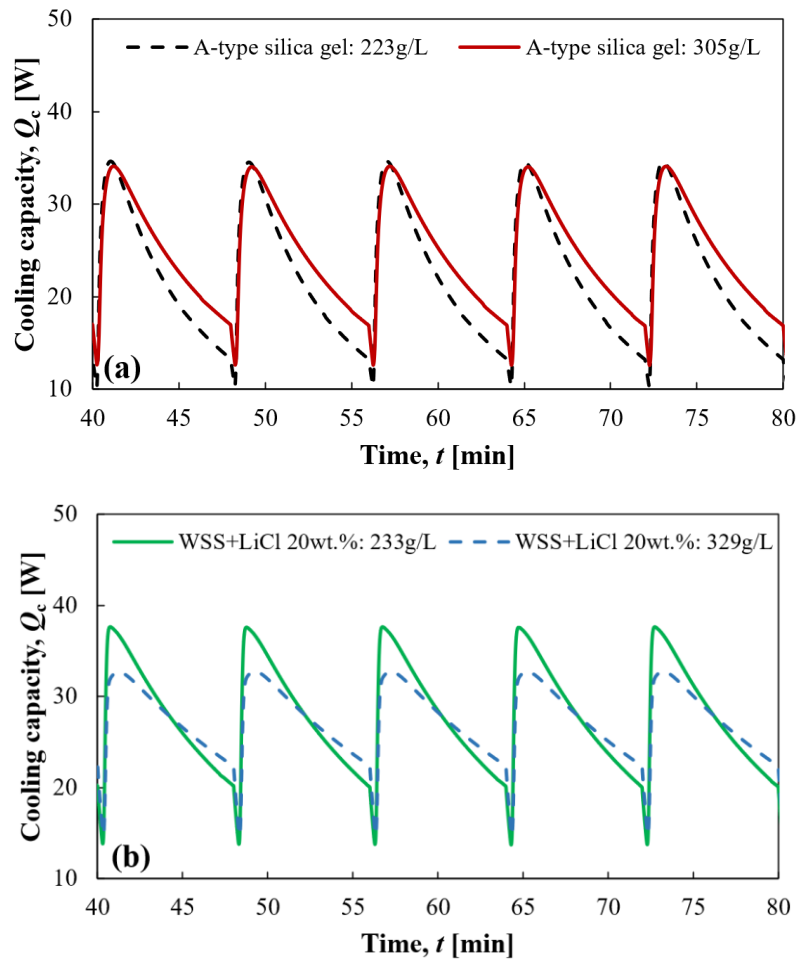
Fig. 4. 15 Comparison of cooling capacity according to filled density:
(a) A-type silica gel, (b) WSS+LiCl 20 wt.%

Fig. 4. 16 presents the adsorption amount based on the filled density for both adsorbents. Increasing the cycle time did not positively affect the A-type silica gel (223 g/L), because it nearly achieved the equilibrium adsorption amount. However, the WSS composite exhibited a higher adsorption capability owing to its large equilibrium adsorption amount. This implies that systems employing adsorbers with a moderate adsorption rate may be operated with a longer cycle time to reduce the heat loss that occurs when switching between the adsorption and desorption modes.
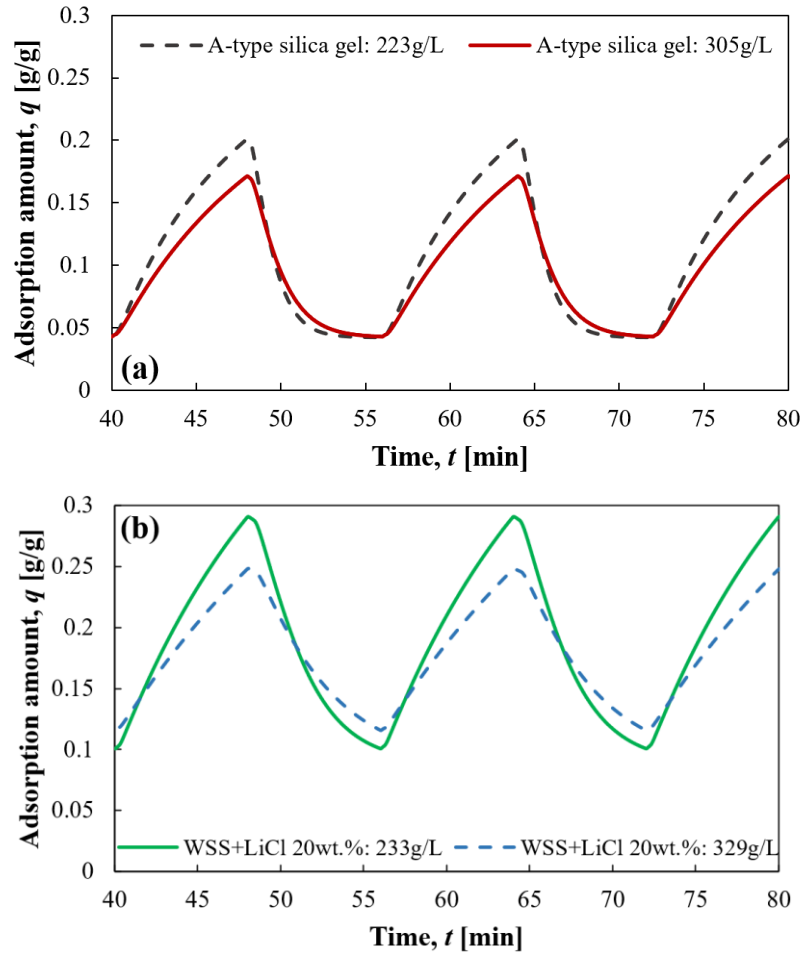
Fig. 4. 16 Comparison of adsorption amount according to filled density: (a) A-type silica gel, (b) WSS+LiCl 20 wt.%

Fig. 4. 17 (a) and (b) illustrate the effect of the half cycle time on the cooling capacity and heating capacity, respectively. Here, the half cycle time includes precooling time and adsorption time, and it is assumed that they are the same as the sum of preheating and desorption time. The cooling and heating capacity tended to decrease with an increase in the adsorption time because the adsorption rate decreased during the adsorption process, owing to the reduced adsorption driving force (q^*-q). The adsorbers exhibited dissimilar decrements owing to their different adsorption dynamics and equilibrium characteristics. Hence, the optimal cycle time must be calculated by considering the adsorption dynamics and equilibrium characteristics of the adsorbers.

Fig. 17 (c) and (d) present the variations in the specific cooling power (SCP) and COP,

respectively, with respect to the half cycle time. The COP should be considered when evaluating an AHP, as well as other heat-pump systems. Additionally, the SCP is an important performance indicator of an AHP and represents the attainable cooling capacity based on the unit mass of the adsorbent. The SCP values of the materials with lower filling densities were higher than those of the materials with higher filling densities. This implies that the adsorbent was used more efficiently in the heat exchanger with the lower filling density. The general trends of the SCP resembled and were dependent on the cooling capacity. WSS+LiCl 20 wt.% (329 g/L) exhibited the smallest SCP variation (relatively constant value) with respect to the half cycle time. As the cycle time increased, the sensible heat loss that occurred when the mode was switched from adsorption to desorption accounted for a relatively small portion among the entire load. Hence, the COPs of the systems employing the adsorbers tended to increase when the adsorption time increased. The COP for the case of the WSS composite was improved by 6–17% compared with that for the A-type silica gel, indicating the effectiveness of the WSS composite However, the SCP value obtained in this study was relatively lower than the value obtained from the numerical study of Kowsari et al. [62] using SWS-1L. The highest SCP found in their research was 554 W/kg when assuming that the entire cycle time is two times of adsorption and pre-cooling time. The WSS composite yields the lower value (512 W/kg) at the same working condition even though it has the lower filled density (233 g/L) and the heat exchanger thickness (12 mm). Therefore, further researches on the effects of particle size of the host material and impregnated chloride on the system performance are required. Table 4. 5 summarizes a comparison of the AHP performance based on adsorption times of 8 and 16 min. As mentioned in previous sections, the WSS composite, particularly the adsorber with the higher filled density, exhibited smaller decrements in the cooling capacity and SCP and a greater increment in the COP.
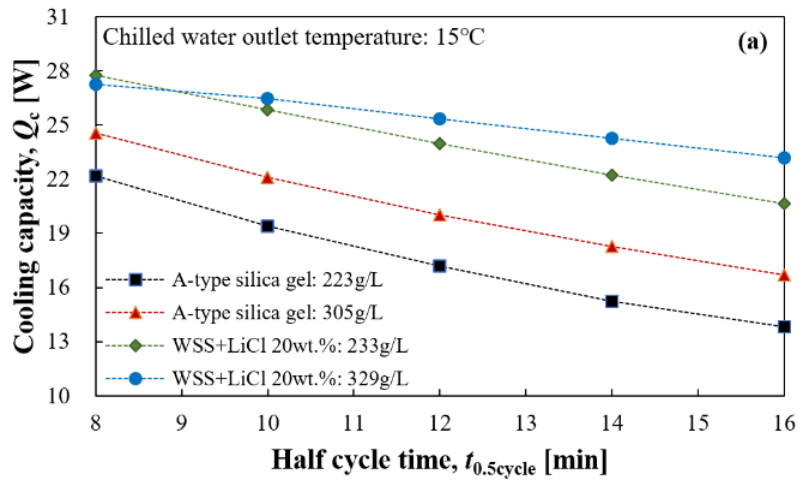
(a) Cooling capacity
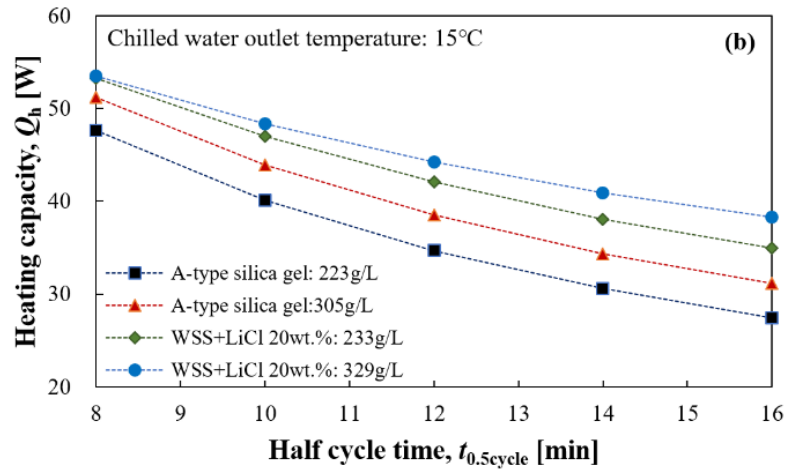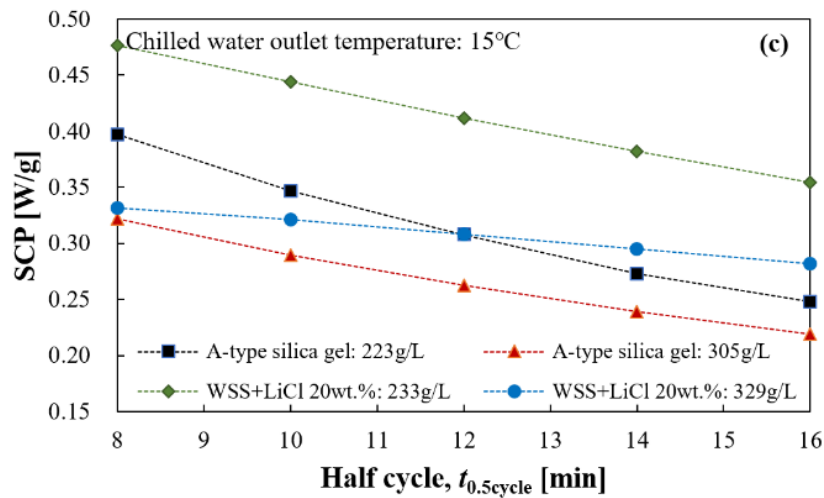
(b) Heating capacity
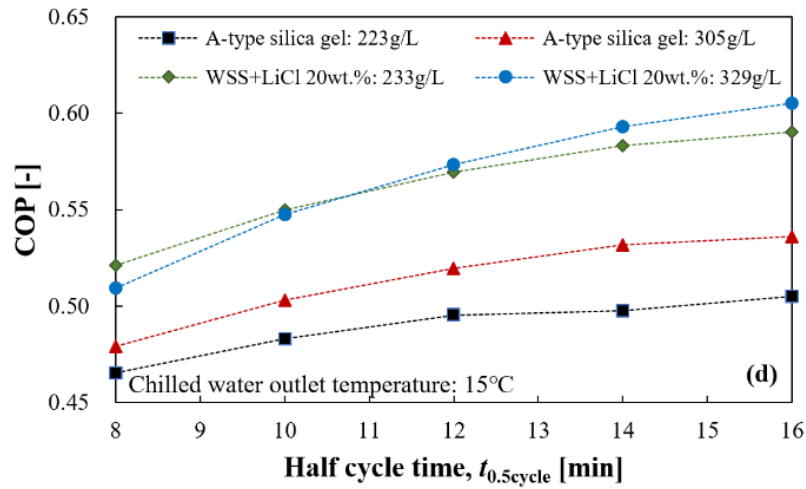
(c) SCP

(d) COP

Fig. 4. 17 Effect of half cycle time on (a) cooling capacity, (b) heating capacity, (c) SCP, (d) COP

Table 4. 5 Comparison of AHP performance between half cycle time of 8 min and 16 min

HEX	S1			S2			W1			W2		
No.	Q_c	SCP	COP	Q_c	SCP	COP	Q_c	SCP	COP	Q_c	SCP	COP
8 min	22.2	0.40	0.46	24.5	0.32	0.48	27.7	0.47	0.52	27.3	0.33	0.51
16 min	13.8	0.25	0.50	16.7	0.22	0.53	20.6	0.35	0.59	23.1	0.28	0.60
%	60.9	60.0	8.0	46.7	45.5	9.4	34.5	34.3	11.9	18.2	17.9	15.0

4.5 SUMMARY

In this study, an AHP system was simulated based on experimentally estimated heat and mass transfer characteristics to minimize the error resulting from traditional evaluations of heat and mass transfer. Four heat exchangers filled with an A-type silica gel and WSS impregnated with 20 wt.% LiCl at different filling densities were used to estimate the heat and mass transfer characteristics.

The mass transfer coefficient of each adsorber was calculated using the LDF model considering thermal effects. The simulation model, which was created by utilizing the estimated overall mass transfer coefficient, yielded adsorption amounts similar to those obtained experimentally. Additionally, the overall heat transfer coefficient was experimentally evaluated by changing the adsorbent temperature from 80 to 30 °C to realize the actual working conditions of an AHP. The reliability of the obtained *UA* value was verified by comparing the calculated and experimentally measured adsorbent temperatures.

The experimentally obtained heat and mass transfer coefficients were substituted into a mathematical model for a more accurate and practical estimation of the AHP performance. The cooling capacity and SCP tended to decrease as the adsorption time increased because of the decreasing adsorption rate. The COP tended to increase with an increase in the adsorption time. The decrements and increments of the parameters of the adsorbers differed owing to their different adsorption dynamics and equilibrium characteristics. Therefore, the optimization of the cycle time, considering the adsorption dynamics and equilibrium characteristics of the adsorbers, is necessary. In future studies, the analysis on long term-operations (i.e., during daytime) will be conducted based on this zero-dimensional AHP model, thermally supported by a solar collector. This appears to be promising because of the advantages of fast and simple calculations. Additionally, the system performance as well as energy and exergy analyses according to various operating parameters will be provided in future studies.

Finally, the WSS composite material exhibited a COP that was 6–17 % higher than that of the A-type silica gel. This indicates the effectiveness of the WSS composite compared with the frequently used A-type silica gel.

4.6 REFERENCE

[1]   Z. Lu, R. Wang, Z. Xia, L. Gong, Experimental investigation adsorption chillers using micro-porous silica gel–water and compound adsorbent-methanol, Energy Convers. Manag. 65 (2013) 430–437.

[2]   M.B. Elsheniti, O.A. Elsamni, R.K. Al-dadah, S. Mahmoud, E. Elsayed, K. Saleh, Adsorption Refrigeration Technologies, in: Sustain. Air Cond. Syst., InTech, 2018.

[3]   Y.. Aristov, G. Restuccia, G. Cacciola, V.. Parmon, A family of new working materials for solid sorption air conditioning systems, Appl. Therm. Eng. 22 (2002) 191–204.

[4]   I.I. El-Sharkawy, On the linear driving force approximation for adsorption cooling applications, Int. J. Refrig. 34 (2011) 667–673.

[5]   K. Daou, R.Z. Wang, Z.Z. Xia, Development of a new synthesized adsorbent for refrigeration and air conditioning applications, Appl. Therm. Eng. 26 (2006) 56–65.

[6]   X. Zheng, T.S. Ge, R.Z. Wang, Recent progress on desiccant materials for solid desiccant cooling systems, Energy. 74 (2014) 280–294.

[7]   H. Zhang, Y. Yuan, Q. Sun, X. Cao, L. Sun, Steady-state equation of water vapor sorption for CaCl2-based chemical sorbents and its application, Sci. Rep. 6 (2016) 34115.

[8]   Y.I. Aristov, B. Dawoud, I.S. Glaznev, A. Elyas, A new methodology of studying the dynamics of water sorption/desorption under real operating conditions of adsorption heat pumps: Experiment, Int. J. Heat Mass Transf. 51 (2008) 4966–4972.

[9]   Y.I. Aristov, I.S. Glaznev, A. Freni, G. Restuccia, Kinetics of water sorption on a CaCl2-in-silica-gel-pores sorbent: The effects of the pellet size and temperature, Kinet. Catal. 47 (2006) 770–775.

[10]   B.B. Saha, A. Chakraborty, S. Koyama, Y.I. Aristov, A new generation cooling device employing CaCl2-in-silica gel-water system, Int. J. Heat Mass Transf. 52 (2009) 516–524.

[11]   A. Kurokawa, J. Togawa, Y. Nabeshima, K. Nagano, The Evaluation of the Moisture Sorption Mechanism of Chloride-Impregnated Wakkanai Siliceous Shale, KAGAKU KOGAKU RONBUNSHU. 37 (2011) 394–399.

[12]   S. Nakabayashi, K. Nagano, M. Nakamura, J. Togawa, A. Kurokawa, Improvement of water vapor adsorption ability of natural mesoporous material by impregnating with chloride salts for development of a new desiccant filter, Adsorption. 17 (2011) 675–686.

[13]   H. Liu, K. Nagano, J. Togawa, A composite material made of mesoporous siliceous shale impregnated with lithium chloride for an open sorption thermal energy storage system, Sol. Energy. 111 (2015) 186–200.

[14] A. Sapienza, I.S. Glaznev, S. Santamaria, A. Freni, Y.I. Aristov, Adsorption chilling driven by low temperature heat: New adsorbent and cycle optimization, Appl. Therm. Eng. 32 (2012) 141–146.

[15] A. Sapienza, A. Velte, I. Girnik, A. Frazzica, G. Füldner, L. Schnabel, Y. Aristov, "Water - Silica Siogel" working pair for adsorption chillers: Adsorption equilibrium and dynamics, Renew. Energy. 110 (2017) 40–46.

[16] S. Santamaria, A. Sapienza, A. Frazzica, A. Freni, I.S. Girnik, Y.I. Aristov, Water adsorption dynamics on representative pieces of real adsorbers for adsorptive chillers, Appl. Energy. 134 (2014) 11–19.

[17] L. Schnabel, M. Tatlier, F. Schmidt, A. Erdem-Şenatalar, Adsorption kinetics of zeolite coatings directly crystallized on metal supports for heat pump applications (adsorption kinetics of zeolite coatings), Appl. Therm. Eng. 30 (2010) 1409–1416.

[18] A. Frazzica, G. Füldner, A. Sapienza, A. Freni, L. Schnabel, Experimental and theoretical analysis of the kinetic performance of an adsorbent coating composition for use in adsorption chillers and heat pumps, Appl. Therm. Eng. 73 (2014) 1022–1031.

[19] Y.I. Aristov, M.M. Tokarev, A. Freni, I.S. Glaznev, G. Restuccia, Kinetics of water adsorption on silica Fuji Davison RD, Microporous Mesoporous Mater. 96 (2006) 65–71.

[20] A. Freni, L. Bonaccorsi, L. Calabrese, A. Caprì, A. Frazzica, A. Sapienza, SAPO-34 coated adsorbent heat exchanger for adsorption chillers, Appl. Therm. Eng. 82 (2015) 1–7.

[21] K. Wang, S. Qiao, X. Hu, Study of isosteric heat of adsorption and activation energy for surface diffusion of gases on activated carbon using equilibrium and kinetics information, Sep. Purif. Technol. 34 (2004) 165–176.

[22] I. Medveď, R. Černý, Surface diffusion in porous media: A critical review, Microporous Mesoporous Mater. 142 (2011) 405–422.

[23] B. Sun, A. Chakraborty, Thermodynamic frameworks of adsorption kinetics modeling: Dynamic water uptakes on silica gel for adsorption cooling applications, Energy. 84 (2015) 296–302.

[24] A. Fenti, S. Salvestrini, Analytical solution of the Langmuir-based linear driving force model and its application to the adsorption kinetics of boscalid onto granular activated carbon, React. Kinet. Mech. Catal. 125 (2018).

[25] A. Patton, B.D. Crittenden, S.P. Perera, Use of the Linear Driving Force Approximation to Guide the Design of Monolithic Adsorbents, Chem. Eng. Res. Des. 82 (2004) 999–1009.

[26] A. Sakoda, M. Suzuki, Fundamental study on solar powered adsorption cooling system, J. Chem. Eng. Japan. 17 (1984) 52–57.

[27] M. Verde, K. Harby, R. de Boer, J.M. Corberán, Performance evaluation of a waste-heat driven adsorption system for automotive air-conditioning: Part I –

Modeling and experimental validation, Energy. 116 (2016) 526–538.

[28] L.X. Gong, R.Z. Wang, Z.Z. Xia, C.J. Chen, Design and performance prediction of a new generation adsorption chiller using composite adsorbent, Energy Convers. Manag. 52 (2011) 2345–2350.

[29] M.H. Chahbani, J. Labidi, J. Paris, Modeling of adsorption heat pumps with heat regeneration, Appl. Therm. Eng. 24 (2004) 431–447.

[30] Z. Xu, J.G. Cai, B.C. Pan, Mathematically modeling fixed-bed adsorption in aqueous systems, J. Zhejiang Univ. Sci. A. 14 (2013) 155–176.

[31] K. Wang, S. Qiao, X. Hu, Study of isosteric heat of adsorption and activation energy for surface diffusion of gases on activated carbon using equilibrium and kinetics information, Sep. Purif. Technol. 34 (2004) 165–176.

[32] J. Solsvik, H.A. Jakobsen, A Survey of Multicomponent Mass Diffusion Flux Closures for Porous Pellets: Mass and Molar Forms, Transp. Porous Media. 93 (2012) 99–126.

[33] H. Demir, M. Mobedi, S. Ülkü, Effects of porosity on heat and mass transfer in a granular adsorbent bed, Int. Commun. Heat Mass Transf. 36 (2009) 372–377.

[34] A.D. Grekova, L.G. Gordeeva, Y.I. Aristov, Composite "LiCl/vermiculite" as advanced water sorbent for thermal energy storage, Appl. Therm. Eng. 124 (2017) 1401–1408.

[35] Y.I. Aristov, I.S. Glaznev, I.S. Girnik, Optimization of adsorption dynamics in adsorptive chillers: Loose grains configuration, Energy. 46 (2012) 484–492.

[36] J.H. Hills, Non-isothermal adsorption in a pellet, Chem. Eng. Sci. 46 (1991) 69–74.

[37] A. Freni, G. Maggio, F. Cipitì, Y.I. Aristov, Simulation of water sorption dynamics in adsorption chillers: One, two and four layers of loose silica grains, Appl. Therm. Eng. 44 (2012) 69–77.

[38] Marlinda, A.S. Uyun, T. Miyazaki, Y. Ueda, A. Akisawa, Marlinda, A.S. Uyun, T. Miyazaki, Y. Ueda, A. Akisawa, Performance Analysis of a Double-effect Adsorption Refrigeration Cycle with a Silica Gel/Water Working Pair, Energies. 3 (2010) 1704–1720.

[39] I.I. El-Sharkawy, H. AbdelMeguid, B.B. Saha, Potential application of solar powered adsorption cooling systems in the Middle East, Appl. Energy. 126 (2014) 235–245.

[40] I.P. Koronaki, E.G. Papoutsis, V.D. Papaefthimiou, Thermodynamic modeling and exergy analysis of a solar adsorption cooling system with cooling tower in Mediterranean conditions, Appl. Therm. Eng. 99 (2016) 1027–1038.

[41] S. Riffat, Y. Su, Y. Ding, Thermochemical cooling system based on adsorption pumping pipe, Int. J. Low-Carbon Technol. 11 (2014) 35–41.

[42] A. Li, K. Thu, A. Bin Ismail, K.C. Ng, A heat transfer correlation for transient vapor uptake of powdered adsorbent embedded onto the fins of heat exchangers, Appl. Therm. Eng. 93 (2016) 668–677.

[43] M. Verde, K. Harby, J.M. Corberán, Optimization of thermal design and geometrical parameters of a flat tube-fin adsorbent bed for automobile air-conditioning, Appl. Therm. Eng. 111 (2017) 489–502.

[44] A. Rezk, R.K. Al-Dadah, S. Mahmoud, A. Elsayed, Effects of contact resistance and metal additives in finned-tube adsorbent beds on the performance of silica gel/water adsorption chiller, Appl. Therm. Eng. 53 (2013) 278–284.

[45] S.T.O., Silica gel/water based adsorption cooling system employing compact fin-tube heat exchanger, 九州大学, 2013.

[46] K. Grabowska, M. Sosnowski, J. Krzywanski, K. Sztekler, W. Kalawa, A. Zylka, W. Nowak, The Numerical Comparison of Heat Transfer in a Coated and Fixed Bed of an Adsorption Chiller, J. Therm. Sci. 27 (2018) 421–426.

[47] M. Sosnowski, J. Krzywanski, K. Grabowska, R. Gnatowska, Polyhedral meshing in numerical analysis of conjugate heat transfer, EPJ Web Conf. 180 (2018) 02096.

[48] K. Grabowska, J. Krzywański, K. Sztekler, W. Kalawa, W. Nowak, Fuzzy logic approach in the analysis of heat transfer in a porous sorbent bed of the adsorption chiller, Tech. Sci. 4 (2018) 281–290.

[49] H. Liu, K. Nagano, J. Togawa, H. Liu, K. Nagano, J. Togawa, Performance of LiCl Impregnated Mesoporous Material Coating over Corrugated Heat Exchangers in a Solid Sorption Chiller, Energies. 11 (2018) 1565.

[50] S.H. Seol, K. Nagano, J. Togawa, A new experimental method to separate interfacial and internal mass transfer on coated adsorbent, Appl. Therm. Eng. 159 (2019) 113869.

[51] A. Sharafian, C. McCague, M. Bahrami, Impact of fin spacing on temperature distribution in adsorption cooling system for vehicle A/C applications, Int. J. Refrig. 51 (2015) 135–143.

[52] J. Ammann, P. Ruch, B. Michel, A.R. Studart, Quantification of heat and mass transport limitations in adsorption heat exchangers: Application to the silica gel/water working pair, Int. J. Heat Mass Transf. 123 (2018) 331–341.

[53] J. Ammann, B. Michel, P.W. Ruch, Characterization of transport limitations in SAPO-34 adsorbent coatings for adsorption heat pumps, Int. J. Heat Mass Transf. 129 (2019) 18–27.

[54] S. Jribi, T. Miyazaki, B.B. Saha, A. Pal, M.M. Younes, S. Koyama, A. Maalej, Equilibrium and kinetics of CO 2 adsorption onto activated carbon, Int. J. Heat Mass Transf. 108 (2017) 1941–1946.

[55] T. OUCHI, S. TAKATA, Y. HAMAMOTO, H. MORI, A. ETOH, Adsorption Equilibrium and Desorption Rate of Adsorbent Coated on Heat Transfer Plate,

Trans. JAPAN Soc. Mech. Eng. Ser. B. 79 (2013) 2602–2606.

[56] M. Tatlıer, B. Tantekin-Ersolmaz, A. Erdem-Şenatalar, A novel approach to enhance heat and mass transfer in adsorption heat pumps using the zeolite–water pair, Microporous Mesoporous Mater. 27 (1999) 1–10.

[57] H.-J. Bart, S. Scholl, eds., Innovative Heat Exchangers, Springer International Publishing, Cham, 2018.

[58] T. Bello-Ochende, L. Liebenberg, J.P. Meyer, Constructal design: Geometric optimization of micro-channel heat sinks, S. Afr. J. Sci. 103 (2007) 483–489.

[59] B. Shao, L. Wang, J. Li, Z. Sun, Application of thermal resistance network model in optimization design of micro-channel cooling heat sink, Int. J. Numer. Methods Heat Fluid Flow. 19 (2009) 535–545.

[60] W.M. Alaian, E.A. Elnegiry, A.M. Hamed, Experimental investigation on the performance of solar still augmented with pin-finned wick, Desalination. 379 (2016) 10–15.

[61] M. Verde, L. Cortés, J.M. Corberán, A. Sapienza, S. Vasta, G. Restuccia, Modelling of an adsorption system driven by engine waste heat for truck cabin A/C. Performance estimation for a standard driving cycle, Appl. Therm. Eng. 30 (2010) 1511–1522.

[62] M. Mohammadzadeh Kowsari, H. Niazmand, M.M. Tokarev, Bed configuration effects on the finned flat-tube adsorption heat exchanger performance: Numerical modeling and experimental validation, Appl. Energy. 213 (2018) 540–554.

CHAPTER 5. SIMULATION ON ANNUAL PERFORMANCE OF SOLAR AHP USING WSS COMPOSITE FOR LOW-CARBON AIR CONDITIONING

5.1 INTRODUCTION

Environmental issues resulted from energy usage has been continued despite researches and efforts to reduce electricity consumption. International Institute of Refrigeration (IIR) defined that the refrigeration and air-conditioning sector consume approximately 17% of the overall electricity use of the worldwide [1]. Aside from the environmental pollution which is produced when generating electricity for the operation of cooling systems, the most of refrigerants of vapor compression-cooling systems themselves are harmful to environment. The most representative CFCs and HCFCs are well known to results in deplete the ozone layer [2]. Thermal-driven cooling systems give significant energy saving compared to traditional vapor compression systems and have low GWP and ODP [3]. As a part of the heat-driven systems, adsorption heat pump (AHP) has attracted huge interest due to its eco-friendly operation and applicability of low-level heat sources less than 100°C. AHP systems have an advantage compared to absorption cycles that the heat source with the lower temperature can be used [4,5]. Agnieszka and Szaflik [6] compared the cooling performance of the adsorption and absorption chillers at the driving temperature between 55 and 95 °C, showing strong limitation to the lowest possible driving temperature. Utilization of solar energy makes the AHP far more attractive because it significantly decreases fossil energy input for the operation the system. Followings introduces previous studies related to the solar adsorption heat pump systems. Yong et al. [7] investigated the performance of a solar adsorption cooling system by using a lumped numerical modeling, according to four different collectors: single and double glazed cover, transparent insulation material cover. Koronaki et al. [8] examined the application of an AHP under climatic conditions of eastern Mediterranean area based on a mathematical modeling. They also provided overall energy and exergy efficiencies of the cooling system using hybrid photovoltaic-thermal (PV/T) collector. El-Sharkawy et al. [9] compared performances of the AHP in two cases which are with and without the hot water buffer storage by using a mathematical modeling. They addressed that the time which shows the maximum cooling capacity is revealed different for these two cases with and without the hot water tank. According to Zhang et al. [10], the cooling capacity is affected by the initial temperature of the hot water which is dependent on the heat capacity of water in the tank. Thus, optimum initial temperature and water volume in the tank need

to be evaluated for the optimal performance. Di et al. [11] also insisted necessity of a buffer tank in order to get the better performance in case of lacking solar radiation. It was also pointed out in the paper that the thermal capacity ratio between the adsorbent and the metal affects the regeneration heat and COP. Habib et al. [12] distinctively applied activated carbon-methanol and activated carbon fiber (ACF)-ethanol working pairs to the solar AHP system to compare their performance with that of the silica gel-water system. Even though the ACF-ethanol presented the highest uptake, the silica gel-water pair showed the highest cooling capacity due to the large evaporation heat of the water. Alam et al. [13] emphasized that cycle time is the most influential parameter for a solar adsorption cooling system, and the number of required solar collectors may be reduced by optimizing the cycle time. Zhai and Wang [14] provided the result showing that the initial temperature of regeneration water greatly affect the cooling capacity of a AHP system. That is, sharp increase of the cooling performance was observed when the initial hot water temperature increases from 55 ℃ to 60 ℃. Pan and Wang [15] proposed the new operation strategy of a AHP system based on a mathematical modelling, which showed enhanced the utilization efficiency of solar cooling system without any decrease in cooling capacity. The research work of Alahmer et al. [16] using TRANSYS presented that the solar cooling system reduces electrical power consumption by 28~34% compared to the conventional vapor compression cooling system. Sim [17] also used TRANSYS to suggest the optimum solar collector area with respect to its lifecycle saving. Zhai et al. [18] installed a solar AHP system at the Shanghai Research Institute of Building Science. They could obtain average cooling power of 15.3kW using AHP, referring solar fraction of 0.71. Habib et al. [19] applied experimentally obtained heat source temperature data from 22 units of solar collectors into a mathematical model of an AHP. They introduced a two-stage and four beds cooling system which enables effective operation when the heat source temperature is below 60 ℃.

As shown in the previous researches listed above, the performance of solar AHP systems is strongly dependent on conditions of the regeneration water. Thus, effective use of the obtained thermal energy through the solar collector is required. An AHP system inevitably undergoes sensible heat loss when switching the adsorption and desorption mode. Therefore, the adsorbent having large adsorption capacity enables the system to go through less frequent switching between adsorption and desorption.

Composite "salt inside porous matrix" is an adsorbent that exhibits an enhanced equilibrium adsorption capacity compared with that of traditional working pairs. Various composite materials have been studied in a lot of researches [20–25].

As a part of them, our research team also has previously reported the enhanced adsorption capacity of a natural mesoporous material called Wakkanai siliceous shale (WSS) by impregnating several kinds of chlorides and verified the its applicability as a host matrix. Nakabayashi et al. [26] suggested an appropriate impregnation amount of chlorides based on water sorption amount and pore volume to prevent a carryover. Togawa et al. [27] conducted the salt-leakage test of the WSS impregnated with 20 wt.% of LiCl to ensure that there is no carryover under the working condition of AHP. Liu et al. [28] proved the stability of WSS impregnated with LiCl by repeating adsorptions (0.55 g/g, 25 ℃, RH 95 %) and desorption (0.1 g/g, 60 ℃, RH 5 %) for 250 repetitions. Also as presented in our recent research, WSS + LiCl 20 wt.% exhibited a higher adsorption capability, which allows the system to be operated with a longer cycle time to reduce the heat loss occurs when switching between adsorption and desorption modes [29].

Therefore, this research aims to present application effect of the WSS impregnated with 20 wt.% of lithium chloride to the solar adsorption heat pump system. The mathematical model is used to analyze the cooling performance under the various operating conditions. The zero-dimensional lumped modeling of AHP systems, which has been proposed by numerous researchers, employs the LDF model to calculate mass transfer and energy balance equations to calculate heat transfer, respectively [30–32]. Because of the advantages of fast and simple calculations, this zero-dimensional AHP model enables the analysis on long term-operations (i.e., seasonal and annual) of AHP thermally supported by a solar collector. With this perspective, the present study provides analysis of annual cooling performance of AHP based on the mathematical model under the different weather conditions. Four metropolises having distinct climatic characteristics are selected: Tokyo (35 º N, 139 º E), Florida (28 º N, 81 º W), Hawaii (19 º N, 155 º W), Dubai (25 º N, 55 º E). Lastly, the economic analysis of solar AHP system is provided to show economic competitiveness of the system.

5.2 SYSTEM DESCRIPTION AND SIMULATION METHODOLOGY

Fig. 5. 1 describes a schematic diagram of the cooling system applying a solar adsorption heat pump (AHP) and electric heat pumps (EHP). Firstly, the solar AHP system consists of two main categories which are AHP unit and the solar thermal system. The adsorption unit includes two adsorbers, an evaporator and a condenser. The basic working principle of the AHP is as following. The evaporated water vapor from the evaporator is adsorbed by the adsorbents, which is filled between the heat exchanger fins. The heat of adsorption is removed by the circulating cooling water, and absorbed heat is released through the cooling tower. At the same time, the other adsorber which finished the adsorption process undergoes the desorption process by supplying the hot water generated from a solar thermal system. The desorbed water vapor then goes to the condenser to be condensed, and the system switches the role of two adsorbers to obtain continuous cooling effect. The other main components of the solar AHP system includes a solar collector, a hot water storage tank and an auxiliary heat source as a back-up thermal source. Because of near coincidence of the peak cooling load with available solar energy [16], the solar AHP system is advantageous to operate together with a traditional electric heat pumps. The detailed description of the cooling load allocation to these two cooling systems will be provided in following Chapter 5.5.

Fig. 5. 2 shows operating strategy of the cooling system AHP and EHP systems. The first loop decides whether to use auxiliary heat or not. To explain, the auxiliary heating device (natural gas in this study) starts to provide thermal energy to the hot water storage tank to heat it up, if the obtainable cooling capacity from the AHP powered by solar energy is not enough to cover the cooling load. The supply of auxiliary thermal energy stops if the temperature of regeneration water reaches to 80 °C. In case that the cooling load still exceeds the cooling capacity of the AHP, the EHP starts to operate to cover the rest of the cooling load.
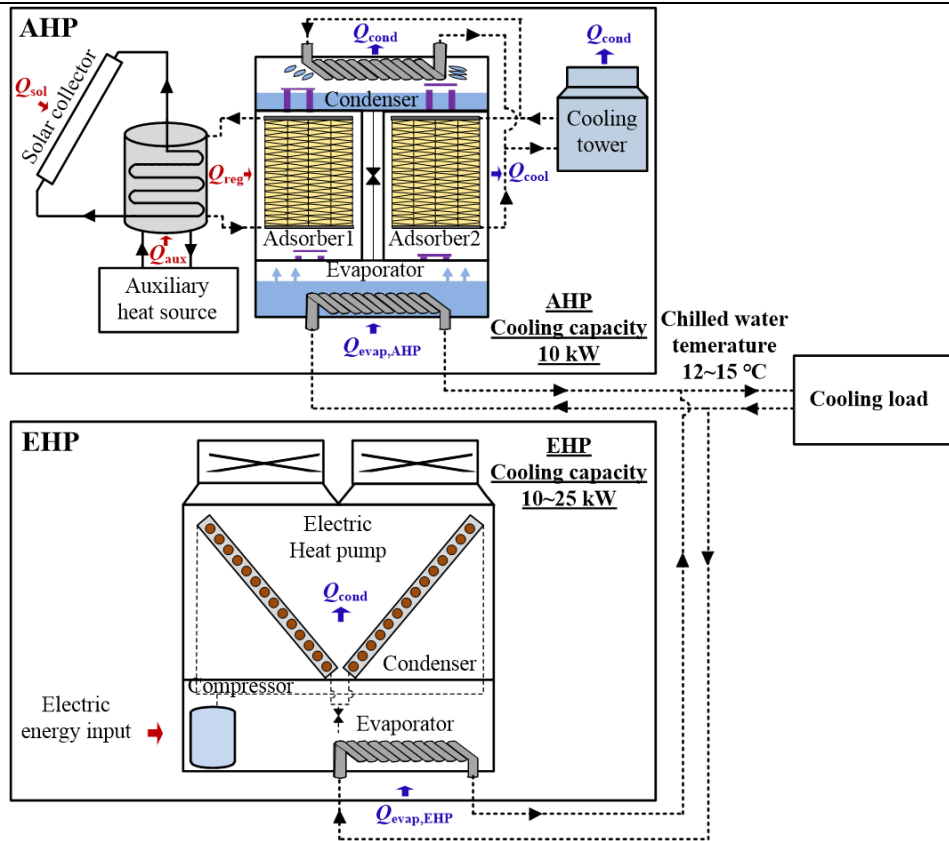
Fig. 5. 1 Schematic diagram of the cooling system applying AHP and EHP
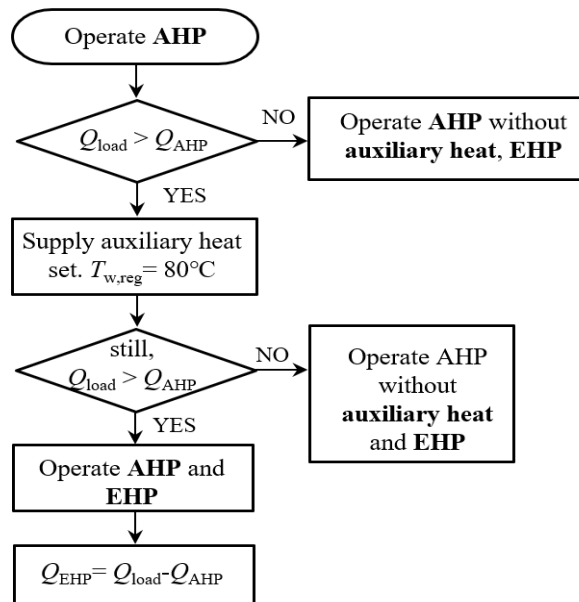
Fig. 5. 2 Operating strategy of the cooling system applying AHP and EHP

5.3 MATHEMATICAL MODELLING OF SOLAR AHP SYSTEM

5.3.1 Adsorbent Equilibrium and Kinetic

The equilibrium adsorption amount of WSS + LiCl 20 wt.% can be described by the equation proposed by Yahia et al.[33]. On the other hand, the equilibrium adsorption amount of the A-type silica gel is expressed using the equation proposed by Li et al. [34], as shown in Eq. (2-22) and (2-23) of Chapter 2.

The adsorption kinetic based on the LDF theory is expressed by Eq. (4-3) and (4-4) in Chapter 4 which includes thermal effect on the kinetic characteristics [35]. The slope and the y-intercept of the Eq. (4-4) are derived from the previous research on the gravimetric estimation of the mass transfer, introduced in Chapter 4 [29].

5.3.2 Adsorption/ Desorption Model

Energy balance equations applied to the mathematical modeling are as shown followings. Firstly, the bed 1 starts from the desorption mode. The adsorbent temperature (T_a) and water outlet temperature ($T_{b,w,o}$) are calculated by Eq. (5-1)~ (5-3).

In the Eq. (5-1), the heat flux which is supplied to the control volume is calculated by temperature difference between water inlet and outlet, and the one exiting from the system is calculated with temperature difference between the regeneration water and the adsorbent. The heat transfer effectiveness (ε) was derived from our previous research introduced in Chapter 4 [29].

$$\left(C_{a1} + C_{metal} + M_a q C_{p,w}\right)\frac{dT_{a1}}{dt} = M_a \frac{dq}{dt}\Delta H(T_{a1}) + \dot{Q}_1 \tag{5-1}$$

$$C_{b1,w}\frac{dT_{b1,w,o}}{dt} = \dot{m}_{b,w}C_{p,w}\left(T_{b1,w,i} - T_{b1,w,o}\right) - \dot{Q}_1 \tag{5-2}$$

$$\dot{Q}_1 = \varepsilon_{b1}\dot{m}_{b1,w}C_{p,w}\left(T_{b1,w,i} - T_{a1}\right) \tag{5-3}$$

Similarly, in the adsorption bed 2, adsorbent temperature and water outlet temperature during the adsorption process are obtained by following Eq. (5-4)~ (5-6).

$$\left(C_{a2} + C_{metal} + M_a q C_{p,w}\right)\frac{dT_{a2}}{dt}$$

$$= M_a \frac{dq}{dt}\left\{\Delta H(T_{b2}) - C_{p,v}(T_{a2} - T_{evap})\right\} - \dot{Q}_2 \tag{5-4}$$

$$C_{b2,w}\frac{dT_{b2,w,o}}{dt} = -\dot{m}_{b2,w}C_{p,w}\left(T_{b2,w,o} - T_{b2,w,i}\right) - \dot{Q}_2 \tag{5-5}$$

$$\dot{Q}_2 = \varepsilon_{b2}\dot{m}_{b2,w}C_{p,w}\left(T_{a2} - T_{b2,w,i}\right) \tag{5-6}$$

5.3.2 Evaporator and Condenser Model

The condensation rate is expressed with the energy conservation equation as shown in Eq. (5-7). Also, the variation of water outlet temperature is calculated through the energy conservation equation of Eq. (5-8) and (5-9).

$$\dot{m}_{cond} = \frac{\dot{m}_{cond,w}C_{p,w}(T_{cond,w,o} - T_{cond,w,i})}{C_{p,v}\left(T_{cond,v,i} - T_{cond}\right) + h(P_{cond})} \tag{5-7}$$

$$C_{cond,w}\frac{dT_{cond,w,o}}{dt} = \dot{m}_{cond,w}C_{p,w}\left(T_{cond,w,i} - T_{cond,w,o}\right) - \dot{Q}_{cond} \tag{5-8}$$

$$\dot{Q}_{cond} = \varepsilon_{cond}\dot{m}_{cond,w}C_{p,w}\left\{\begin{array}{l}\left(\alpha(T_{cond,w,i} - T_{cond}) + \right.\\ \left.(1-\alpha)(\frac{T_{cond,w,o} - T_{cond}}{1 - \varepsilon_{cond}})\right\}\end{array}\right. \tag{5-9}$$

Those for the case of the evaporator can be yield with the same calculation method Eq. (5-10) ~ (5-12).

$$\dot{m}_{evap} = \frac{-\dot{m}_{evap,w}C_{p,w}(T_{evap,w,i} - T_{evap,w,o})}{C_{p,w}\left(T_{cond} - T_{evap}\right) - h(P_{evap})} \tag{5-10}$$

$$C_{evap,w}\frac{dT_{evap,w,o}}{dt} = \dot{m}_{evap,w}C_{p,w}\left(T_{evap,w,i} - T_{evap,w,o}\right) - \dot{Q}_{evap} \tag{5-11}$$

$$\dot{Q}_{\text{evap}} = \varepsilon_{\text{evap}} \dot{m}_{\text{evap,w}} C_{\text{p,w}} \left\{ \begin{array}{c} \left(\alpha(T_{\text{evap,w,i}} - T_{\text{evap}}) + \right. \\ \left. (1 - \alpha)(\dfrac{T_{\text{evap,w,o}} - T_{\text{evap}}}{1 - \varepsilon_{\text{evap}}}) \right\} \end{array} \right. \tag{5-12}$$

5.3.3 Solar Thermal System Model

The energy balance absorbed by the collector is established by following Eq. (5-13), where $F_{\text{R}}\tau\alpha$ is intercept efficiency of the collector [-], $F_{\text{R}}U_{\text{L}}$ is the first-order coefficient [W/(m^{2}K)]. In this research, $F_{\text{R}}\tau\alpha$ value of 0.64 and $F_{\text{R}}U_{\text{L}}$ value of 0.89 W/(m^{2}K) are derived from Reda et al. [36]. The terms on the left side describes transient temperature variation of the stored water. The first term of the right side depicts input energy through the collector which is proportional to the solar radiation and collector area. The second term refers to the heat transfer from the collector toward ambient. Third term shows heat transfer amount to the AHP system for the desorption process. Lastly, as presented in Eq. (5-14), $\dot{Q}_{\text{L}}$ defines heat loss from the storage tank to the ambient which can be expressed proportional to the water volume. The heat loss coefficient of 6.84 W/(m^{3}K) is applied in this research [37].

$$C_{tw} \frac{dT_{tw}}{dt} = F_R A_{SC} I(\tau\alpha) - F_R U_L A_{SC}(T_{tw} - T_{amb})$$
$$- \dot{m}_{b1,w} C_{p,w}(T_{tw} - T_{b1,w,o}) - \dot{Q}_L \tag{5-13}$$

$$\dot{Q}_L = 6.84(T_{\text{tw}} - T_{\text{amb}})V_{\text{tw}} \tag{5-14}$$

5.4 SIMULATION CONDITIONS AND COOLING LOAD

5.4.1 Meteorological Information

In this research, climate conditions of four metropolises having distinct weather characteristics are applied to the mathematical model. Fig. 5. 3 and Fig. 5. 4 provide annual ambient temperature and daily average solar radiation at four cities, respectively. The weather data were derived from the website of 'Climate One Building' [38]. Relatively strong vertical fluctuation in solar radiation is observed in the cases of Tokyo and Florida. On the other hand, it can be easily noticed that the daily solar radiation in Dubai rarely shows vertical fluctuation, which refers to stable utilization of the solar energy. Another climate characteristic of Dubai is long cooling period and extremely high ambient temperature especially from May to September. Hawaii of U.S. also presents long cooling period. However, the ambient temperature distribution throughout the year is quite moderate, rather than showing obviously high values during the concentrated period.
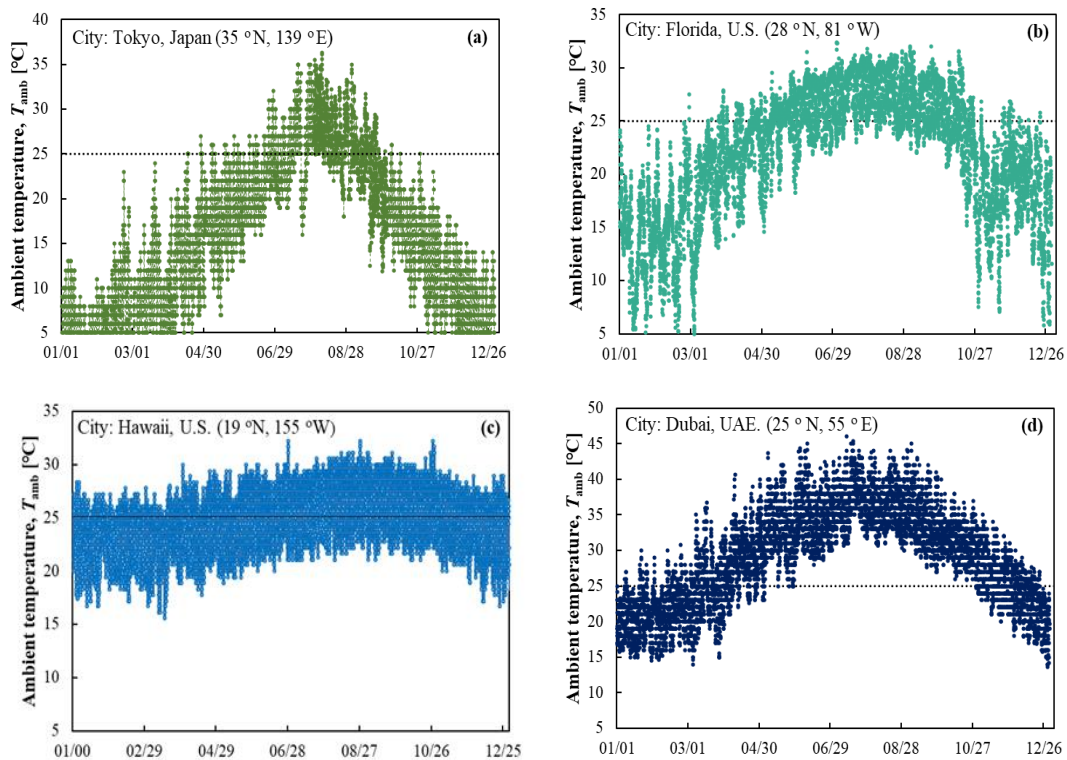
Fig. 5. 3 Annual ambient temperatures at four cities:
(a) Tokyo, Japan, (b) Florida, U.S., (c) Hawaii, U.S., (d) Dubai, UAE.
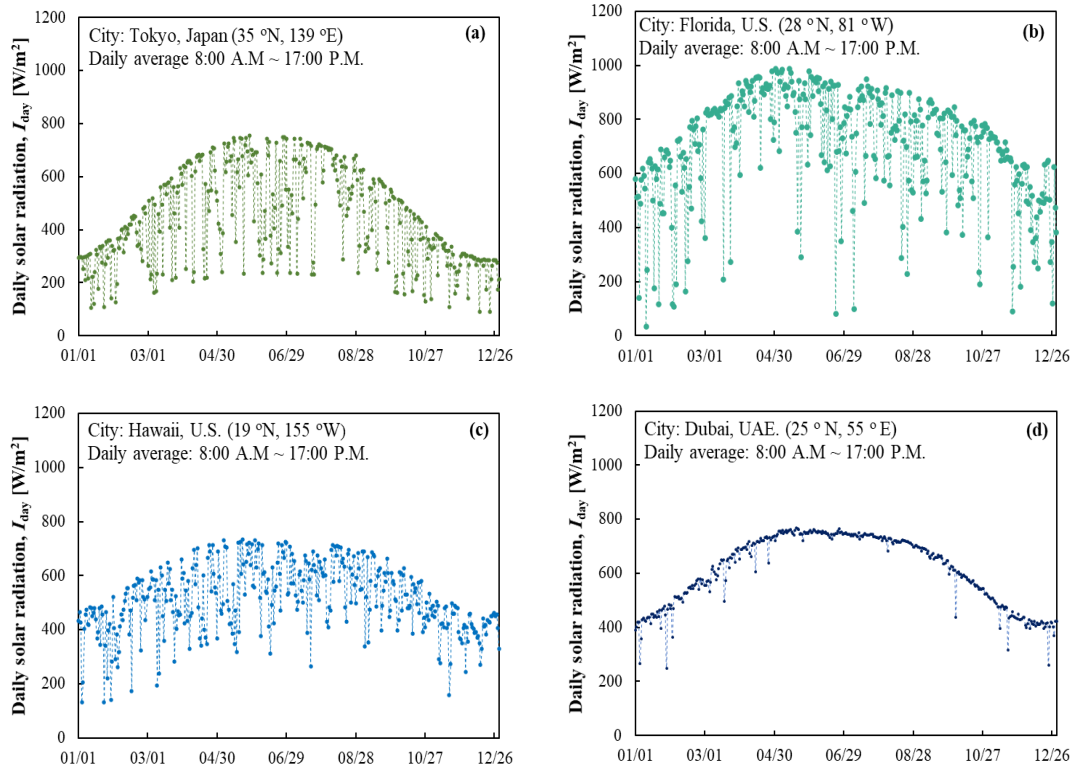
Fig. 5. 4 Daily average values of radiation throughout the year at four cities: (a) Tokyo, Japan, (b) Florida, U.S. (c) Hawaii, U.S., (d) Dubai, UAE.

5.4.2 Cooling Load Calculation

Fig. 5. 5 depicts monthly total and maximum cooling load of four cities. The building energy simulation program named 'EnergyPlus^{TM}' was used for the calculation. The target building was considered as a small-scale office building requires cooling demand from 8 A.M. to 8 P.M. Its detailed design specifications are listed in Table 5. 1. As presented in Fig. 5. 4 and Fig. 5. 5, the cooling load characteristics of the four cities are strongly dependent on the climate conditions. Cooling demand is observed during whole year in Dubai, and it shows especially high cooling demand from May to September. The total cooling load in Florida tended to be concentrated around these periods as well. Hawaii also required cooling system all the year round, however period which shows especially high cooling demand was not observed. Although the maximum cooling load in Tokyo is higher than that of Hawaii during the summer, its total cooling load is lower which implies relatively sporadic cooling load distribution.
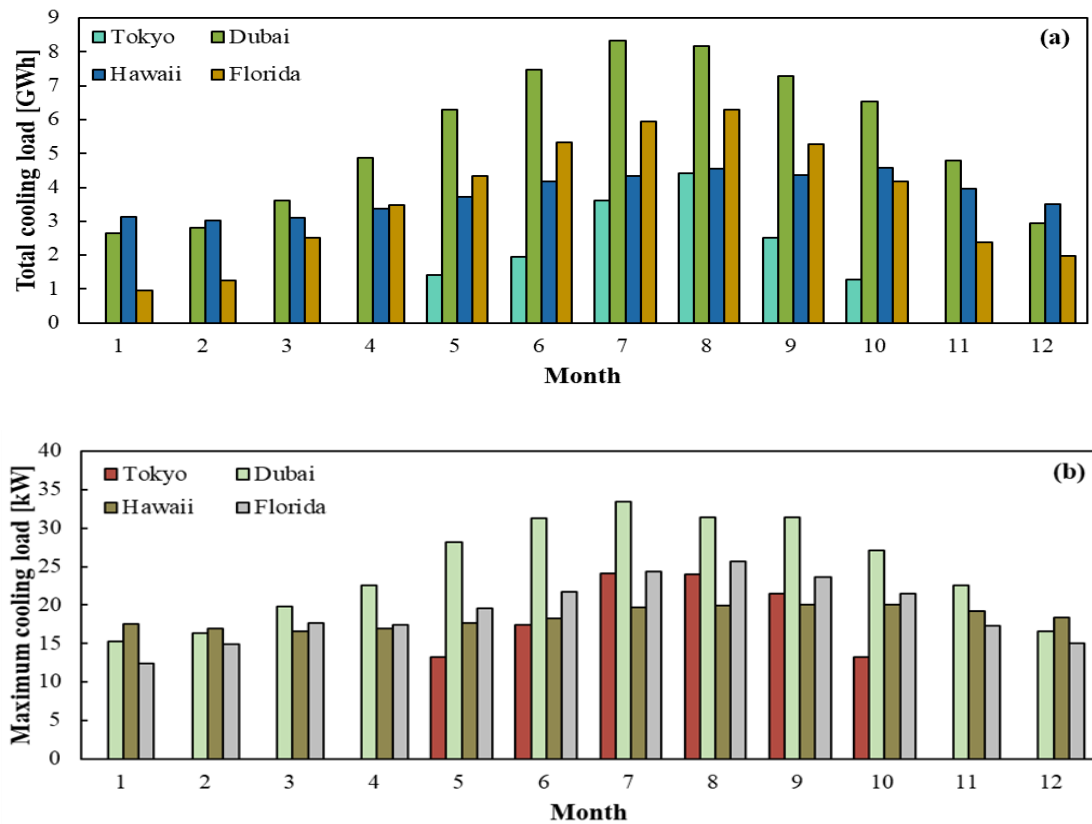
Fig. 5. 5 Monthly (a) total cooling load and (b) maximum cooling load

Table 5. 1 Cooling load calculation conditions of the target building

Parameters	Values
Floor area [m^2/floor]	200 (2 story)
People [person/m^2]	0.15
Lights [W/m^2]	12
Electric equipment [W/m^2]	11
Infiltration per person [m^3/h]	25
Roof (U [W/m^{2}K])	0.284
Floor (U [W/m^{2}K])	1.45
Interior walls (U [W/m^{2}K])	2.58
Exterior walls (U [W/m^{2}K])	0.99
Window (U [W/m^{2}K])	6.42
Window-wall ratio [%]	24

5.5 SIMULATION RESULTS AND DISCUSSIONS

5.5.1 System Performance in Different Cities

Fig. 5. 6 compares the cooling capacity obtained by AHP and EHP in August. The maximum AHP cooling capacity was approximately 10 kW in all cities. The sum of AHP cooling energies of Tokyo and Hawaii were 2554 and 3025 kWh, respectively. It can also be observed that the peak load of Tokyo is higher than Hawaii due to high ambient temperature and solar radiation in the concentrated period. Florida presented relatively stable AHP cooling performance. The peak cooling load of Florida was obviously higher than that of Tokyo and Hawaii, due to the high solar radiation. Meanwhile, it is revealed that AHP works the most stably in Dubai because of uniform solar radiation throughout the month, showing the sum of AHP cooling energy around 3190 kWh.

Fig. 5. 7 represents comparison of heat capacity obtained by solar energy and auxiliary heat source. The maximum solar heat energy of four cities was shown similar around 25 kW. The clear difference was found from stability of solar radiation. As mentioned earlier, Dubai presented climatic characteristic of constant solar radiation, which can be considered as a huge advantage in applying AHP in the cooling system. The auxiliary heat supports solar collectors in case of insufficient radiation and larger cooling demand than the cooling capacity of AHP with currently obtainable solar thermal energy. Use of natural gas as the auxiliary heat source is assumed in this research. As presented in the Fig. 5. 2, the combustion of the natural gas is dependent on cooling load and obtainable regeneration water temperature.

Fig. 5. 8 depicts hourly variation of regeneration and chilled water temperature in August. The variation of the hot water changed in accordance with the solar radiation, and its temperature distributed around 80 ℃ in general. Because of stable solar radiation, the regeneration water temperature in Dubai was highly constant.
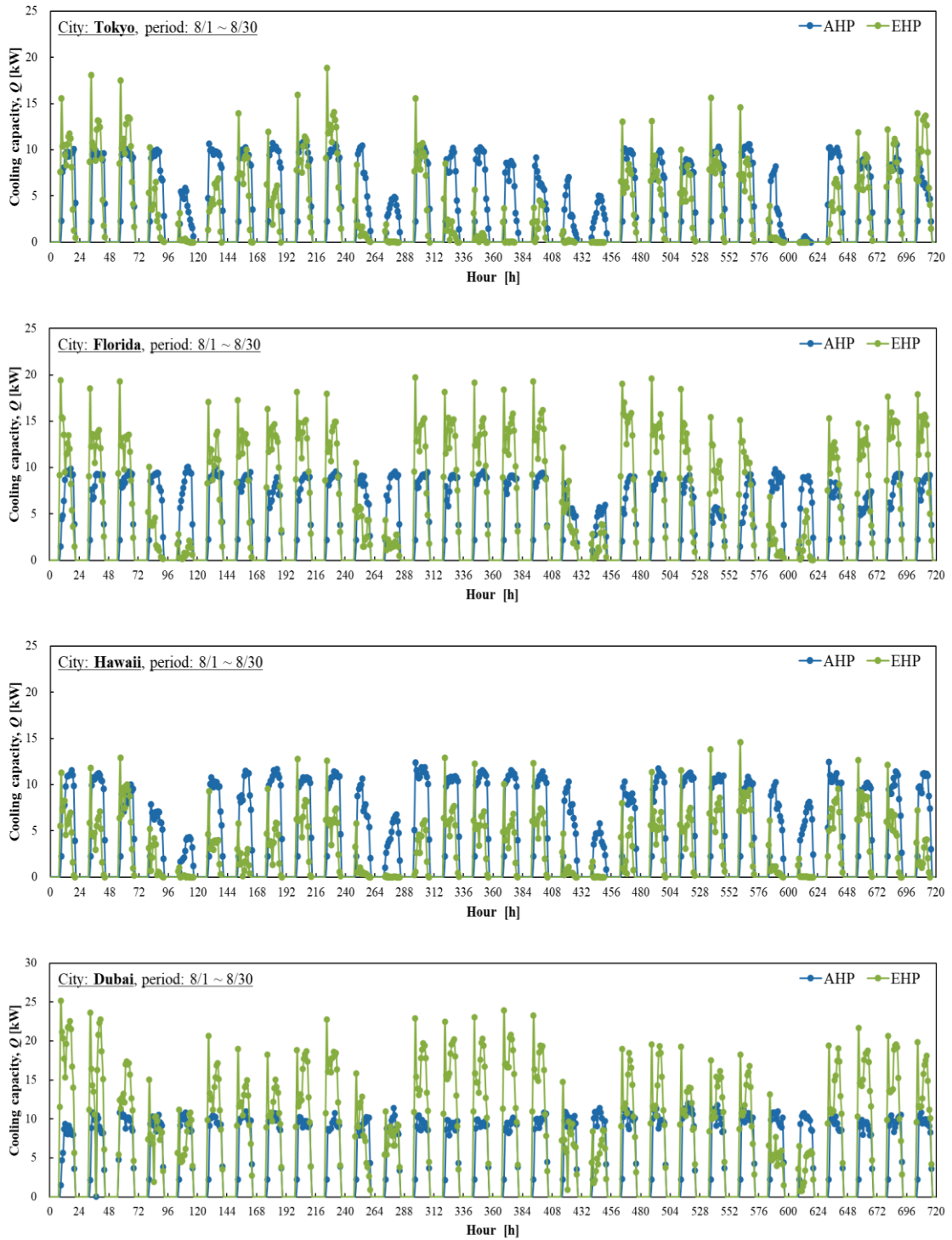
Fig. 5. 6 Comparison of cooling capacity obtained by AHP and EHP at different cities
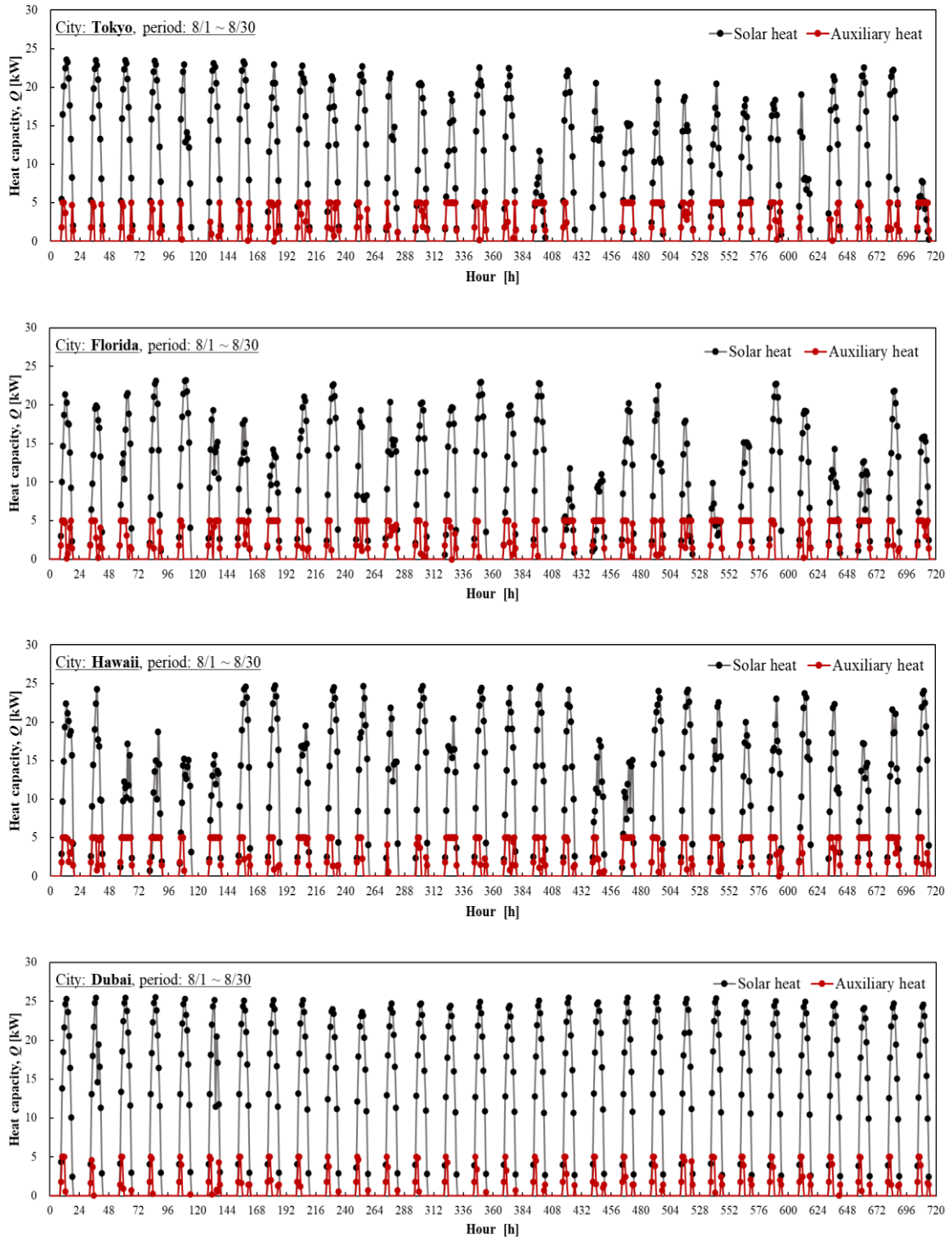
Fig. 5. 7 Comparison of heat capacity obtained by auxiliary heat and solar heat at different cities
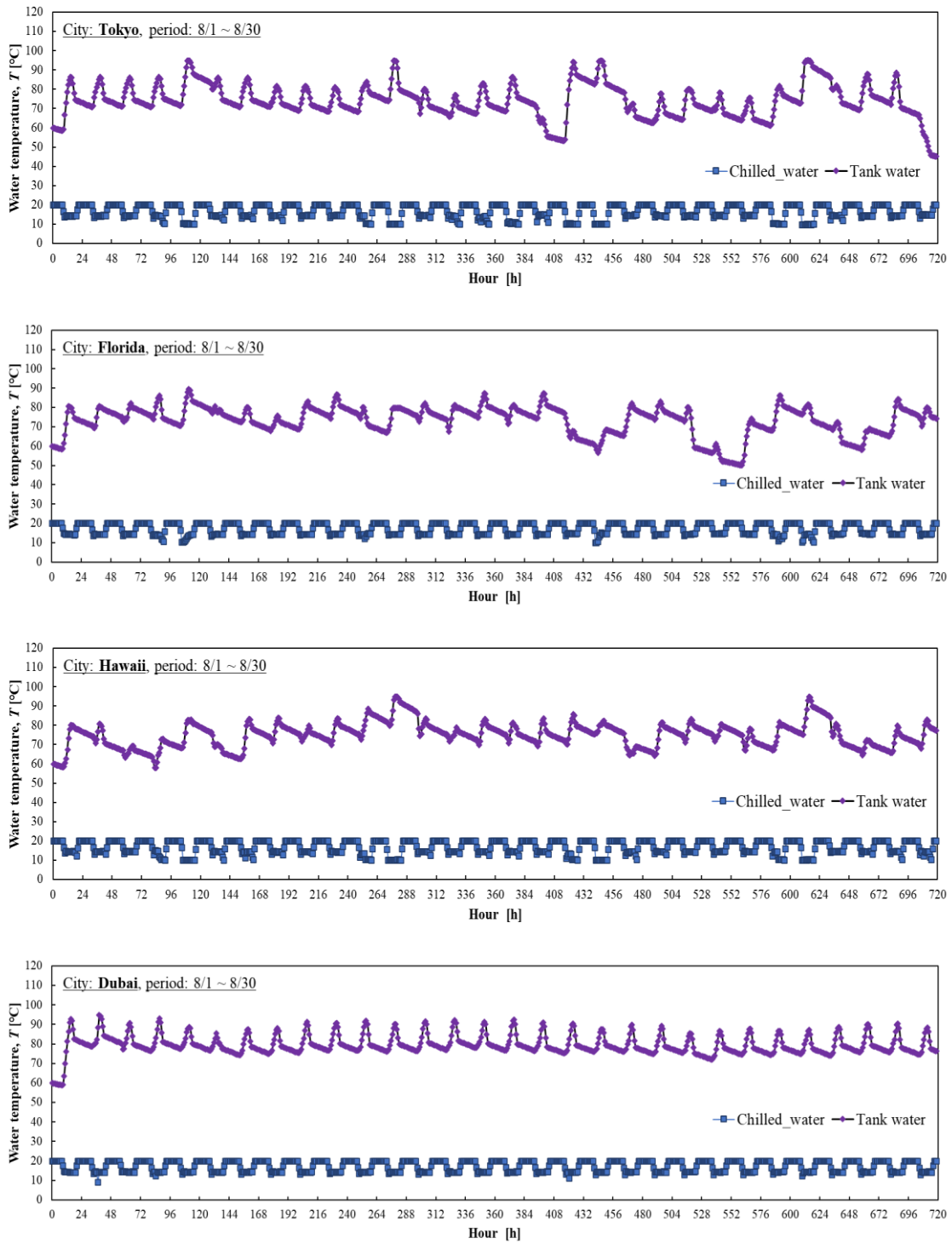
Fig. 5. 8 Hourly variation of regeneration water and chilled water temperature of AHP in August

5.5.2 Performance Parameter of Solar AHP

- Solar Collector Area

Fig. 5. 9 shows effect of solar collector area on the cooling capacity and regeneration water temperature. As the area of solar collector changes from 34 to 50 m^2 (47 %), approximately 20 °C higher peak temperature was obtained. The AHP cooling capacity is strongly concerned with the regeneration water temperature. At the beginning of the daytime, the higher AHP cooling capacity was obtained owing to the more rapid temperature increase of regeneration water when using the larger collecting area. The difference in cooling performance of AHP resulted from altering collector area was reduced near the peak temperature. It was observed that the regeneration water temperature starts to decrease from approximately 3 P.M. as absorption of solar radiation decreases. In the latter part of operating hours, the larger collector area also resulted in the larger AHP cooling capacity due to the continued effect of the higher peak temperature. The EHP covers the shortage of cooling capacity over the entire cooling load except for the load handled by AHP. Therefore, the cooling capacity handled by EHP decreased as the regeneration water temperature increased, that is, the cooling capacity of AHP increased. It also tended to increase around noon as the cooling load rose due to the daily highest solar radiation.
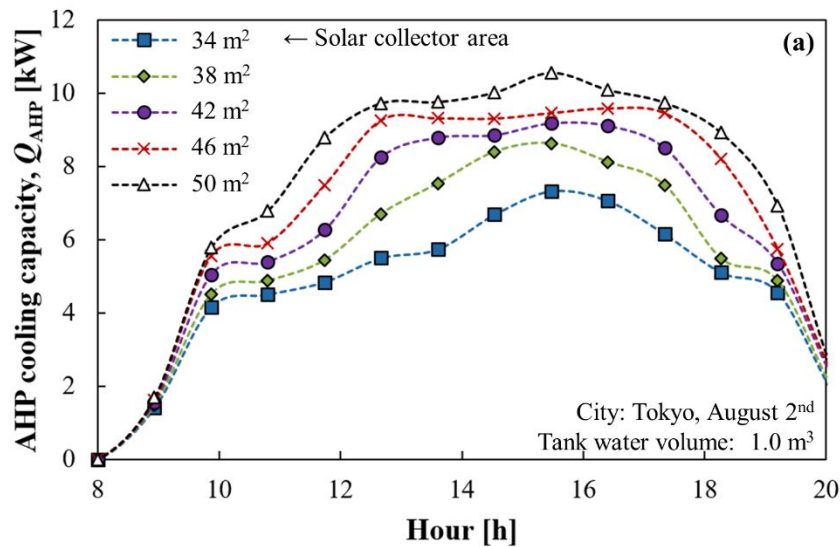
(a) AHP cooling capacity
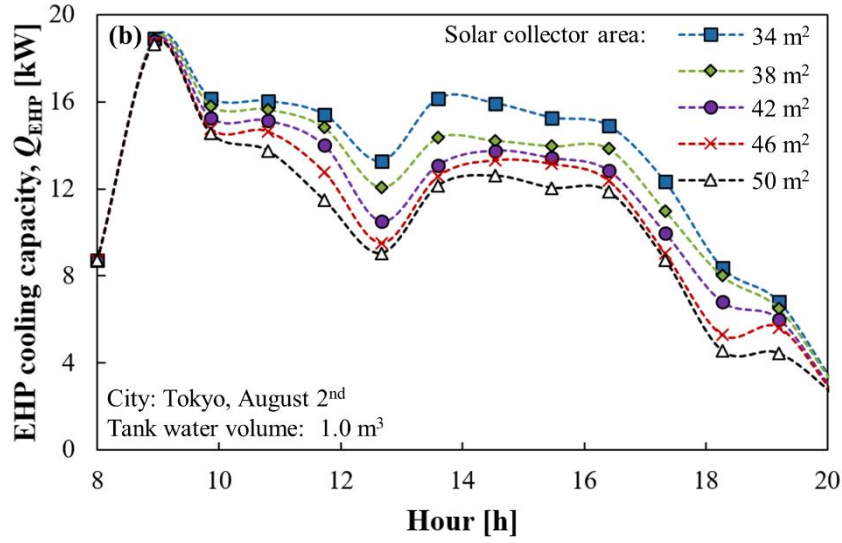
(b) EHP cooling capacity
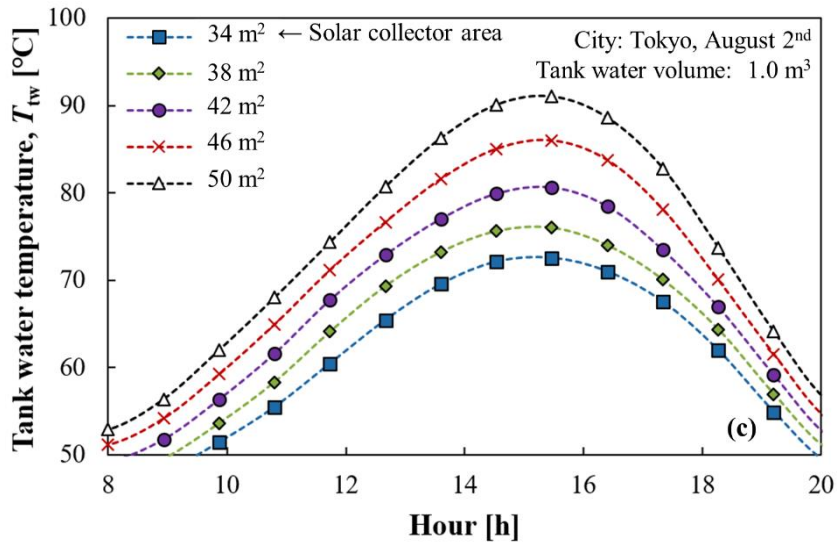
(c) Tank water temperature

Fig. 5. 9 Effect of solar collector area on the cooling capacity of (a) AHP, (b) EHP, and (c) regeneration water temperature

- Water Tank Volume

Fig. 5. 10 depicts the effect of water volume in the tank as changing it from 0.5 m^3 to 2.5 m^3. It was notable that the water temperature rises the most rapidly and reaches to the highest temperature for the case of 0.5 m^3 due to the lowest thermal capacity which is proportional to weight of water. Because of the rapid increase, in the case with water tank

volume of 0.5 m³, the cooling capacity of AHP before reaching to the peak temperature. In the same principle, the water temperature in the storage tank decreased rapidly as the solar radiation was reduced, resulting in less AHP cooling capacity at the latter part of the operating hours. In contrast, the case with water tank volume of 2.5 m³ presented the lowest peak temperature for the same reason. This case, however, showed relatively uniform temperature distribution throughout the operating hours due to the high thermal capacity.

Detailed information about effect of solar collector area and water volume in the tank are summarized in Table 5. 2.
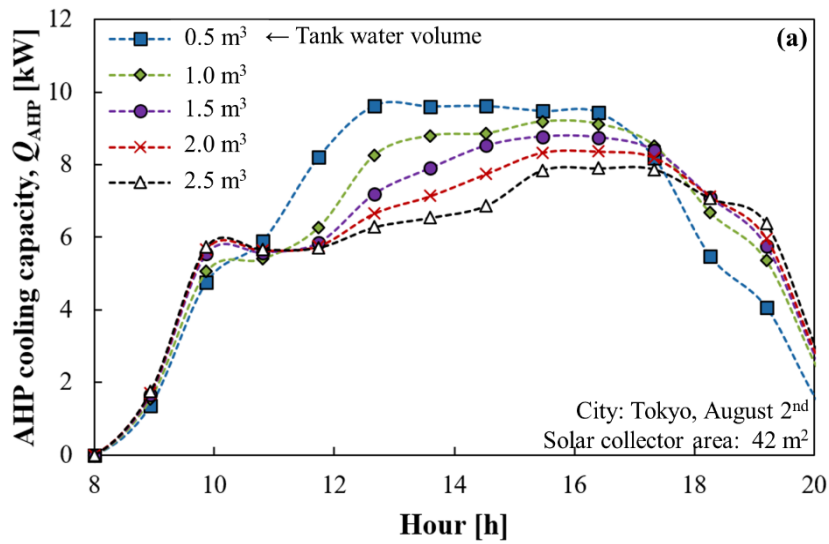
(a) AHP cooling capacity
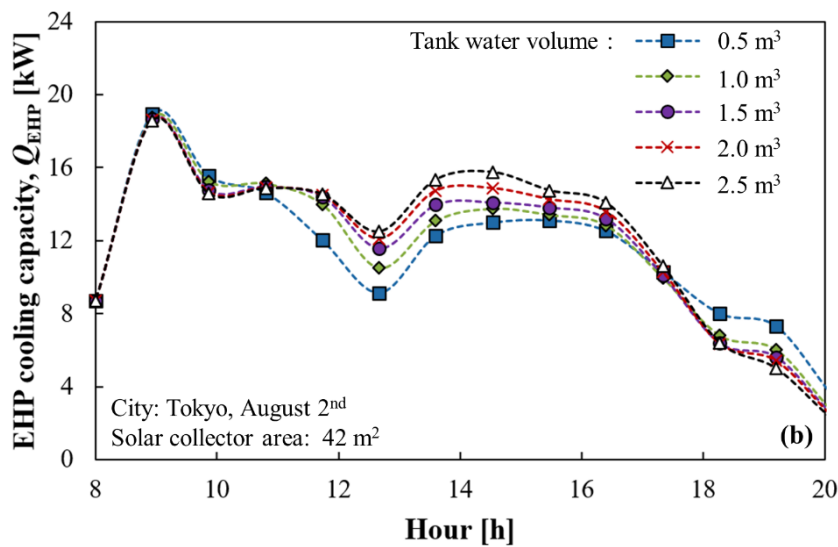
(b) EHP cooling capacity
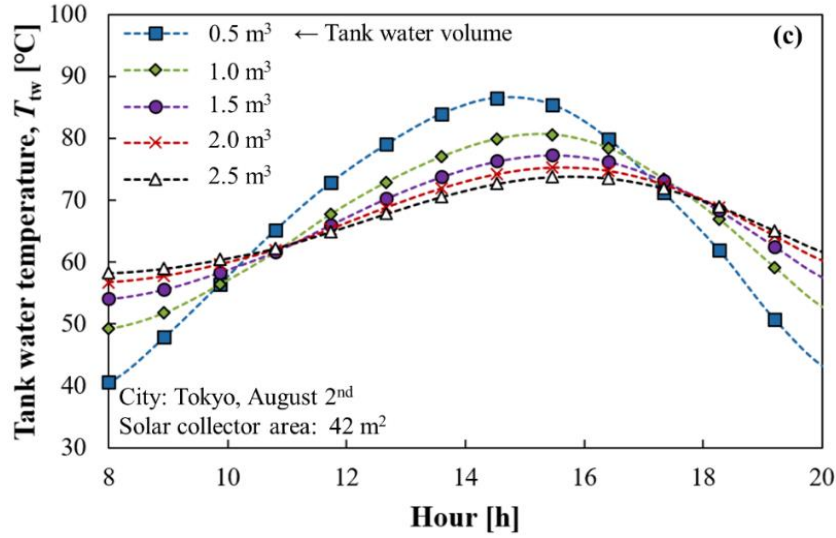
(c) Tank water temperature

Fig. 5. 10 Effect of tank volume on the cooling capacity of
(a) AHP, (b) EHP, and (c) regeneration water temperature

Table 5. 2 Effect of solar collector area and water volume in the tank on monthly AHP cooling
energy [kWh] in August

Solar collector area [m²]	Water volume in tank [m³]				
	0.5	1.0	1.5	2.0	2.5
34	1508.4	1471.4	1439.4	1411.1	1387.6
38	1692.8	1667.8	1636.4	1600.8	1566.4
42	1855.0	1848.8	1828.4	1797.3	1761.3
46	2009.5	2004.4	1995.5	1976.0	1946.7
50	2140.8	2153.2	2149.1	2141.2	2120.4

- Half Cycle Time

As mentioned earlier, AHP system repeats switch of adsorption and desorption mode which results in inevitable sensible heat loss to heat up heat exchanger metals and adsorbent. This sensible heat loss can be reduced by extending cycle time as long as the adsorbent is still capable to adsorb water vapor. That is why the adsorbent having large

adsorption capacity is advantageous to lessen frequency of switching between adsorption and desorption. As presented in previous researches [26–28], the composite material WSS + LiCl 20 wt.% exhibited a higher adsorption capability. Fig. 5. 11 (a) shows change of tank water temperature during operating hours for the cases of various half cycle time, and Fig. 5. 11 (b) describes effects of half cycle time on cooling capacity of AHP using different adsorber.

From Fig. 5. 11 (a), it can be discovered that the obtainable regeneration water temperature differs according to the cycle time. The average temperature of the regeneration water for the half cycle time of 14 minutes was about 9.7 ℃ higher than the case of 8 minutes. The reason can be explained as followings. The temperature of regeneration water in the water tank was calculated based on Eq. (20). The third term which indicates consumed energy for the regeneration is the main factor to hinder rise of the water temperature. This energy loss increases as repeating to cool down (approx. 30℃) and heat up (approx. 80℃) the adsorber more frequently. For this reason, the higher regeneration water temperature was obtained for the cases of the longer cycle time throughout the operating hours. However, it is noteworthy that adsorption capacity and rate need to be considered when it comes to extending the cycle time. Our previous research has revealed that the A-type silica gel reaches the equilibrium faster than WSS+LiCl 20 wt.%, due to the less adsorption equilibrium amount and the higher adsorption rate [29]. This characteristic resulted in more drastic decrease in AHP cooling capacity of the case applying the A-type silica gel when extending the cycle time, in spite of supplying regeneration water with the higher temperature (Fig. 5. 11 (b)). On the other hand, for the case applying WSS+LiCl 20 wt.%, approximately 14 % of increase in AHP cooling performance was observed as extending the half cycle time from 8 minute to 14 minute. Also, decrease of the cooling capacity was more clear for the cases with lower filling density (223g/L, 233g/L) because they reach the adsorption equilibrium faster than the cases with the higher filling density (303g/L, 329g/L).
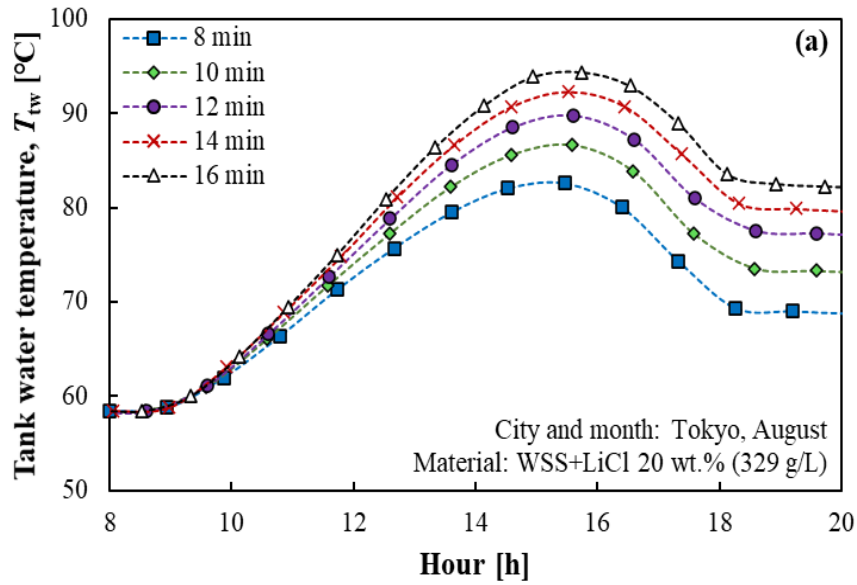
(a) Tank water temperature
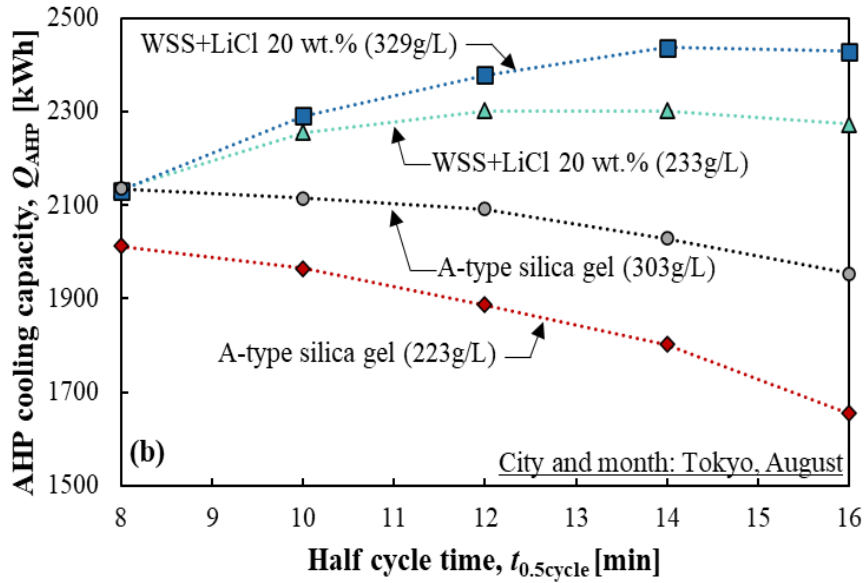
(b) AHP cooling capacity

Fig. 5. 11 Effect of cycle time on (a) tank water temperature, (b) cooling capacity of A HP using different adsorber in August

- *Auxiliary Heat*

The auxiliary heat source provides supplemental energy together with solar thermal energy to operate AHP in this research. As presented in the Fig. 5. 12, the combustion of

the natural gas is dependent on cooling load and obtained regeneration water temperature. That is, the auxiliary energy is designed to be supplied if radiation is insufficient thereby the cooling demand is larger than the cooling capacity of AHP with currently obtainable solar thermal energy. Also, the supply of auxiliary thermal energy stops if the cooling load is properly managed or the temperature of the temperature of regeneration water exceeds 80 ℃.

Fig. 5. 12 shows comparison of monthly energy input according to auxiliary heat capacity in August. The cooling energy of AHP tended to increase as supplying auxiliary thermal energy. Because of stable solar radiation in Dubai as mentioned earlier, it presented the lowest auxiliary energy input. Fig. 5. 12 also provides comparison of monthly price of input energy. The input energy includes electricity cost for operating EHP and natural gas cost for operating AHP. The assumed price of electricity and natural gas are summarized in Table 5. 3. In all cities, total energy input cost tended to increase as increasing the auxiliary heat capacity although obtainable cooling energy from AHP increases as well. The difference in the input cost between the cases with 5kW auxiliary heat capacity and without auxiliary energy was around 17 % in Tokyo and Florida. Dubai presented the smallest difference in the input energy cost since the lowest amount of auxiliary energy was spent. However, Hawaii presented somewhat larger difference than others because of high natural gas cost. For the case of Hawaii, the difference in the input cost between the cases with 5kW auxiliary heat capacity and without auxiliary energy was around 30 %. As shown in Fig. 5. 12, supplying auxiliary heat by burning natural gas helps AHP systems to produce more cooling energy. However, it was hard to acquire economic benefit due to the cost of input energy. If the circumstance that waste heat around 80 ℃ is obtainable is assumed, application of AHP systems becomes more attractive. For example, when assuming that a gas engine generator operated by natural gas generates electricity for lighting, electric equipment and fans of the target building, the waste heat obtained while cooling down the gas engine can be used as an auxiliary heat source of the AHP system. Maeda et al. revealed that the waste heat around 90 ℃ can be acquired by the engine coolant of the vehicles [39]. Fig. 5. 13 shows electric power consumption for lightings, electric equipment, fans and the sum of them and waste heat capacity obtainable from the coolant. In this case, the annual AHP cooling energy is expected to increase about 10 % compared to the case without supplying auxiliary heat.
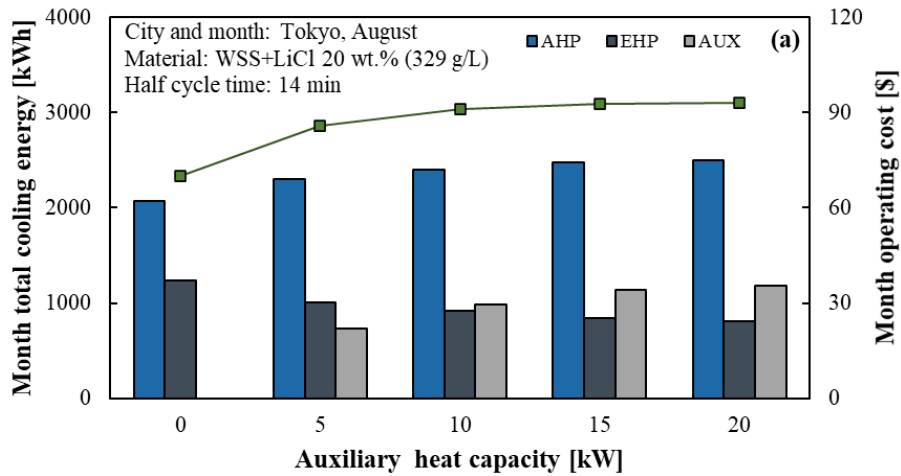
(a) Tokyo
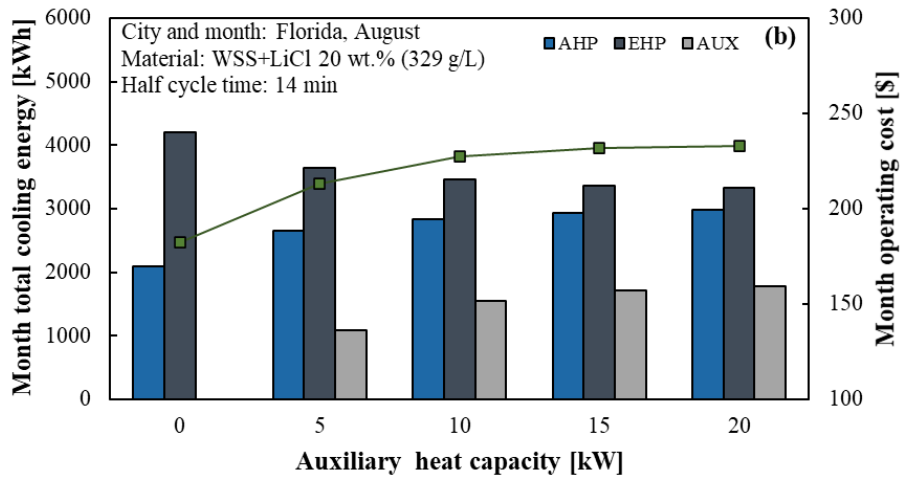
(b) Florida
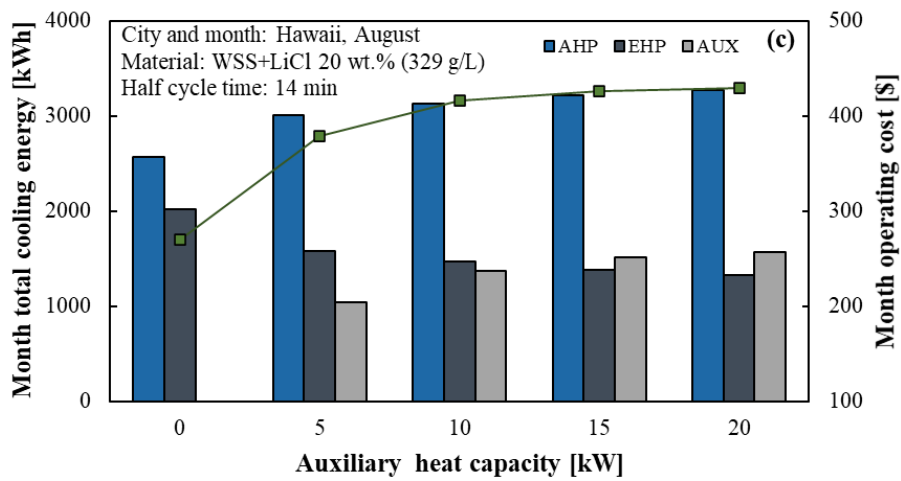
(c) Hawaii
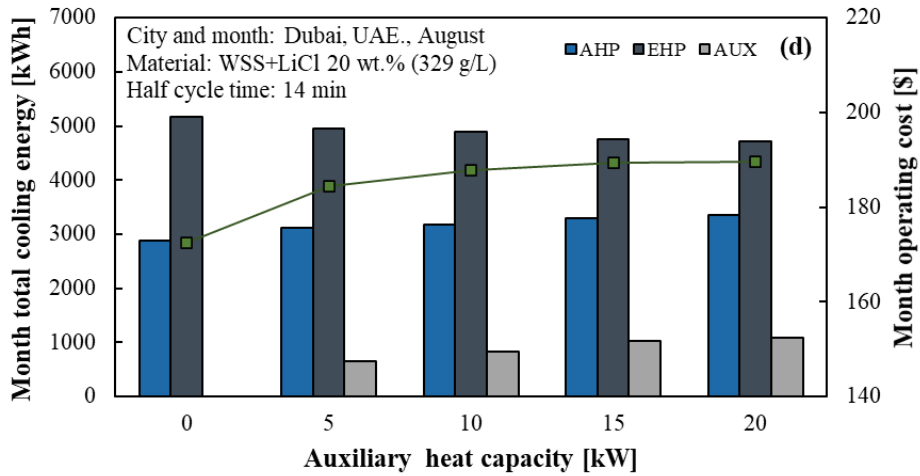
(d) Dubai

Fig. 5. 12 Comparison of energy and cost input according to auxiliary heat at different cities: (a) Tokyo, Japan, (b) Florida, U.S.,(c) Hawaii, U.S., (d) Dubai, UAE.
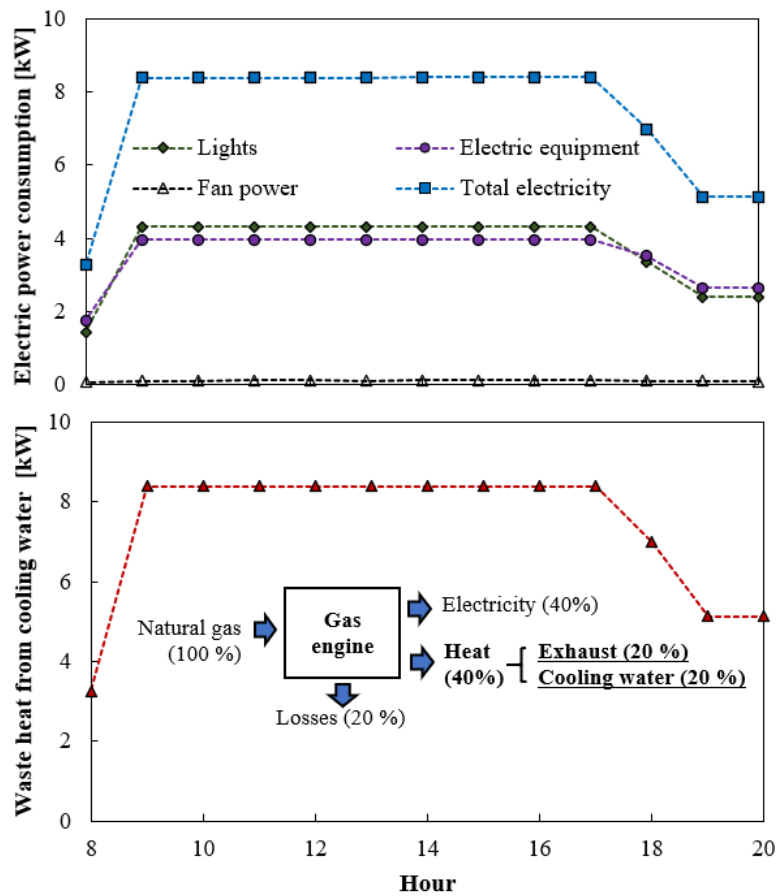
Fig. 5. 13 Electric power consumption for lightings, electric equipment, fans and waste heat capacity

- Exergy Analysis

The definition of exergy is known as the maximum amount of achievable work which can be provided by the system and certain energy source. Thus it indicates the loss of obtainable energy resulted from the generation of entropy in the irreversible system. The reference temperature for the exergy analysis is 298.15 K, and all processes are considered to be at cyclic steady state [40,41].

The exergy for a specific stream with reference temperature is presented as shown in Eq. (5-15).

$$\varphi = (h - h_0) - T_0(s - s_0) \tag{5-15}$$

Fig. 5. 14 describes control volume of each AHP component, and the calculation of irreversibility of each component is shown in Eq. (5-16) ~ (5-19). The total irreversibility indicates the sum of irreversibility of each component.

$$\dot{I}_{ad} = \left(1 - \frac{T_0}{T_a}\right) Q_{ad} + \dot{m}_{w,1}\varphi_{w,1} - \dot{m}_{w,2}\varphi_{w,2} \tag{5-16}$$

$$\dot{I}_{des} = -\left(1 - \frac{T_0}{T_a}\right) Q_{des} + \dot{m}_{w,3}\varphi_{w,3} - \dot{m}_{w,4}\varphi_{w,4} \tag{5-17}$$

$$\dot{I}_{cond} = \dot{m}_{w,5}\varphi_{w,5} + \dot{m}_{r,7}\varphi_{r,7} - \dot{m}_{w,6}\varphi_{w,6} - \dot{m}_{r,8}\varphi_{r,8} \tag{5-18}$$

$$\dot{I}_{evap} = \dot{m}_{w,9}\varphi_{w,9} + \dot{m}_{r,11}\varphi_{r,11} - \dot{m}_{w,10}\varphi_{w,10} - \dot{m}_{r,12}\varphi_{r,12} \tag{5-19}$$

Lastly, the exergy efficiency is estimated based on following Eq. (5-20) [40].

$$\eta_\varphi = \frac{\dot{m}_{w,9}\varphi_{w,9} - \dot{m}_{w,10}\varphi_{w,10}}{(\dot{m}_{w,3}\varphi_{w,3} - \dot{m}_{w,4}\varphi_{w,4}) - W_P} \tag{5-20}$$

Fig. 5. 15 (a) depicts irreversibility of AHP components and exergy efficiency during operating hours. Irreversibility of ad/desorption process is higher than that of evaporator and condenser. In general, the irreversibility tended to increase as the heat source temperature rises. The reason for this can be analyzed that the entropy generation increased as the heat source temperature increased. Meanwhile, as presented in Fig. 5. 15

(b), the total irreversibility decreased as extending the cycle time. Sharifzadeh et al. also has revealed that the irreversibility of AHP components decreases as time passes in one cycle [42]. Therefore, exergy efficiency tended to increase accordingly.

(a) Adsorption bed

$\dot{m}_{w,1}$ c.v $\dot{m}_{w,2}$

Q_a
Adsorbent (T_a)

(b) Desorption bed

$\dot{m}_{w,3}$ c.v $\dot{m}_{w,4}$

Q_a
Adsorbent (T_a)

(c) Condenser

$\dot{m}_{r,7}$

c.v

$\dot{m}_{w,5}$ $\dot{m}_{w,6}$

Refrigerant

$\dot{m}_{r,8}$

(d) Evaporator

$\dot{m}_{r,12}$

c.v

Refrigerant

$\dot{m}_{w,9}$ $\dot{m}_{w,10}$

$\dot{m}_{r,11}$
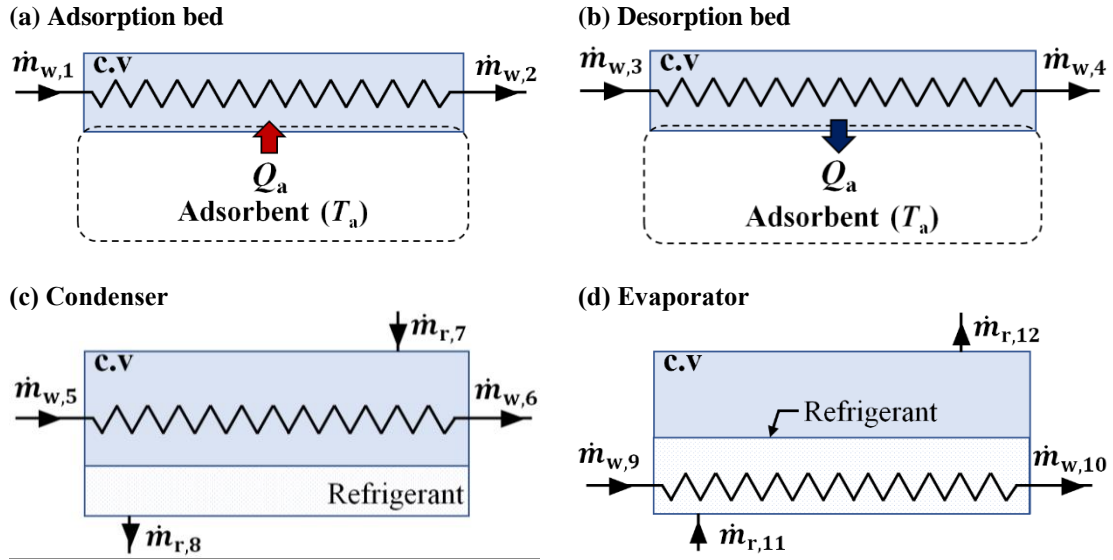
Fig. 5. 14 Control volumes of each component of AHP for exergy analysis
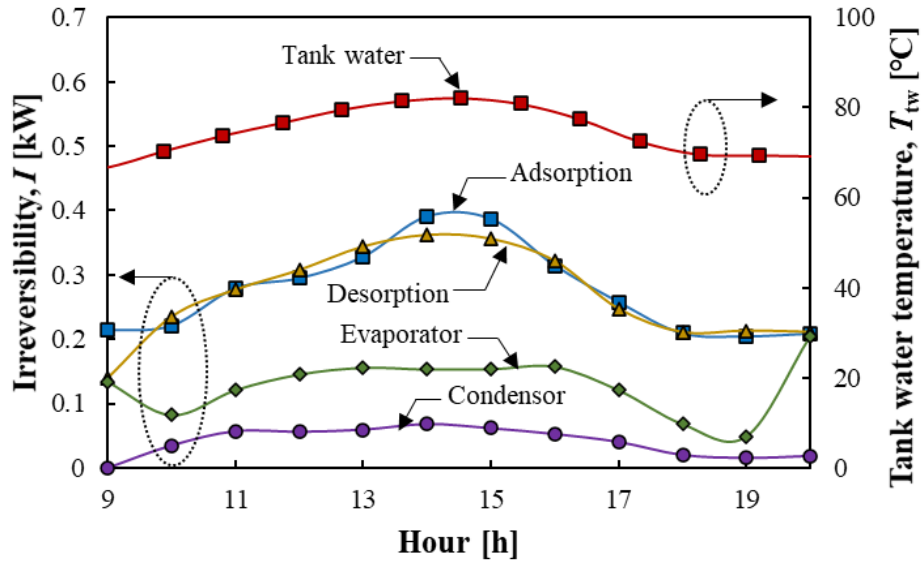
(a) Irreversibility of AHP components
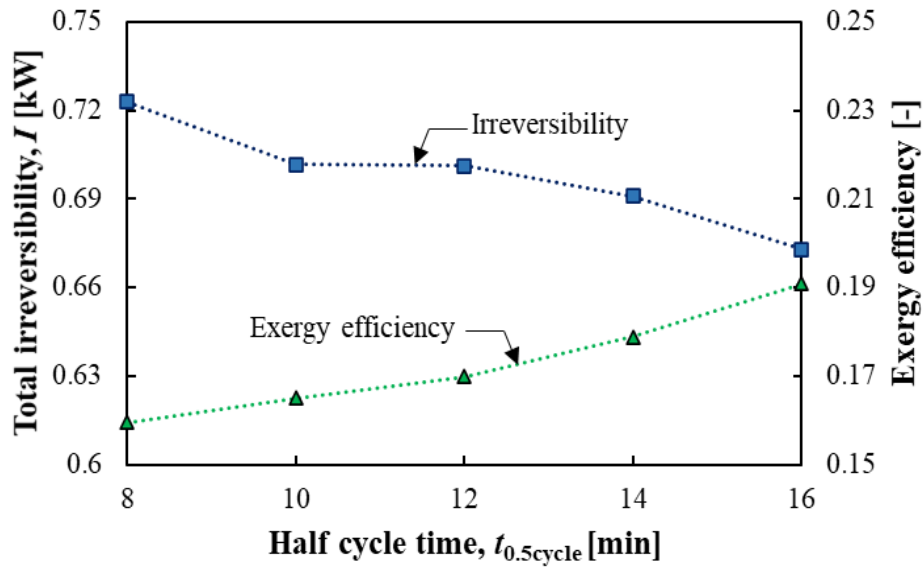
(b) Total irreversibility and exergy efficiency

Fig. 5. 15 (a) Irreversibility of AHP components and (b) total irreversibility and exergy efficiency during operating time

As shown in Fig. 5. 16, the irreversibility tended to increase as the heat source temperature rises. The reason for this can be analyzed that the entropy generation increased as the heat source temperature increased. In terms of the exergy efficiency, the inlet temperature of chilled water affected more than the temperature of regeneration water does. Since most of exergy loss occurs from the adsorption and desorption process [42], which inevitably undergoes large temperature change, it is expected to reduce entire irreversibility by applying heat recovery.
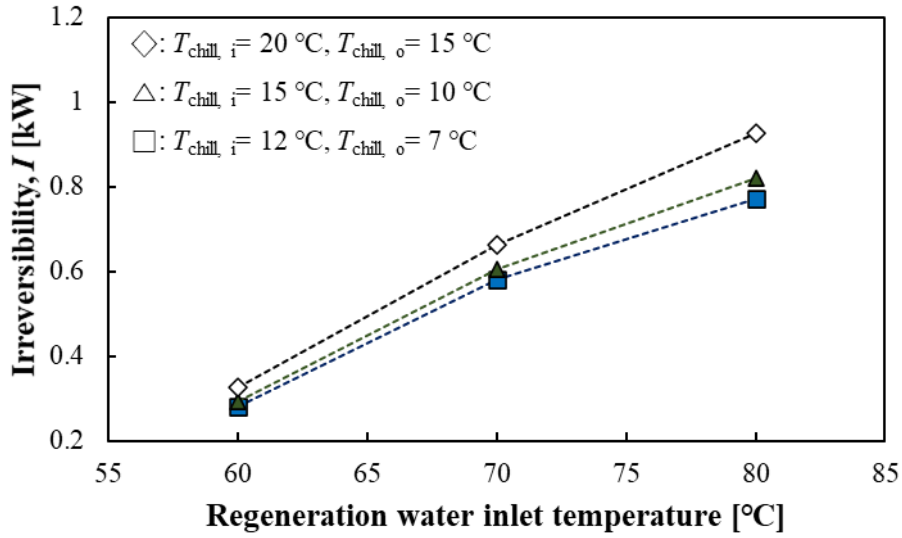
(a) Irreversibility
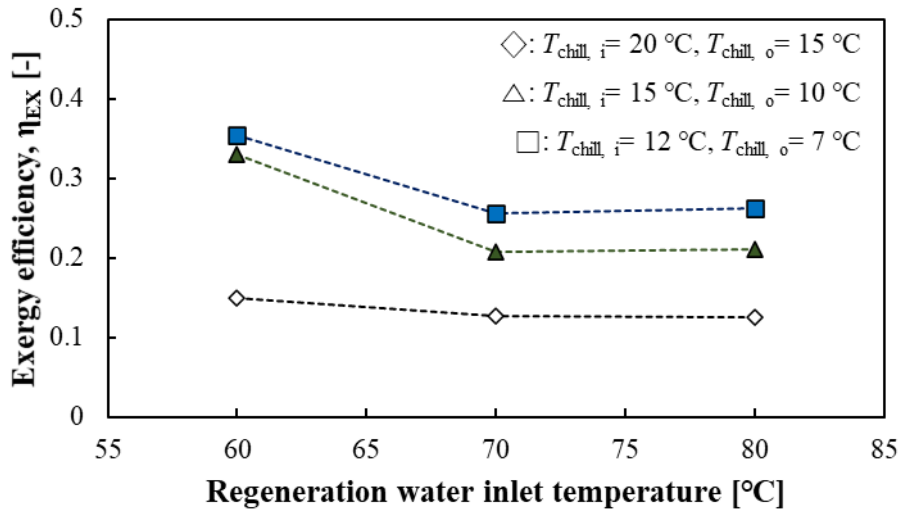
(b) Exergy efficiency

Fig. 5. 16 (a) irreversibility and (b) exergy efficiency according to regeneration temperature and chilled water temperature

5.5.3 Annual Operation of Solar AHP and Economic Analysis

Utilization of solar energy makes the AHP attractive because it significantly decreases fossil energy input for the operation the system. On the other hand, it implies at the same time that entire performance of a solar assisted AHP system is dependent on the solar radiation. Furthermore, annual distribution of cooling load is another important information since it implies how long the AHP can be used usefully in a year.

Fig. 5. 17 describes annual distribution of cooling load and obtainable cooling capacity from AHP and EHP in different cities. The hourly cooling load during the cooling period was arranged with descending order. It also describes the cooling capacity of both AHP and EHP at the moment separately. This enables the analysis on the annual cooling load with hourly-unit and gives information about the portion of cooling load taken care by AHP and EHP in the moment.

Firstly, Tokyo presented nearly 5.5 month (12 hour operation per day) of cooling periods in a year. As also shown in Fig. 5. 17, the maximum cooling load in Tokyo was 24.1 kW, however the period that the cooling load exceeds 10 kW was less about 750 hours. During the annual cooling periods, total cooling energies come from AHP and EHP are 7.9 GJ and 4.8 GJ, respectively. Florida required the longer cooling period compared to Tokyo. The period that the cooling load exceeds 10 kW exceeded 2000 hours. Total cooling energies come from AHP and EHP are 24.8 GJ and 19.4 GJ, respectively. On the other hand, Dubai showed all year round cooling hours. The highest maximum cooling load of 32.9 kW, and the period that the cooling load exceeds 10 kW was longer than 3000 hours in a year. The annual cooling energies generated by AHP and EHP are 34.4 GJ and 31.2 GJ, respectively. Hawaii also presented similar cooling load characteristics with Dubai. Instead, the peak cooling load was much lower (20 kW) than that of Dubai, even lower then Tokyo. However, Hawaii also required cooling all year round, which is advantageous in terms of utilization of an AHP system. The annual cooling energies generated by AHP and EHP are 28.5 GJ and 18.0 GJ, respectively. It is noteworthy that the AHP cooling energy in Dubai was about 20 % higher than that of in Hawaii due to stable solar radiation.
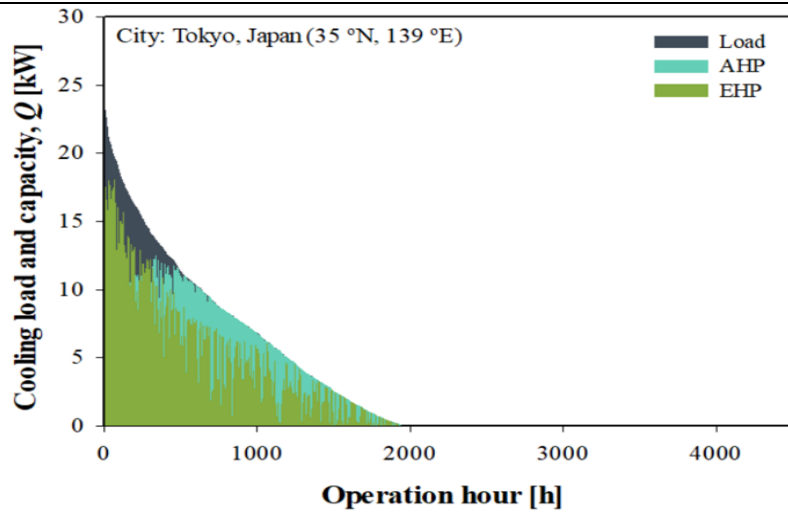
(a) Tokyo
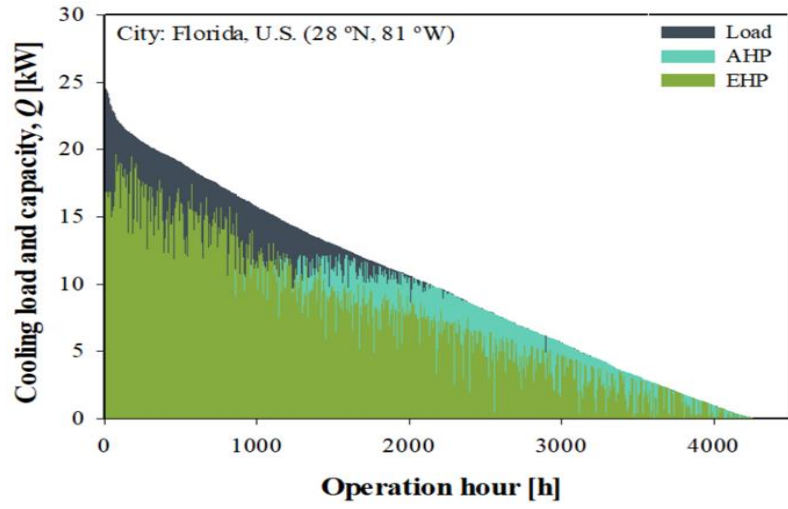
(b) Florida
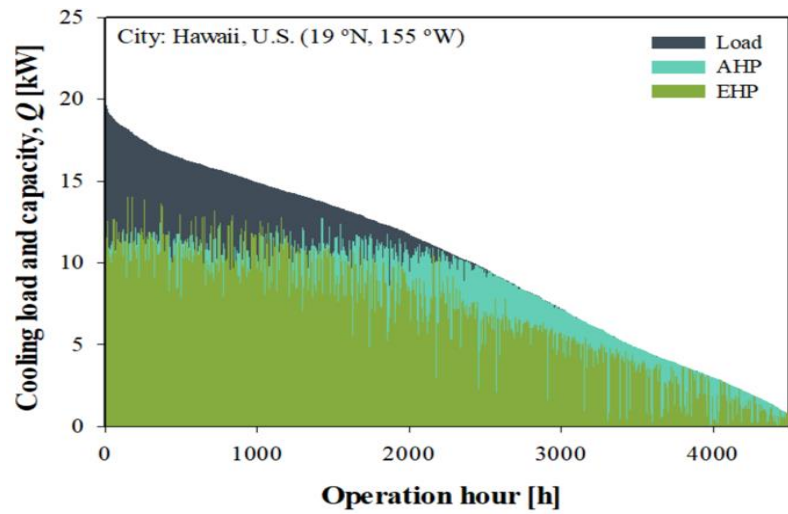
(c) Hawaii
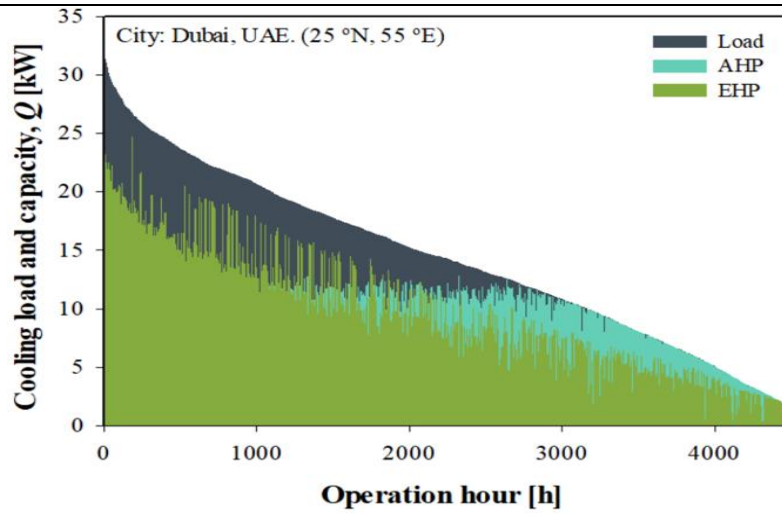
(d) Dubai

Fig. 5. 17 Annual distribution of cooling load and cooling capacity from AHP and EHP

Fig. 5. 18 depicts the accumulation of monthly AHP cooling energy in different cities. For the case of Tokyo, the accumulation of cooling energy from the AHP was merely 35 % of that of Hawaii because of relatively short cooling period. The obtained AHP cooling energy in Hawaii is also similar with that of Dubai from January to March, but the gap between them tended to get wider as approaching to the hottest season. As a result, the difference in the annual AHP cooling energy between these two cities was 20 %.
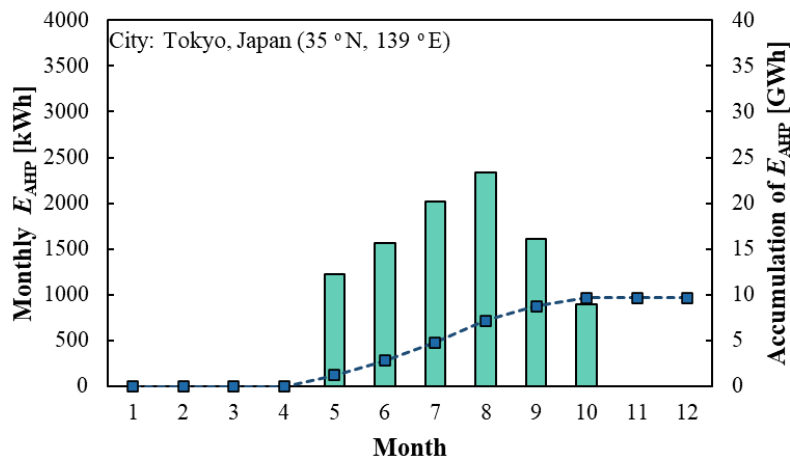
(a) Tokyo
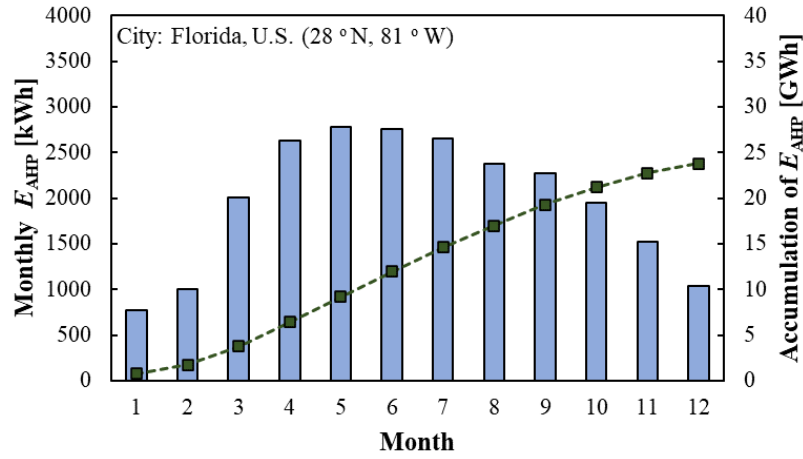
(b) Florida
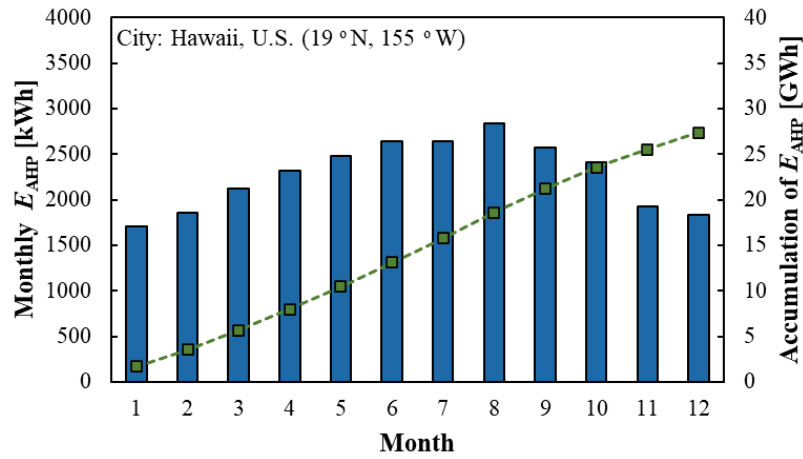
(c) Hawaii
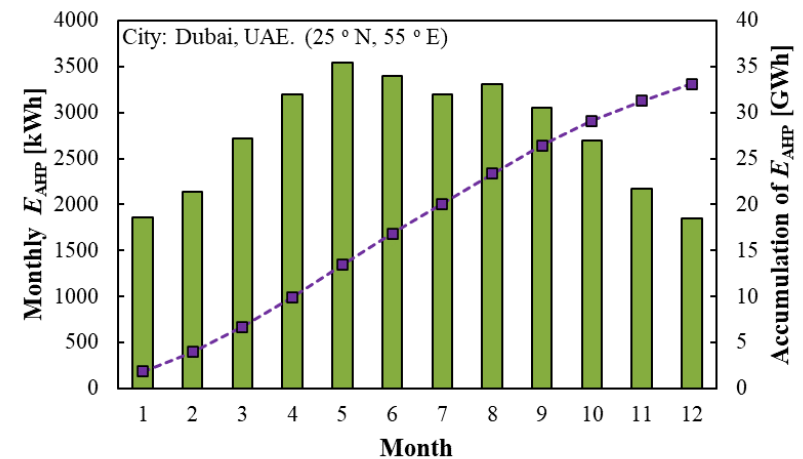
(d) Dubai

Fig. 5. 18 Annual AHP cooling energy distribution and accumulation

Table 5. 3 summarizes the economic parameters used to estimate the application of the AHP system in aspects of the cost. Fig. 5. 19 represent monthly cost saving from AHP and its accumulation with the unit of U.S. dollar. It is noteworthy that not only the amount of AHP cooling energy but also the electricity price should be considered together to estimate cost saving coming from operating AHP. The electrical power consumption of EHP was assumed based on the COP, and the COP of electrical chiller was calculated by Eq. (5-21) as a function of ambient temperature [43]. Table 5. 4 shows summary of initial and cost saving from AHP in different cities.

$$COP_{EHP} = 0.0035 T_{amb}{}^2 - 0.3372\, T_{amb} + 10.287 \tag{5-21}$$
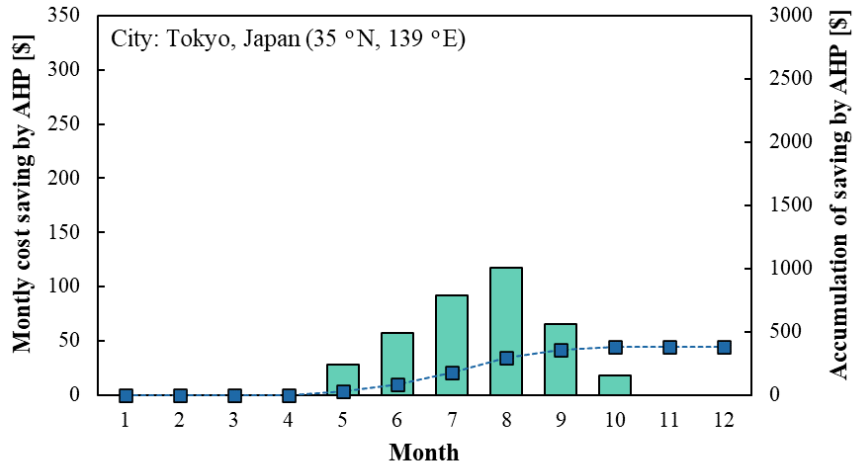
(a) Tokyo
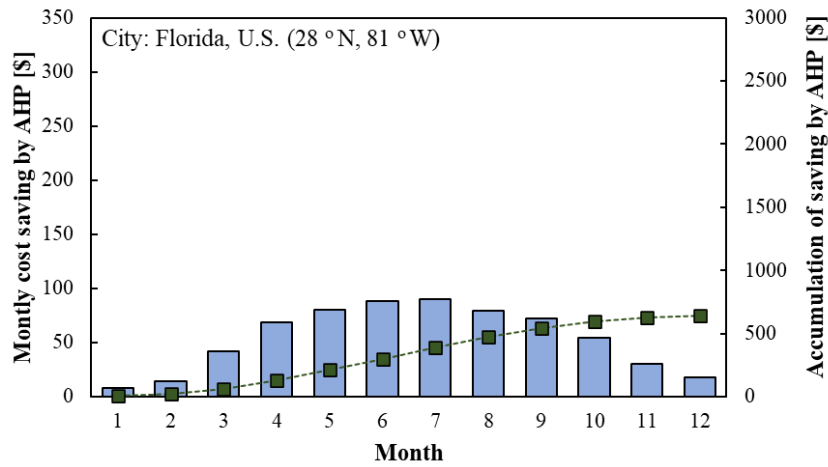
(b) Florida
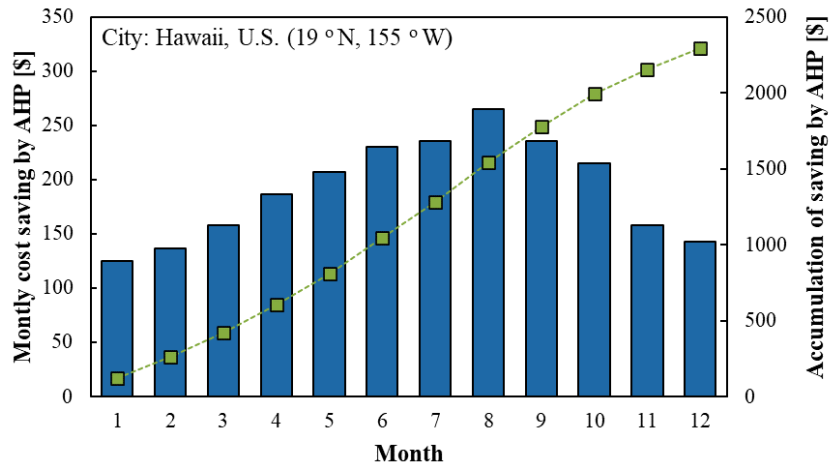
(c) Hawaii
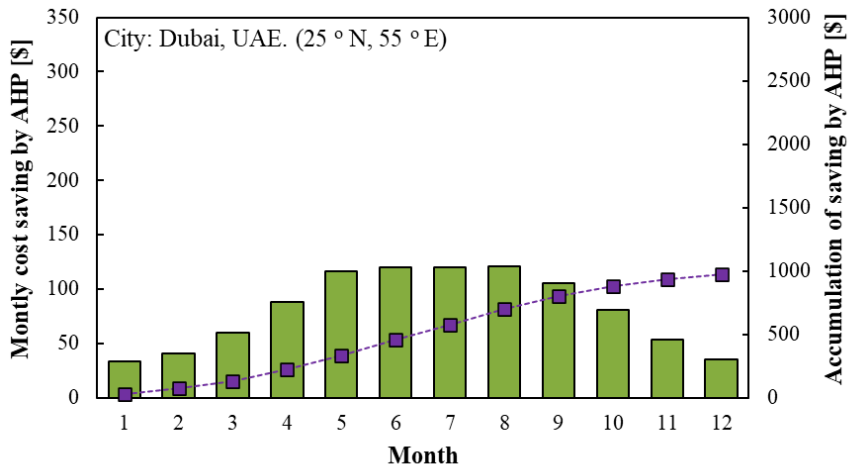
(d) Dubai

Fig. 5. 19 Monthly cost saving from AHP and accumulation

Table 5. 3 Summary of cost related to solar adsorption heat pump system

Parameters	Cost	Value
Solar collector [36]	$ 140/m^2	42 m^2
Adsorption heat pump (AHP) [44]	$ 1000/kW	10 kW
Water storage tank	$ 960/m^3	1 m^3
Cooling tower [45]	$ 170/kW	10 kW
EHP installation cost [45]	$ 340/kW	10 kW
Electricity and Natural gas	$/ kWh	-
- Tokyo	0.2 and 0.04	-
- Hawaii	0.36 and 0.16	-
- Florida	0.13 and 0.05	
- Dubai	0.1 and 0.04	-

Table 5. 4 Summary of initial and cost saving from AHP in different cities

City, county	Initial cost [$]	Annual saving from AHP [$]	Payback period [year]
Hawaii, U.S.	AHP: $ 18,540	$ 2,295.2	6.6
Dubai, UAE.	EHP: $ 3,400	$ 973.6	15.6
Florida, U.S.	Difference:	$ 645.4	23.5
Tokyo, Japan	$ 15,140	$ 378.2	40.0

It seems to be hard to expect cost saving from the solar assisted AHP system installed in Tokyo and Florida in two decades due to the short cooling period and relatively cheap electricity price. It can be noticed that much higher cost saving can be obtainable in Hawaii than in Dubai, although obtainable AHP cooling energy in Dubai was rather 20 % higher than in Hawaii. That is because the electricity in Hawaii is much expensive than that of in Dubai. The electricity price in UAE is very cheap as they are one of the oil-

producing country. Based on the economic analysis, the low electricity price in Dubai diminishes the advantages of application of AHP such as all year round cooling demand and stable solar radiation.

On the other hand, electricity in Hawaii is greatly expensive, about four times expensive than mainland of the U.S. The main reason why the electricity in Hawaii expensive can be found from the geographical characteristic of it; it is isolated in the middle of the Pacific Ocean. Therefore, all the fuels to generate electricity are transported through seaways. Since it is more cost effective to ship more dense fuels such as crude oil compared to ship natural gas or coal, the major fuel used for the generation in Hawaii is oil which is relatively more expensive than other fossil fuels [46]. Also the price of natural gas is much expensive than in the mainland for the same reason. For this reason, Hawaii is greatly charming to apply a solar assisted AHP system. About this point, Lambert and Beyene [47] also have pointed out that the high usage percentage of the cooling system together with a high electricity price result in significant operating cost savings.

According to the accumulation of saving by AHP and economic information in Table 3, the estimated payback periods in Hawaii and Dubai are 6.6 years and 15.6 years, respectively. Another advantage coming from applying an AHP system is to reduce CO_2 emission since it consumes less electricity. Fig. 5. 20 shows monthly CO_2 emission reduction from AHP in different cities.
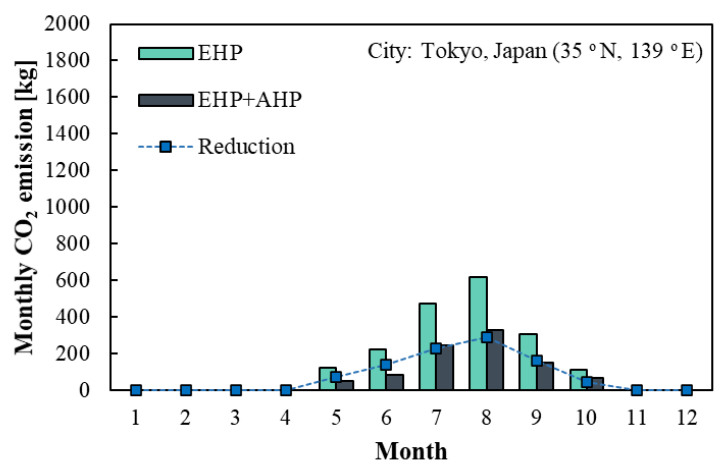
(a) Tokyo
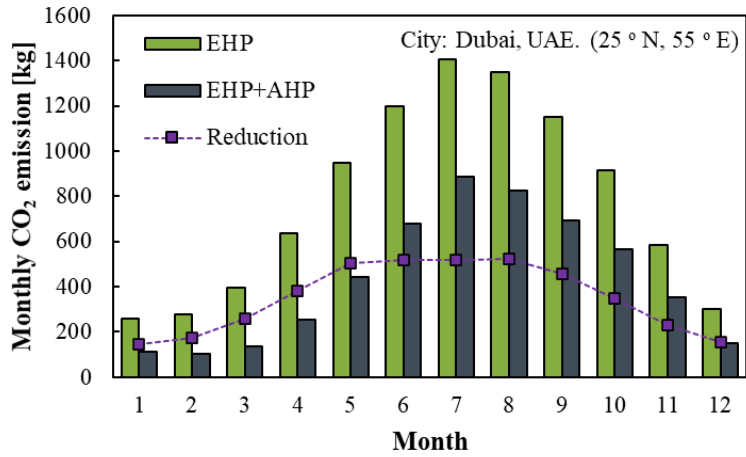
(b) Florida
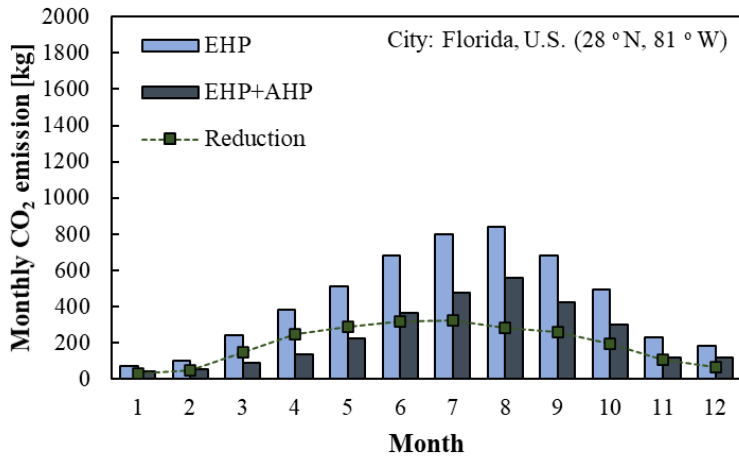
(c) Hawaii
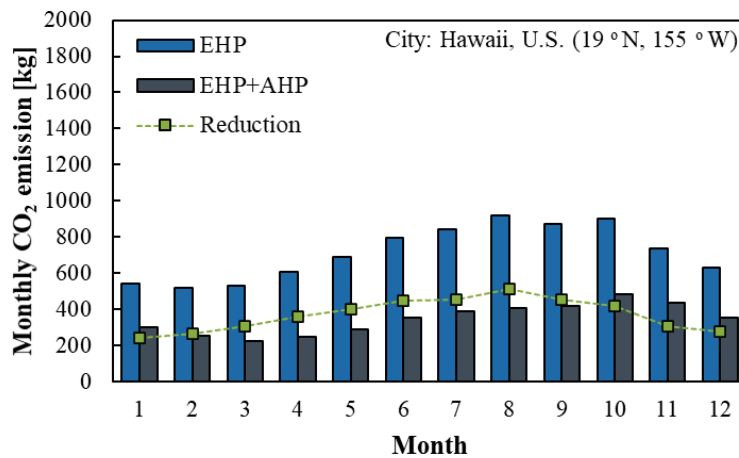
(d) Dubai

Fig. 5. 20 Comparison of monthly CO_2 emission of EHP 100% and AHP+EHP

163

Table 5. 5 summarizes comparison of CO_2 emission reduction from AHP in different cities.

The reduction of CO_2 emission by applying AHP was proportional to the AHP cooling energy, and the emission factors which differ according to the cities are also considered. Since the emission factor tends to decrease as the portion of renewable energy and nuclear power increase throughout the world [48–50], the entire emission amount is expected to decrease in accordance with the trend.

Table 5. 5 Comparison of CO_2 emission reduction from AHP in different cities

City, county	Emission factor [kgCO$_2$/kWh]	CO_2 emission amount[ton/year]		
		EHP 100%	EHP+AHP	Reduction
Hawaii, U.S.	0.695	8.58	4.14	4.43
Dubai, UAE.	0.433	9.42	5.21	4.22
Florida, U.S.	0.466	5.21	2.90	2.31
Tokyo, Japan	0.492	1.85	0.92	0.93

5.6 SUMMARY

This chapter shows research on the annual cooling performance of the solar assisted AHP which uses a composite natural mesoporous material as an adsorbent. The analysis was based on the mathematical model applying four difference climate conditions (Tokyo, Florida, Dubai, Hawaii). The system performances under the various operating conditions were studied, and following results were obtained.

The regeneration water temperature in Dubai was highly constant because of the stable solar radiation, which implies a substantial advantage in applying AHP. As the area of solar collector changes from 34 to 50 m^2 (47 %), approximately 20 ℃ higher peak temperature was obtained. Because of the rapid increase in the case of smallest water volume (0.5 m^3), the AHP cooling capacity in this case rose rapidly at the beginning of the operating hours. However, with the same reason, the water temperature in the storage tank decreased rapidly as the solar radiation was reduced, resulting in less AHP cooling capacity at the latter part of the operating hours.

The higher regeneration water temperature was obtained by extending the half cycle time due to the reduced sensible heat loss which occurs during the switching of ad/desorption. The average temperature of the regeneration water for the half cycle time of 14 minutes was about 9.7 ℃ higher than the case of 8 minutes. When the A-type silica gel was applied, the more drastic drop in AHP cooling capacity was observed as extending the cycle time due to its less adsorption capacity. Meanwhile, the case applying WSS+LiCl 20 wt.% showed about 14 % of increase in AHP cooling performance as extending the half cycle time from 8 minute to 14 minute.

Although achievable AHP cooling energy in Dubai was higher than in Hawaii, much higher cost saving can be obtainable in Hawaii than in Dubai owing to the high electricity cost of Hawaii. The estimated payback periods in Hawaii and Dubai are 6.6 years and 15.6 years, respectively.

The CO_2 emission could be reduced by applying an AHP system since it saves electric consumption. The reduction was proportional to the cooling energy from AHP. The average reduction ratio of four cities was about 47 % by applying an AHP system.

5.7 REFERENCE

[1]   UNEP, Refrigeration, Air Conditioning and Heat Pumps, 2018 Assessment Report, 2018.

[2]   M.F. Raiyan, O. Abdur Rehman, Effects of Chlorine based refrigerants on atmosphere and search for alternative refrigerants-A review, 2017.

[3]   R. Narayanan, Heat-driven cooling technologies, 2017.

[4]   S. Akhtar, T.S. Khan, S. Ilyas, M.S. Alshehhi, Feasibility and Basic Design of Solar Integrated Absorption Refrigeration for an Industry, Energy Procedia. 75 (2015) 508–513.

[5]   J. Cerezo Román, R. Javier Romero Domínguez, A. Rodríguez Martínez, P. Soto Parra, Thermal Analysis of an Absorption and Adsorption Cooling Chillers Using a Modulating Tempering Valve, in: Zero Net Zero Energy, IntechOpen, 2019: p. 13.

[6]   K. Agnieszka, W. Szaflik, Absorption and adsorption chillers applied to air conditioning systems, Arch. Thermodyn. 31 (2010) 77–94.

[7]   L. Yong, K. Sumathy, Modeling and simulation of a solar powered two bed adsorption air conditioning system, Energy Convers. Manag. 45 (2004) 2761–2775.

[8]   I.P. Koronaki, E.G. Papoutsis, V.D. Papaefthimiou, Thermodynamic modeling and exergy analysis of a solar adsorption cooling system with cooling tower in Mediterranean conditions, Appl. Therm. Eng. 99 (2016) 1027–1038.

[9]   I.I. El-Sharkawy, H. AbdelMeguid, B.B. Saha, Potential application of solar powered adsorption cooling systems in the Middle East, Appl. Energy. 126 (2014) 235–245.

[10]   G. Zhang, D.C. Wang, J.P. Zhang, Y.P. Han, W. Sun, Simulation of operating characteristics of the silica gel–water adsorption chiller powered by solar energy, Sol. Energy. 85 (2011) 1469–1478.

[11]   J. Di, J.Y. Wu, Z.Z. Xia, R.Z. Wang, Theoretical and experimental study on characteristics of a novel silica gel-water chiller under the conditions of variable heat source temperature, Int. J. Refrig. 30 (2007) 515–526.

[12]   K. Habib, B.B. Saha, S. Koyama, Study of various adsorbent-refrigerant pairs for the application of solar driven adsorption cooling in tropical climates, Appl. Therm. Eng. 72 (2014) 266–274.

[13]   K.C.A. Alam, B.B. Saha, A. Akisawa, Adsorption cooling driven by solar collector: A case study for Tokyo solar data, Appl. Therm. Eng. 50 (2013) 1603–1609.

[14]   X.Q. Zhai, R.Z. Wang, Experimental investigation and theoretical analysis of the solar adsorption cooling system in a green building, Appl. Therm. Eng. 29 (2009) 17–27.

[15]   Q.W. Pan, Study on operation strategy of a silica gel-water adsorption chiller in solar cooling application, Sol. Energy. 172 (2018) 24–31.

[16]   A. Alahmer, X. Wang, R. Al-Rbaihat, K.C. Amanul Alam, B.B. Saha, Performance evaluation of a solar adsorption chiller under different climatic conditions, Appl. Energy. 175 (2016) 293–304.

[17]   L.F. Sim, Numerical modelling of a solar thermal cooling system under arid weather conditions, Renew. Energy. 67 (2014) 186–191.

[18]   X.Q. Zhai, R.Z. Wang, J.Y. Wu, Y.J. Dai, Q. Ma, Design and performance of a solar-powered air-conditioning system in a green building, Appl. Energy. 85 (2008) 297–311.

[19]   K. Habib, B. Choudhury, P.K. Chatterjee, B.B. Saha, Study on a solar heat driven dual-mode adsorption chiller, Energy. 63 (2013) 133–141.

[20]   H. Chen, Q. Cui, Y. Tang, X. Chen, H. Yao, Attapulgite based LiCl composite adsorbents for cooling and air conditioning applications, Appl. Therm. Eng. 28 (2008) 2187–2193.

[21]   A.D. Grekova, L.G. Gordeeva, Y.I. Aristov, Composite "LiCl/vermiculite" as advanced water sorbent for thermal energy storage, Appl. Therm. Eng. 124 (2017) 1401–1408.

[22]   L.X. Gong, R.Z. Wang, Z.Z. Xia, C.J. Chen, Adsorption Equilibrium of Water on a Composite Adsorbent Employing Lithium Chloride in Silica Gel, J. Chem. Eng. Data. 55 (2010) 2920–2923.

[23]   K. Daou, R.Z. Wang, Z.Z. Xia, Development of a new synthesized adsorbent for refrigeration and air conditioning applications, Appl. Therm. Eng. 26 (2006) 56–65.

[24]   Y.. Aristov, G. Restuccia, G. Cacciola, V.. Parmon, A family of new working materials for solid sorption air conditioning systems, Appl. Therm. Eng. 22 (2002) 191–204.

[25]   Y.I. Aristov, I.S. Glaznev, A. Freni, G. Restuccia, Kinetics of water sorption on a CaCl2-in-silica-gel-pores sorbent: The effects of the pellet size and temperature, Kinet. Catal. 47 (2006) 770–775.

[26]   S. Nakabayashi, K. Nagano, M. Nakamura, J. Togawa, A. Kurokawa, Improvement of water vapor adsorption ability of natural mesoporous material by impregnating with chloride salts for development of a new desiccant filter, Adsorption. 17 (2011) 675–686.

[27]   J. Togawa, A. Kurokawa, K. Nagano, Water sorption property and cooling performance using natural mesoporous siliceous shale impregnated with LiCl for adsorption heat pump, Appl. Therm. Eng. 173 (2020) 115241.

[28]   H. Liu, K. Nagano, J. Togawa, A composite material made of mesoporous siliceous shale impregnated with lithium chloride for an open sorption thermal energy storage system, Sol. Energy. 111 (2015) 186–200.

[29] S.H. Seol, K. Nagano, J. Togawa, Modeling of adsorption heat pump system based on experimental estimation of heat and mass transfer coefficients, Appl. Therm. Eng. 171 (2020) 115089.

[30] M. Verde, L. Cortés, J.M. Corberán, A. Sapienza, S. Vasta, G. Restuccia, Modelling of an adsorption system driven by engine waste heat for truck cabin A/C. Performance estimation for a standard driving cycle, Appl. Therm. Eng. 30 (2010) 1511–1522.

[31] M. Verde, K. Harby, R. de Boer, J.M. Corberán, Performance evaluation of a waste-heat driven adsorption system for automotive air-conditioning: Part I – Modeling and experimental validation, Energy. 116 (2016) 526–538.

[32] L.X. Gong, R.Z. Wang, Z.Z. Xia, C.J. Chen, Design and performance prediction of a new generation adsorption chiller using composite adsorbent, Energy Convers. Manag. 52 (2011) 2345–2350.

[33] M. Ben Yahia, Y. Ben Torkia, S. Knani, M.A. Hachicha, M. Khalfaoui, A. Ben Lamine, Models for type VI adsorption isotherms from a statistical mechanical formulation, Adsorpt. Sci. Technol. 31 (2013) 341–357.

[34] A. Li, A. Bin Ismail, K. Thu, M.W. Shahzad, K.C. Ng, B.B. Saha, Formulation of Water Equilibrium Uptakes on Silica Gel and Ferroaluminophosphate Zeolite for Adsorption Cooling and Desalination Applications, Evergreen. 1 (2014) 37–45.

[35] T. OUCHI, S. TAKATA, Y. HAMAMOTO, H. MORI, A. ETOH, Adsorption Equilibrium and Desorption Rate of Adsorbent Coated on Heat Transfer Plate, Trans. JAPAN Soc. Mech. Eng. Ser. B. 79 (2013) 2602–2606.

[36] A.M. Reda, A.H.H. Ali, M.G. Morsy, I.S. Taha, Design optimization of a residential scale solar driven adsorption cooling system in upper Egypt based, Energy Build. 130 (2016) 843–856.

[37] Z. Zhou, L. Wang, C. Li, A. Ebert, Performance analysis of a collective solar domestic water-heating system in the temperate zone of Yunnan Province, China, J. Eng. Sci. Technol. Rev. 9 (2016) 60–65.

[38] climate.onebuilding, (n.d.). climate.onebuilding.org/.

[39] S. Maeda, K. Thu, T. Maruyama, T. Miyazaki, Critical Review on the Developments and Future Aspects of Adsorption Heat Pumps for Automobile Air Conditioning, Appl. Sci. 8 (2018) 2061.

[40] G. Gutiérrez-Urueta, A. Huicochea, P. Rodríguez-Aumente, W. Rivera, Energy and Exergy Analysis of Water-LiBr Absorption Systems with Adiabatic Absorbers for Heating and Cooling, Energy Procedia. 57 (2014) 2676–2685.

[41] V. Baiju, C. Muraleedharan, Exergy Assessment of Single Stage Solar Adsorption Refrigeration System Using ANN, ISRN Mech. Eng. 2012 (2012) 1–10.

[42] M. Sharifzadeh, M. Ghazikhani, H. Niazmand, Temporal exergy analysis of adsorption cooling system by developing non-flow exergy function, Appl.

Therm. Eng. 139 (2018) 409–418.

[43] R. Porumb, B. Porumb, M. BǍlan, Baseline Evaluation of Potential to Use Solar Radiation in Air Conditioning Applications, Energy Procedia. 85 (2016) 442–451.

[44] M. Ebrahimi, A. Keshavarz, 2 - CCHP Technology, in: M. Ebrahimi, A.B.T.-C.C. Keshavarz   Heating and Power (Eds.), Elsevier, Boston, 2015: pp. 35–91.

[45] A. Alahmer, X. Wang, K.C.A. Alam, Dynamic and Economic Investigation of a Solar Thermal-Driven Two-Bed Adsorption Chiller under Perth Climatic Conditions, Energies. 13 (2020) 1005.

[46] R. Fares, 3 Reasons Hawaii Put the Brakes on Solar and Why the Same Won't Happen in Your State, Sci. Am. (2015). https://blogs.scientificamerican.com/plugged-in/3-reasons-hawaii-put-the-brakes-on-solar-and-why-the-same-won-t-happen-in-your-state/.

[47] M.A. Lambert, A. Beyene, Thermo-economic analysis of solar powered adsorption heat pump, Appl. Therm. Eng. 27 (2007) 1593–1611.

[48] J. Liu, Q. Yang, Y. Zhang, W. Sun, Y. Xu, Analysis of CO2 Emissions in China's Manufacturing Industry Based on Extended Logarithmic Mean Division Index Decomposition, Sustainability. 11 (2019) 226.

[49] E.& I.S. Department for Business, 2019 Government Greenhouse Gas Conversion Factors For Company Reporting, 2019.

[50] K. Treyer, C. Bauer, The environmental footprint of UAE's electricity sector: Combining life cycle assessment and scenario modeling, Renew. Sustain. Energy Rev. 55 (2016) 1234–1247.

CHAPTER 6. ENERGY AND EXERGY ANALYSIS BASED ON EXPERIMENTS OF 1kW-SCALE AHP

6.1 INTRODUCTION

Thermal-driven cooling systems give significant energy saving compared to traditional vapor compression systems and have low GWP and ODP [1]. As a part of the heat-driven systems, adsorption heat pump (AHP) has attracted huge interest due to its eco-friendly operation and applicability of low-level heat sources less than 100℃. AHP systems have an advantage compared to absorption cycles that the heat source with the lower temperature can be used [2,3]. Followings introduces experimental researches of AHP systems.

Grisel et al. [4] conducted experimental research using plate/fin heat exchangers where grains of silica gel were inserted between the fins. One reactor contained six heat exchanger units, and the system operated between the cycle time of 5 and 30 minutes in which COP and SCP changes from 0.48 to 0.85 and 0.23 and 0.22 kW/kg, respectively. Atiya et al. [5] applied finned-tube heat exchangers containing silica gel grains between the fins. They could obtain the average cooling power of 0.66 kW and SCP of 0.16 kW/kg, by using about 4 kg of silica gel grains. Wang [6] tested the performance of an silica gel-AHP utilizing low grad heat source between 55 to 67 ℃. They revealed that cooling water temperature greatly affects cooling capacity especially when the hot water temperature is low. By using the low degree heat source around 60 ℃, Pan et al. [7] could produce cooling effect and SCP of 0.07~0.11 kW/kg, however the chilled water temperature was around 18.8 ℃. Kashiwagi et al. [8] experimentally verified that the two or three-stage AHP systems can be run properly with low heat source temperature between 40 to 60 ℃. The authors mentioned that the system could utilize very low grade waste heat source although COP of the systems is quite low. Experimentally studied the multi-bed AHP systems applying heat [9] and mass recovery [10] can be also found. Wirajati et al. [11] also applied low-temperature heat source around 60 ℃ to the two-stage AHP system to produce chilled water around 9 ℃. Esaki et al. [12] proposed a double-effect AHP system using FAM-Z01 which can be utilized with low-grade waste heat between 60 to 80 ℃. In the system, the desorbed water vapor from the first desorption bed is condensed by the heat exchanger inside of the second desorption bed, generating condensation heat to the adsorbent in the second desorption bed. For this principle, they insisted that the higher COP is obtainable from a double-effect AHP system compared to that of a single-effect

chiller. Myat et al. [13] conducted experimental research using FAM-Z01-coated heat exchanger as an adsorber. They compared cooling performance of the AHP system according to the heat source temperature and the cycle time. The results presented that the average cooling performance is less affected by the cycle time when the heat source temperature becomes lower. Maaitah et al. [14] presented experimental research using an activated carbon-methanol working pair to produce chilled water ranging 7 to 12 °C. They applied an air-cooled condenser, thus analysis on the effect of cooling temperature from 25 to 50 °C was provided. They insisted that the activated carbon-methanol working pair can give the better cooling performance compared to the traditional silica gel-water working pair, especially when the cooling temperature is as high as 50 °C. Utilization of solar energy makes the AHP far more attractive because it significantly decreases fossil energy input for the operation the system [15–18]. Wang [19] conducted experimental research on the adsorption chillers integrated with heat pipes. The system applying such heat pipes presented 77% enhanced heat transfer coefficient compared to the traditional activated carbon-methanol system.

Composite "salt inside porous matrix" is an adsorbent that exhibits an enhanced equilibrium adsorption capacity compared with that of traditional working pairs. Various composite materials have been studied in a lot of researches [20–25]. In the research of Aristov et al. using SWS-9L (LiNO$_3$/silica KSK) [26], effects of ad/desorption time composition at certain fixed total cycle time were studied. The total cycle time was varied 385~600 second, and precooling and preheating time were fixed. Freni et al. [27] gave the effects of thermal conductivity on the cooling performance, which emphasizes enhancement of heat transfer of the adsorption bed. The experiment on the coated adsorbent presented much higher specific cooling power than that of the pallet types. Also, they tested the new composite of silica gel modified by calcium nitrate (Ca(NO$_3$)$_2$) in the relatively low regeneration temperature [28]. The isoteric diagram is calculated from experimentally obtained equilibrium adsorption data.

As a part of reaches using the composite adsorbent, our research team also has previously reported the enhanced adsorption capacity of a natural mesoporous material called Wakkanai siliceous shale (WSS) by impregnating several kinds of chlorides and verified the its applicability as a host matrix [29–32]. This chapter provides experimental investigation of AHP systems using 1kW-scale experimental system applying WSS

impregnated with 20 wt.% of LiCl. The adsorbent is filled between the fins of corrugated aluminum heat exchangers. The heat exchangers are kept in the transparent acrylic chamber of the AHP system to observe the valve action and condensed water inside of the system. Based on the experimental data, thermodynamic characteristics regarding energy and exergy are analyzed.

6.2 EXPERIMENTAL AHP SYSTEM

6.2.1 Description on 1kW AHP System

The 1kW-scle AHP unit consists of an evaporator, a condenser and two adsorbers. The cylinder-shape unit whose diameter is 450 mm is made of transparent acrylic, and the thickness of the wall is about 20 mm. The total height of the unit is about 1140 mm which consist of the condenser chamber (270 mm), adsorbers chambers (720 mm) and the evaporator chamber (150 mm), respectively. In each adsorber contains four pieces of corrugate fin type heat exchangers (400×300×12 mm) in which the WSS+LiCl 20 wt.% is filled between its fins. The total weight of the adsorbent in both adsorbers is about 4.1 kg. The heat exchangers (235×110×25 mm) are inserted in the evaporator and the condenser. Four self-actuating plastic ball valves having diameter of 55 mm are installed to divide the adsorber and the evaporator. The accumulated water in the bottom of the adsorber chambers can be recovered to evaporator chamber. On the other hand, four self-actuating plate valves having diameter of 50 mm are installed to divide the adsorber and the condenser. Both ball type valves and plate type valves are controlled by vapor pressure differences, preventing revere flow of the vapor from the adsorber to the evaporator or from the condenser to the adsorber. The evaporator chamber is covered by the polystyrene foam to reduce heat loss.

As shown in Fig. 6. 1, the hot water for regeneration is heated by an electric heater, and the heated water is stored in the insulated tank with volume of 300 L. Meanwhile the cooling water for removing heat of adsorption is provided from the electric chillers. The heat source for the evaporator is also supplied by the other electric chiller having the cooling capacity around 1 kW. The cooling and condensation capacities in this study are designed to more than 1 kW, thus the auxiliary heating and cooling are supplied by a tube heater and additional plate heat exchanger, respectively. Fig. 6. 2 and Fig. 6. 3 show the

actual feature of a transparent evaporator and condenser. The PT-100 and pressure sensors are installed to measure the temperature and pressure of the water flow. The flowrates of each component is measured by a flowmeter. Solenoid valves are used to control the operation modes of adsorption and desorption.
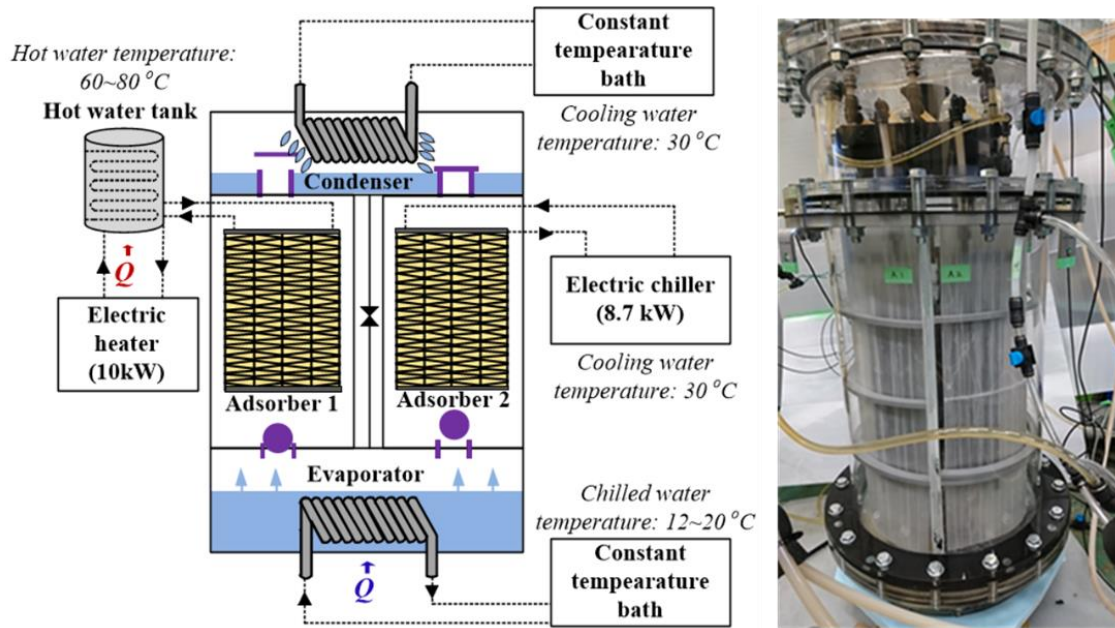
Fig. 6. 1 Schematic diagram of AHP system and actual feature of 1kW-scale unit
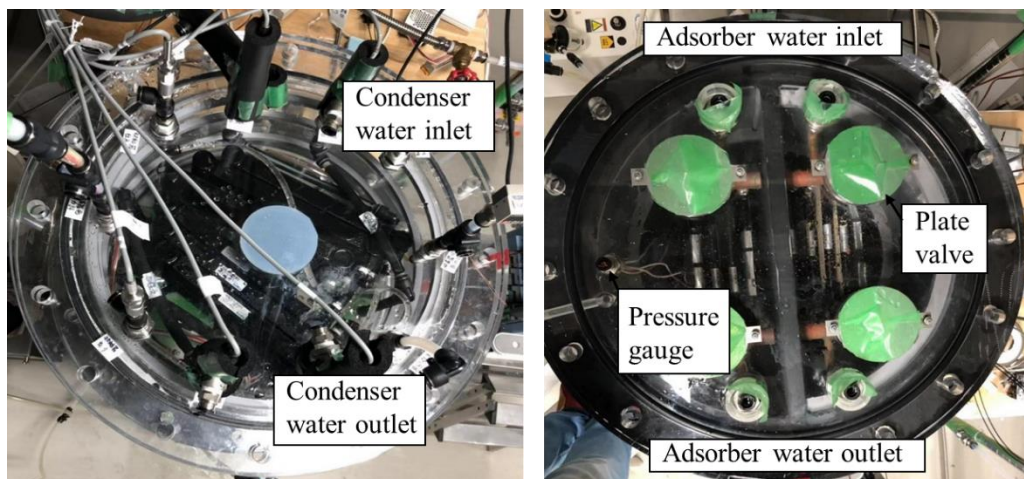
Fig. 6. 2 Actual feature of chamber: condenser-desorber
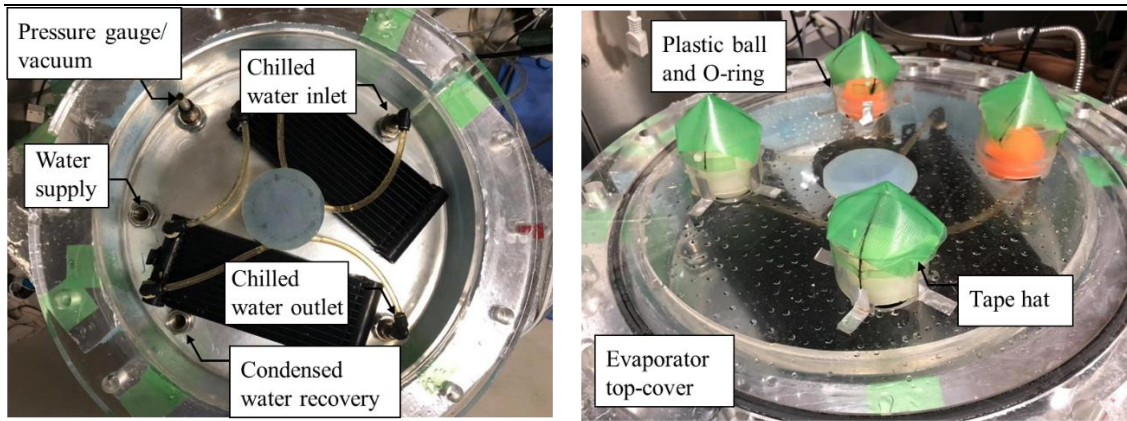
Fig. 6. 3 Actual feature of chambers: evaporator-adsorber

6.2.2 Adsorbers Filled with WSS+LiCl 20 wt.%

WSS+LiCl 20 wt.% is filled between the fins of the corrugated heat exchanger made of aluminum alloy. As mentioned earlier, the geometric size of the heat exchanger is 400×300×12 mm, and its blank weight and volume are about 850 (±10) g and 1.44 L, respectively. The gap between the water channels is about 8 mm. Since the adsorbent containing chloride which may bring out the concerns regarding corrosion, the surface of the heat exchanger is coated by the thin epoxy resin layer to avoid corrosion issues. After filling the slurry state adsorbent into to space between fins, the heat exchanger is dried in the oven at the temperature of 120 °C. Eight heat exchangers are prepared with the same process and the same filling amount so far as possible. The mass of dry adsorbent in one heat exchanger is approximately 500(±15) g. Detailed specifications of each adsorption heat exchanger is summarized in Table 6. 1, and Fig. 6. 4 depicts preparation and installation of adsorbent-filled heat exchangers.

Table 6. 1 Specifications heat exchangers used in 1kW-scale experimental system

Adsorber	Adsorber 1				Adsorber 2			
Heat exchanger No. [-]	A	B	C	D	E	F	G	H
Weight of HEX [kg]	0.845	0.835	0.855	0.835	0.835	0.850	0.845	0.850
Weight of adsorbent [kg]	0.535	0.520	0.500	0.555	0.520	0.490	0.485	0.490
Total adsorbent weight [kg]	2.11				1.99			
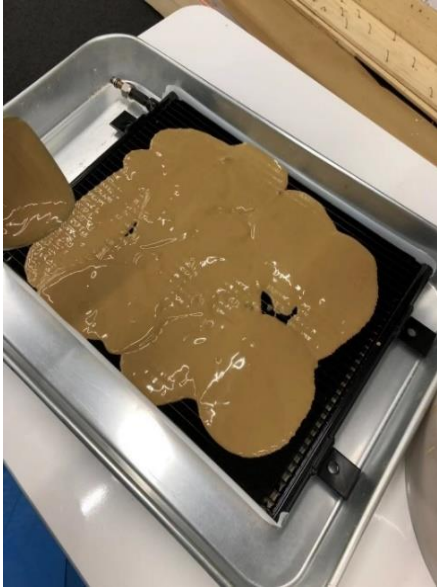
(a) Filling slurry state adsorbent into heat exchanger

(b) Drying process in the oven at temperature of 120 ºC
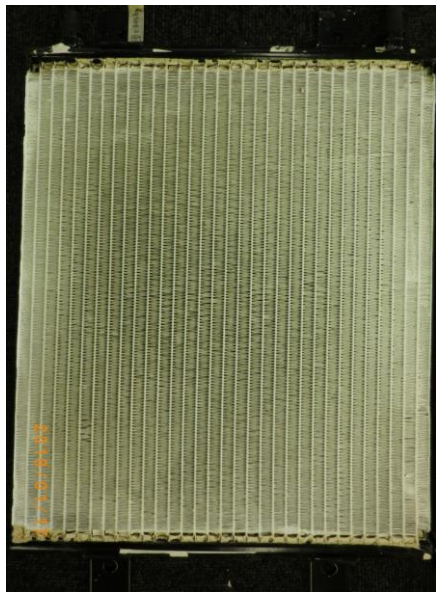
(c) Prepared adsorption heat exchanger after drying

(d) Installed feature of adsorbers in the transparent chamber

Fig. 6. 4 Preparation and installation of adsorbent-filled heat exchangers

6.2.3 Experimental Methodology

Before starting the experiments, hot water of 80 °C is supplied to both adsorbers while operating the vacuum pump to remove the residual air and the desorbed water vapor. Similarly, the residual air and evaporated water vapor are eliminated by the vacuum pump. The pressure at the evaporator and the condenser just before starting the experiment were about 2.4 kPa and 4.3 kPa, respectively, which properly correspond with the saturation temperature of the water inlet temperature of each component. The pressure of adsorbers is about 4.5 kPa, being affected by the condensation pressure.

As starting the experiment and data recording, the cooling water with temperature about 30 °C circulates the adsorber corresponding to the adsorption process, thereby the adsorption resulting in the evaporation occurs consequently. In this experimental investigation, the half cycle time was varied from 8 to 16 minute, the regeneration temperature is changed from 60 to 80 °C, the chilled water temperature is controlled from 7 to 15 °C. The temperature and flowrate data are recorded every second by a logger and analyzed to evaluate system performance.
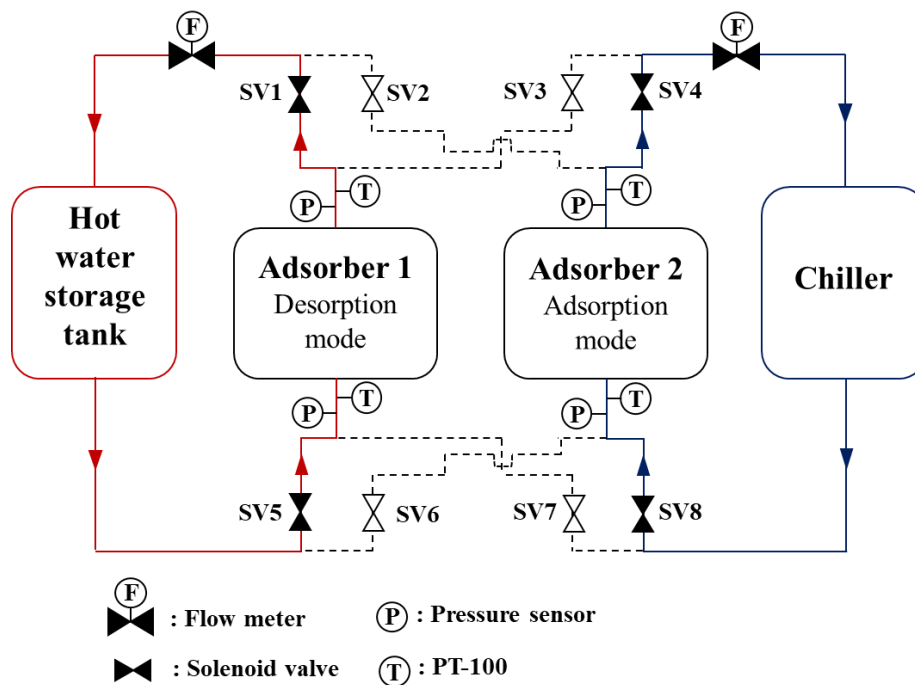
Fig. 6. 5 Control of water flows for adsorption and desorption modes

6.3 EXPERIMENTAL RESULTS AND DISCUSSIONS

6.3.1 Temperature and Pressure Profile

Fig. 6. 6 presents inlet and outlet water temperature profiles of the adsorbers. The experiments were conducted at the half cycle time of 12 minutes. The inlet temperature of regeneration water was kept around 80 (± 0.5) ℃, and that of cooling water for the adsorption process was controlled as 30 (± 1.5) ℃. Low temperature heat source of 20 (±0.6) ℃ flowed through the evaporator to be chilled. The outlet temperature of the chilled water ranged from 10 to 17 ℃. As presented in Fig. 6. 7, the condensation pressure and the desorption pressure were coupled, and the evaporation pressure and the adsorption pressure were also connected. The evaporation and the adsorption pressure tended to decrease at the beginning of the cycle due to the induced adsorption by cooling the adsorber. Compared to the pressure change of this low-pressure components, the pressure at the condenser and the desorption bed increased more rapidly at the beginning of the cycle. The reason for this difference comes from difference between adsorption and desorption rate. As presented in the chapter 4, the mass transfer rate is proportional to the adsorbent temperature. Therefore, the mass transfer during the desorption process which exchanges heat at the higher temperature level occurs faster, resulting in the more rapid increase in the pressure as well.

Fig. 6. 8 shows inlet and outlet water temperature profiles of the condenser and evaporator. The inlet water temperatures of the condenser and the evaporator are controlled almost constant with 30 and 20 ℃. It can be noticed that, for the case of condenser, the temperature difference between inlet and outlet water becomes almost zero. This implies that the condensation and the desorption process may be considered finished at the end of the cycle. On the other hand, the temperature difference for the case of evaporator reveled quite different; the difference still existed at the end of the cycle. This difference can be confirmed from Fig. 6. 9, based on the condensation and evaporation heat capacity. Lastly, Fig. 6. 10 and Fig. 11 depict change of regeneration and cooling capacity according to the elapsed time. Since the adsorbers undergo sudden switching from the high temperature level to the low temperature level, the heat capacity at first several seconds of every cycle was greatly high. It can be observed that the cooling capacity did not converged to zero even at the end of the cycle, for the same reason

provided above.
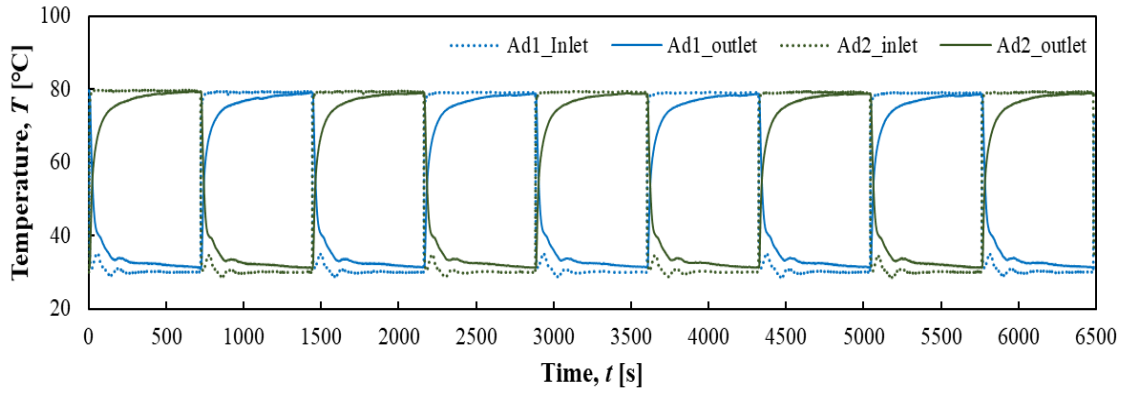
Fig. 6. 6 Inlet and outlet water temperature profiles of the adsorbers
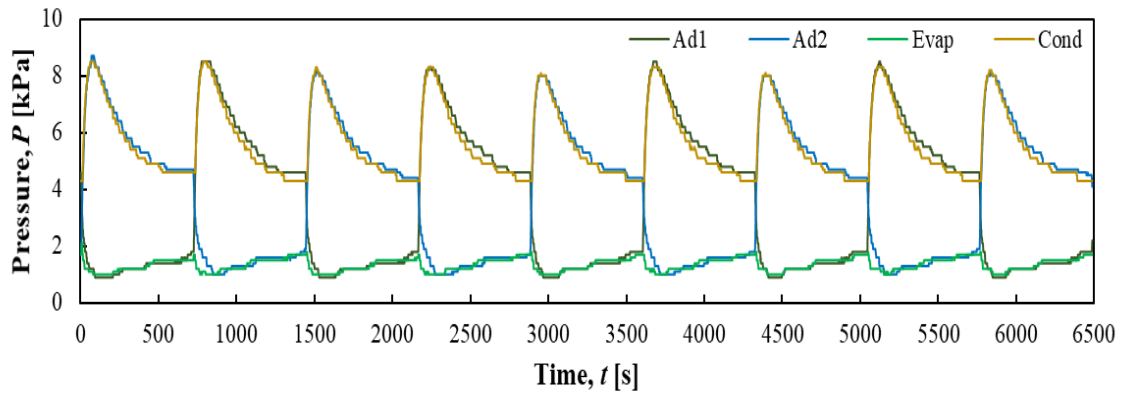
Fig. 6. 7 Pressure profiles in each component of the AHP system
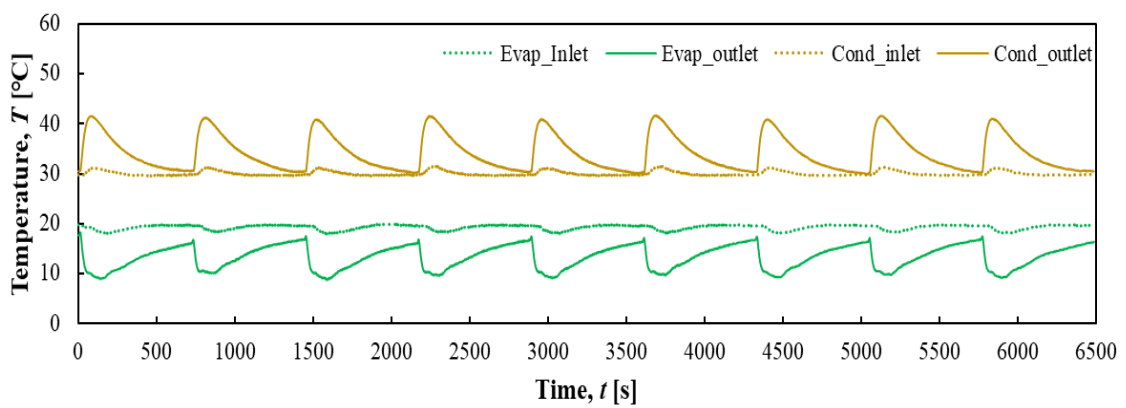
Fig. 6. 8 Inlet and outlet water temperature profiles of the condenser and evaporator
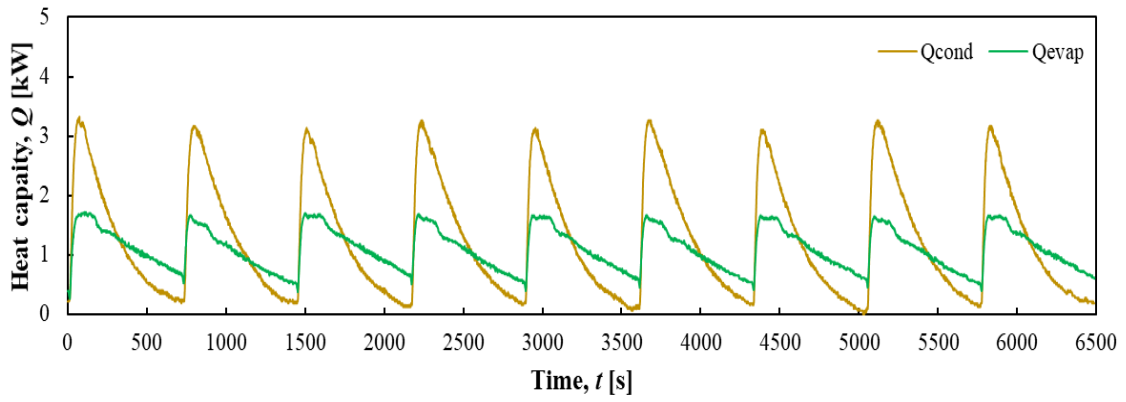
Fig. 6. 9 Comparison of condensation and evaporation capacity
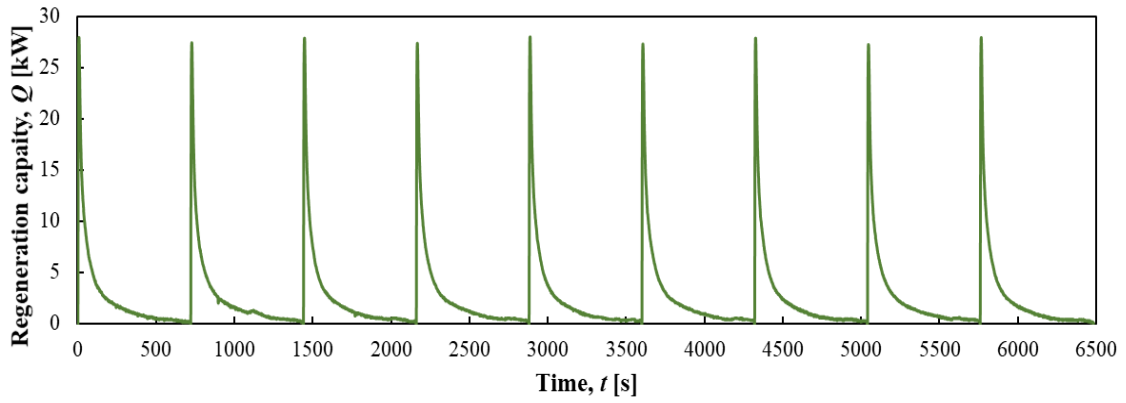
Fig. 6. 10 Change of regeneration capacity according to the elapsed time
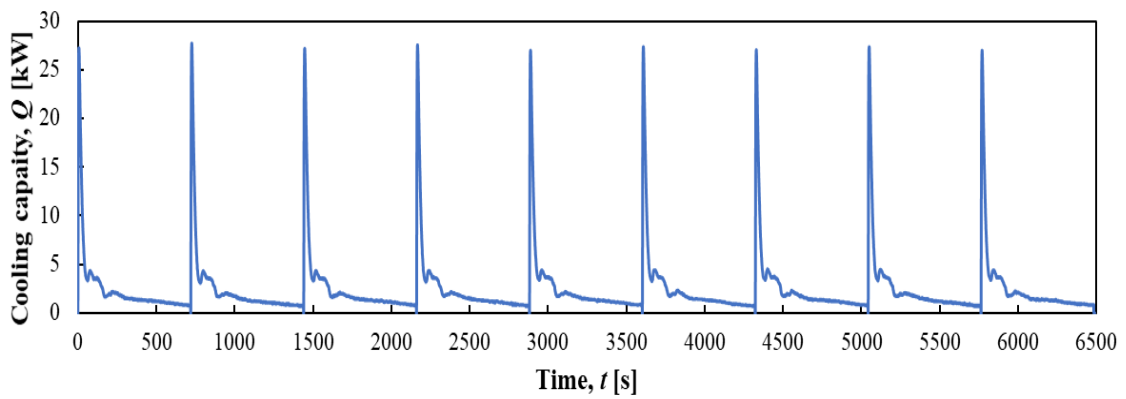
Fig. 6. 11 Change of cooling capacity according to the elapsed time

6.3.2 Effect of Cycle Time

Fig. 6. 12 presents cooling capacity according to the various half cycle time during the adsorption process. The cooling capacity tended to decrease as proceeding the adsorption process. This is because the driving force which induces the adsorption phenomena was reduced as the adsorbent adsorbs water vapor. As the half cycle time becomes longer, the difference between the peak cooling capacity and the value at the end of the cycle became large. However, the cooling capacity was still obtainable even at the half cycle time 16 minute due to the large adsorption capacity of the WSS composite. Fig. 6. 12 also compares experimentally obtained cooling capacity and the calculated cooling capacity by the mathematical model introduced in the chapter 4. In general, the differences between the average value of experimental and the calculated cooling capacity were around 3 to 8 %.
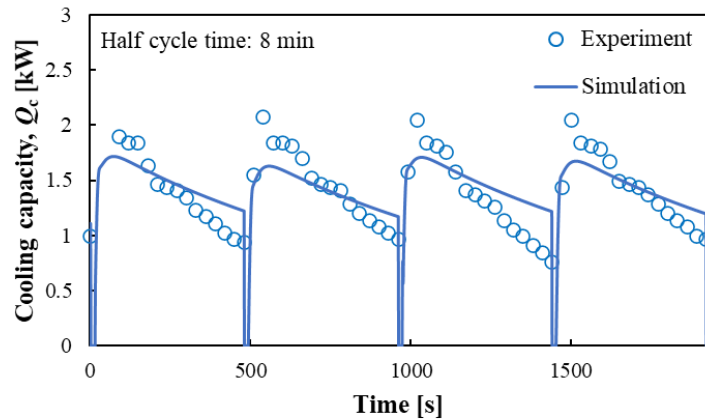
(a) Half cycle time of 8 min
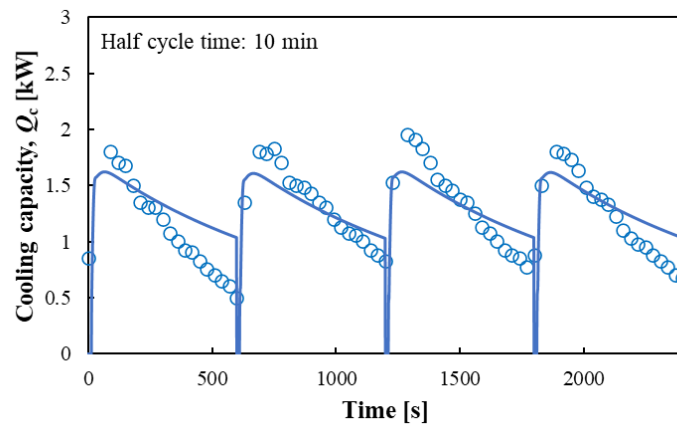
(a) Half cycle time of 10 min
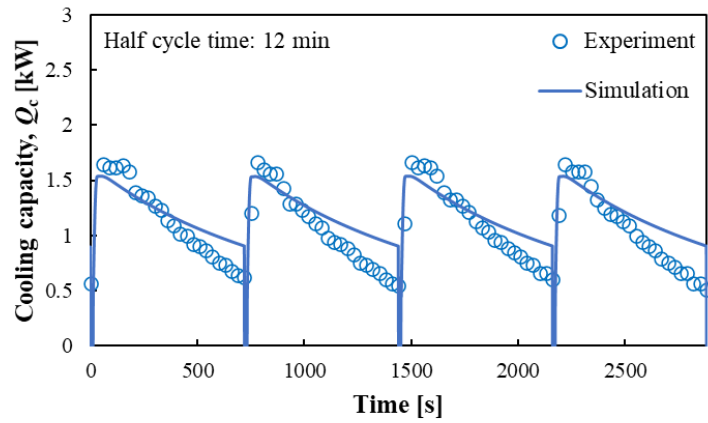
(c) Half cycle time of 12 min
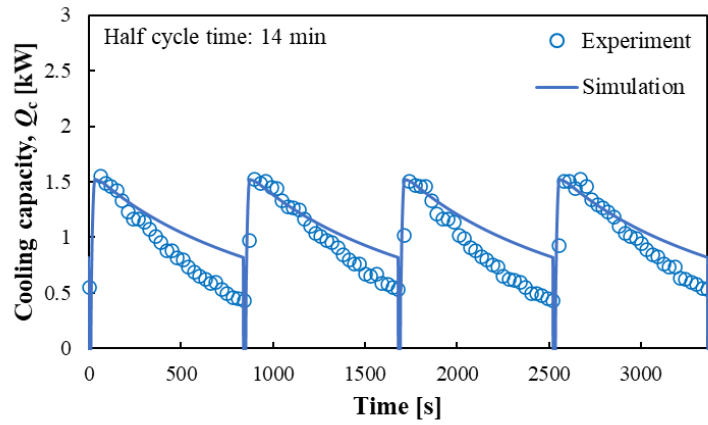
(d) Half cycle time of 14 min
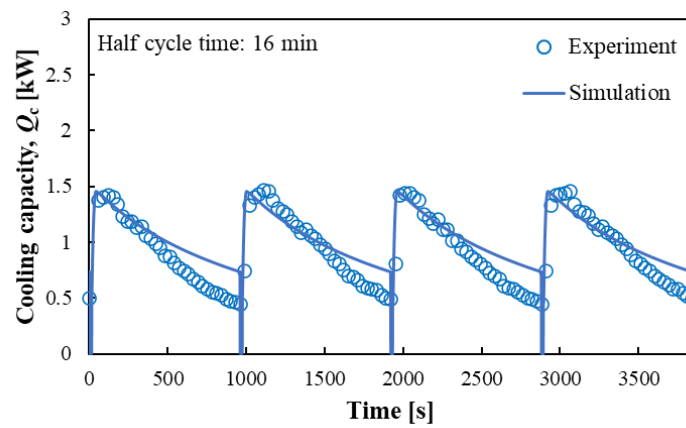
(e) Half cycle time of 16 min

Fig. 6. 12 Cooling capacity profiles according to the half cycle time

Fig. 6. 13 shows the effects of half cycle time on COP and SCP. Both COP and SCP are normally used to estimate the performance of AHP systems. As shown in Eq. (6-3), COP refers to the balance of the input and output energy, same as other types of cooling systems. Meanwhile, SCP represents the attainable cooling capacity based on the unit mass of the adsorbent. This implies that how the adsorbent used efficiently in the AHP system. As the cycle time increased, the sensible heat loss that occurred when the mode was switched from adsorption to desorption accounted for a relatively small portion among the entire load. Hence, the COP of the systems employing the adsorbers tended to increase when the adsorption time increased. SCP tended to decrease with an increase in the half cycle time because the adsorption rate decreased during the adsorption process, owing to the reduced adsorption driving force.

$$Q_c = \int_{t_{i,ad}}^{t_{e,ad}} \dot{m}_{w,evap} c_{p,w} \left(T_{w,i,evap} - T_{w,o,evpap} \right) dt \qquad (6\text{-}1)$$

$$Q_h = \int_{t_{i,h}}^{t_{e,h}} \dot{m}_{w,des} c_{p,w} \left(T_{w,i,des} - T_{w,o,des} \right) dt \qquad (6\text{-}2)$$

$$\text{COP} = \sum Q_c / \sum Q_h \qquad (6\text{-}3)$$

$$\text{SCP} = \sum Q_c / (m_{ad} \cdot t_{cycle}) \qquad (6\text{-}4)$$
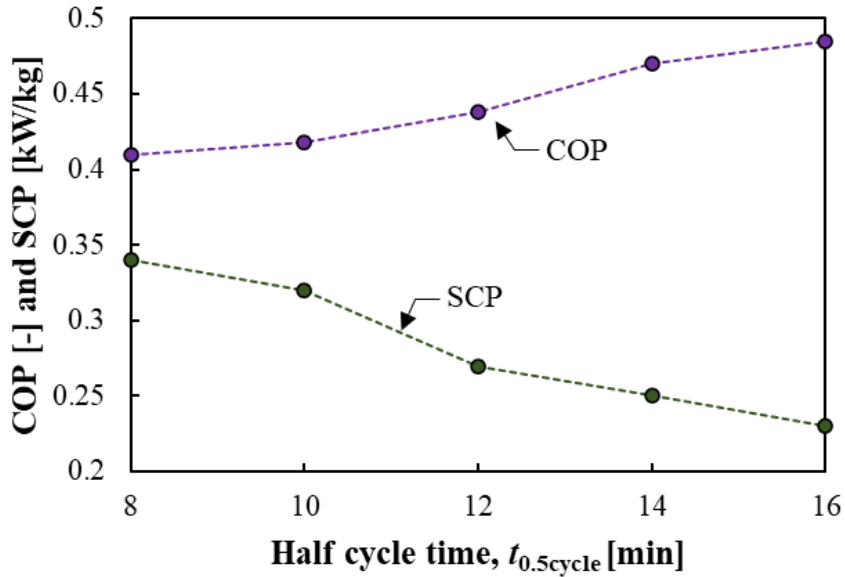
Fig. 6. 13 Effect of half cycle time on COP and SCP

6.3.3 Effect of Regeneration and Chilled Water Temperature

Fig. 6. 14 and Fig. 6. 15 depict effects of regeneration temperature and heat source temperature of SCP and COP. Firstly, the regeneration temperature significantly affected the cooling performance of the AHP system. The reason is because the adsorption capacity decreases as the regeneration water temperature decreases. That is, the adsorbent which finished the desorption process remains less dry condition as supplying regeneration water with the lower temperature. The cooling capacity when the regeneration temperature is 70 °C was about 36 % reduced than that of the case with the regeneration water of 80 °C. Meanwhile, the decrease in the cooling capacity was much more severe when applying the regeneration water of 60 °C.

The SCP also tended to decrease as lowering the inlet water temperature at the evaporator. That is because the temperature of evaporation heat source is strongly concerned with the evaporation and adsorption pressure. As the evaporation and the adsorption pressure decreases, obtaining chilled water with the lower temperature is possible, however, the equilibrium adsorption amount at the corresponding pressure decreases at the same time. This eventually results in decrease of the adsorption capacity and rate. From the experimental investigation, it was proved that accruing the chilled water around 7 °C is possible by using AHP system when the regeneration water above 70 °C. As presented in Fig.6. 15, COP also decreased as supplying the lower temperature heat source. COP was less dependent on the regeneration water temperature because the portion of sensible heat loss also decreases as the regeneration water temperature decreases.
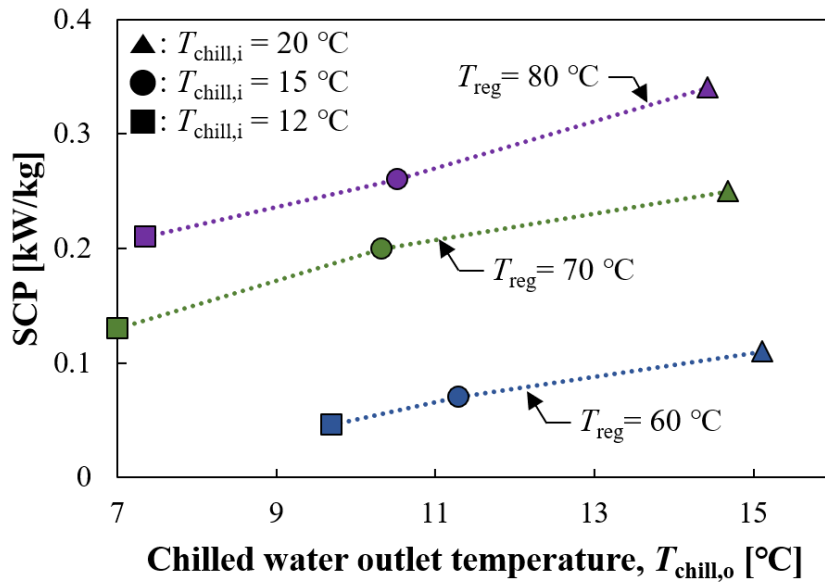
Fig. 6. 14 Effect of regeneration temperature and heat source temperature on SCP
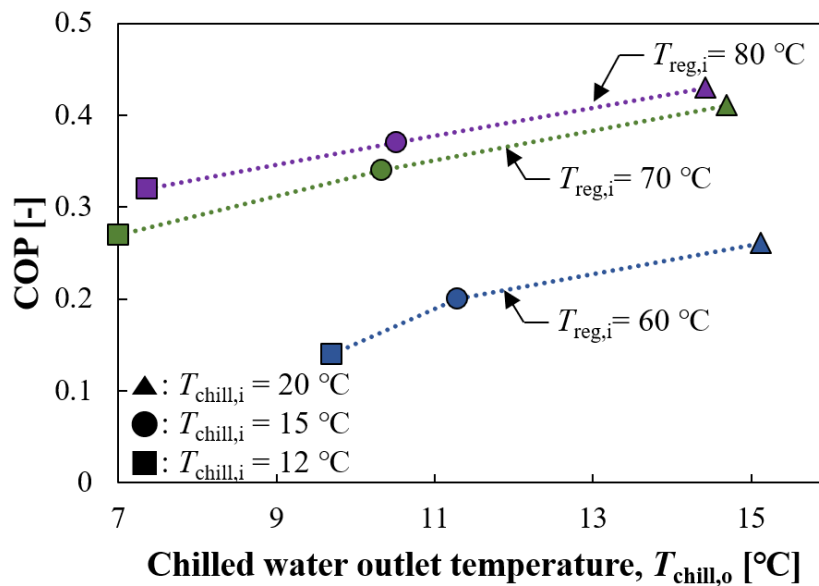
Fig. 6. 15 Effect of regeneration temperature and heat source temperature on COP

6.3.4 Exergy Analysis Based on Experimental Results

The definition of exergy is known as the maximum amount of achievable work which can be provided by the system and certain energy source. Thus it indicates the loss of obtainable energy resulted from the generation of entropy in the irreversible system. The reference temperature for the exergy analysis is 298.15 K, and all processes are considered to be at cyclic steady state [33,34]. Irreversibility of each component and exergy efficiency for exergy analysis is calculated based on Eq. (5-16)~(5-20) of chapter 5. As shown in Fig. 6. 16, the irreversibility tended to increase as the heat source temperature rises. The reason for this can be analyzed that the entropy generation increased as the heat source temperature increased. In terms of the exergy efficiency (Fig. 6. 17), the inlet temperature of chilled water affected more than the temperature of regeneration water does. Since most of exergy loss occurs from the adsorption and desorption process [35] as shown in Fig. 6. 18, which inevitably undergoes large temperature change, it is expected to reduce entire irreversibility by applying heat recovery. About this statement, Fig. 6. 19 presents simulation analysis on effect of the circulate heat recovery on the irreversibility.
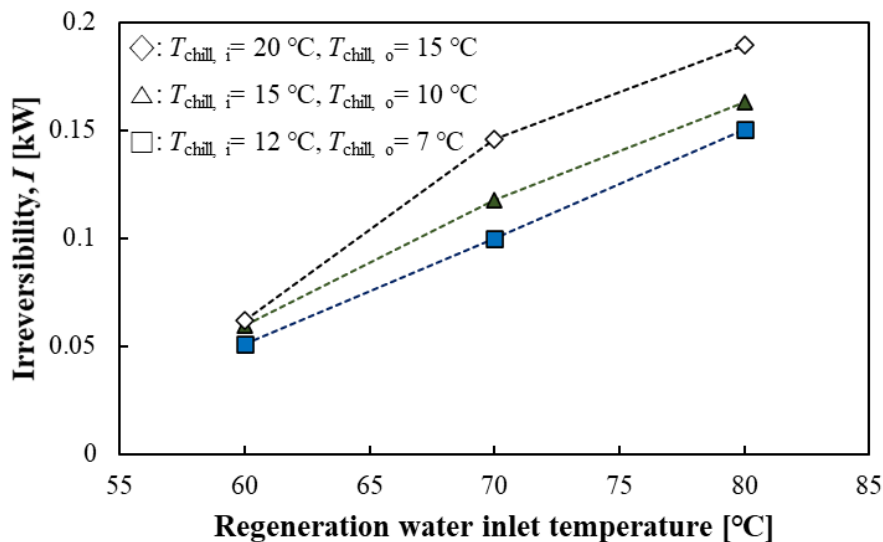
Fig. 6. 16 Irreversibility according to temperature of regeneration water and chilled water
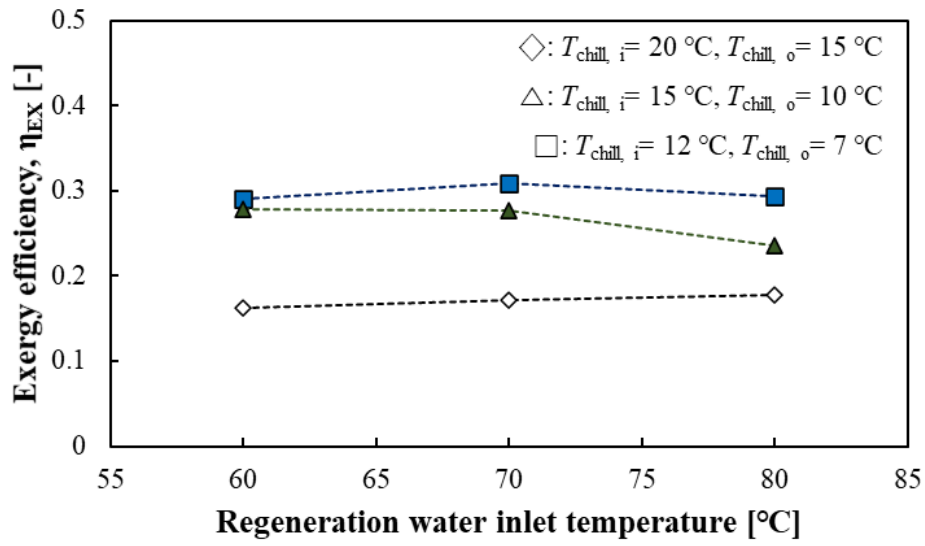
Fig. 6. 17 Exergy efficiency according to temperature of regeneration water and chilled water
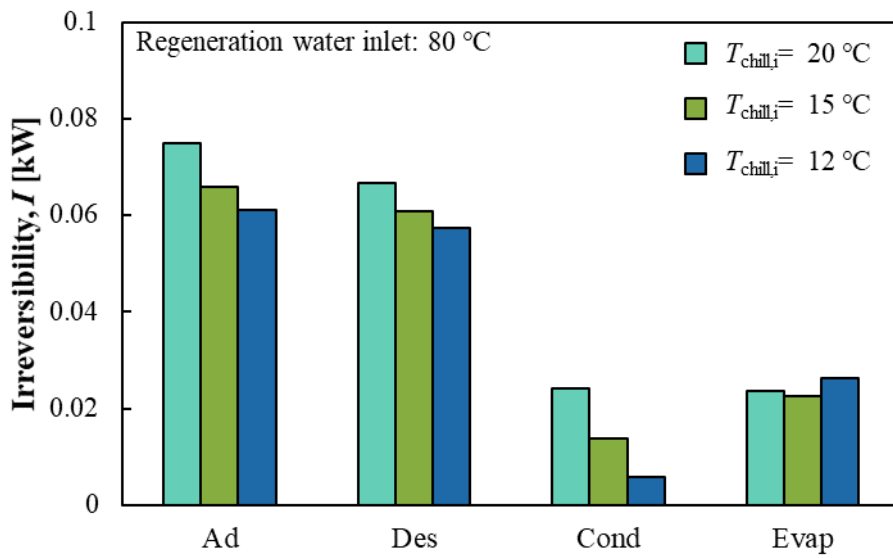
Fig. 6. 18 Irreversibility of each component according to temperature of chilled water

As expected, the irreversibility during the adsorption and desorption process are greatly reduced by applying the heat recovery. That is because the temperature jump or drop at the beginning of the process becomes moderate due to the recovered heat, without inputting any thermal energy outside of the system. The irreversibility also tended to decrease as increasing the heat recovery time since its effect is proportional to the duration time. The optimized heat recovery time may be decided based on the cooling performance of AHP according to the heat recovery time, as shown in Fig. 6 20.
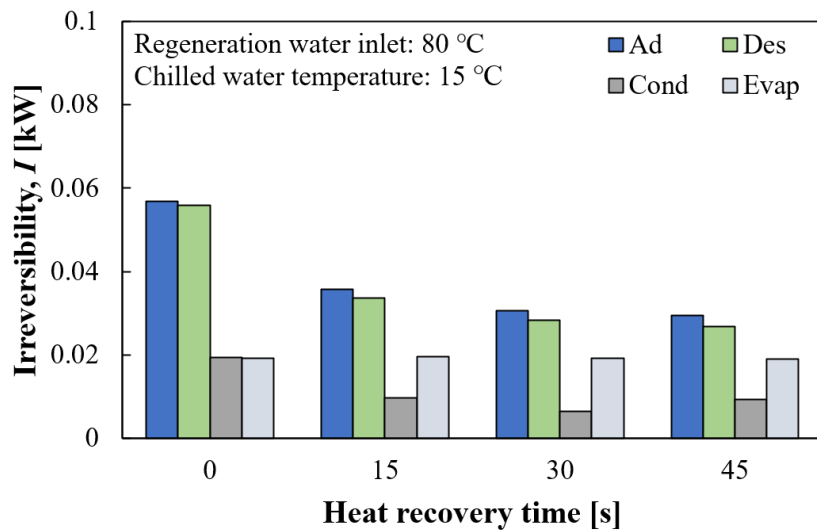
Fig. 6. 19 Irreversibility of each component according to heat recovery time
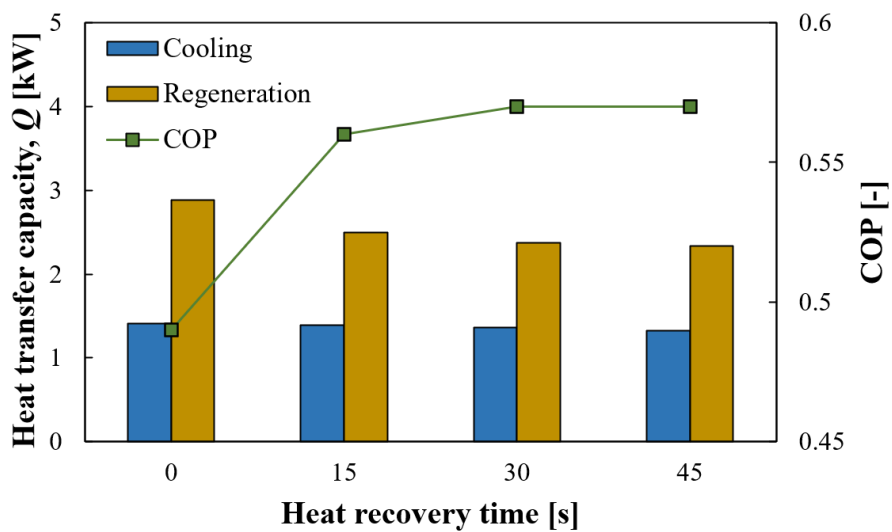
Fig. 6. 20 Cooling performance of AHP according to heat recovery time

6.4 SUMMARY

In this chapter, experimental investigation on energy and exergy analysis of AHP systems using 1kW-scale system were provided. The WSS composite adsorbent with 20 wt.% of LiCl is filled between the fins of corrugated aluminum heat exchangers. During the experiments, the half cycle time was varied from 8 to 16 minute, the regeneration temperature is changed from 60 to 80 ℃, the chilled water temperature is controlled from 7 to 15 ℃. Followings summarize the major contents of this chapter.

1) The pressure of that of the condenser and the desorption bed increased more rapidly compared to the adsorber and evaporator at the beginning of the cycle, due to the dependency of mass transfer rate on the adsorbent temperature.

2) The cooling capacity tended to decrease as proceeding the adsorption process due to the reduced driving force. As the half cycle time becomes longer, the difference between the peak cooling capacity and the value at the end of the cycle became large. It was confirmed that the cooling capacity was still obtainable even at the half cycle time 16 minute due to the large adsorption capacity of the WSS composite.

3) The COP of the systems employing the adsorbers tended to increase when the adsorption time increased. That was because the sensible heat loss that occurred when the mode was switched from adsorption to desorption accounted for a relatively small portion among the entire load.

4) The cooling capacity when the regeneration temperature is 70 ℃ was about 36 % reduced than that of the case with the regeneration water of 80 ℃. Meanwhile, the decrease in the cooling capacity was much more severe when applying the regeneration water of 60 ℃. COP was less dependent on the regeneration water temperature because the portion of sensible heat loss also decreases as the regeneration water temperature decreases.

5) The SCP tended to decrease as lowering the inlet water temperature at the evaporator,

because the equilibrium adsorption amount at the corresponding pressure decreases at the same time.

6) The irreversibility tended to increase as the heat source temperature rises since the entropy generation increased as the heat source temperature increased. The inlet temperature of chilled water affected more than the temperature of regeneration water does; the lower irreversibility was observed at the lower chilled water temperature.

7) Since most of exergy loss occurs from the adsorption and desorption process, which inevitably undergoes large temperature change, it is expected to reduce entire irreversibility by applying heat recovery.

6.5 REFERENCE

[1]   R. Narayanan, Heat-driven cooling technologies, 2017.

[2]   S. Akhtar, T.S. Khan, S. Ilyas, M.S. Alshehhi, Feasibility and Basic Design of Solar Integrated Absorption Refrigeration for an Industry, Energy Procedia. 75 (2015) 508–513.

[3]   J. Cerezo Román, R. Javier Romero Domínguez, A. Rodríguez Martínez, P. Soto Parra, Thermal Analysis of an Absorption and Adsorption Cooling Chillers Using a Modulating Tempering Valve, in: Zero Net Zero Energy, IntechOpen, 2019: p. 13.

[4]   R.J.H. Grisel, S.F. Smeding, R. de Boer, Waste heat driven silica gel/water adsorption cooling in trigeneration, Appl. Therm. Eng. 30 (2010) 1039–1046.

[5]   M. a Atiya, F. a Lattieff, A. a Al-hemiri, Experimental Performance of a Finned-tube Silica Gel Adsorption Chiller for Air-Conditioning Application, Al-Khwarizmi Eng. J. 10 (2014) 68–77.

[6]   D.C. Wang, Z.X. Shi, Q.R. Yang, X.L. Tian, J.C. Zhang, J.Y. Wu, Experimental research on novel adsorption chiller driven by low grade heat source, Energy Convers. Manag. 48 (2007) 2375–2381.

[7]   Q. Pan, J. Peng, R. Wang, Experimental study of an adsorption chiller for extra low temperature waste heat utilization, Appl. Therm. Eng. 163 (2019) 114341.

[8]   T. Kashiwagi, A. Akisawa, B. Saha, S. Koyama, K. Ng, H. Chua, Development of Waste Heat Driven Multi-Bed, MultiStage Regenerative Adsorption Chiller, (2004).

[9]   K.C. Ng, X. Wang, Y.S. Lim, B.B. Saha, A. Chakarborty, S. Koyama, A. Akisawa, T. Kashiwagi, Experimental study on performance improvement of a four-bed adsorption chiller by using heat and mass recovery, Int. J. Heat Mass Transf. 49 (2006) 3343–3348.

[10]   A.S. Uyun, T. Miyazaki, Y. Ueda, A. Akisawa, Experimental Investigation of a Three-Bed Adsorption Refrigeration Chiller Employing an Advanced Mass Recovery Cycle, Energies. 2 (2009) 531–544.

[11]   I. Wirajati, A. Akisawa, Y. Ueda, T. Miyazaki, EXPERIMENTAL INVESTIGATION OF A REHEATING TWO-STAGE ADSORPTION CHILLER APPLYING FIXED CHILLED WATER OUTLET CONDITIONS, Heat Transf. Res. 46 (2015) 293–309.

[12]   T. Esaki, N. Kobayashi, T. Matsuda, Evaluation of the Characteristic of Adsorption in a Double-Effect Adsorption Chiller with FAM-Z01, J. Mater. Sci. Chem. Eng. 04 (2016) 8–19.

[13]   A. Myat, N. Kim Choon, K. Thu, Y.-D. Kim, Experimental investigation on the optimal performance of Zeolite–water adsorption chiller, Appl. Energy. 102 (2013) 582–590.

[14] A.A. Al-Maaitah, F.M. Hadi, Experimental Investigation of Two Stages Adsorption Chiller with Four Generators Utilizing Activated Carbon and Methanol as Working Pair, Int. J. Curr. Eng. Technol. 77 (2017) 2277–4106. http://inpressco.com/category/ijcet.

[15] X.Q. Zhai, R.Z. Wang, J.Y. Wu, Y.J. Dai, Q. Ma, Design and performance of a solar-powered air-conditioning system in a green building, Appl. Energy. 85 (2008) 297–311.

[16] Z.X. Yuan, Y.X. Li, C.X. Du, Experimental System of Solar Adsorption Refrigeration with Concentrated Collector, J. Vis. Exp. (2017).

[17] D.C. Wang, Y.J. Wang, J.P. Zhang, X.L. Tian, J.Y. Wu, Experimental study of adsorption chiller driven by variable heat source, Energy Convers. Manag. 49 (2008) 1063–1073.

[18] Z.S. Lu, R.Z. Wang, Experimental performance investigation of small solar air-conditioning systems with different kinds of collectors and chillers, Sol. Energy. 110 (2014) 7–14.

[19] R.Z. Wang, Efficient adsorption refrigerators integrated with heat pipes, Appl. Therm. Eng. 28 (2008) 317–326.

[20] H. Chen, Q. Cui, Y. Tang, X. Chen, H. Yao, Attapulgite based LiCl composite adsorbents for cooling and air conditioning applications, Appl. Therm. Eng. 28 (2008) 2187–2193.

[21] A.D. Grekova, L.G. Gordeeva, Y.I. Aristov, Composite "LiCl/vermiculite" as advanced water sorbent for thermal energy storage, Appl. Therm. Eng. 124 (2017) 1401–1408.

[22] L.X. Gong, R.Z. Wang, Z.Z. Xia, C.J. Chen, Adsorption Equilibrium of Water on a Composite Adsorbent Employing Lithium Chloride in Silica Gel, J. Chem. Eng. Data. 55 (2010) 2920–2923.

[23] K. Daou, R.Z. Wang, Z.Z. Xia, Development of a new synthesized adsorbent for refrigeration and air conditioning applications, Appl. Therm. Eng. 26 (2006) 56–65.

[24] Y.. Aristov, G. Restuccia, G. Cacciola, V.. Parmon, A family of new working materials for solid sorption air conditioning systems, Appl. Therm. Eng. 22 (2002) 191–204.

[25] Y.I. Aristov, I.S. Glaznev, A. Freni, G. Restuccia, Kinetics of water sorption on a CaCl2-in-silica-gel-pores sorbent: The effects of the pellet size and temperature, Kinet. Catal. 47 (2006) 770–775.

[26] Y.I. Aristov, A. Sapienza, D.S. Ovoshchnikov, A. Freni, G. Restuccia, Reallocation of adsorption and desorption times for optimisation of cooling cycles, Int. J. Refrig. 35 (2012) 525–531.

[27] A. Freni, F. Russo, S. Vasta, M. Tokarev, Y.I. Aristov, G. Restuccia, An advanced solid sorption chiller using SWS-1L, Appl. Therm. Eng. 27 (2007) 2200–2204.

[28] A. Freni, A. Sapienza, I.S. Glaznev, Y.I. Aristov, G. Restuccia, Experimental testing of a lab-scale adsorption chiller using a novel selective water sorbent "silica modified by calcium nitrate," Int. J. Refrig. 35 (2012) 518–524.

[29] S. Nakabayashi, K. Nagano, M. Nakamura, J. Togawa, A. Kurokawa, Improvement of water vapor adsorption ability of natural mesoporous material by impregnating with chloride salts for development of a new desiccant filter, Adsorption. 17 (2011) 675–686.

[30] J. Togawa, A. Kurokawa, K. Nagano, Water sorption property and cooling performance using natural mesoporous siliceous shale impregnated with LiCl for adsorption heat pump, Appl. Therm. Eng. 173 (2020) 115241.

[31] H. Liu, K. Nagano, J. Togawa, A composite material made of mesoporous siliceous shale impregnated with lithium chloride for an open sorption thermal energy storage system, Sol. Energy. 111 (2015) 186–200.

[32] S.H. Seol, K. Nagano, J. Togawa, Modeling of adsorption heat pump system based on experimental estimation of heat and mass transfer coefficients, Appl. Therm. Eng. 171 (2020) 115089.

[33] G. Gutiérrez-Urueta, A. Huicochea, P. Rodríguez-Aumente, W. Rivera, Energy and Exergy Analysis of Water-LiBr Absorption Systems with Adiabatic Absorbers for Heating and Cooling, Energy Procedia. 57 (2014) 2676–2685.

[34] V. Baiju, C. Muraleedharan, Exergy Assessment of Single Stage Solar Adsorption Refrigeration System Using ANN, ISRN Mech. Eng. 2012 (2012) 1–10.

[35] M. Sharifzadeh, M. Ghazikhani, H. Niazmand, Temporal exergy analysis of adsorption cooling system by developing non-flow exergy function, Appl. Therm. Eng. 139 (2018) 409–418.

CHAPTER 7. FUTURE RESEARCHES AND GENERAL CONCLUSIONS

7.1 FUTURE RESEARCH TOPICS

7.1.1 Hybrid Cooling System with AHP and CO_2 Compression

Since it is a thermally driven system, AHP has the advantage of easily being combined with other types of systems. AHP systems are often used in the cascade cooling systems with a vapor compression system [1,2]. That is, the evaporator of the AHP system takes a role of the condenser of the vapor compression system to reduce energy consumption of the compressor by lowering condensation pressure. If the working fluid for the vapor compression system is CO_2, the application effect is more visible because the combination prevents the CO_2 cycle from exceeding the critical point. Since both working fluids used in two combined systems are natural refrigerant, this kind of system has an advantage of environmentally friendly operation. Furthermore, the vapor density of CO_2 is exceptionally high compared to other working fluids, it has an advantage of reducing component size. However, the high pressure level and relatively low COP compared to HCFC and HFC refrigerants has been considered as a disadvantage. One of the reason for this relatively low cooling performance is high vapor quality of CO_2 at the evaporator inlet [3].
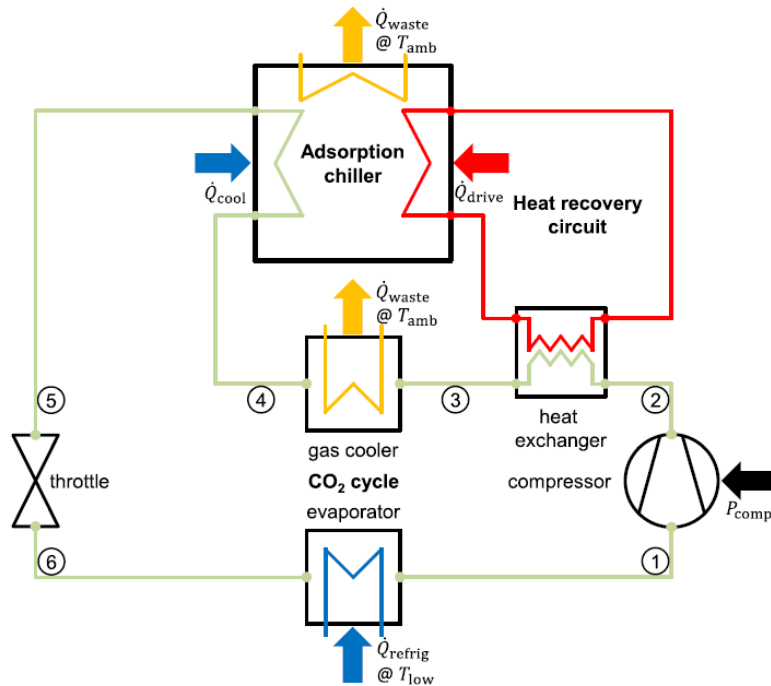
Fig. 7. 1 Schematic diagram of the hybrid system combining CO_2 cycle and AHP [4]

In recent paper, another form of the hybrid system of AHP with CO_2 compression was introduced by Gibelhaus et al. [4] to relieve this problem. The suggested system has a characteristic that it utilizes the internal heat source rather than bringing external input energy. That is, the hot gas from the compressor outlet is used as a heat source of the combined AHP system. On the other hand, the cooling capacity of the AHP system cools down the gas at the outlet side of the gas cooler. Therefore, the gas at the outlet of the gas cooling is cooled again by the AHP cycle before being expanded, resulting in the lower vapor quality after the expansion. Fig. 7. 1 describes the schematic diagram of the system, and Fig. 7. 2 shows a P-h diagram of the CO_2 cycle of the hybrid system.

Based on this approach, followings seem to worth to conduct more study and research for further development. Firstly, the optimization of high level pressure seems to be required. The optimization of high pressure transcritical CO_2 system has been dealt with a lot of reaches [5]. For this hybrid cycle, the effect of AHP according to the high level pressure needs to be considered together. That is because the temperature of gas at the compressor outlet is greatly changed with respect to the high level pressure, and the cooling performance of AHP and vapor quality of CO_2 cycle are highly dependent on it. Also, optimization of adsorbers is required because the performance of the hybrid system is dependent on how AHP consumes the limited heat source effectively.
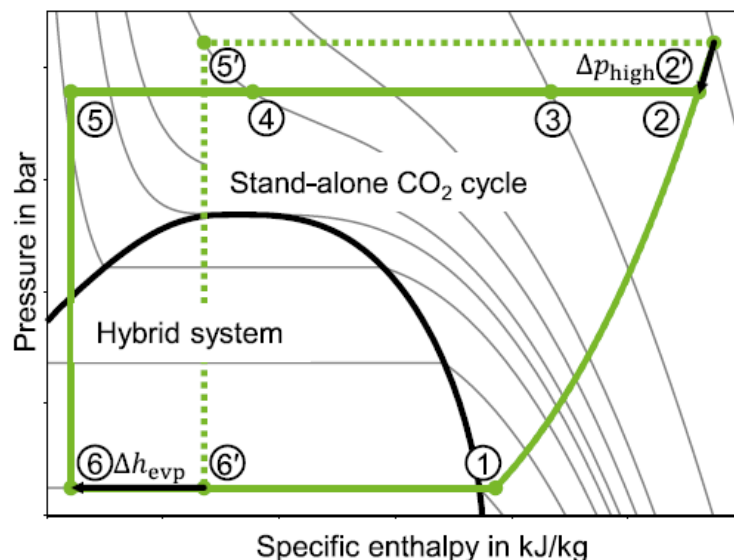
Fig. 7. 2 P-h diagram of the hybrid system combining CO_2 cycle and AHP [4]

7.1.2 Combined AHP with Power Generation

As a part of cogeneration systems, a lot of researches have been conducted by utilizing AHP systems [6,7]. Jiang et al. [8] suggested a cogeneration cycle generating electricity and chilled water at the same time with one connected resorption cycle. Al-Mousawi et al. [9] proposed combined AHP system for cooling system with expander for generating electricity. In the proposed system, the pressure of desorption increases as supplying hot water around 80 °C. The expander operates as the pressure difference between the desorption and condensation occurs.
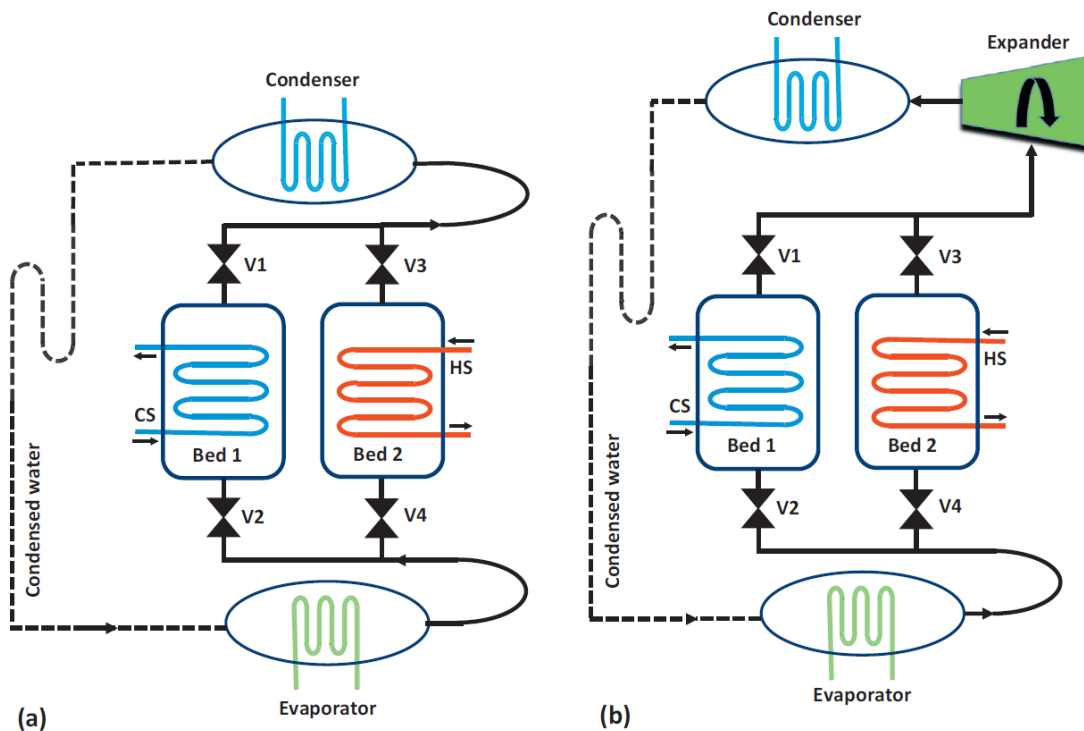
Fig. 7. 3 Schematic diagram of (a) basic AHP system (b) combined AHP with power generation

This approach seems to be worth to conduct more research because there can be several factors which may affect both cooling performance and electricity generation. Firstly, there can be severer performance difference according to the working pairs. Since typical AHP systems operate at sub-atmospheric pressure, the trivial pressure difference of these working pairs may be difficult to operate an expander properly. Therefore, additional analysis of various working fluids considering thermal and physical properties of working fluids seems to be essential for the future research. Secondly, the operating

strategy needs to be different since combining two different cycles. For instance, controlling vapor flow from the desorption bed to the expander needs to be optimized because the expander inlet pressure is inevitably unsteady due to the characteristic of AHP. As the inlet pressure gradually decreases, it is expected that the turbine efficiency also decreases. This may be relieved by controlling operation strategy such as multi-bed operation with a different number of beds undergoing adsorption and desorption process.

7.2 GENERAL CONCLUSIONS OF THE THESIS

Because of increasing concerns about energy saving and environmental issues resulted from air-conditioning, AHP has been considered as one of promising solution to relieve the problems. Furthermore, recently increasing interest on utilization of waste heat and reduced price of solar collectors are good opportunity for AHP systems to be more widespread. However, limitations such as expensive initial cost, relatively large system volume and low COP compared to other types of cooling system need to be improved. Therefore, as a part of effort to overcome these hinderances, this study presented several research topics in each chapter and could make conclusions as followings.

In Chapter 1, comprehensive review of various AHP systems was provided. The advantages which make AHP system promising were clarified, and disadvantages to improve are also pointed out. Various AHP systems, several representative working pairs and commercialized AHP units were also introduced.

In Chapter 2, the natural mesoporous material based composite adsorbent impregnated with lithium chloride was introduced. The obvious enhancement of the equilibrium adsorption amount was obtained by impregnating LiCl into the pure WSS. The maximum applicable amount of the lithium chloride for preventing carryover was determined to be 20 wt.%, based on its pore volume. However, one major concern of applying the composite adsorbent is stability. To investigate physical stability after the impregnation, the experiments comparing the physical and equilibrium adsorption properties were conducted. WSS hardly showed change in physical properties after impregnation and the equilibrium adsorption amount also did not changed. Therefore, it was concluded that WSS is expected to be utilized as a host matrix of composite adsorbent in terms of both enhanced equilibrium adsorption amount and physically stable pore structures.

In Chapter 3, the mass transfer characteristics of water vapor on the coated adsorbent layer were studied. The coated type adsorbers have advantage of the better heat transfer from the metal of heat exchanger to the coated layer, and the adsorbent can be used more effectively. The mass transfer characteristic of the coated layer was dependent on

thickness of the layer. Here, the mass transfer was divided into interfacial and internal to estimate effect of coated thickness, by using a novel experimental method. The experimentally obtained and calculated overall mass transfer coefficients based on the LDF model were matched acceptably, implying the applicability of the suggested experimental method.

In Chapter 4, the mass and heat transfer characteristics of the filled type adsorbers were studied. The mass transfer coefficient of each adsorber was calculated using the LDF model considering thermal effects. During the experiments, the adsorbent temperature was controlled by adjusting the temperature of the cooling water from 30 to 60 °C. The overall heat transfer coefficient was experimentally evaluated by changing the adsorbent temperature from 80 to 30 °C to realize the actual working conditions of an AHP. The experimentally obtained heat and mass transfer coefficients were substituted into a mathematical model for a more accurate and practical estimation of the AHP performance. WSS composite material exhibited a COP that was 6–17 % higher than that of the A-type silica gel. This indicates the effectiveness of the WSS composite compared with the frequently used A-type silica gel.

In Chapter 5, the simulation analysis on the annual cooling performance of the solar assisted AHP which WSS composite as an adsorbent was conducted. The analysis was based on the mathematical model applying four difference climate conditions (Tokyo, Florida, Dubai, Hawaii). An AHP system inevitably undergoes sensible heat loss when switching the adsorption and desorption mode. WSS + LiCl 20 wt.% exhibited high adsorption capability, which allows the system to be operated with a longer cycle time to reduce the heat loss occurs when switching between adsorption and desorption modes. Indeed, the average temperature of the regeneration water for the half cycle time of 14 minutes was about 9.7 °C higher than the case of 8 minutes. Thus, WSS+LiCl 20 wt.% showed about 14 % of increase in AHP cooling performance as extending the half cycle time from 8 minute to 14 minute. The payback periods estimated based on the annual energy saving obtained from AHP and the local electricity cost were 6.6 years for Hawaii, 15.6 years for Dubai, respectively.

In Chapter 6, thermodynamic characteristics regarding energy and exergy are analyzed based on the experimental data using 1 kW-scale AHP system. The cooling capacity when the regeneration temperature is 70 ℃ was about 36 % reduced than that of the case with the regeneration water of 80 ℃. Meanwhile, the decrease in the cooling capacity was much more severe when applying the regeneration water of 60 ℃. The irreversibility tended to increase as the heat source temperature rises since the entropy generation increased as the heat source temperature increased. The inlet temperature of chilled water affected more than the temperature of regeneration water does; the lower irreversibility was observed at the lower chilled water temperature. Since most of exergy loss occurs from the adsorption and desorption process, which inevitably undergoes large temperature change, it is expected to reduce entire irreversibility by applying heat recovery.

In Chapter 7, several future research topics were introduced. Based on the advantage of being easily combined with other types of cycles, it seems that various challenges regarding hybrids cycles of AHP systems will be possible. It is also expected that system characteristics will be quite different from the basic AHP systems for the case of the hybrid system with other types of cycles. Therefore, these hybrid cycles will be attractive topics as future researches.

To sum up, AHP systems are greatly attractive in terms of saving operating cost and reducing emission of greenhouse gas. Although there still hurdles for an AHP system to overcome, it is strongly believed that researches in terms of its various aspects throughout the world will finally bring us the more developed technology. Furthermore, interest on utilization of waste heat, spreading out solar collectors with more reasonable price especially from China, price reduction by the mass production of high-performance adsorbent are also positive factors for AHP systems to spread out.

The world has been facing environmental issues during recent decades. As a part of effort to solve the problem, the low-carbon air conditioning through AHP systems are highly suggested.

7.3 REFERENCE

[1]   V. Palomba, E. Varvagiannis, S. Karellas, A. Frazzica, Hybrid Adsorption-Compression Systems for Air Conditioning in Efficient Buildings: Design through Validated Dynamic Models, Energies. 12 (2019) 1161.

[2]   S. Vasta, V. Palomba, D. La Rosa, W. Mittelbach, Adsorption-compression cascade cycles: An experimental study, Energy Convers. Manag. 156 (2018) 365–375. https://linkinghub.elsevier.com/retrieve/pii/S0196890417311135.

[3]   A. Cavallini, F. Tecnica, V. Venezia, I.P. Pd, European Seminar – Properties of CO2 as a refrigerant, Carbon N. Y. (2002).

[4]   A. Gibelhaus, N. Fidorra, F. Lanzerath, U. Bau, J. Köhler, A. Bardow, Hybrid refrigeration by CO2 vapour compression cycle and water-based adsorption chiller: An efficient combination of natural working fluids, Int. J. Refrig. 103 (2019) 204–214.

[5]   L. Yang, H. Li, S.-W. Cai, L.-L. Shao, C.-L. Zhang, Minimizing COP loss from optimal high pressure correlation for transcritical CO2 cycle, Appl. Therm. Eng. 89 (2015) 656–662.

[6]   F.N. Al-Mousawi, R. Al-Dadah, S. Mahmoud, Integrated adsorption-ORC system: Comparative study of four scenarios to generate cooling and power simultaneously, Appl. Therm. Eng. 114 (2017) 1038–1052.

[7]   L. Jiang, L. Wang, R. Wang, P. Gao, F. Song, Investigation on cascading cogeneration system of ORC (Organic Rankine Cycle) and CaCl2/BaCl2 two-stage adsorption freezer, Energy. 71 (2014) 377–387.

[8]   L. Jiang, L.W. Wang, A.P. Roskilly, R.Z. Wang, Design and performance analysis of a resorption cogeneration system, Int. J. Low-Carbon Technol. 8 (2013) i85–i91.

[9]   F.N. Al-Mousawi, R. Al-Dadah, S. Mahmoud, Different bed configurations and time ratios: Performance analysis of low-grade heat driven adsorption system for cooling and electricity, Energy Convers. Manag. 148 (2017) 1028–1040.

ACKNOWLEDGEMENT

First of all, I would like to express my sincere gratitude to my supervisor Professor Nagano. 3 years I spent in his laboratory was one of the most valuable experience in my life. Of course, a lot of things were too tough for me at the beginning. I was clumsy at dealing with the new research topic and having hard time to get used to the new life. In this hard time, Professor Nagano supported me with his sincere passion rather than pressing me. He tried to listen to student's voice, and we could notice his consideration. I will cherish all advises from Professor Nagano and experiences in here to become the better researcher. I appreciate again for giving me the chance to undergo this precious experience.

I would like to thank Professor Katsura, Professor Hayama, Professor Hamada and Professor Tabe for their service on my doctoral committee and precious comments for developing my research.

Also, I would like to say special thanks to Dr. Togawa for training me as a member of 'Adsorption Team'. In retrospect, offering his time only for my experiments is not easy at all. Dr. Togawa has not expressed any complain about my annoying questions. I do know well that all of our team members owe him, and I will not forget his support. I should not forget to express thanks to Ms. Kurokawa who contributed to academic development of 'Adsorption Team'. I wish to thank our team members Mr. Hefang, Ms. Tang, Ms. Izawa for sharing valuable knowledges.

I appreciate Professor Sakata, Mr. Nakamura and Mr. Kusaka for supporting me with sincere heart whenever I face problems. I would like to say thanks to Dr. Award and Dr. Ali for giving me a lot of academic advices. Let us plan various co-work research in the near future.

Being alone in abroad sometimes made me depressed. Every time I feel depressed, I used to be encouraged by Korean group especially Professor Lee and Mr. Chae. I would like to say thanks to all Korean members in Hokkaido University. I also would like to thank many students in our laboratory especially the leader Mr. Shoji.

The doctoral course itself and living in foreign country alone were more tough than I expected. Every time I feel frustrated, I used to be mentally supported by the fact that all of professors that I respect have undergone the same road as I am standing. They

encouraged me only by the presence. I would like to express sincere gratitude to Professor Yoon Jung-In, Professor Choi Kwang-Hwan, Professor Son Chang-Hyo, Professor Kim Jong-Soo, Professor Kum Jong-Soo, Professor Kim Eun-Pil and Professor Jeong Seok-Kwon, in Pukyong National University of Korea.

During the doctoral course, I sometimes used to feel by myself becoming narrow-mind person. I would like to give a special shout out to my friends Moon Jung-Hyun and Kang In-Ho for cheering me up.

Finally, I would like to dedicate this thesis to my father. I always have felt as if he is standing behind me to support me. Thank you so much for being my hero. I also would like to express gratitude to my mother. I will not forget that I am standing upon your sacrifice and do my best to be your pride. To my sister, thank you for helping my days in Japan, and I will not forget your support. Lastly, I promise my girlfriend Lee Hae-In to never forget anything about our relationship I have felt during the doctoral course.

<div align="right">

2020. 08. 18

With All My Heart

Sung-Hoon SEOL

</div>